AN EVALUATION OF REPAIR METHODS FOR CANTILEVER BRIDGE PIERS

by

SUSAN EILEEN SCOTT, BS

THESIS

Presented to the Faculty of the Graduate School of

the University of Texas at Austin

in Partial Fulfillment

of the Requirements

for the Degree of

MASTER OF SCIENCE IN ENGINEERING

THE UNIVERSITY OF TEXAS AT AUSTIN

May 1997

AN EVALUATION OF REPAIR METHODS

FOR CANTILEVER BRIDGE PIERS

APPROVED BY

SUPERVISING COMMITTEE:

Michael E. Kreger

James O. Jirsa

ACKNOWLEDGMENTS

I would like to thank, etc., etc..

UT:

Professors: Dr. Michael E. Kreger, Dr. James O. Jirsa

GRA: Bradley Wood, Scott Armstrong, Ruben Salas, Sarah Billington

URA: Mohammed Najah, Mohamed Elmrabet

Staff:

TxDOT: Gustavo Morales-Valentin, Scott Armstrong

Fellowship: McKays and Stanley Finch Memorial Fellowship

ABSTRACT

AN EVALUATION OF REPAIR METHODS

FOR CANTILEVER BRIDGE PIERS

by

Susan Eileen Scott, MSE

The University of Texas at Austin, 1996

Supervising Professor: Michael E. Kreger

Cantilever bridge piers are occasionally used in place of standard symmetrical hammerhead bents in areas where limited right-of-way prevents placement of the bents directly under the roadway. This design produces extremely high moments in the joint region, where the caniliver overhang joins the vertical pier. Many bents of this type were used in the I-10/I-35 highway interchange in San Antonio. A design flaw was discovered in the joint of these bents, and field investigations revealed significant cracking in this region in several of the bents.

Earlier phases of Texas Department of Transportation Project 1364, "Design of Large Structural Members Utilizing Partial Prestressing," examined the strength of the deficient joint regions and designs for future bents with increased strength, while this study examines

various methods for repairing and retrofitting existing bents to bring them up to full design strength.

Three types of cantilever bridge piers were used in the San Antonio interchange. One type contained only mild reinforcement, another utilized post-tensioning in the overhang but not in the pier, while the third was post-tensioned throughout. The last type did not exhibit the joint design flaw, so the study concentrated on the other two. Scale models of each type of pier were constructed and tested. Several repair options, including various methods of internal and external post-tensioning, were designed, constructed, and tested. The different repair options were then evaluated and compared based on ultimate strength, serviceability, cost, constructibility, and aesthetics. The results of the tests, evaluations, and comparisons are presented in this report, along with recommendations for the Texas Department of Transportation on the most suitable repair method.

TABLE OF CONTENTS

LIST OF TABLES xvi

LIST OF FIGURES xvii

CHAPTER 1: INTRODUCTION 1

1.1 General Problem Statement 1

1.2 Scope of Research 3

1.2.1 Earlier Phases 3

1.2.2 Current Phases 3

1.3 Objectives 4

1.4 Organization 5

CHAPTER 2: BACKGROUND 6

2.1 Introduction 6

2.2 Reinforcement Layout 7

2.2.1 Bents with Post-Tensioned Overhangs 7

2.2.2 Reinforced Concrete Bents x

2.2.3 Fully Prestressed Bents x

2.3 Field Performance x

2.3.1 Relevance of Field Performance to Laboratory Study x

2.3.2 Bents with Post-Tensioned Overhangs x

2.3.2.1 Pier D-36C x

2.3.2.2 Pier D-37C x

2.3.2.3 Pier D-38C x

2.3.2.4 Pier D-39C x

2.3.2.5 Pier C-11C x

2.3.3 Reinforced Concrete Bents x
2.3.3.1 Pier I-3C x
2.3.3.2 Pier I-4C x
2.3.3.3 Pier I-5C x
2.3.3.4 Pier I-2C x
2.3.3.5 Pier C-11C x

CHAPTER 3: DESIGN, CONSTRUCTION, AND TESTING OF UNREPAIRED CANTILEVER BENT MODELS 30

3.1 Introduction x
3.2 Design x
3.2.1 Selection of Representative Bent 7
3.2.2 Scale Factor 7
3.2.3 Selection of Superstructure Type and Loading Points 7
3.2.4 Overhang Depth 7
3.2.5 Joint Size 7
3.2.6 Column and Overhang Length 7
3.2.7 Column and Overhang Reinforcement 7
3.2.8 Footing Design 7
3.2.9 Calculation of Moment Capacity 7
3.2.10 Identification of Specimens 7
3.3 Materials x
3.3.1 Concrete 7
3.3.2 Mild Steel Reinfocement 7
3.3.3 Post-Tensioning Bars 7
3.3.4 Post-Tensioning Hardware 7
3.3.5 Grout 7
3.4 Fabrication x
3.4.1 Reinforcing Cages 7

3.4.2 Formwork 7
3.4.3 Placement and Consolidation of Concrete 7
3.4.4 Finishing, Curing, and Form Removal 7
3.5 Test Set-Up x
3.5.1 Loading Frame and Rams 7
3.5.2 Floor Anchorage System 7
3.5.3 Instrumentation and Data Collection 7
3.5.3.1 Strain Gauges x
3.5.3.2 Displacement Gauges x
3.5.3.3 Pressure Transducers x
3.5.3.4 Data Acquisition System x
3.6 Test Procedure x
3.6.1 Installation of Specimen 7
3.6.1.1 Specimen Placement and Preparation x
3.6.1.2 Tie-Down Attachment x
3.6.1.3 Gauge Installation x
3.6.2 Static Load Steps 7
3.6.3 Post-Tensioning Operation 7
3.6.4 Crack Identification 7
3.6.5 Strain and Displacement Measurements 7
3.6.6 Crack Width Measurements 7
3.6.7 Photographs 7
3.6.8 Completion of the Tests 7

CHAPTER 4: REPAIR METHODS 70

4.1 Introduction x
4.2 Prestressed Concrete Specimen (POJ-PS-100) x
4.2.1 External Vertical Post-Tensioning (POJ-PS-100-RP1) 7
4.2.1.1 Concept x

4.2.1.2 TxDOT Design x
4.2.1.3 Scaled and Modified Design x
4.2.1.4 Details x
4.2.1.5 Materials x
4.2.1.6 Fabrication x
4.2.1.7 Installation x
4.2.1.8 Test Procedure x
4.2.2 Modified External Vertical Post-Tensioning (POJ-PS-100-RP2) 7
4.2.2.1 Rationale and Design x
4.2.2.2 Details x
4.2.2.3 Test Procedure x
4.3 Reinforced Concrete Specimen (POJ-RC2) x
4.3.1 External Diagonal Post-Tensioning (POJ-RC2-RP1) 7
4.3.1.1 Concept x
4.3.1.2 Design x
4.3.1.3 Details x
4.3.1.4 Materials x
4.3.1.5 Fabrication and Installation x
4.3.1.6 Test Procedure x
4.3.2 Internal Vertical Post-Tensioning (POJ-RC2-RP2) 7
4.3.2.1 Concept x
4.3.2.2 Design x
4.3.2.3 Details x
4.3.2.4 Materials x
4.3.2.5 Fabrication and Installation x
4.3.2.6 Test Procedure x
4.3.2.7 Modification (POJ-RC2-RP2a) x
4.3.3 Internal Vertical Post-Tensioning (POJ-RC2-RP2) 7
4.3.3.1 Concept x
4.3.3.2 Modification of Specimen x

4.3.3.3 Modification of Test Procedure x
4.4 Discarded Repair Options x
4.4.1 External Horizontal and Vertical Post-Tensioning 7
4.4.2 Internal Diagonal Post-Tensioning 7
4.4.3 Concrete Strut 7
4.4.4 Steel Haunch 7
4.4.5 Internal Horizontal and Vertical Post-Tensioning 7

CHAPTER 5: PRESENTATION OF TEST RESULTS 120

5.1 Introduction x
5.2 Tests on Prestressed Concrete Specimens x
5.2.1 POJ-PS-100 7
5.2.1.1 Strength x
5.2.1.2 Deflection x
5.2.1.3 Cracking x
5.2.2 POJ-PS-100-RP1 7
5.2.2.1 Strength x
5.2.2.2 Deflection x
5.2.2.3 Cracking x
5.2.2.4 Repair Performance x
5.2.3 POJ-PS-100-RP2 7
5.2.3.1 Strength x
5.2.3.2 Deflection x
5.2.3.3 Cracking x
5.2.3.4 Repair Performance x
5.3 Tests on Reinforced Concrete Specimens x
5.3.1 POJ-RC2 7
5.3.1.1 Strength x
5.3.1.2 Deflection x

5.3.1.3 Cracking x
5.3.2 POJ-RC2-RP1 7
5.3.2.1 Strength x
5.3.2.2 Deflection x
5.3.2.3 Cracking x
5.3.2.4 Repair Performance x
5.3.3 POJ-RC2-RP2 7
5.3.3.1 Strength x
5.3.3.2 Deflection x
5.3.3.3 Cracking x
5.3.4 POJ-RC2-RP2a 7
5.3.4.1 Strength x
5.3.4.2 Deflection x
5.3.4.3 Cracking x
5.4 POJ-RC2-RP2s x
5.4.1 Strength 7
5.4.2 Deflection 7
5.4.3 Cracking 7

CHAPTER 6: DISCUSSION OF TEST RESULTS 170

6.1 Introduction x
6.2 Tests on Prestressed Concrete Specimens x
6.2.1 POJ-PS-100 7
6.2.2 POJ-PS-100-RP1 7
6.2.2.1 Specimen Performance x
6.2.2.2 Performance of Repair Components x
6.2.3 POJ-PS-100-RP2 7
6.2.3.1 Specimen Performance x
6.2.3.2 Performance of Repair Components x

6.3 Tests on Reinforced Concrete Specimens x
6.3.1 POJ-RC2 7
6.3.2 POJ-RC2-RP1 7
6.3.2.1 Specimen Performance x
6.3.2.2 Performance of Repair Components x
6.3.3 POJ-RC2-RP2 7
6.3.4 POJ-RC2-RP2a 7
6.4 Shear Test (POJ-RC2-RP2s) x

CHAPTER 7: PERFORMANCE AND COST COMPARISONS 185

7.1 Introduction x
7.2 Projected Ultimate Strength x
7.3 Effectiveness/Performance at Service Load x
7.3.1 Deflections 7
7.3.2 Crack Control 7
7.4 Effectiveness/Performance at Factored Load x
7.4.1 Deflections 7
7.4.2 Cracking and Overall Distress 7
7.5 Cost/Constructibility x
7.5.1 General 7
7.5.2 Costs of Material and Labor 7
7.5.3 Installation Time 7
7.6 Other Factors x
7.6.1 Durability/Service Life 7
7.6.2 Aesthetics 7

CHAPTER 8: CONCLUSIONS AND RECOMMENDATIONS 215

8.1 Introduction x

8.2 Summary x
8.2.1 Background 8
8.2.2 Scope 8
8.2.3 Limitations 8
8.3 Conclusions x
8.3.1 Specimen Performance at Factored Load / ϕ 8
8.3.1.1 Strength x
8.3.1.2 Stiffness x
8.3.2 Specimen Performance at Service Load 8
8.3.2.1 Cracking x
8.3.2.2 Stiffness x
8.3.3 Other Factors 8
8.3.3.1 Installation Cost x
8.3.3.2 Durability/Service Life x
8.3.3.3 Aesthetics x
8.4 Recommendations x
8.4.1 Repair Method 8
8.4.1.1 Post-Tensioned Bents x
8.4.1.2 Reinforced Concrete Bents x
8.4.2 Continued Monitoring 8
8.4.3 Further Research 8

REFERENCES 225

VITA 226

LIST OF TABLES

Table 3.1: Scaling of Reinforcement 6
Table 3.2: Concrete Mix Design..... 6
Table 3.3: Properties of Mild Reinforcing Bars 7
Table 3.4: Grout Mix Design..... x
Table 3.5: Major Load Steps x

Table 4.1: Loading Sequence x

Table 5.1: Number of Cracks in Specimen POJ-PS-100 at Dead Load x
Table 5.2: Maximum Crack Widths in Specimen POJ-PS-100 at Dead Load x
Table 5.3: Number of Cracks in Specimen POJ-PS-100-RP1 at Service Load..... x
Table 5.4: Maximum Crack Widths in Specimen POJ-PS-100-RP1 at Service Load..... x
Table 5.5: Number of Cracks in Specimen POJ-PS-100-RP2 at Service Load..... x
Table 5.6: Maximum Crack Widths in Specimen POJ-PS-100-RP2 at Service Load..... x
Table 5.7: Number of Cracks in Specimen POJ-RC2 at its Ultimate Load..... x
Table 5.8: Maximum Crack Widths in Specimen POJ-RC2 at its Ultimate Load x
Table 5.9: Number of Cracks in Specimen POJ-RC2-RP1 at Service Load x
Table 5.10: Maximum Crack Widths in Specimen POJ-RC2-RP1 at Service Load..... x
Table 5.11: Number of Cracks in Specimen POJ-RC2-RP2 at Service Load x
Table 5.12: Maximum Crack Widths in Specimen POJ-RC2-RP2 at Service Load..... x
Table 5.13: Number of Cracks in Specimen POJ-RC2-RP2a at Service Load x
Table 5.14: Maximum Crack Widths in Specimen POJ-RC2-RP2a at Service Load x

Table 7.1: Original Calculated Strength Estimates and Maximum
Normalized Test Loads..... x
Table 7.2: Unit Costs of Repair Components..... x

LIST OF FIGURES

Figure 1.1: Configuration of Cantilever Bridge Pier, Showing Each Region of the Bent 2

Figure 2.1: Example of Fully Prestressed Cantilever Bent 6
Figure 2.2: Example of Reinforced Concrete Cantilever Bent 6
Figure 2.3: Example of Reinforced Concrete Bent with Fully Post-Tensioned Overhang 7
Figure 2.4: Schematic of Pier, Overhang, and Joint Regions in Cantilever Bent, Showing Assumed Critical Sections for Original Design x
Figure 2.5: Layout of Reinforcement in Bent with Post-Tensioned Overhang x
Figure 2.6: Available and Required Development Length for Pier Reinforcement in Bent with Post-Tensioned Overhang x
Figure 2.7: Crack at Critical Section in Bent with Post-Tensioned Overhang x
Figure 2.8: Free-Body Diagram of Bent Cut through Critical Section x
Figure 2.9: Layout of Reinforcement in Reinforced Concrete Bent x
Figure 2.10: Available and Required Development Length of Overhang Reinforcement in Reinforced Concrete Bent x
Figure 2.11: Diagonal Crack at Critical Section in Reinforced Concrete Bent x
Figure 2.12: Free-Body Diagram of Overhang with Diagonal Crack through the Joint x
Figure 2.13: Pattern of Cracks in Pier D-36C x
Figure 2.14: Pattern of Cracks in Pier D-37C x
Figure 2.15: Pattern of Cracks in Pier D-38C x
Figure 2.16: Pier D-39C x
Figure 2.17: Pattern of Cracks in Pier C-11C x
Figure 2.18: Pattern of Cracks in Pier I-3C x
Figure 2.19: Pattern of Cracks in Pier I-4C x
Figure 2.20: Pattern of Cracks in Pier I-5C x

Figure 2.21: Elevation of Pier I-2C x
Figure 2.22: Pattern of Cracks in Pier I-2C x

Figure 3.1: Full-Scale, Two-Lane Precast Superstructure Design 6
Figure 3.2: Cantilever Bent with Critical Live Load Distribution on Superstructure 6
Figure 3.3: Loading Points for Model Bent 7
Figure 3.4: Dimensions of Model Bent x
Figure 3.5: Layout of Reinforcement in Model Bent with Post-Tensioned Overhang x
Figure 3.6: Layout of Reinforcement in Reinforced Concrete Model Bent x
Figure 3.7: Details of Reinforcement in Model Bent with Post-Tensioned Overhang x
Figure 3.8: Details of Reinforcement in Reinforced Concrete Model Bent x
Figure 3.9: Footing Design for Model Bent x
Figure 3.10: Example of Spreadsheet for Calculating Moment Capacity x
Figure 3.11: Equilibrium of Bent Cut through Critical Section x
Figure 3.12: Format of Specimen Labelling x
Figure 3.13: Results of Concrete Compressive Strength Tests x
Figure 3.14: Typical Tensile Test Results for Mild Reinforcing Bars x
Figure 3.15: Results of Tensile Test for 1.59 cm (5/8 in.) Diameter Post-Tensioning Bars x
Figure 3.16: Post-Tensioning Hardware x
Figure 3.17: Compressive Strength Test Results for Grout x
Figure 3.18: Formwork Sections and Assembled Formwork x
Figure 3.19a: Loading Frame x
Figure 3.19b: Loading Frame with Columns Cut Away to Show Rams and Floor Anchorage x
Figure 3.20: Locations of Strain Gauges in Post-Tensioned Specimen x
Figure 3.21: Locations of Strain Gauges in Reinforced Concrete Specimen x

Figure 3.22: Locations of Displacement Gauges x
Figure 3.23: Grid Lines on Specimen x

Figure 4.1: TxDOT Design for External Vertical Post-Tensioning 6
Figure 4.2: Scaled, Modified Design for Specimen 6
Figure 4.3: Dimensions of Top Beam Assembly 7
Figure 4.4: Dimensions of Side Plate Assemblies..... x
Figure 4.5: Locations of Strain Gauges on Repair Components x
Figure 4.6: Locations of Displacement Gauges on Repair Components..... x
Figure 4.7: Stressing Sequence for External Vertical Post-Tensioning Bars x
Figure 4.8: Modified Bar Layout for External Vertical Post-Tensioning x
Figure 4.9: Effective Applied Force from Horizontal and Diagonal Post-Tensioning Bars x
Figure 4.10: Layout of External Diagonal Post-Tensioning x
Figure 4.11: Normal and Shear Forces Produced in the Specimen by Diagonal Post-Tensioning x
Figure 4.12: Crack at New Critical Section x
Figure 4.13: Effect of Plate Length..... x
Figure 4.14: Plate Size and Position for External Post-Tensioning System..... x
Figure 4.15: Details of Side Plate Assembly for External Diagonal Post-Tensioning..... x
Figure 4.16: Details of Top Plate Assembly for External Diagonal Post-Tensioning x
Figure 4.17: Forces from Post-Tensioning Bars, Anchor Bolts, and Friction..... x
Figure 4.18: Example of Anchor Bolt Shear Test Results x
Figure 4.19: Cracks in Specimen Due to Anchor Bolt Tensioning Superimposed on Cracks from the Previous Test..... x
Figure 4.20: Locations of Strain Gauges on Repair Components x
Figure 4.21: Locations of Displacement Gauges on Repaired Specimen x
Figure 4.22: Schematic of Internal Post-Tensioning..... x
Figure 4.23 Location of Post-Tensioning Bars in Profile x
Figure 4.24: Plan View Location of Post-Tensioning Bars..... x

Figure 4.25: Epoxy Distribution in Holes x
Figure 4.26: Stressing Sequence for Vertical Internal Post-Tensioning x
Figure 4.27 Location of Holes in Plan and Profile Views x
Figure 4.28: Location of Diagonal Crack in Pier I-4C x
Figure 4.29: Specimen Tie-Down Systems x
Figure 4.30: Reconfigured Loading Frame x
Figure 4.31: Expected Diagonal Crack and Holes Cored through Shear Friction Steel x
Figure 4.32: Schematic of External Horizontal and Vertical Post-Tensioning x
Figure 4.33 Schematic of Internal Diagonal Post-Tensioning x
Figure 4.34: Layout of Concrete Strut x
Figure 4.35: Layout of Steel Haunch x
Figure 4.36: Schematic of Internal Horizontal and Vertical Post-Tensioning x

Figure 5.1: Pier Reinforcement Strains in the Joint of Specimen POJ-PS-100..... 6
Figure 5.2: Tip Displacement vs. Normalized Load Response for
Specimen POJ-PS-100 6
Figure 5.3: Crack Patterns on Specimen POJ-PS-100 at Dead Load 7
Figure 5.4: Distribution of Dead Load Crack Widths in Each Region of
Specimen POJ-PS-100 x
Figure 5.5: Pier Reinforcement Strains in the Joint of Specimen POJ-PS-100-RP1 x
Figure 5.6: Tip Displacement vs. Normalized Load Response for
Specimen POJ-PS-100-RP1 x
Figure 5.7: Crack Patterns on Specimen POJ-PS-100-RP1 at Factored Load / ϕ x
Figure 5.8: Distribution of Service Load Crack Widths in Each Region of
Specimen POJ-PS-100-RP1 x
Figure 5.9: Vertical Displacement in the Top Beam for Specimen POJ-PS-100-RP1..... x
Figure 5.10: Vertical Slippage of the Side Plates on Specimen POJ-PS-100-RP1 x
Figure 5.11: Movement of the Side Plates Normal to Specimen POJ-PS-100-RP1,
Measured at Each Row of Bolts..... x
Figure 5.12: Pier Reinforcement Strains in the Joint of Specimen POJ-PS-100-RP2 x

Figure 5.13: Tip Displacement vs. Normalized Load Response for Specimen POJ-PS-100-RP2 x
Figure 5.14: Crack Patterns on Specimen POJ-PS-100-RP2 at Ultimate Load x
Figure 5.15: Distribution of Service Load Crack Widths in Each Region of Specimen POJ-PS-100-RP2 x
Figure 5.16: Vertical Displacement in the Top Beam for Specimen POJ-PS-100-RP2 x
Figure 5.17: Vertical Slippage of the Side Plates on Specimen POJ-PS-100-RP2 x
Figure 5.18: Pier Reinforcement Strains in the Joint of Specimen POJ-RC2 x
Figure 5.19: Tip Displacement vs. Normalized Load Response for Specimen POJ-RC2 x
Figure 5.20: Crack Patterns on Specimen POJ-RC2 at its Ultimate Load x
Figure 5.21: Distribution of Service Load Crack Widths in Each Region of Specimen POJ-RC2 x
Figure 5.22: Pier Reinforcement Strains in the Joint of Specimen POJ-RC2-RP1 x
Figure 5.23 Tip Displacement vs. Normalized Load Response for Specimen POJ-RC2-RP1 x
Figure 5.24: Crack Patterns on Specimen POJ-RC2-RP1 at Factored Load / ϕ x
Figure 5.25: Distribution of Service Load Crack Widths in Each Region of Specimen POJ-RC2-RP1 x
Figure 5.26: Horizontal Component of Crack Width for Growth of Main Joint Crack on Specimen POJ-RC2-RP1 x
Figure 5.27 Normalized Load vs. Plate Slippage Curves for Specimen POJ-RC2-RP1 x
Figure 5.28: Pier Reinforcement Strains in the Joint of Specimen POJ-RC2-RP2 x
Figure 5.29: Tip Displacement vs. Normalized Load Response for Specimen POJ-RC2-RP2 x
Figure 5.30: Crack Patterns on Specimen POJ-RC2-RP2 at Factored Load / ϕ x
Figure 5.31: Distribution of Service Load Crack Widths in Each Region of Specimen POJ-RC2-RP2 x
Figure 5.32 Displacement on Either Side of Main Joint Crack on

Specimen POJ-RC2-RP2 x
Figure 5.33: Horizontal Component of Crack Width for Growth of Main
Joint Crack on Specimen POJ-RC2-RP2 x
Figure 5.34 Pier Reinforcement Strains in the Joint of Specimen POJ-RC2-RP2a x
Figure 5.35: Tip Displacement vs. Normalized Load Response for
Specimen POJ-RC2-RP2a x
Figure 5.36: Crack Patterns on Specimen POJ-RC2-RP2a at Factored Load / ϕ x
Figure 5.37: Distribution of Service Load Crack Widths in Each Region of
Specimen POJ-RC2-RP2a x
Figure 5.38 Displacement on Either Side of Main Joint Crack on
Specimen POJ-RC2-RP2a x
Figure 5.39 Horizontal Component of Crack Width for Growth of Main
Joint Crack on Specimen POJ-RC2-RP2a x
Figure 5.40: Strut-and-Tie Model of Specimen POJ-RC2-RP2s x
Figure 5.41: Tip Displacement vs. Normalized Load Response for
Specimen POJ-RC2-RP2s x
Figure 5.42: Crack Patterns on Specimen POJ-RC2-RP2 at Ultimate Load x
Figure 5.43: Growth of Main Shear Crack on Specimen POJ-RC2-RP2s
During Loading x

Figure 7.1: Load vs. Increase in Tip Displacement Curves up to Maximum
Tested Load 6
Figure 7.2: Comparison of Service Level Tip Deflection Response for
Specimens with Post-Tensioned Overhangs 6
Figure 7.3: Comparison of Service Level Tip Deflection Response for
Reinforced Concrete Specimens 7
Figure 7.4: Comparison of Service Level Tip Deflection Response for
All Repaired Specimens x
Figure 7.5: Comparison of Service Level Joint Rotations for All Repaired Specimens .. x
Figure 7.6: Comparison of Increase in Joint Rotations from One-Half Dead

Load to Service Load for All Repaired Specimens..... x
Figure 7.7: Average Number of Cracks in Each Region of the Repaired Specimens at Service Load x
Figure 7.8: Average Number of Cracks Emanating from the Back Face of Each Repaired Specimen at Service Load x
Figure 7.9: Comparison of Maximum Crack Widths at Service Load..... x
Figure 7.10: Comparison of Crack Width Distribution at Service Load..... x
Figure 7.11: Comparison of Adjusted Crack Width Distribution at Service Load x
Figure 7.12: Comparison of Tip Deflection Response at Factored Load / ϕ for Specimens with Post-Tensioned Overhangs x
Figure 7.13: Comparison of Tip Deflections at Factored Load / ϕ for Reinforced Concrete Specimens x
Figure 7.14: Comparison of Tip Deflections at Factored Load / ϕ for All Repaired Specimens..... x
Figure 7.15: Comparison of Increase in Joint Rotations from One-Half Dead Load to Factored Load / ϕ for All Repaired Specimens x
Figure 7.16: Comparison of Joint Rotations for Specimens with Internal Post-Tensioning x
Figure 7.17: Comparison of Load-Deflection Curves for Specimens with Internal Post-Tensioning..... x
Figure 7.18: Average Number of Cracks in Each Region of the Repaired Specimens at Factored Load / ϕ x
Figure 7.19: Average Number of Cracks Emanating from the Back Face of Each Repaired Specimen at Factored Load / ϕ x
Figure 7.20: Costs of Selected Repair Options x

REFERENCES

1. Armstrong, Scott D., “Design and Behavior of Large Concrete Cantilever Overhangs with Combinations of Prestresses and Non-Prestressed Reinforcement,” Master’s Thesis, The University of Texas at Austin, August 1994.

2. Salas-Pereira, Ruben M., “Behavior of Structural Concrete Cantilever Piers Using T-Headed Reinforcing Bars and Varied Prestressing Design Criteria,” Master’s Thesis, The University of Texas at Austin, August 1994.

3. Wood, Bradley D., “Title,” PhD Dissertation, The University of Texas at Austin, May 1997.

4. American Concrete Institute, Building Code Requirements for Reinforced Concrete (ACI 318-89), American Concrete Institute, Detroit, 1989.

5. American Association of State Highway and Transportation Officials (AASHTO), Standard Specifications for Highway Bridges, Fifteenth Edition, 1992.

6. American Concrete Institute, Building Code Requirements for Reinforced Concrete (ACI 318-65), American Concrete Institute, Detroit, 1965.

7. Klingner, Richard A., Personal communication, April, 1995.

VITA

Susan Eileen Scott was born in Dayton, Ohio on April 22, 1967 to John Wilmer and Barbara Martin Scott. After graduating from Sandia High School in Albuquerque, New Mexico, she attended the University of Texas at Austin for two years, majoring in chemical engineering and mathematics. She then worked for several years, receiving exposure to civil engineering through the Texas Department of Transportation (TxDOT). In 1991, she returned to the University of Texas at Austin, majoring in civil engineering. In the summer of 1993, she gained field experience as a construction inspector for TxDOT. She received a Bachelor's Degree in Civil Engineering in 1994 and was accepted into the University's graduate program, receiving a graduate fellowship. After completeing her coursework in May of 1996, she accepted a position with Datum Engineering, Inc., a structural engineering firm in Dallas, Texas.

Permanent Address:

This thesis was typed by the author.

CHAPTER 1

INTRODUCTION

1.1 General Problem Statement

The highway interchange between I-10 and I-35 in San Antonio, commonly known as the San Antonio 'Y', involves sections of elevated highway above the existing highway. Due to roadway geometry and limited right-of-way, many sections of the superstructure for the elevated highway could not be supported on hammerhead bents. Instead, the column (pier) of each bent was placed to one side and the superstructure was supported on a cantilever projecting from the top of the column (Figure 1.1). This configuration resulted in extremely high moments in the joint region, where the cantilever and column are joined. During previous research on the bents [Ref. 1, 2, 3], a design flaw was discovered in the detailing of the joint. Due to inadequate development length in the column and overhang reinforcement, tensile forces were unable to flow through the joint from the superstructure support points to the foundation. New calculations performed on the joint indicated a significant deficiency in moment capacity. Field investigations also revealed significant cracking in the joint region of several bents.

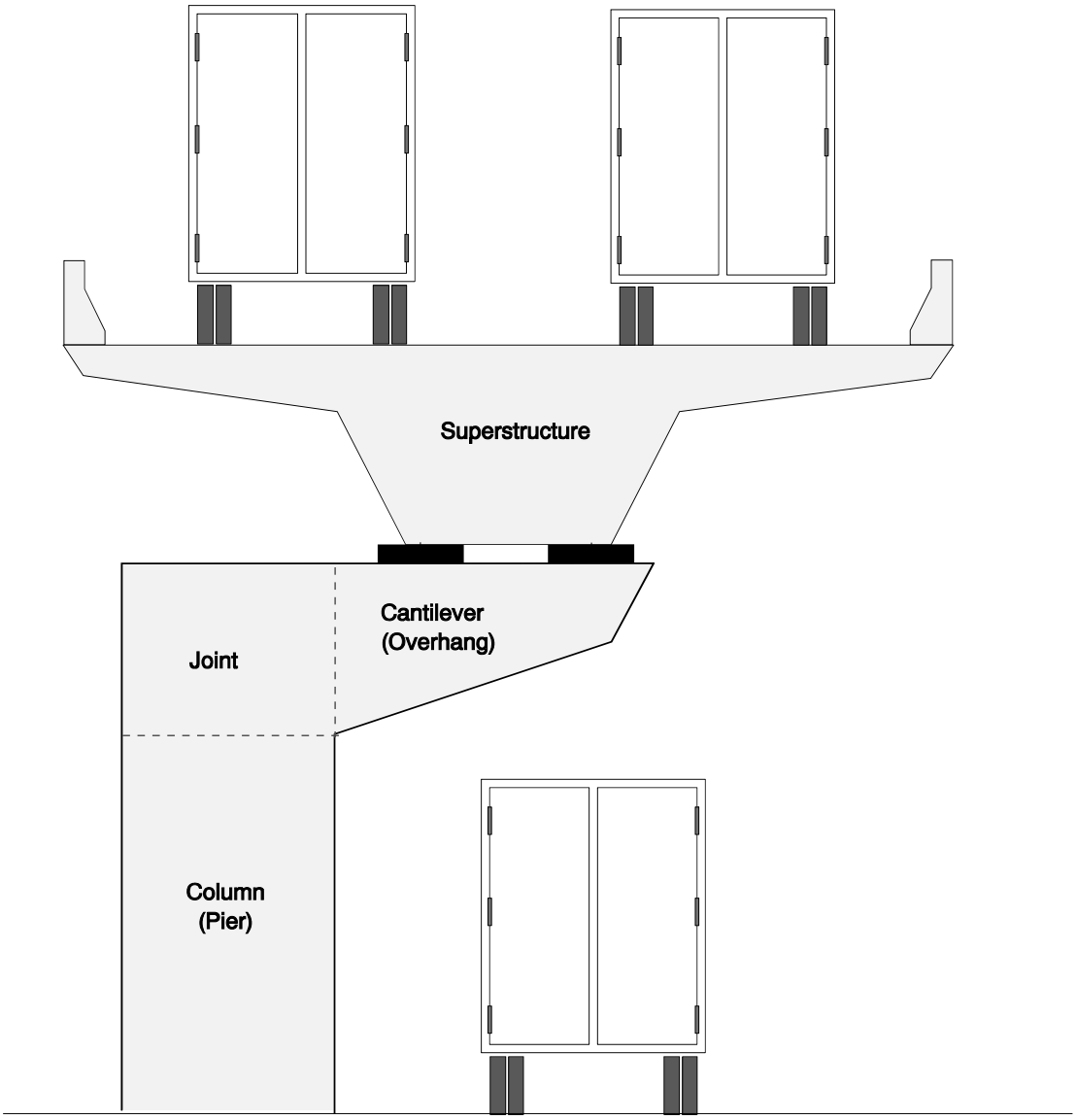

Figure 1.1 Configuration of Cantilever Bridge Pier, Showing Each Region of the Bent

1.2 Scope of Research

1.2.1 Earlier Phases

During previous research involving the bents, the deficiency in the joint region was discovered. A new facet of the overall research study was then initiated to test scale models of typical bents. When the scale models proved to have insufficient moment capacity, the joint region was redesigned to provide a path through which tensile forces could flow. The new designs included the use of T-headed bars and partial prestressing. A complete description of this phase and an evaluation of various joint designs are presented in a dissertation by Wood [Ref. 3]. While the redesigned joints provided adequate moment capacity, this did not solve the problem posed by the existing bents. Therefore, the current phase of the research study was undertaken.

1.2.2 Current Phase

The basis of the current phase of the study was to develop retrofit designs which could be applied to existing bents without excessive disruption of traffic. After various repair schemes were devised, several were selected for fabrication and testing on the scale models of the cantilever bents. Repair methods which successfully resisted factored loads were evaluated based on serviceability, cost, constructilbility, service life, and aesthetics. Based on this evaluation, recommendations are made to the Texas Department of Transportation (TxDOT) as to the most appropriate method for retrofitting deficient bents.

1.3 Objectives

The first objective of this phase of the study was to design several methods for retrofitting the cantilever bents so that they would carry full factored loads. The second objective was to fabricate reduced-scale versions of the most promising repair schemes and test them on scale models of typical bents. The third objective was to compare the different repair methods and develop recommendations based upon effectiveness, cost, constructibility, service life, and aesthetics.

1.4 Organization

This report is organized into eight chapters, as follows:

Chapter 2 explains the background of the research project, including a description of the design flaw and the results of field inspections of existing bents.

Chapter 3 describes the design, construction, and testing procedure for scale models of typical bents, including descriptions of the materials used, the test set-up, and the data acquisition system.

Chapter 4 describes the design, fabrication, and installation of the repair methods, followed by the testing procedures for repaired specimens.

Chapter 5 presents the results of the testing program, both repaired and unrepaired, including deflection, strain, and crack width data.

Chapter 6 discusses the significance of the results presented in Chapter 5.

Chapter 7 evaluates the relative performance, cost, constructibility, service life, and aesthetics of the various repair options.

Chapter 8 summarizes the evaluations of the repair options and makes recommendations based upon those findings.

CHAPTER 2

BACKGROUND

2.1 Introduction

Bridge piers designed to support elevated sections of the I-10/I-35 interchange in San Antonio are of two basic types. One is a hammerhead with loads from the superstructure centered over the pier, resulting in no significant moment in the pier; the other is a cantilever type with the superstructure supported by a cantilever projecting from the top of the pier. Right-of-way restrictions and existing roadway geometry did not permit many of the piers to be placed directly under the superstructure. Superstructure loads on the cantilever bents resulted in high moments in some of the piers.

Because geometry of the superstructure relative to the existing roadway varied considerably, there was not a typical design. However, the cantilever bents consisted of three general types. Those with the longest cantilevers and largest moments were fully prestressed with continuous tendons (Figure 2.1). The others were designed with a reinforced concrete cantilever and pier, or a reinforced concrete pier and a post-tensioned cantilever with post-tensioning provided by straight bars located in the top of the cantilever (Figs. 2.2 and 2.3).

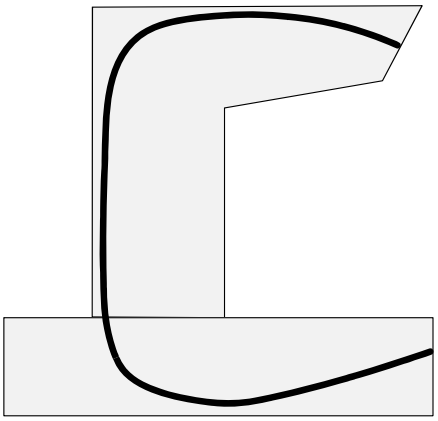

Figure 2.1 Example of Fully Prestressed Cantilever Bent

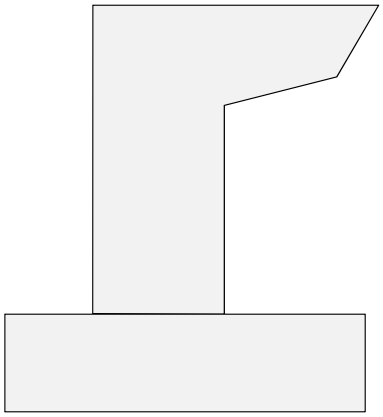

Figure 2.2 Example of Reinforced Concrete Cantilever Bent

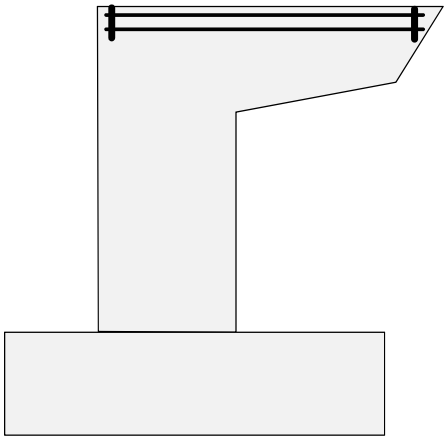

Figure 2.3 Example of Reinforced Concrete Bent with Fully Post-Tensioned Overhang

When reinforcement for the bents was designed, critical sections for moment were assumed to be the interface between the overhang and the joint (the region common to the overhang and pier) and the interface between the column and joint (Figure 2.4). Reinforcement in the overhang and pier was designed to resist moments at the interfaces

between the overhang and joint and between the column and joint, respectively. Design of the joint region did not consider the possibility of diagonal cracks forming in the joint, so the entire joint was assumed to be available for development of longitudinal reinforcement in both the overhang and the pier.

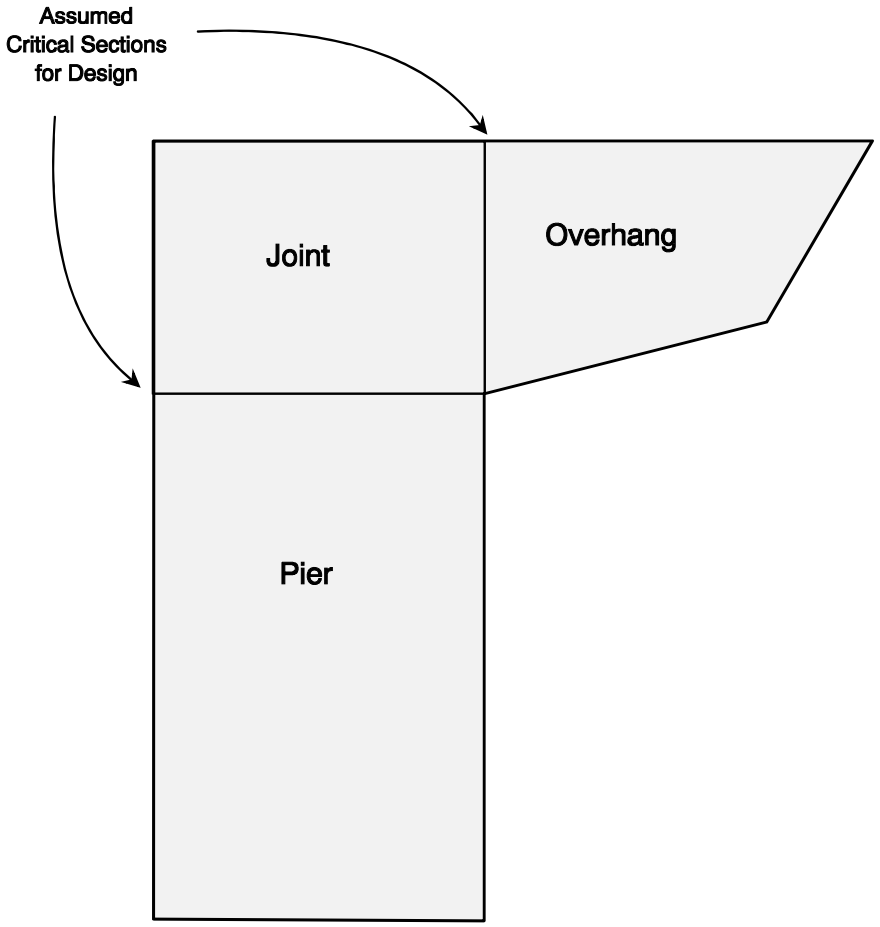

Figure 2.4 Schematic of Pier, Overhang, and Joint Regions in Cantilever Bent, Showing Assumed Critical Sections for Original Design

2.2 Reinforcement Layout

2.2.1 Reinforced Concrete Piers with Post-Tensioned Concrete Overhangs

Many of the cantilever bents in the interchange were designed using reinforced concrete piers and fully post-tensioned overhangs (Figure 2.5). Because the post-tensioning steel is fully effective from one anchorage to the other, any cross-section in the overhang is capable of resisting the design moments. The pier, however, is different. Longitudinal reinforcement in the pier was designed to resist the moment at the interface between the joint and pier. At that cross section, the reinforcement has sufficient anchorage length to develop the necessary stresses. However, if a diagonal section through the joint is examined, high moments must still be resisted, but the available development length for much of the pier longitudinal reinforcement is substantially reduced. This reduction in available anchorage may result in insufficient steel stresses to resist the applied moment. Figure 2.6 compares available development lengths with required development lengths for pier longitudinal reinforcement when a diagonal crack forms from the base of the post-tensioning anchorage in the joint, as shown in Figure 2.7. Such a crack was observed in the field as well as in a related laboratory investigation [Ref. 3].

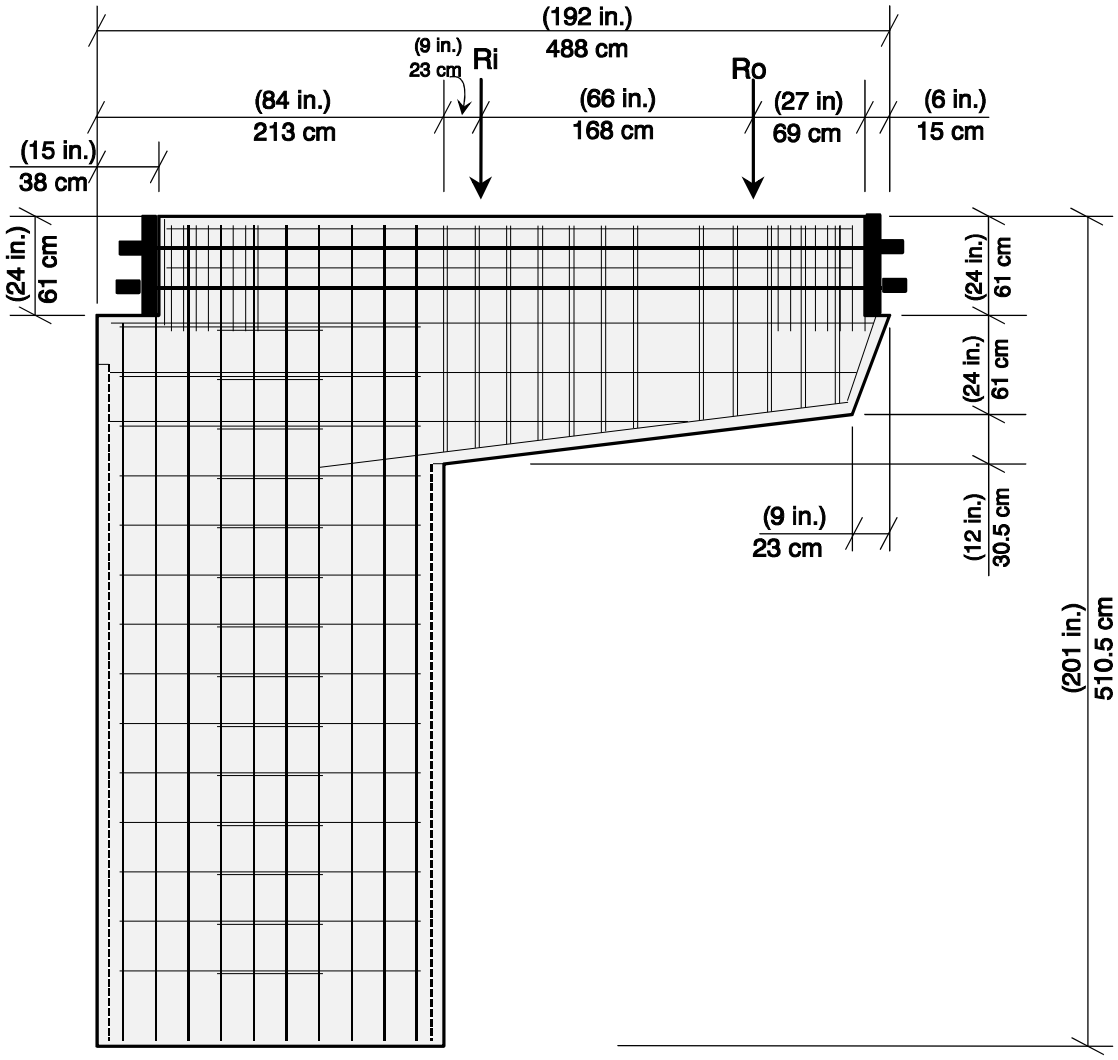

Figure 2.5 Layout of Reinforcement in Bent with Post-Tensioned Overhang [From Ref. 3]

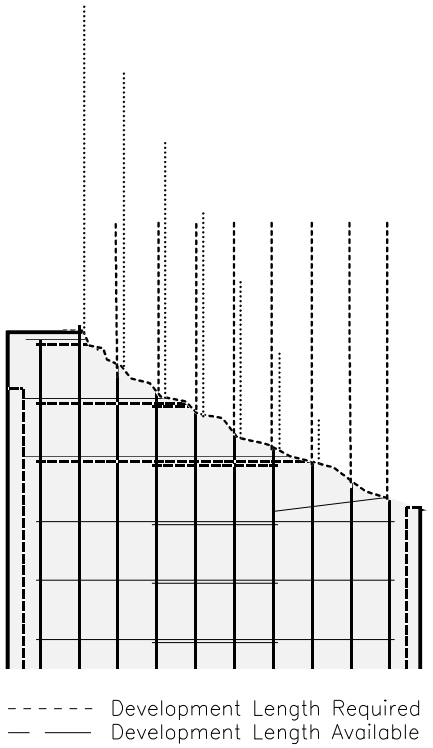

Figure 2.6 Available and Required Development Length for Pier Reinforcement in Bent with Post-Tensioned Overhang

In addition to reducing the anchorage of some of the longitudinal reinforcement, the diagonal crack shown in Figure 2.7 occurs above the end of the outermost layer of longitudinal reinforcement, rendering the primary flexural reinforcement in the pier completely ineffective. The outer layer of longitudinal reinforcement was cut shorter than the other longitudinal bars to accommodate the block-out for the post-tensioning anchorages. Note in Figure 2.7 that the diagonal crack is not intersected by either the primary longitudinal reinforcement in the pier or the post-tensioning steel in the overhang, but only by secondary longitudinal bars in the pier and by side-face reinforcement and shear-friction reinforcement

in the overhang. Not only is the primary steel area greatly diminished, but the moment arm is significantly shorter than intended (Figure 2.8).

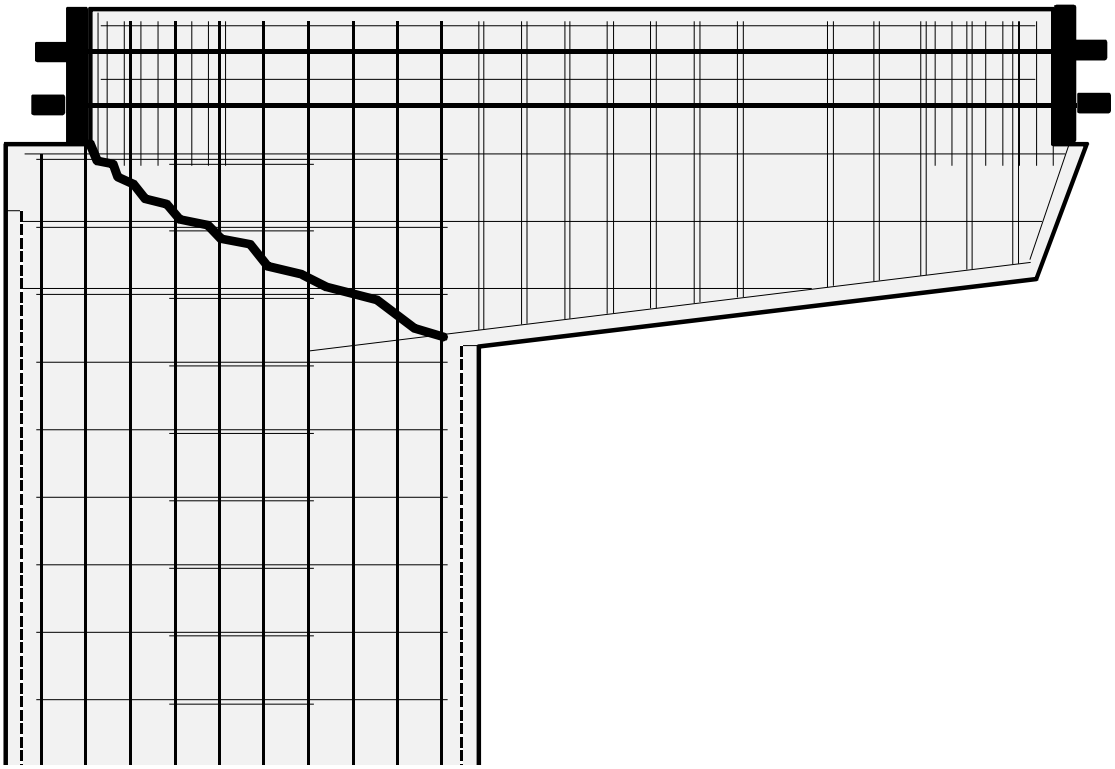

Figure 2.7 Crack at Critical Section in Bent with Post-Tensioned Overhang [Modified from Ref. 3]

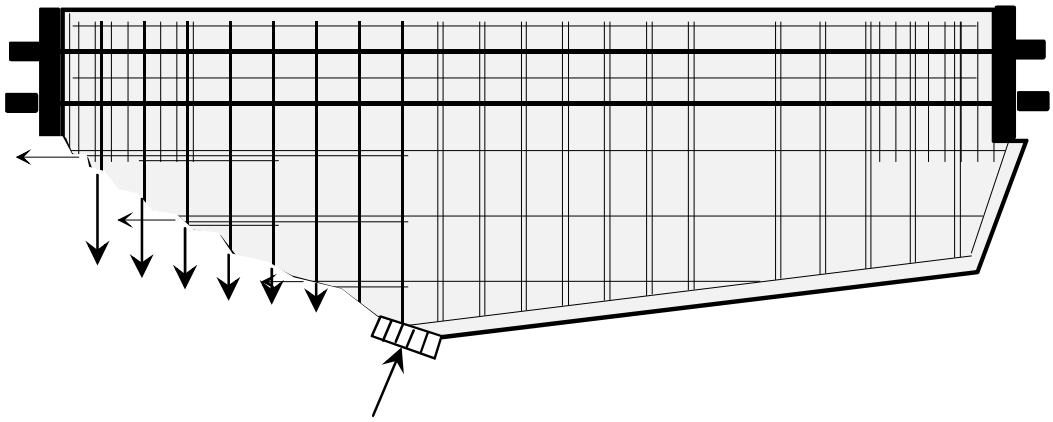

Figure 2.8 Free-Body Diagram of Bent Cut through Critical Section [Modified from Ref. 3]

2.2.2 Reinforced Concrete Bents

For bents built entirely of reinforced concrete (Figure 2.9), there is a deficiency in the development of both the column and overhang reinforcement. Even though the primary reinforcement in reinforced concrete piers continues to the top of the joint, a diagonal section taken through the outer joint corner demonstrates that there is practically no development length for the main pier steel at that location, compared to the 1.35 m (53 in.) required for #11 bars or the 4.12 m (162 in.) required for #14 bars [Ref. 4]. The #11 bars comprising the main overhang steel also require 1.35 m (53 in.) of development length, but again, practically none is provided (Figure 2.10).

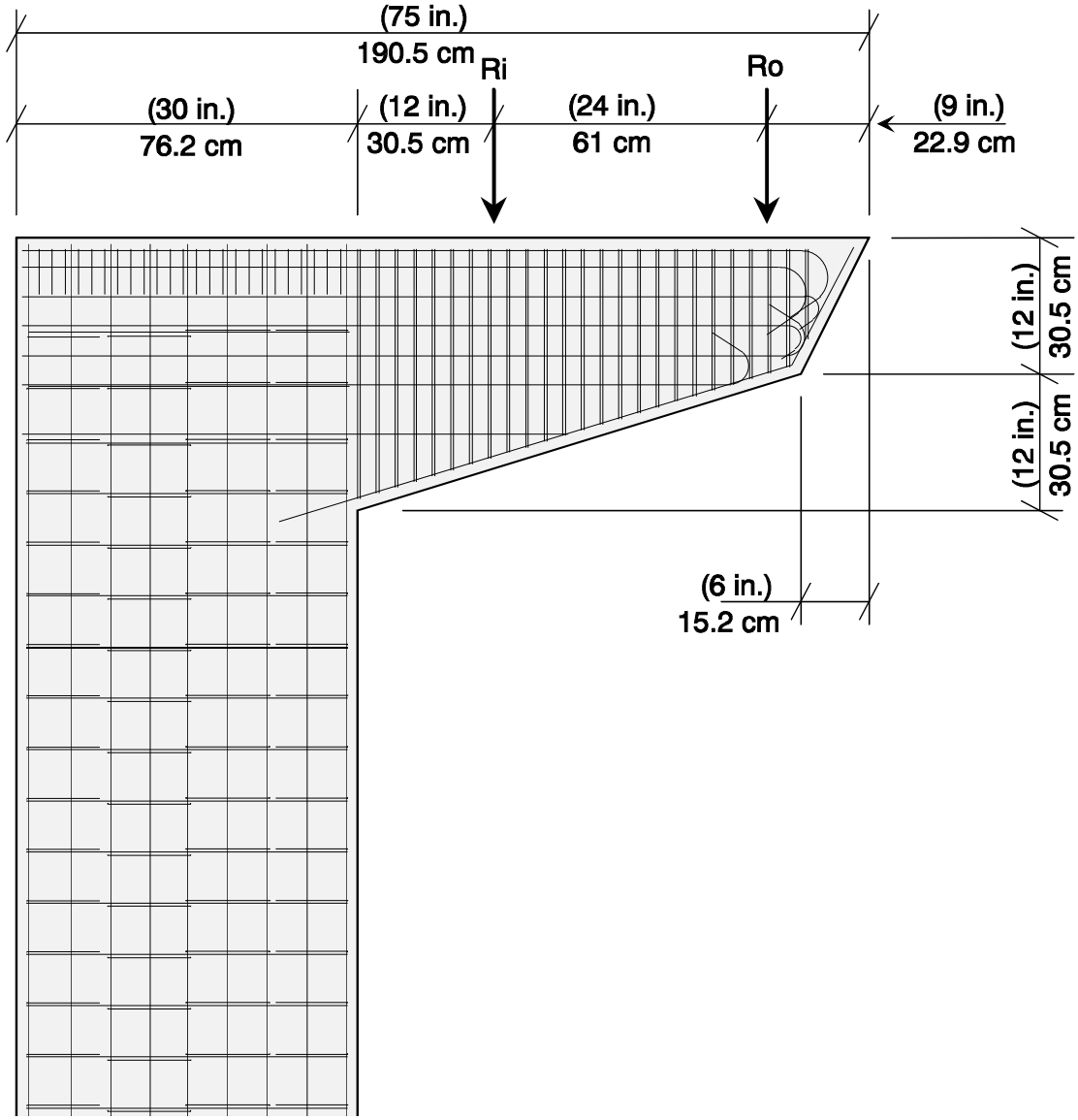

Figure 2.9 Layout of Reinforcement in Reinforced Concrete Bent [From Ref. 3]

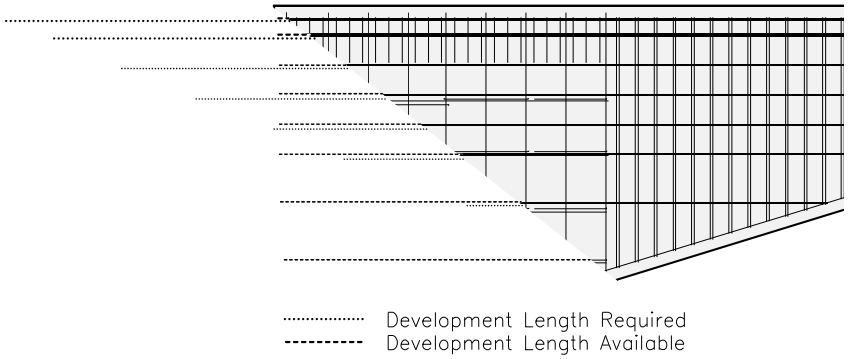

Figure 2.10 Available and Required Development Length of Overhang Reinforcement in Reinforced Concrete Bent

The moment capacity of this bent was calculated for a crack that formed from the exterior corner of the joint toward the interior corner of the bent (Figs. 2.11 and 2.12). As in the case of the cantilever bent with post-tensioned overhang described earlier, this type of cracking has been observed in the field as well as in the laboratory. The moment capacity was substantially less than the intended capacity. Details of this calculation will be provided in a later chapter.

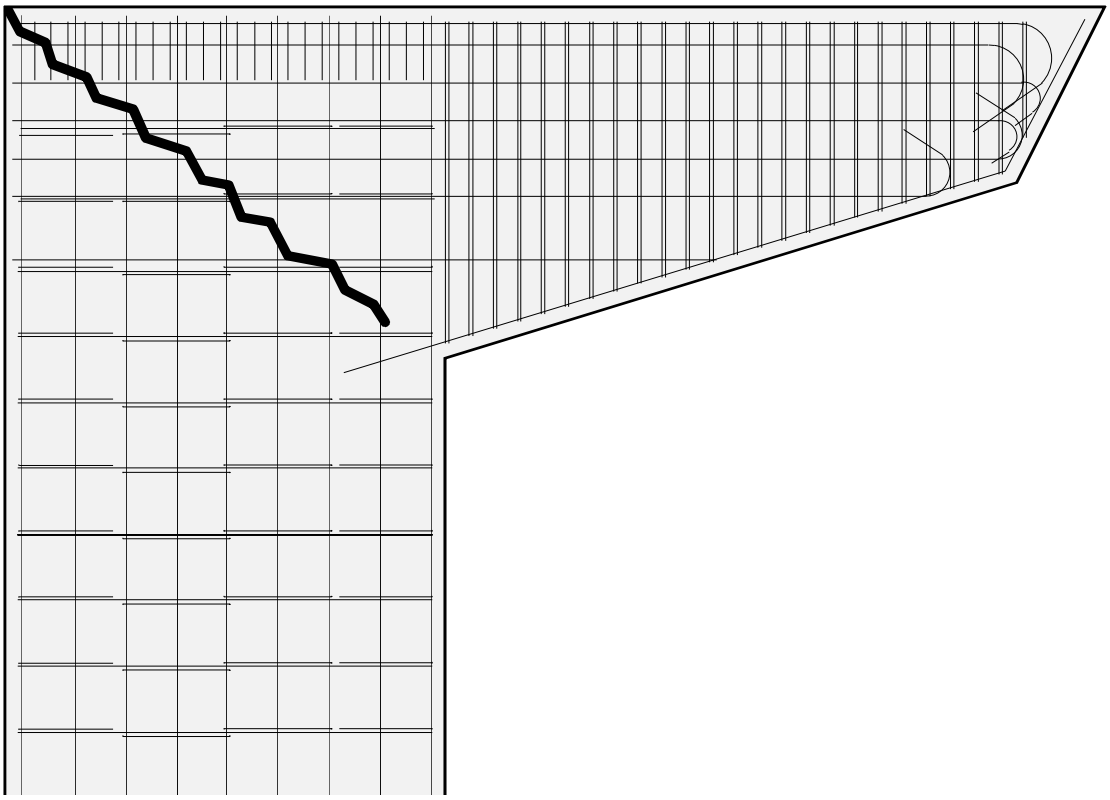

Figure 2.11 Diagonal Crack at Critical Section in Reinforced Concrete Bent [Modified from Ref. 3]

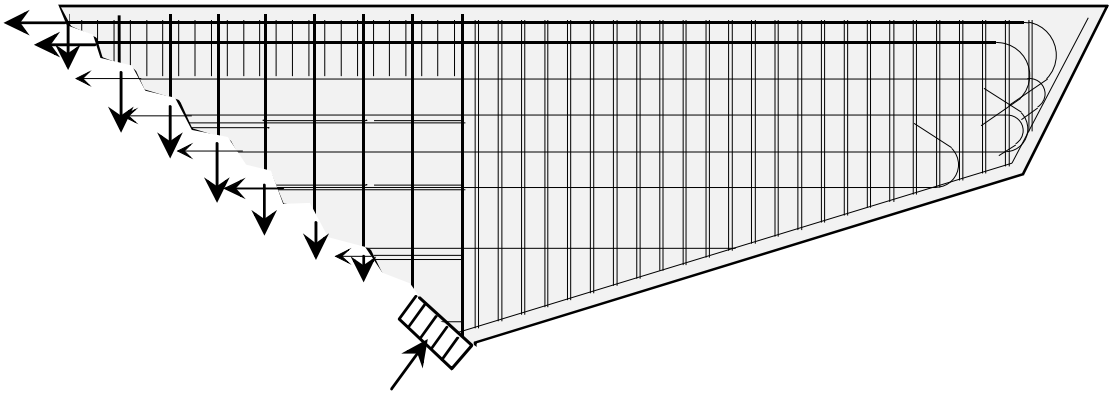

Figure 2.12 Free-Body Diagram of Overhang with Diagonal Crack through the Joint [Modified from Ref. 3]

2.2.3 Fully Prestressed Piers

These bents have continuous post-tensioning tendons that extend from the tip of the overhang, through the joint, down the column, and into the footing (Figure 2.1). The continuity of tension reinforcement avoids the anchorage problems illustrated for the other two types of bents, despite the greater moments resisted by the fully post-tensioned bents. Therefore, fully prestressed bents were not examined in this study.

2.3 Field Performance

2.3.1 Relevance of Field Performance to Laboratory Study

Cracks resembling those described in the previous section for joints of cantilever bents were first observed in a laboratory study conducted by Wood [Ref. 3]. Because the specimens in that study were models of selected bents in San Antonio, and because the specimens failed at loads well below design loads, bents in San Antonio were inspected for damage. The results of the inspection are presented in this section.

2.3.2 Bents with Post-Tensioned Concrete Overhang

Bents with prestressed overhangs, as expected, exhibited no flexural cracks in the overhang or upper joint region. Because of variations in applied moments and in the size and shape of bents, however, some of the bents were more severely stressed than others. The bents which supported superstructure elements positioned closer to the piers showed little or no distress, while those with longer overhangs had a large number of cracks scattered throughout the joint.

2.3.2.1 Pier D-36C

Pier D-36C was the most severely cracked of all the bents, due to its long overhang, extending 4.95 m (16 ft - 3 in.) past the edge of the pier. Both superstructure reactions were located on the overhang. The cracks varied in width up to a maximum size of approximately 2 mm (0.079 in.). As shown in Figure 2.13, the cracks were concentrated in the joint region, with no significant cracking in the pier or overhang. Joint cracks were distributed over most

of the joint, angling slightly downwards. Several cracks initiated at the vertical face of the joint, while others began within the joint. No cracks extended to the top surface of the joint.

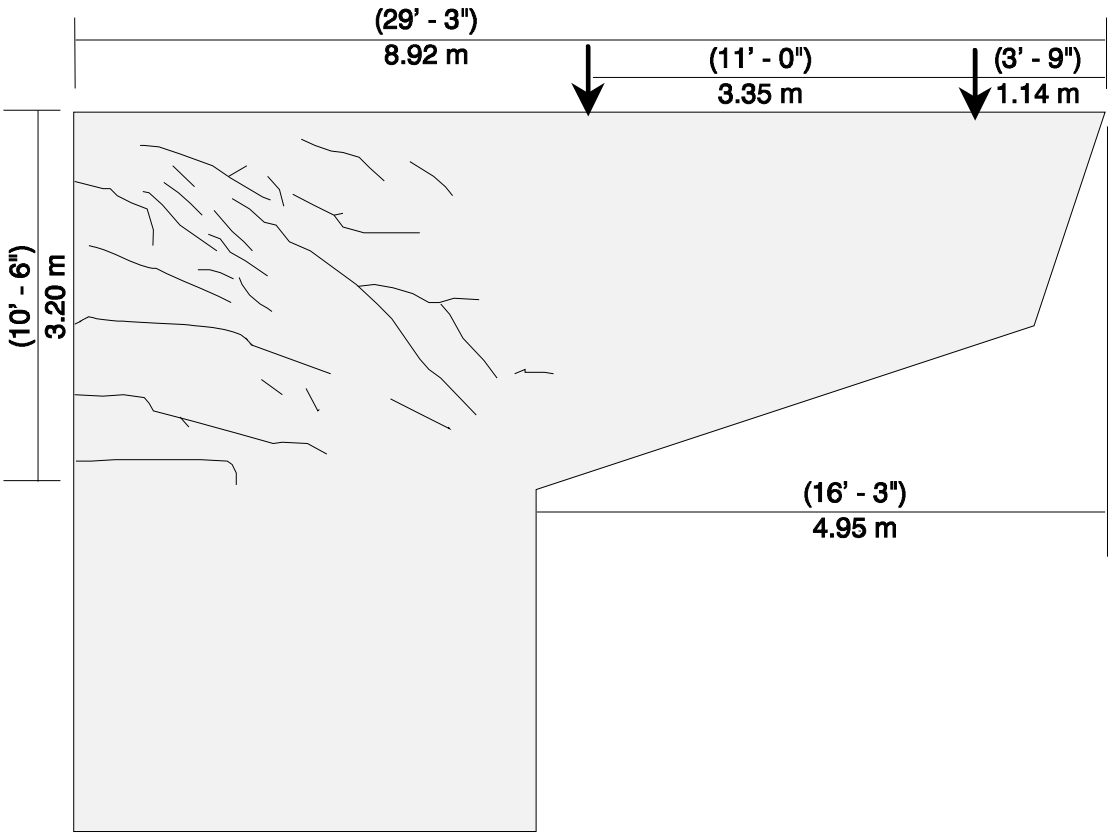

Figure 2.13 Pattern of Cracks in Pier D-36C

2.3.2.2 Pier D-37C

Pier D-37C was slightly less cracked than Pier D-36C, presumably due to the shorter overhang (3.51 m (11 ft, 6 in.)) that resulted in lower moments in the joint. The largest crack width measured was 1.4 mm (0.055 in.). Again, no significant cracks appeared in the pier or overhang. In this bent, the cracks were concentrated toward the back half of the joint and

were more inclined than for Pier D-36C (Figure 2.14). A few cracks began at the vertical face of the joint, but most were completely contained within the joint.

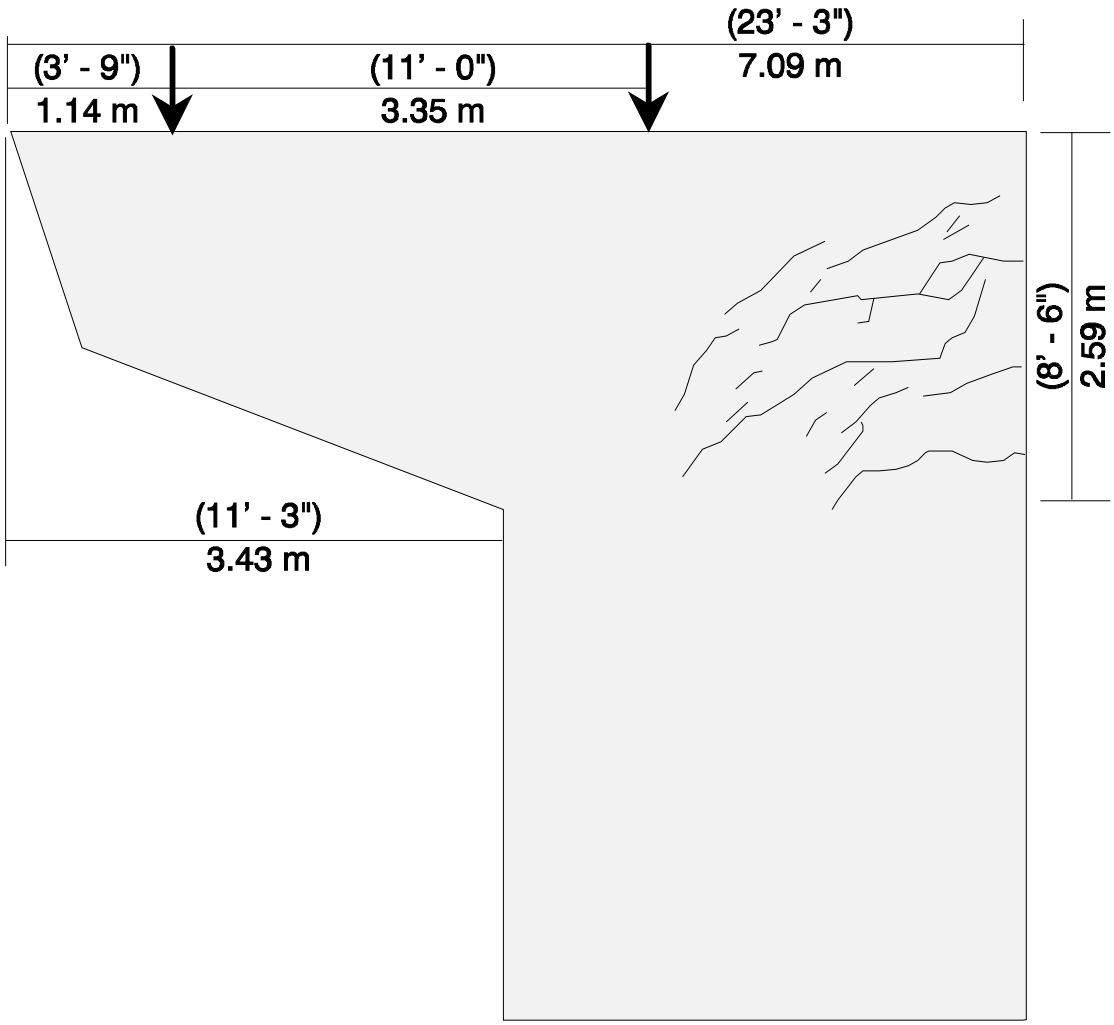

Figure 2.14 Pattern of Cracks in Pier D-37C

2.3.2.3 Pier D-38C

Pier D-38C has a shorter overhang than either D-36C or D-37C, extending 2.97 m (9 ft - 9 in.) beyond the face of the column. The inner bearing pad rests on the joint, rather than on the overhang. As a consequence, only one significant crack was observed, beginning at the vertical face of the column, continuing horizontally for a short distance, then angling downward, as shown in Figure 2.15. This crack was approximately 0.4 mm (0.016 in.) wide.

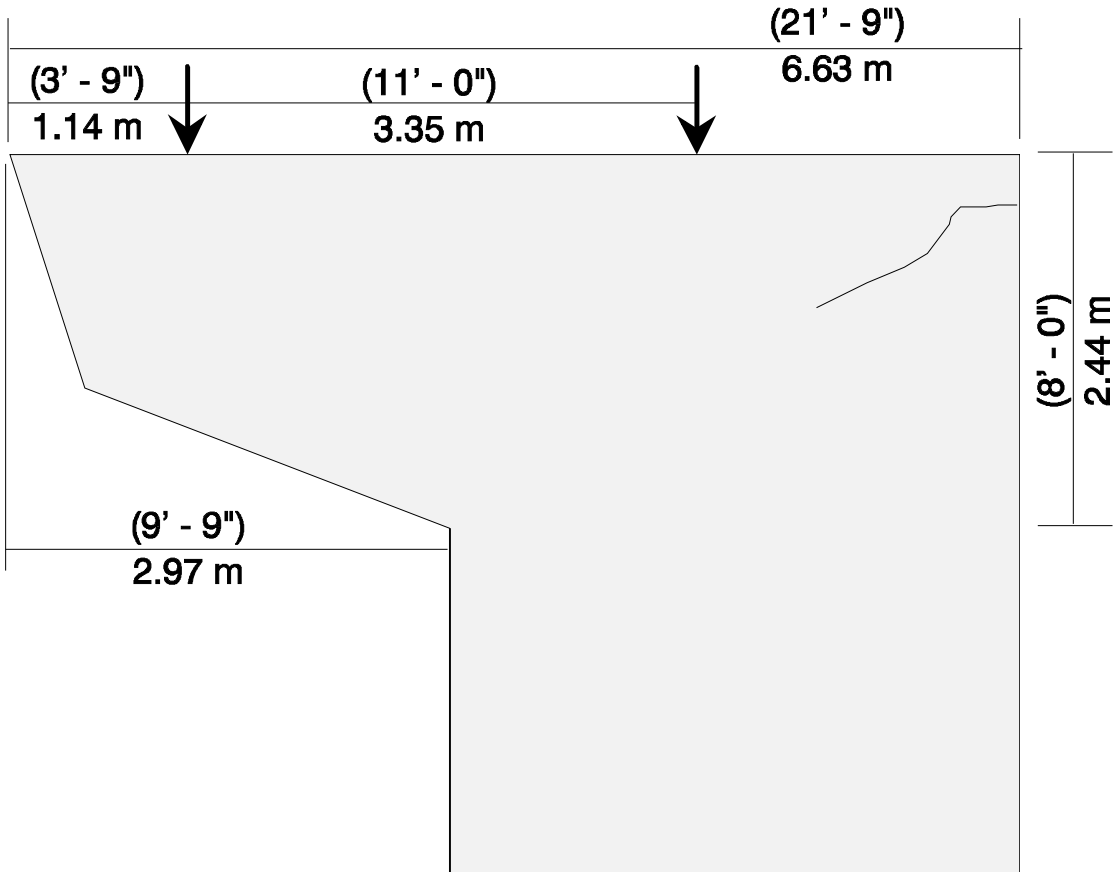

Figure 2.15 Pattern of Cracks in Pier D-38C

2.3.2.4 Pier D-39C

Pier D-39C has the shortest overhang of all of the prestressed piers inspected, at 2.51 m (8 ft - 3 in.), as shown in Figure 2.16. The inner bearing pad rests on the joint and is closer to the outer joint face than to the joint-overhang interface. No significant cracks were observed in this pier.

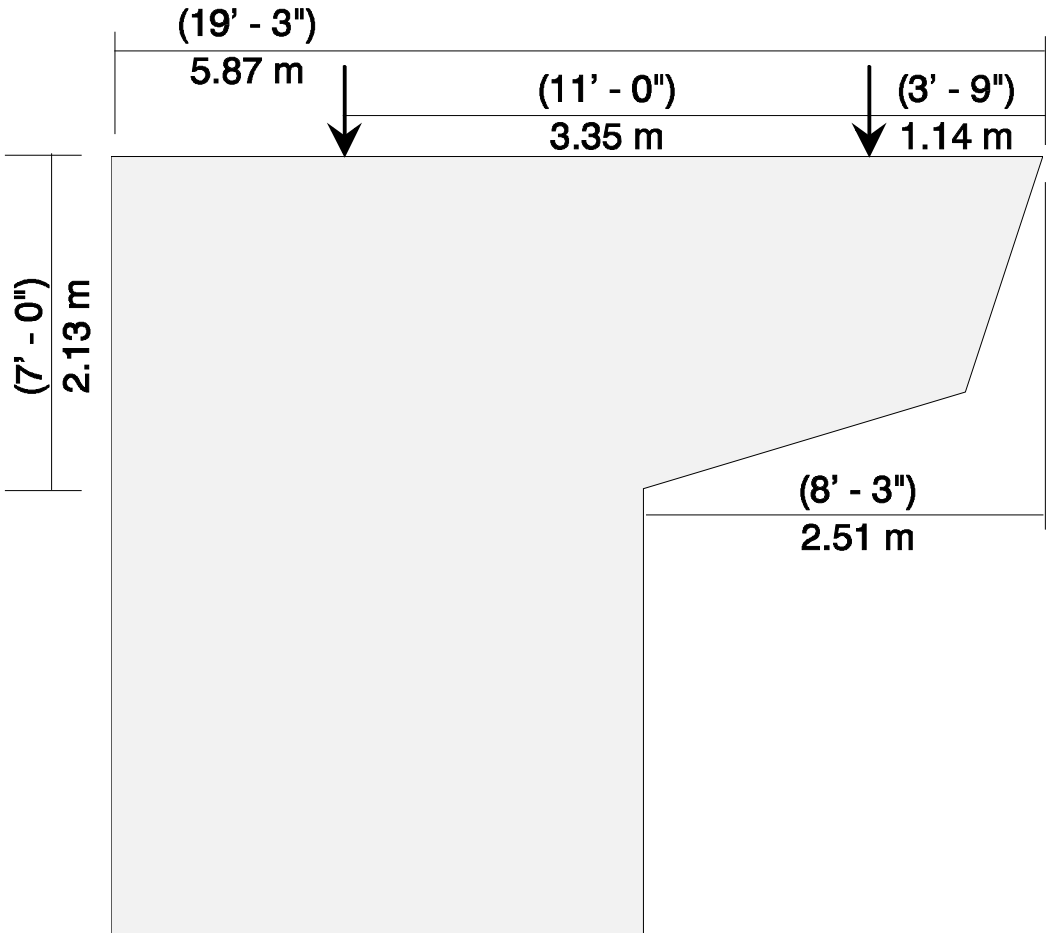

Figure 2.16 Pier D-39C

2.3.2.5 Pier C-11C

Pier C-11C actually cracked under dead load during construction when the superstructure was placed. It was immediately repaired in the field, but no further analysis was performed and no design changes were made in other piers based on the damage sustained by this bent. The repair consisted of internal vertical post-tensioning and epoxy injection of cracks. The overhang was not excessively long, measuring 2.95 m (9 ft - 8 in.), so the severity of the cracking may have been due to the unusually small depth of the pier and overhang, which had been decreased from its original depth due to inadequate clearance. Cracks extended from near the outside corner of the joint to near the inside corner (Figure 2.17). Because the repair was completed before this study was initiated, the crack widths could not be measured before post-tensioning was applied to close them.

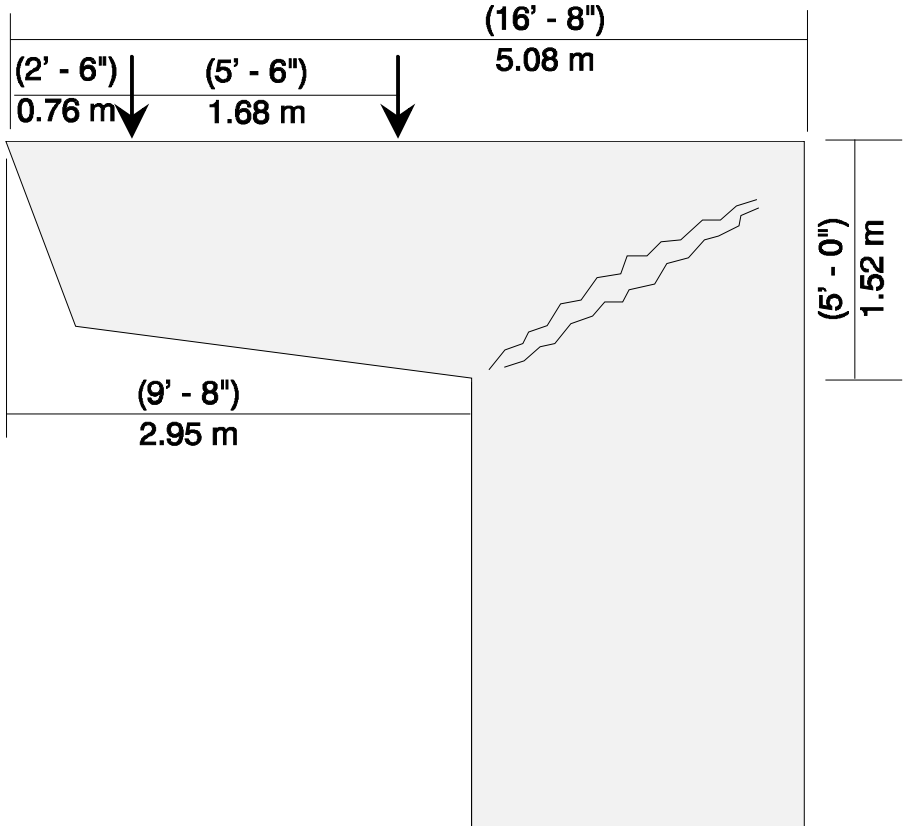

Figure 2.17 Pattern of Cracks in Pier C-11C

2.3.3 Reinforced Concrete Bents

The bents constructed solely of reinforced concrete exhibited cracks in the joint, pier, and overhang regions. Most of the bents of this type were designed with very little eccentricity of the superstructure loads. Often, the inner bearing pad was actually positioned over the joint, rather than on the overhang. In these cases, not only was the applied moment small, but the compression produced by the superstructure load near the joint improved the confinement of the overhang steel and improved its anchorage. No significant cracks were observed in bents with this load configuration.

In bents with both superstructure loads positioned on the overhang, cracks were found. The major cracks tended to occur at the vertical face of the joint, extending diagonally down toward the column, and beneath the inner bearing pad, extending diagonally back toward the joint. The joint region exhibited fewer cracks than the larger piers with post-tensioned overhangs.

2.3.3.1 Pier I-3C

Pier I-3C was the least severely cracked of the reinforced concrete piers inspected. Its overhang extends only 2.51 m (8 ft - 3 in.) beyond the face of the column. The largest crack began at the top of the overhang, almost at the joint/overhang interface, and extended downward and slightly toward the joint. Its maximum width was 0.3 mm (0.012 in.). Two smaller cracks crossed the interface beneath the larger crack. One crack extended from the exterior vertical face of the joint and angled slightly downward. This crack was believed to exist only on the surface of the pier and is therefore of little structural significance. The cracks in Pier I-3C are shown in Figure 2.18.

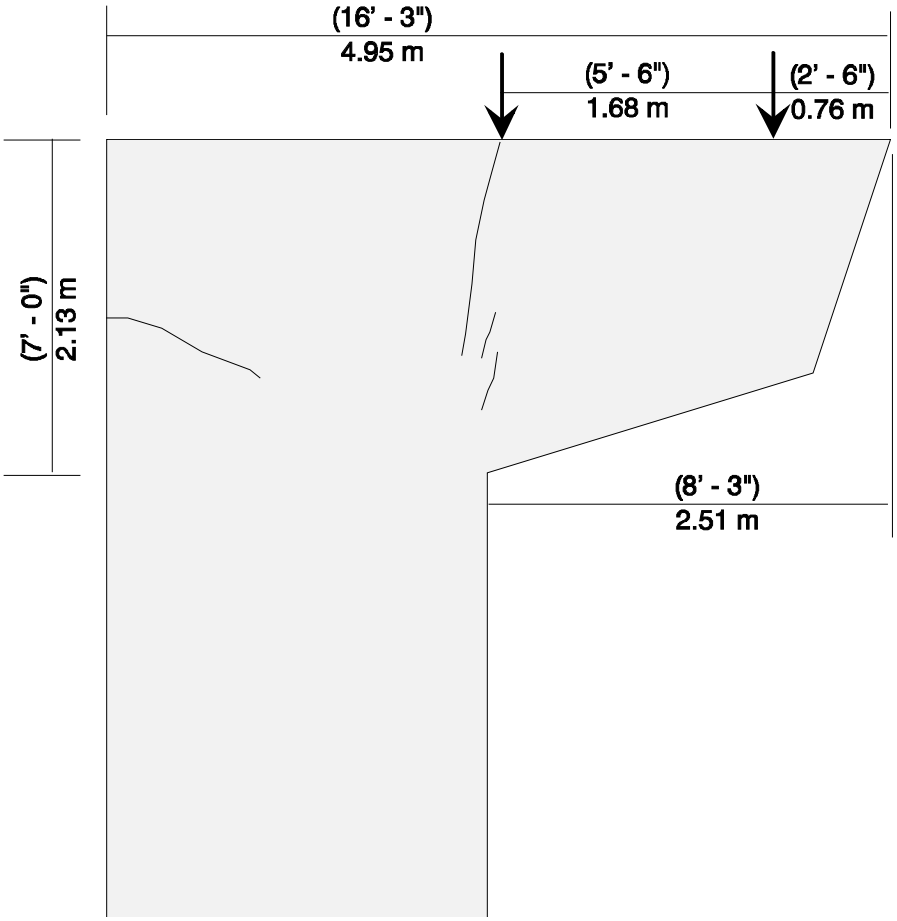

Figure 2.18 Pattern of Cracks in Pier I-3C

2.3.3.2 Pier I-4C

Pier I-4C was designed to resist higher moments than Pier I-3C (having an overhang length of 3.73 m (12 ft - 3 in.)) and consequently showed more cracking. Cracks appeared in the overhang, extending from the inner bearing pad towards the inside corner of the joint. Other cracks began at the vertical and horizontal faces of the joint and also angled toward the inside corner of the joint, as shown in Figure 2.19. The cracks varied in width up to approximately 0.5 mm (0.020 in.).

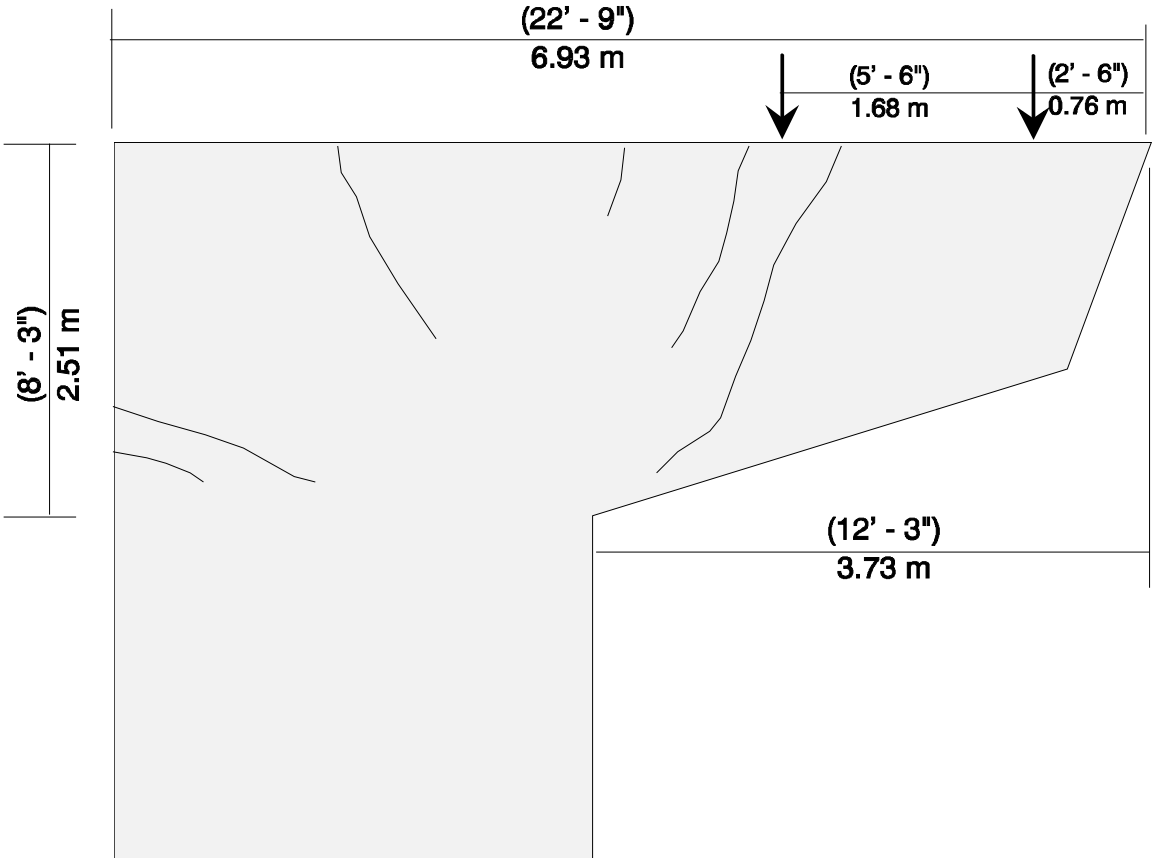

Figure 2.19 Pattern of Cracks in Pier I-4C

2.3.3.3 Pier I-5C

Pier I-5C was designed with the same dimensions and reinforcement as Pier I-4C and displayed very similar crack patterns. The cracks began in the overhang, near the inner bearing pad, and on both faces of the joint, extending toward the inside corner of the joint. The maximum crack width measured was 0.5 mm (0.020 in.). The crack pattern is shown in Figure 2.20.

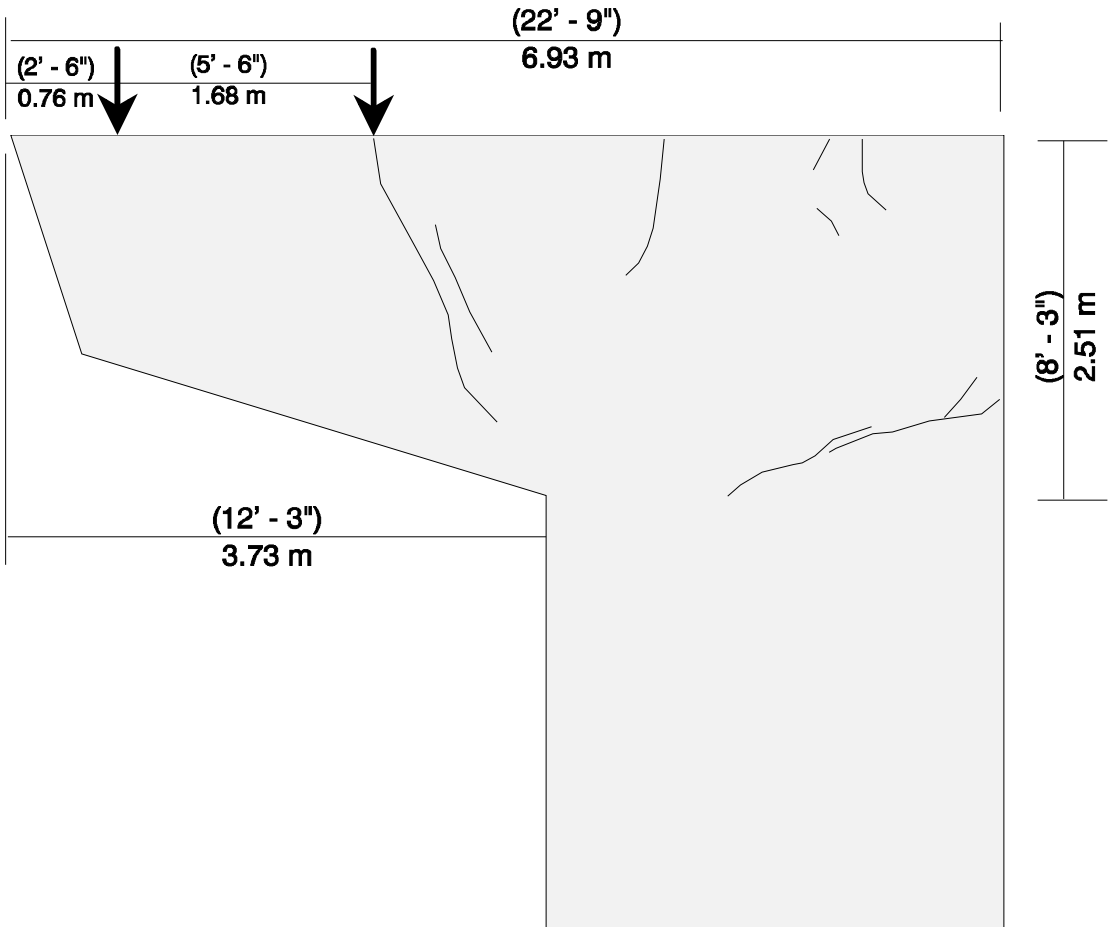

Figure 2.20 Pattern of Cracks in Pier I-5C

2.3.3.4 Pier I-2C

Because of clearance requirements, Pier I-2C was unusual; the superstructure was cast integrally with the pier rather than resting on bearing pads above the bent (Figure 2.21). Although there is post-tensioning in the pier, it is confined to the superstructure region, so the pier is included among the reinforced concrete piers. Pier I-2C exhibited the largest joint crack width of all the bents examined. The crack initiated approximately 25 cm (10 in.)

below the top of the bent and extended horizontally with an increasing downward slope. At the column face, this crack was too large to measure accurately with the scale available, but appeared to be approximately 0.5 cm (0.2 in.). It rapidly narrowed to 3.5 mm (0.138 in.) within approximately 25 cm (10 in.). Other cracks were observed throughout the joint area, as shown in Figure 2.22. Because this pier was unique, it was not examined specifically in the study.

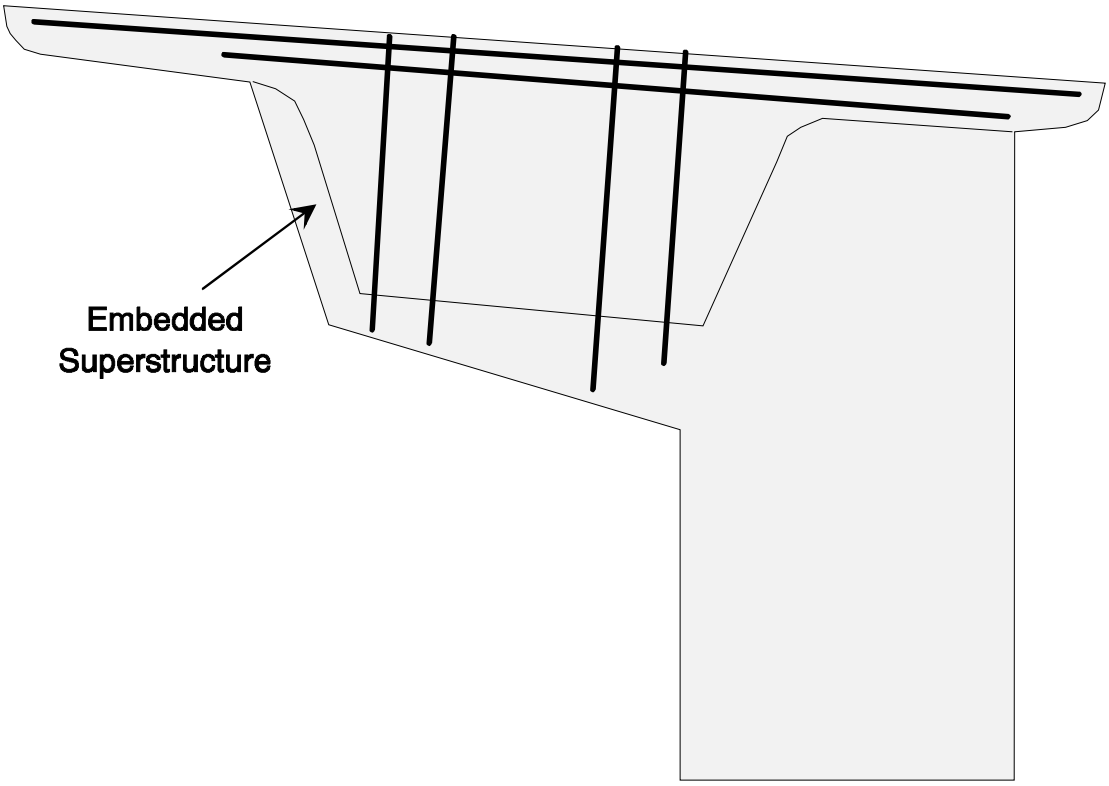

Figure 2.21 Elevation of Pier I-2C

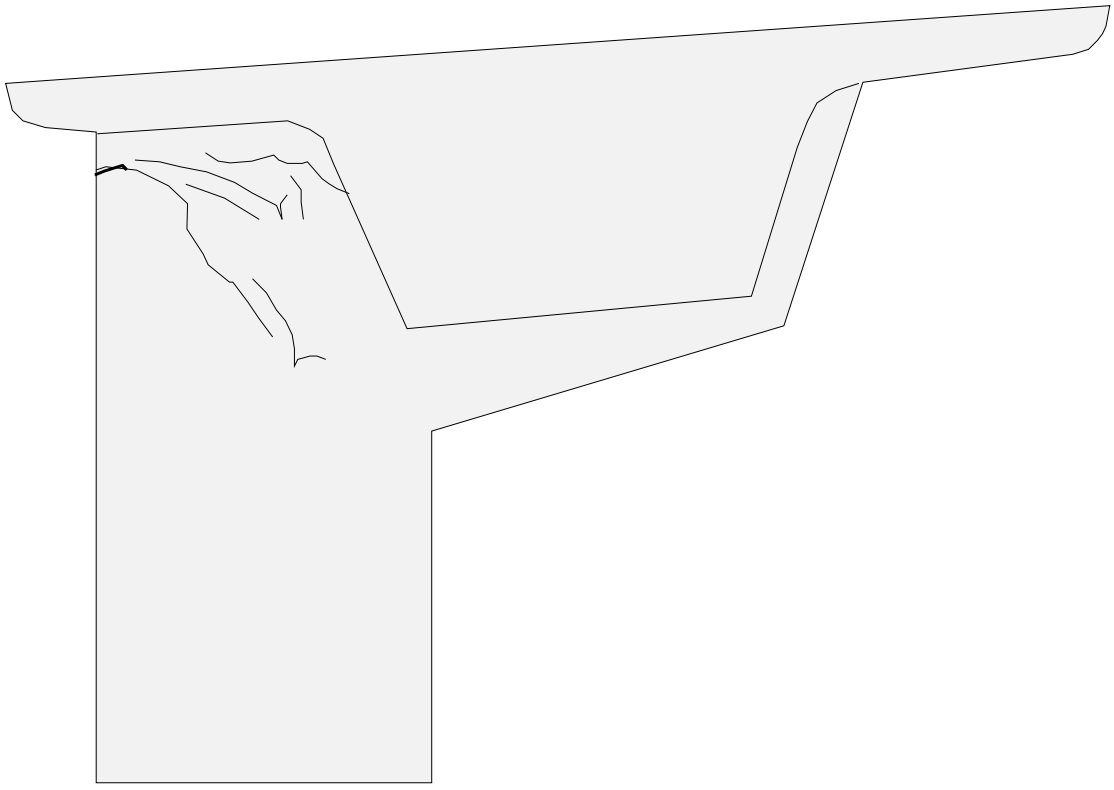

Figure 2.22 Pattern of Cracks in Pier I-2C

CHAPTER 3

DESIGN, CONSTRUCTION, AND TESTING OF UNREPAIRED CANTILEVER BENT MODELS

3.1 Introduction

This chapter explains the process involved in designing representative scale models of typical cantilever bridge bents. It describes the procedures and equipment used for the construction and testing of two basic model specimens, reinforced concrete and post-tensioned, before any repairs were made to either.

3.2 Design

3.2.1 Selection of Representative Bent

The wide variety of sizes and shapes of actual bents precluded the possibility of testing all possible configurations, so a representative sample of a reinforced concrete bent was chosen. The chosen bent was designed similar to Pier I-4C, but with #11 bars for primary longitudinal reinforcement in the overhang and #14 bars for longitudinal reinforcement in the column. The dimensions of the reinforced concrete specimen were selected based on the representative bent, and the specimen with the post-tensioned overhang was designed using the same dimensions for convenience in construction and analysis.

3.2.2 Scale Factor

Previous tests on overhangs of the cantilever bents were performed on models constructed at a 1:5.5 scale. It was decided that, to better understand the joint behavior, a larger scale should be used. Several scale factors were considered, and it was found that a factor of 2.75 provided the best match between bars used to represent the full-scale bents and those used in the reduced-scale models. Number 11 bars in the overhang of the full-scale reinforced concrete bent scaled approximately to #4 bars, and #14 bars in the column scaled approximately to #5 bars. The full-size bars and their scaled counterparts are shown in Table 3.1. Because of a lack of smaller post-tensioning bar sizes, the post-tensioning bars were scaled from 3.49 cm (1.375 in.) in diameter to 1.59 cm (0.625 in.) in diameter. The dead and live loads were scaled by the square of the 2.75 scale factor.

Table 3.1 Scaling of Reinforcement [Modified from Ref. 3]

Full-Size Bar	Area of Full-Size Bar		Scaled Area		Scaled Bar	Area of Scaled Bar		% Error
# 14	14.5 cm^2	(2.25 in^2)	1.92 cm^2	(0.298 in^2)	# 5	2.00 cm^2	(0.31 in^2)	4.2
# 11	10.1 cm^2	(1.56 in^2)	1.34 cm^2	(0.208 in^2)	# 4	1.30 cm^2	(0.20 in^2)	-3.0
# 8	5.1 cm^2	(0.79 in^2)	0.67 cm^2	(0.104 in^2)	# 3	0.71 cm^2	(0.11 in^2)	6.0
# 6	2.8 cm^2	(0.44 in^2)	0.37 cm^2	(0.057 in^2)	# 2	0.32 cm^2	(0.05 in^2)	-14
# 4	1.3 cm^2	(0.20 in^2)	0.17 cm^2	(0.026 in^2)	7 ga. wire	0.19 cm^2	(0.03 in^2)	11

3.2.3 Selection of Superstructure Type and Loading Points

The actual box girder superstructure (Figure 3.1) varied between two and four lanes in width, with some non-standard sections used where entrance and exit ramps joined the

main lanes. Piers which were considered to be at risk primarily supported a two-lane superstructure. Loads from the two-lane superstructure were scaled down for designing the model. The distance between bearing pads for the two-lane superstructure elements was 1.68 m (5.5 ft), which scaled to 61.0 cm (2.0 ft).

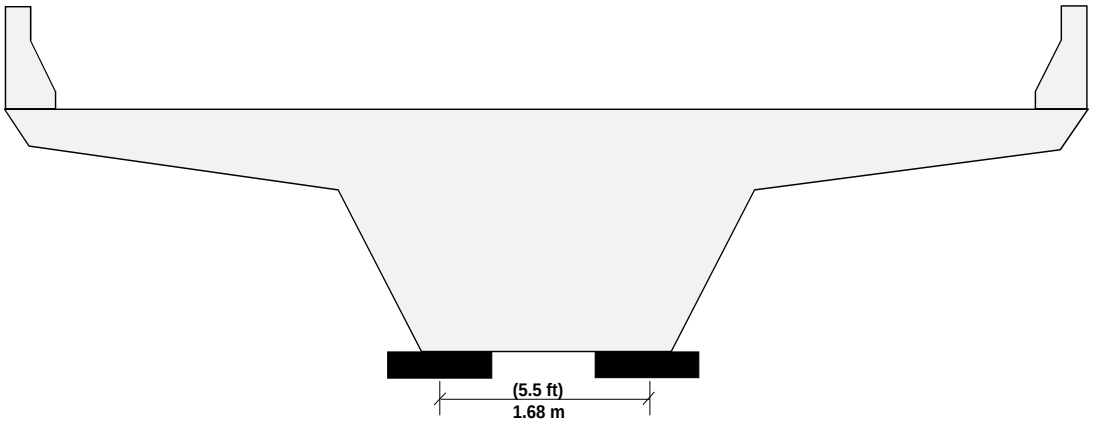

Figure 3.1 Full-Scale, Two-Lane Precast Superstructure Design [From Ref. 3]

Forces due to dead loads were assumed to be divided equally between the two bearing pads. Live loads due to traffic were assumed to be concentrated as far from the column as possible so that moments imposed on the joint would be maximized (Figure 3.2). Forces due to live loads were, therefore, greater on the outer bearing pad than on the inner pad.

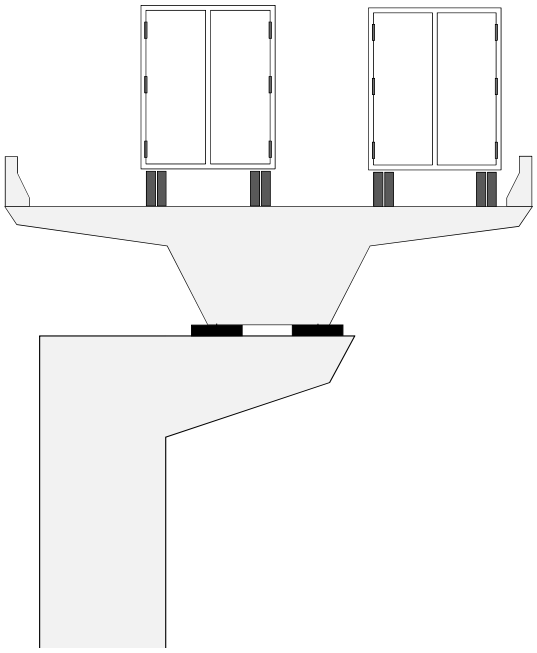

Figure 3.2 Cantilever Bent with Critical Live Load Distribution on Superstructure [From Ref. 3]

The load combination for ultimate load used in design was taken from the AASHTO Standard Specifications for Highway Bridges [Ref. 5] as follows:

$$\gamma [\beta_D D + \beta_L (L+I)] \qquad [3.1]$$

where:

$\gamma = 1.3$

$\beta_D = 1.0$

$\beta_L = 1.67$

This then reduces to:

$$1.3 D + 2.17 L \qquad [3.2]$$

Loads applied to each specimen were scaled by dividing the full-scale superstructure loads by the square of the scale factor. Because self-weight of the test specimen was equal to the self-weight of the full-size bent divided by the cube of the scale factor, additional loads should have been added to compensate for the dead load lost due to scaling. However, because the actual proportions, and hence the self-weight of the specimen, did not correspond exactly to the actual bent, and because the self-weight was insignificant compared to the superstructure dead loads and traffic live loads, the correction was neglected.

3.2.4 Overhang Depth

The depth of the overhang was determined in an earlier study conducted by Armstrong and Salas [Refs. 1, 2], which examined the differences in design methodology between deep beams and corbels. Because the shear span-to-depth ratio separating deep beam and corbel design is 1.0 in the AASHTO Specifications, the distance to the inner load point was chosen to be half the overhang depth at the face of the column, while the distance to the outer load point was chosen to be 1.5 times the depth, making the distance between load points equal to the overhang depth at the column face (Figure 3.3). That depth was thereby fixed at 61.0 cm (24 in.). Because this study originally began as an extension of the work conducted by Armstrong and Salas, the same loading points were used.

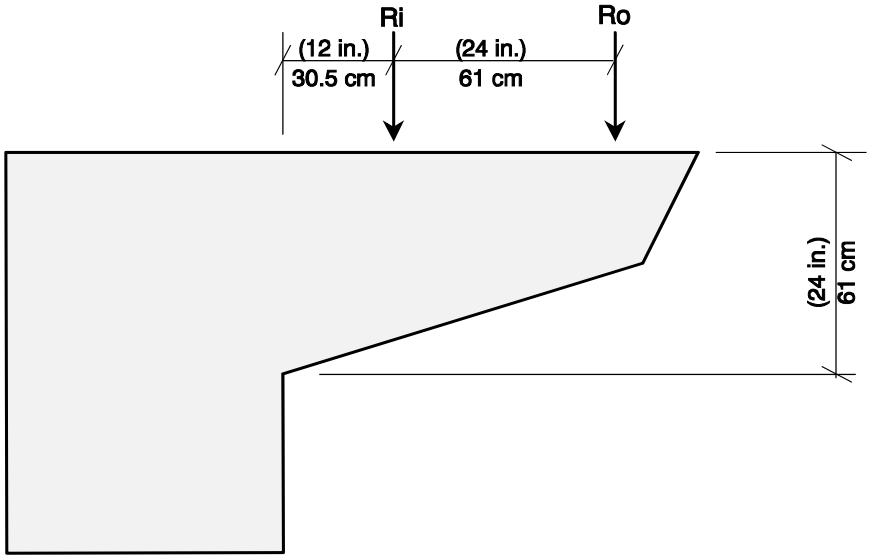

Figure 3.3 Loading Points for Model Bent [From Ref. 3]

3.2.5 Joint Size

Proportions of the joint were tentatively chosen to be similar to those for the Pier I-4C joint which measured 2.51 m (99 in.) high by 3.20 m (126 in.) long. Because the height of the specimen joint had to be the same as the 61.0-cm (24-in.) overhang depth, the joint length was computed as

$$\frac{126}{99} * 61.0 \text{ cm} = 77.6 \text{ cm} \qquad [3.3]$$

Because the deficiency in the cantilever bents was due to a lack of sufficient development length for longitudinal reinforcement in the joint, the model joint had to be designed so the development lengths involved would be comparable to those in the full-scale bents. Because the then-current ACI code [Ref. 4] contains safety factors in its development length equations, the following equations, based on bond strength, from the 1965 code [Ref.

6] were used to provide a more accurate indication of development length required for strength.

$$l_d = \frac{f_y \, d_b}{4 \, U_u} \qquad [3.4]$$

where:

$$U_u = \frac{6.7 \sqrt{f'_c}}{d_b} \leq 560 \text{ for bar sizes less than \#11} \qquad [3.5]$$

$$U_u = 4.2 \sqrt{f'_c} \leq 560 \text{ for bar sizes \#11 and greater} \qquad [3.6]$$

Based on these equations, 34.0 cm (13.4 in.) was computed as the development length for #4 bars, and 42.4 cm (16.7 in.) was computed as the development length for #5 bars. Because available development length for the primary longitudinal reinforcement in the overhang of Pier I-4C, measured from the joint/overhang interface, was approximately twice the required length for the #11 bars, the horizontal dimension of the model joint was taken to be approximately twice the required development length for #4 bars, or 68.1 cm (26.8 in.). The vertical dimension was selected in a similar manner. The height of the joint in Pier I-4C was approximately 1.5 times the development length of #14 bars, so the specimen joint height was taken to be approximately 1.5 times the development length of the #5 bars, or 63.6 cm (25.1 in.). These dimensions being sufficiently close to those based on proportionality, the joint size was fixed at 61.0 cm (24 in.) deep and 76.2 cm (30 in.) long. The width was selected as 61.0 cm (24 in.) to allow space for the necessary reinforcement.

3.2.6 Column and Overhang Length

The column height was chosen to be twice the column depth, to minimize interaction between the footing and joint. The overhang was required to extend slightly beyond the outer loading point. The depth of the overhang was tapered from 61.0 cm (24 in.) at the joint/overhang interface to 30.5 cm (12 in.) just past the edge of the bearing pad for the outer loading point. The final dimensions of the model bent are shown in Figure 3.4.

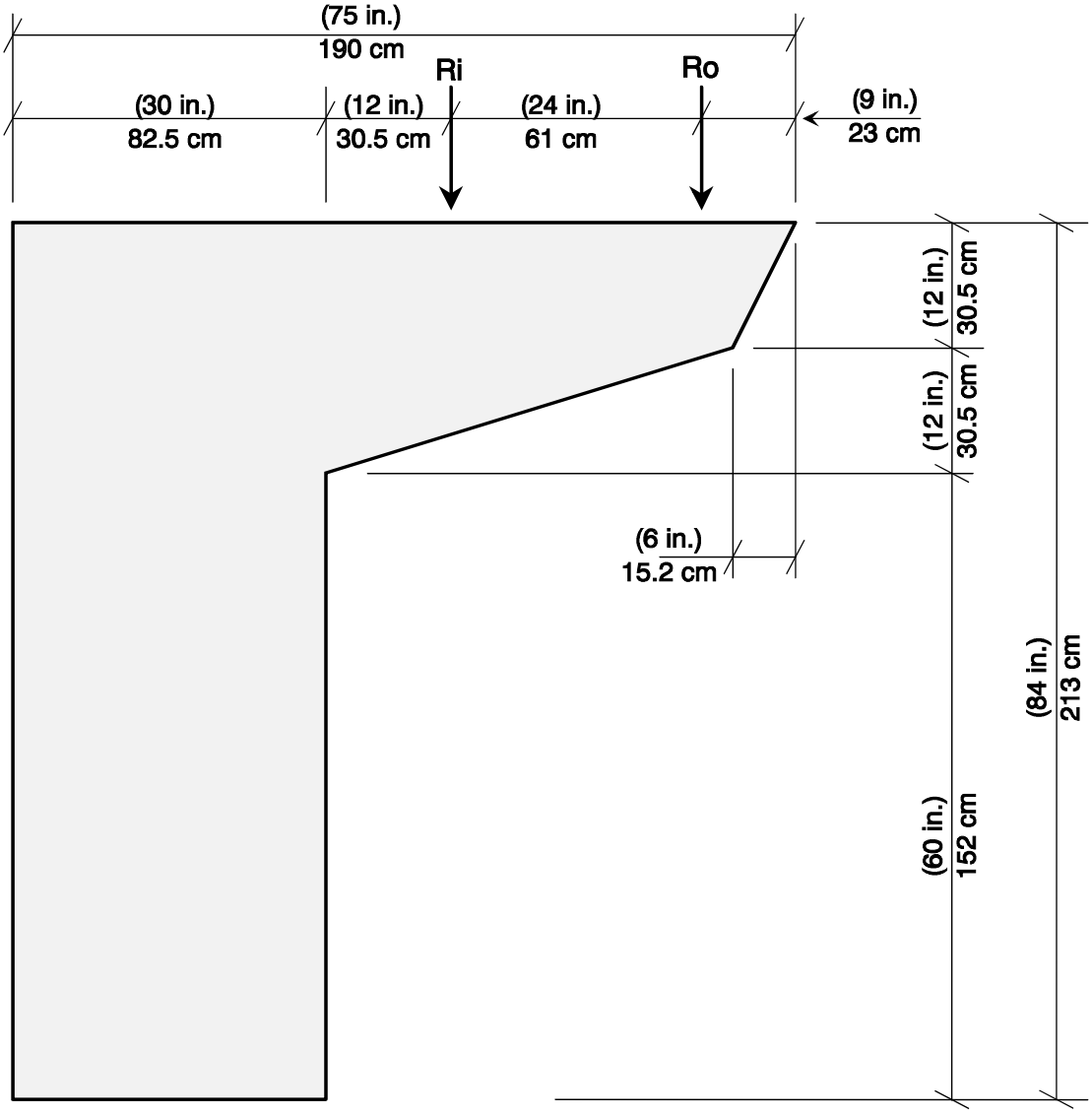

Figure 3.4 Dimensions of Model Bent [From Ref. 3]

3.2.7 Column and Overhang Reinforcement

Based on the previously determined concrete dimensions and bar sizes, the specimens were designed to resist scaled loads at the interfaces, using the same design procedures followed by TxDOT engineers for the original bents. Areas for stirrups, shear

friction steel, and skin steel were calculated, and bar sizes chosen to provide numbers of bars similar to those in the original bents. Column tie spacing was scaled linearly from the full-size spacing. Anchorage zone steel in the post-tensioned specimen was designed to resist bursting stresses imposed by the post-tensioning. The reinforcement layouts are shown in Figures 3.5 and 3.6. Details of the reinforcement are shown in Figures 3.7 and 3.8.

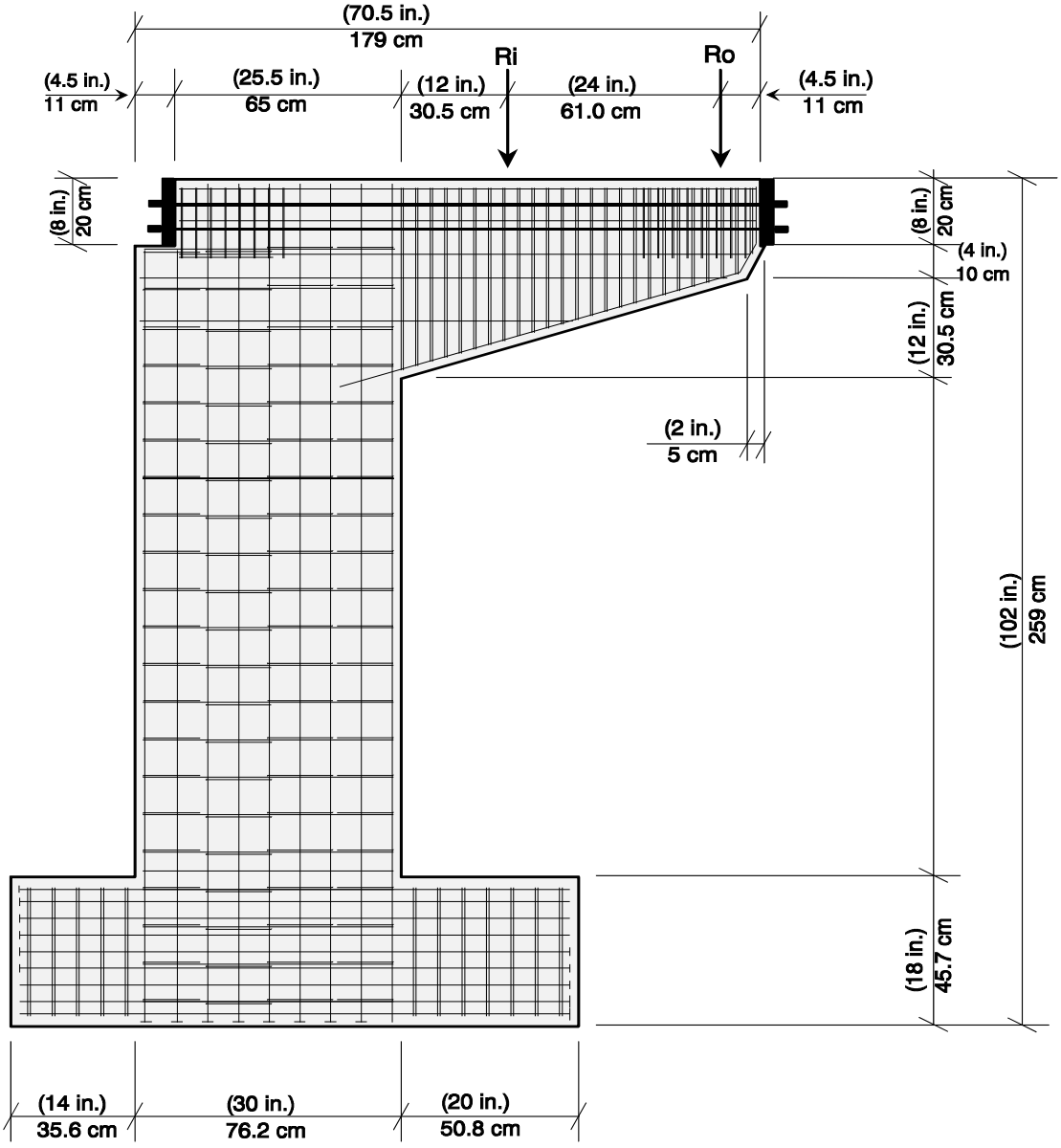

Figure 3.5 Layout of Reinforcement in Model Bent with Post-Tensioned Overhang [From Ref. 3]

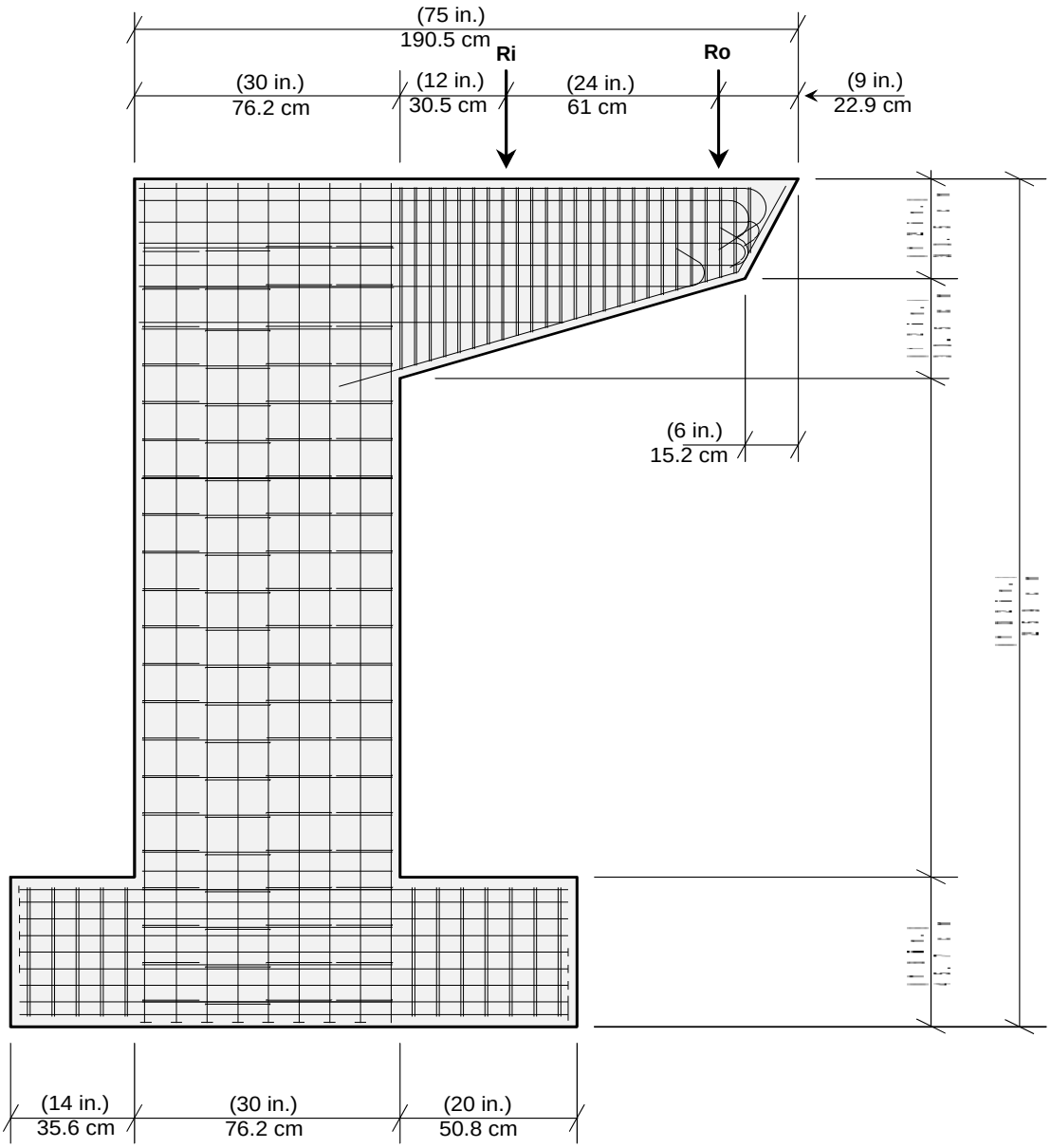

Figure 3.6 Layout of Reinforcement in Reinforced Concrete Model Bent [From Ref. 3]

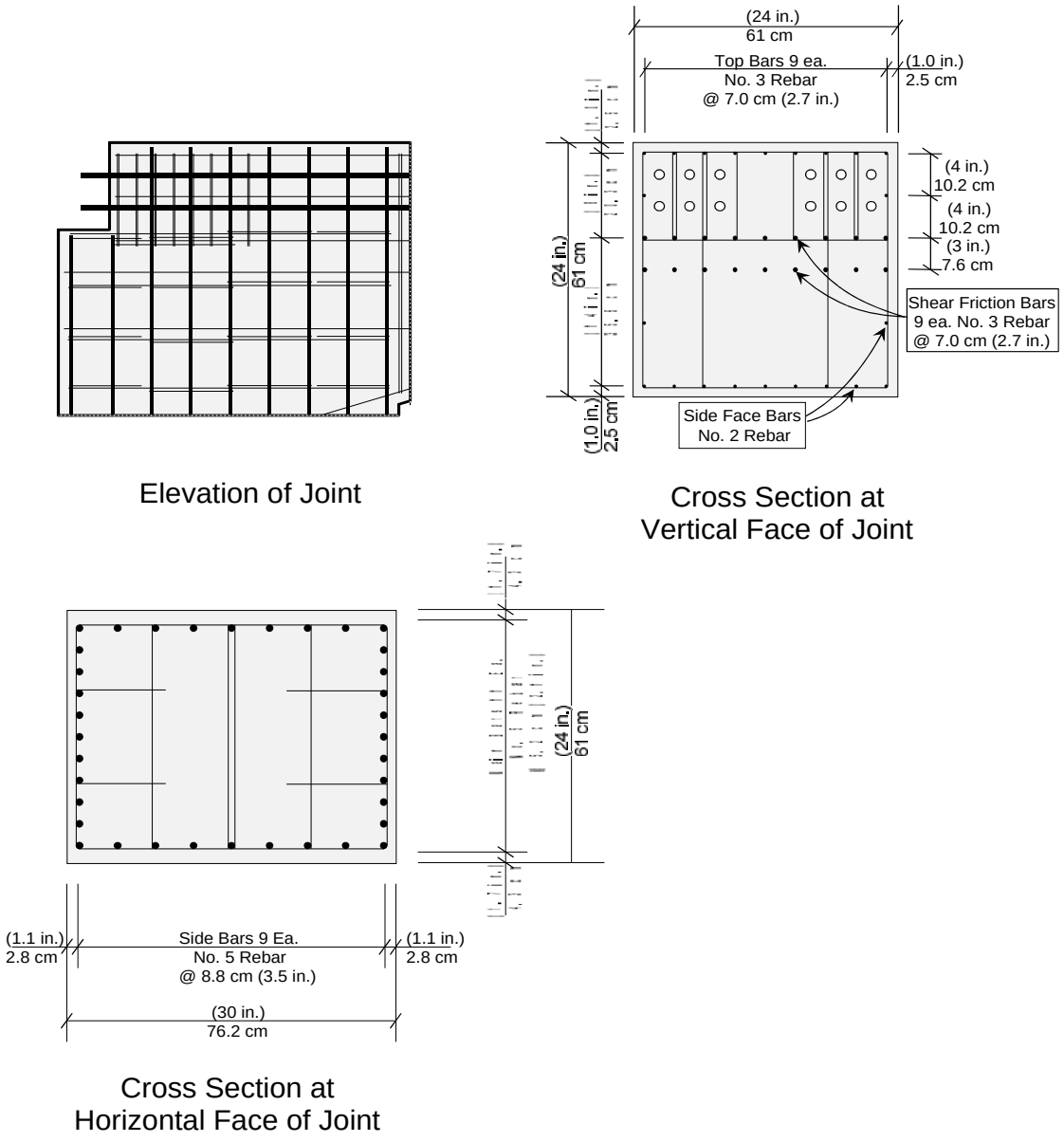

Figure 3.7 Details of Reinforcement in Model Bent with Post-Tensioned Overhang [From Ref. 3]

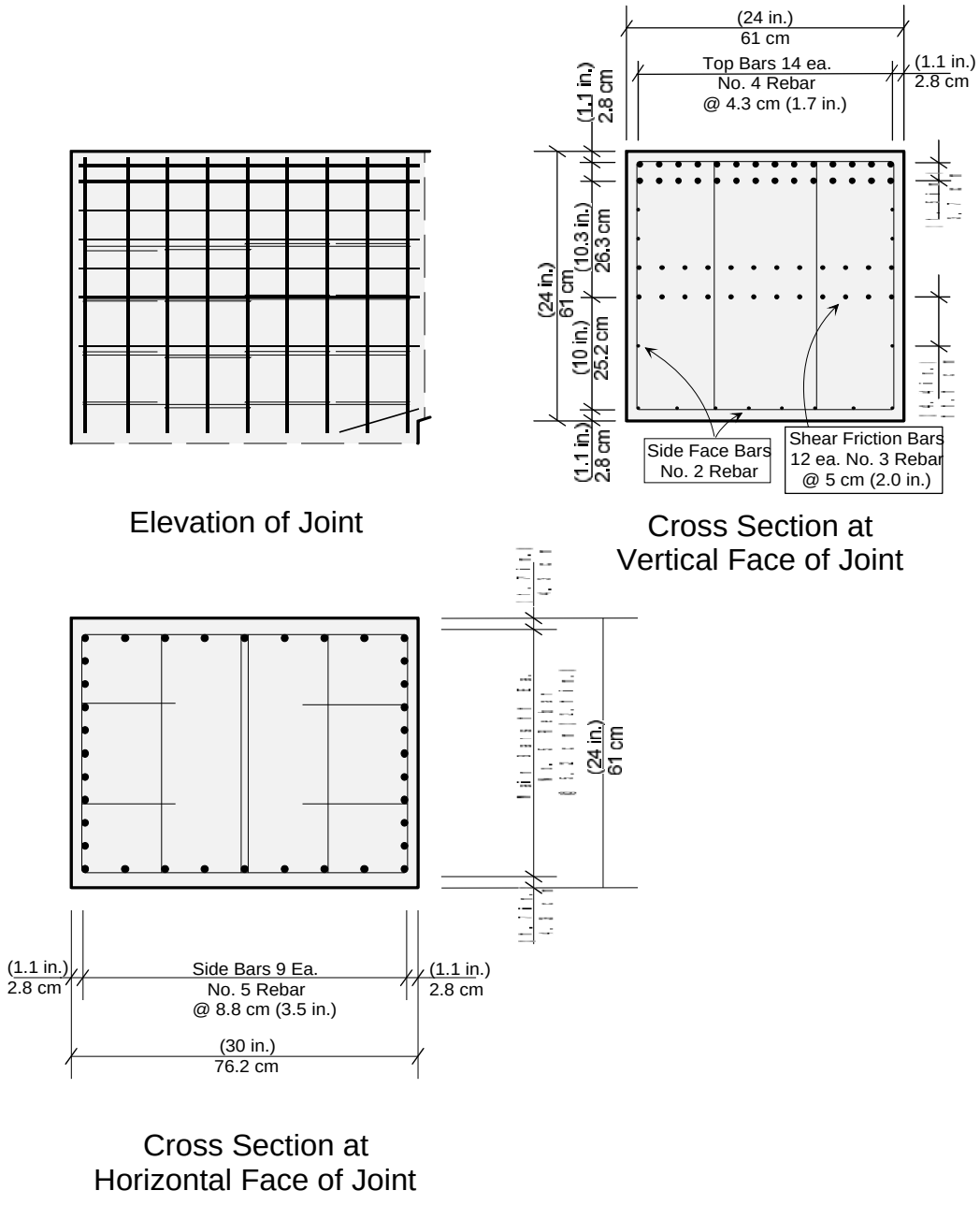

Figure 3.8 Details of Reinforcement in Reinforced Concrete Model Bent [From Ref. 3]

3.2.8 Footing Design

The footing design was not part of the study, so it was simply designed to resist the moments produced by the expected maximum loading. Dimensions were mainly determined by the distance between tie-down locations on the laboratory floor. No attempt was made to reproduce the actual footing. The footing contained T-headed bars for development of the reinforcement in the tensile stress zones, because there was insufficient length and space for straight development or hooks (Figure 3.9). Because the performance of the footing and the base of the column were not the primary focus of the study, the use of T-headed bars did not affect experimental results.

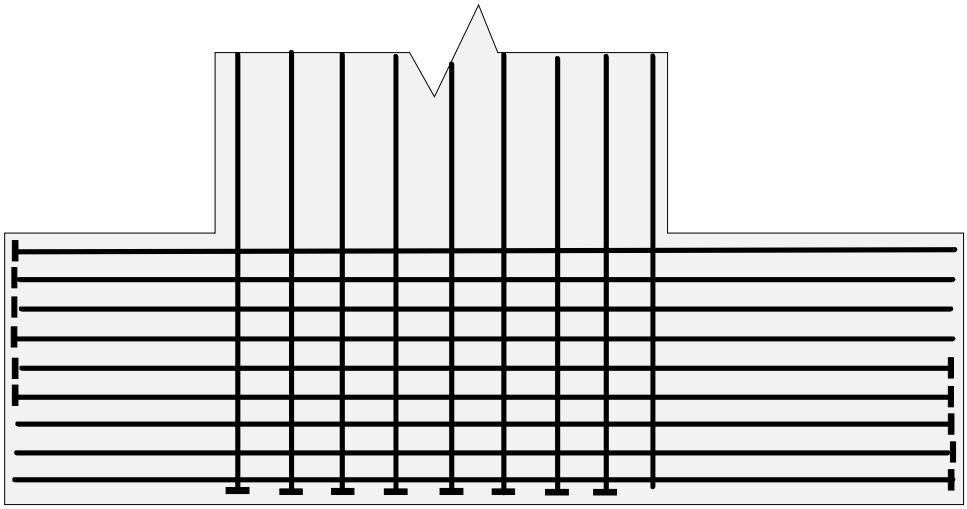

Figure 3.9 Footing Design for Model Bent

3.2.9 Calculation of Moment Capacity

Spreadsheet programs to calculate the actual moment capacity of the connection were written by Wood [Ref. 3]. An example is shown in Figure 3.10. The tensile capacity of a bar with less than the required development length was assumed to be equal to the yield force of the bar multiplied by the ratio of embedment length provided to that required by Eq. 3.3. The spreadsheet assumes a compression zone, calculates the development length and stress in each bar, multiplies the appropriate components of bar forces by respective moment arms, checks for equilibrium, then adjusts its assumptions based on the equilibrium check and iterates until equilibrium is satisfied. A schematic of the resultants of horizontal and vertical bar forces and their moment arms is shown in Figure 3.11. Because the object was to calculate as accurately as possible the actual moment capacity of the bent, all reinforcing steel was included in the calculation.

Figure 3.10 Example of Spreadsheet for Calculating Moment Capacity

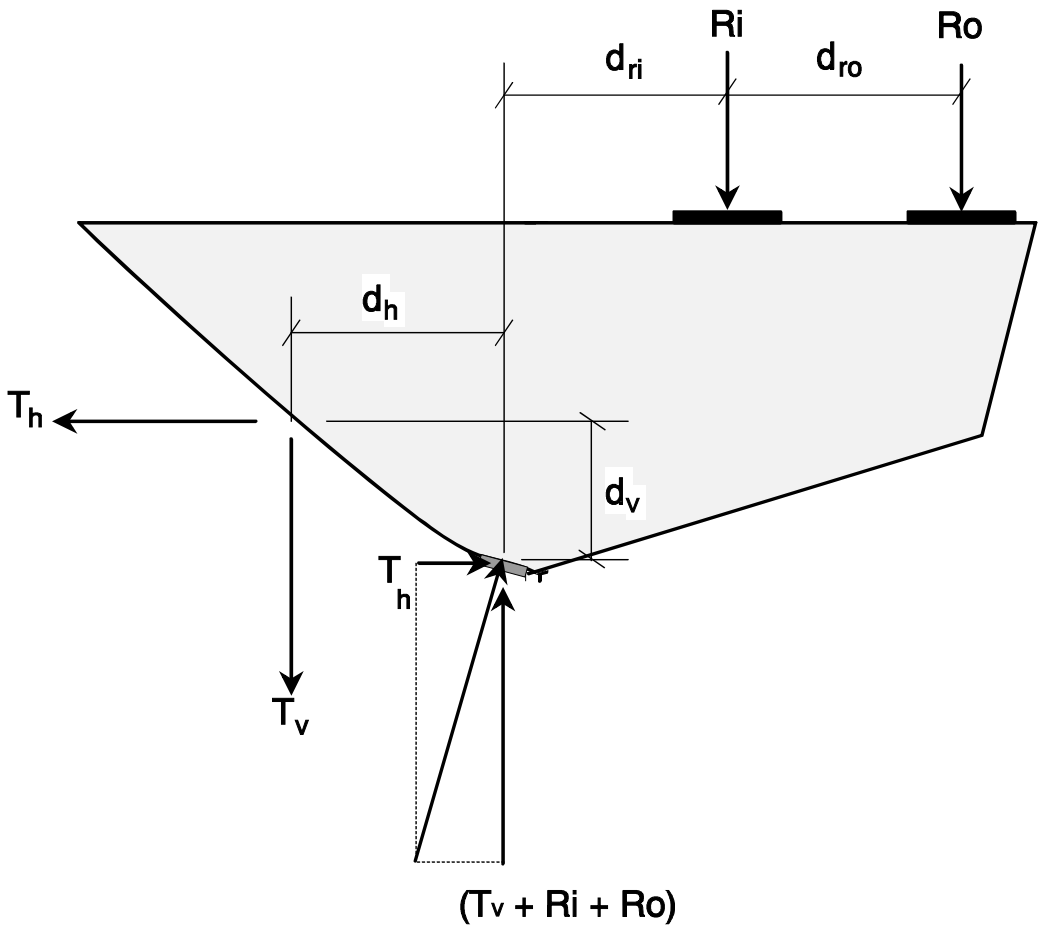

Joint Resistance = Applied Moment

$T_h(d_v) + T_v(d_h) = Ri(d_{ri}) + Ro(d_{ro} + d_{ri})$

Figure 3.11 Equilibrium of Bent Cut through Critical Section [From Ref. 3]

3.2.10 Identification of Specimens

Each specimen and repair was identified by a label indicating the type of structure, type of construction, repair number, and repair modification, if necessary. The format is

shown in Figure 3.12. The code RC2 is used for the reinforced concrete specimens because in an earlier phase of the research program there was another reinforced concrete specimen simply designated with RC. The code PS-100 is used for the specimens with prestressed concrete overhangs because the earlier phase of the study included specimens with various degrees of post-tensioning, including 54 percent and 74 percent.

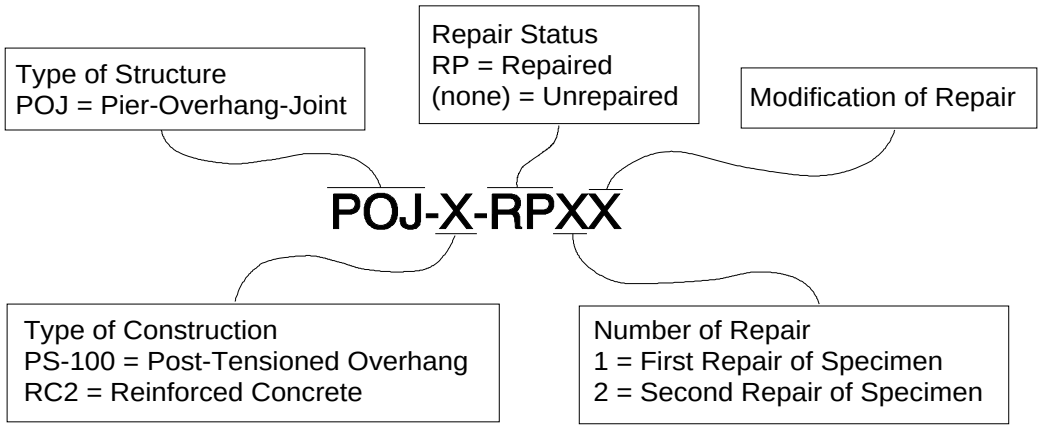

Figure 3.12 Format of Specimen Labelling

3.3 Materials

3.3.1 Concrete

The concrete used was designed for a compressive strength of 34.5 MPa (5000 psi) at seven days. The maximum aggregate size was 0.95 cm (3/8 in.). The mix design is shown in Table 3.2, and the results of compressive strength tests are show in Figure 3.13.

Table 3.2 Concrete Mix Design

Component	Amount	
Cement	334.6 kg	(564 lbs)
3/8" Aggregate	867.9 kg	(1463 lbs)
Sand	967.5 kg	(1631 lbs)
Water	118.6 kg	(200 lbs)
Retarder	965 ml	(25 oz)
Superplasticizer	1737 ml	(45 oz)

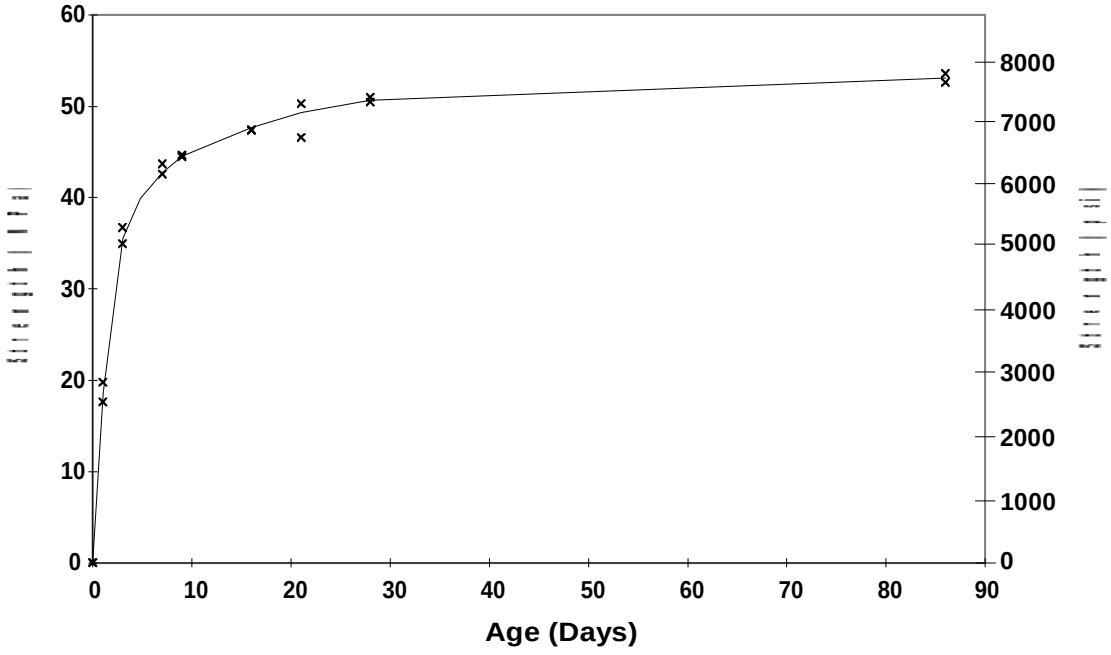

Figure 3.13a Results of Concrete Compressive Strength Tests for Prestressed Concrete Specimen

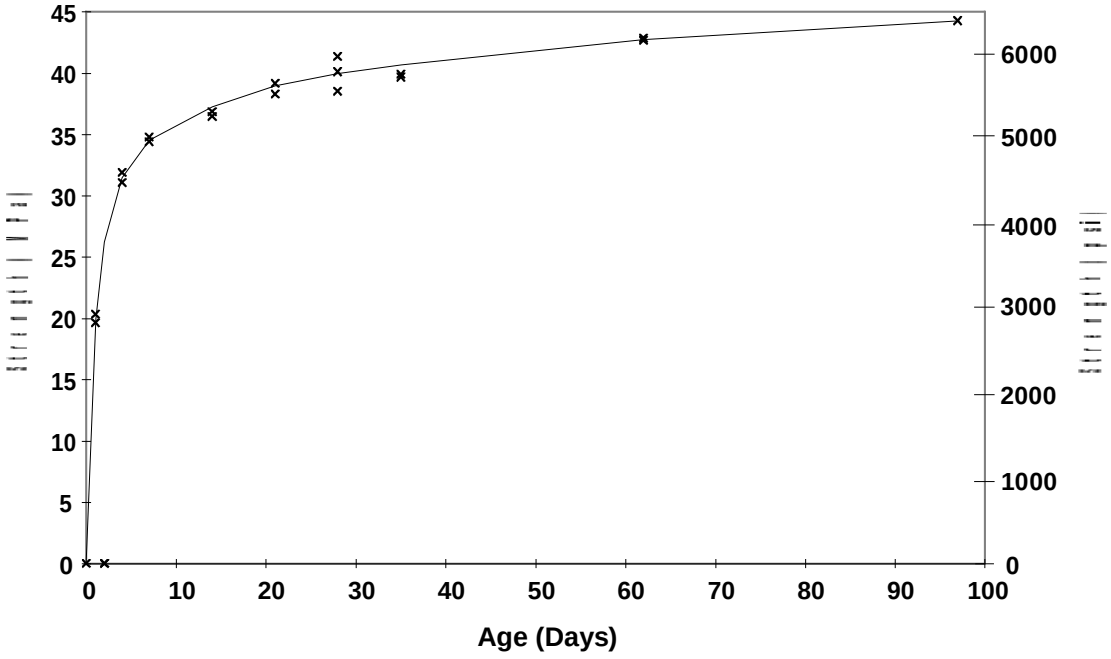

Figure 3.13b Results of Concrete Compressive Strength Tests for Reinforced Concrete Specimen

3.3.2 Mild Steel Reinforcement

Grade 60 reinforcement was used for all #3, #4, and #5 bars. Number 2 bars were Grade 75. Examples of tensile tests are shown in Figure 3.14, and the properties of the various bars are listed in Table 3.3. Undeformed #7 and #9 wire was used for column ties.

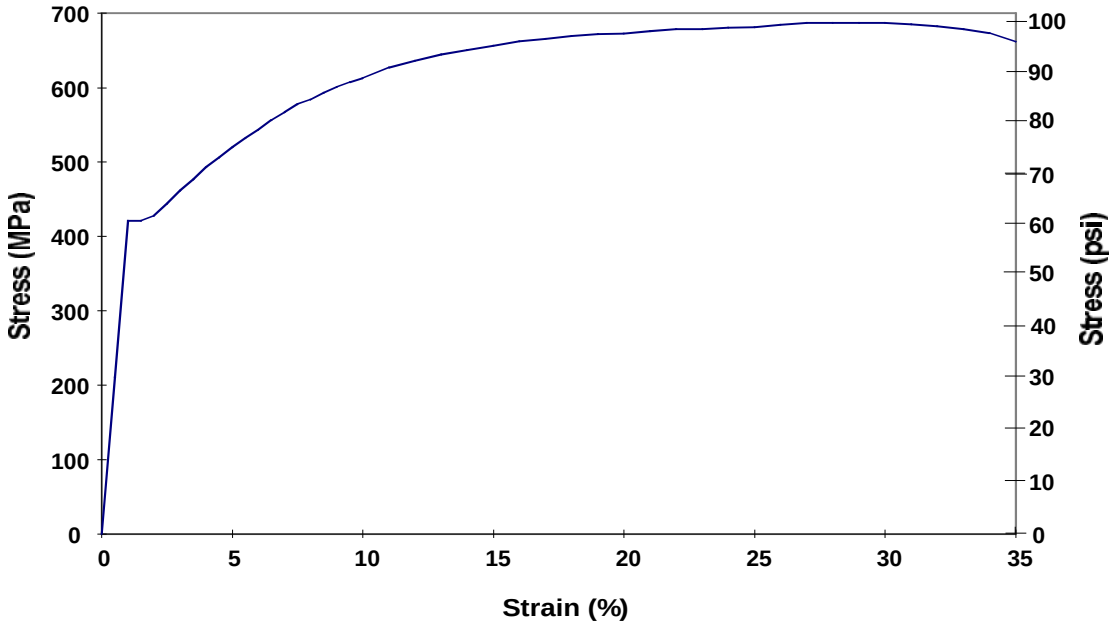

Figure 3.14a Typical Tensile Test Results for #5 Mild Reinforcing Bars

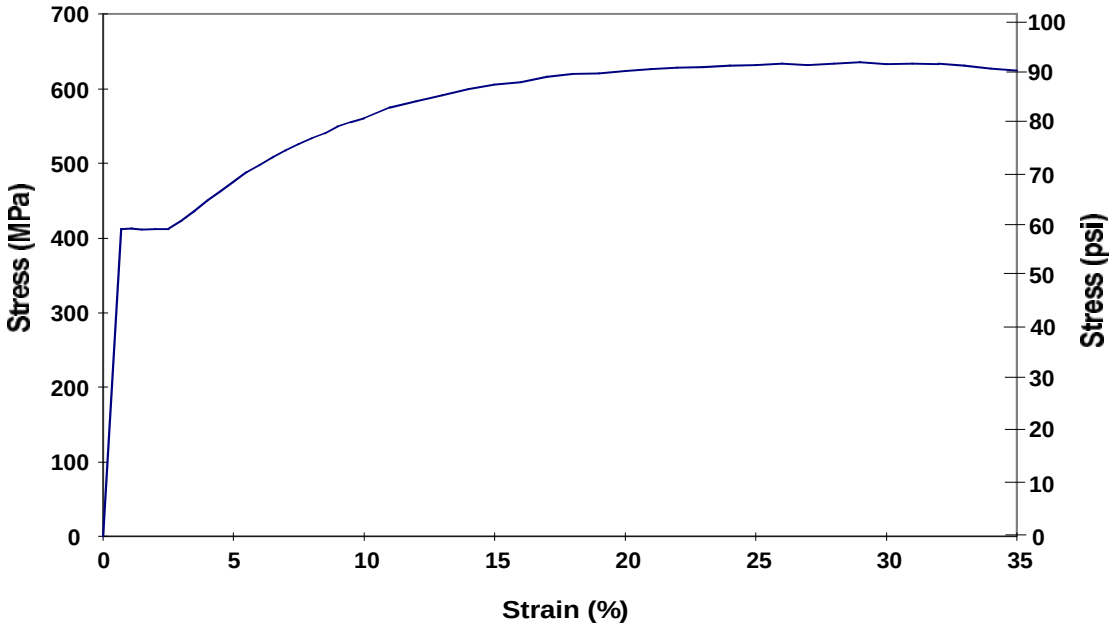

Figure 3.14b Typical Tensile Test Results for #4 Mild Reinforcing Bars

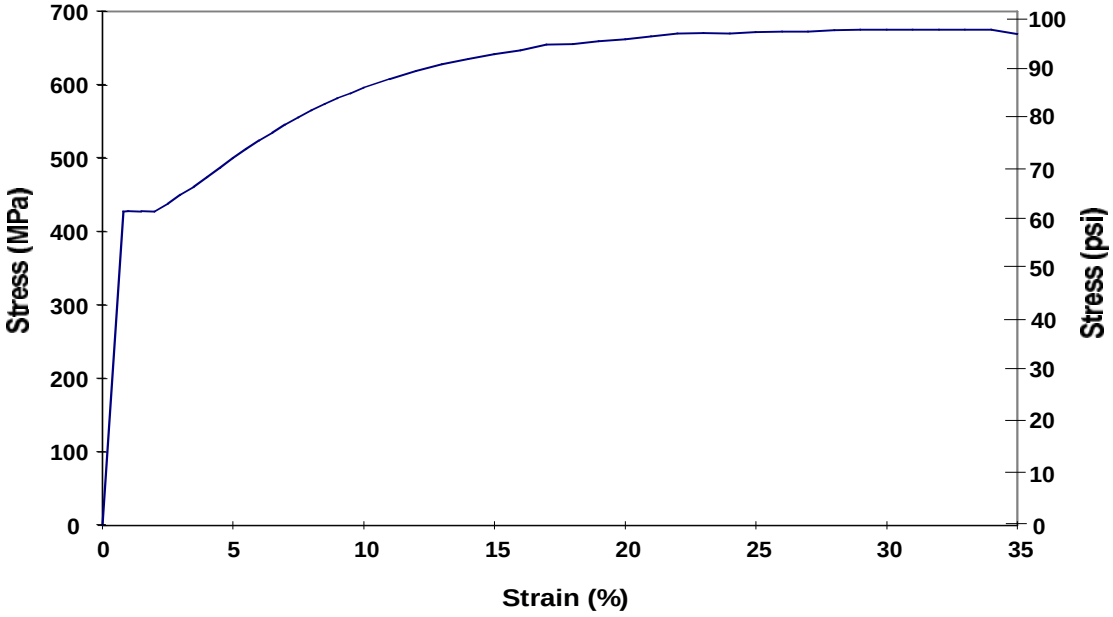

Figure 3.14c Typical Tensile Test Results for #3 Mild Reinforcing Bars

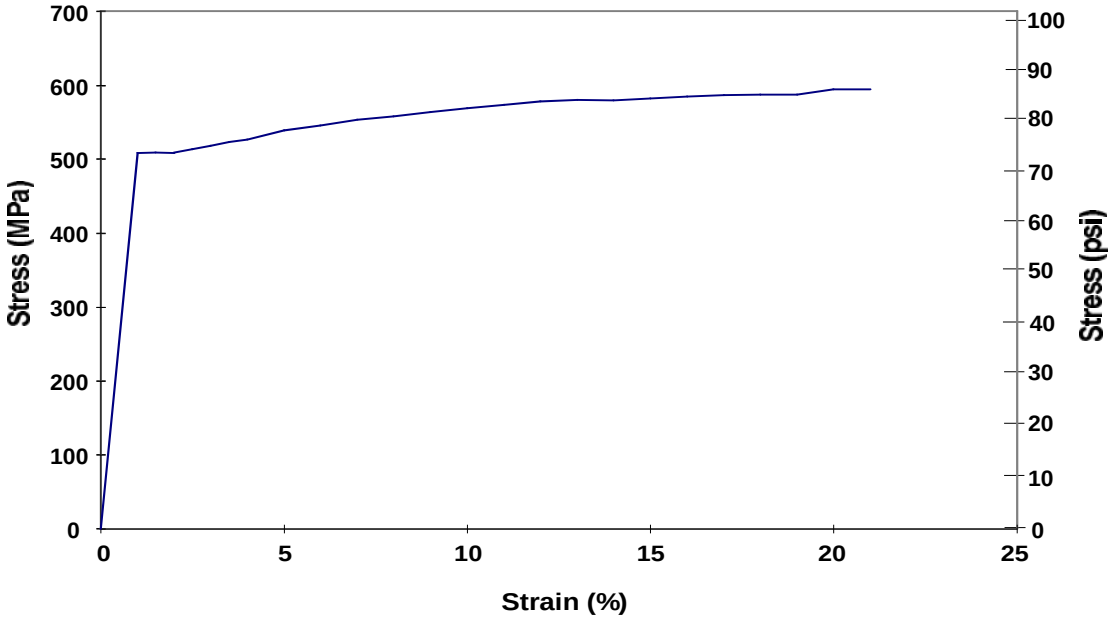

Figure 3.14d Typical Tensile Test Results for #2 Mild Reinforcing Bars

Table 3.3: Properties of Mild Reinforcing Bars

Bar Size	Area		Yield Strength		Ultimate Strength	
# 5	2.00 cm^2	(0.31 in^2)	420 MPa	(61.0 ksi)	691 MPa	(100.3 ksi)
# 4	1.30 cm^2	(0.20 in^2)	412 MPa	(59.8 ksi)	635 MPa	(92.2 ksi)
# 3	0.71 cm^2	(0.11 in^2)	428 MPa	(62.1 ksi)	675 MPa	(98.0 ksi)
# 2	0.32 cm^2	(0.05 in^2)	523 MPa	(75.9 ksi)	595 MPa	(86.3 ksi)

3.3.3 Post Tensioning Bars

Dywidag bars, of 1.59 cm (5/8 in.) diameter, were used for all post-tensioning, both internal and external. Measured yield strength was approximately 772 MPa (112 ksi), while ultimate strength was approximately 967 MPa (140 ksi). An example of tensile test results is shown in Figure 3.15.

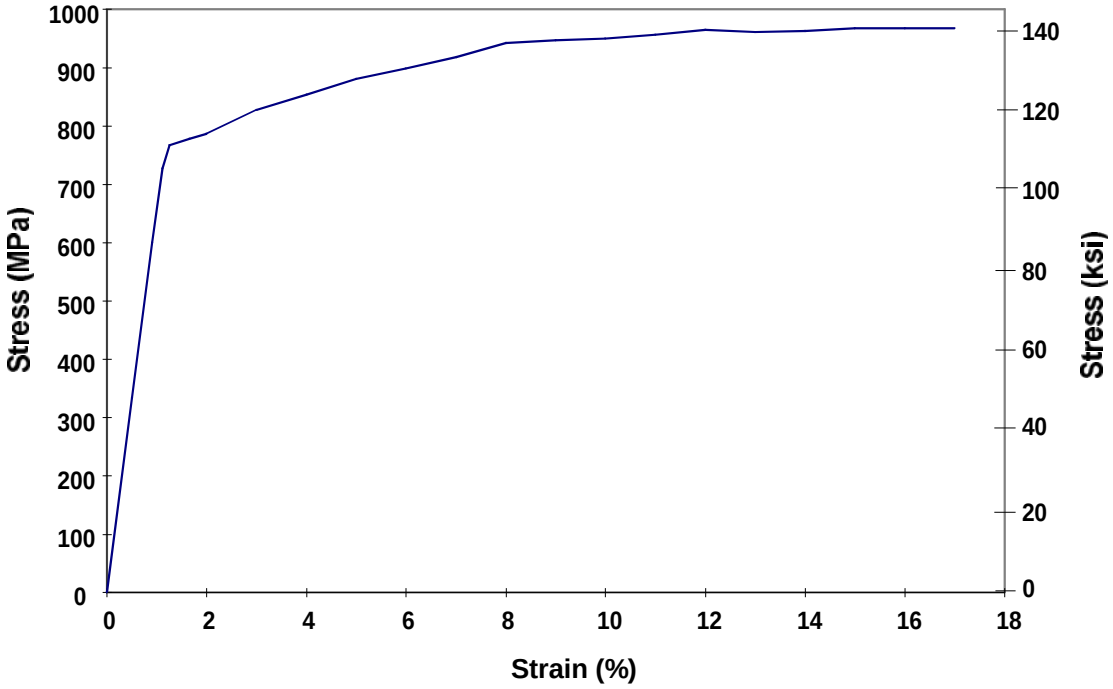

Figure 3.15 Results of Tensile Test for 1.59 cm (5/8 in.) Diameter Post-Tensioning Bars

3.3.4 Post Tensioning Hardware

Dywidag nuts were used to secure all post-tensioning rods. Two nuts were used on each end, with plates to distribute the compressive force across a larger area of concrete, as shown in Figure 3.16.

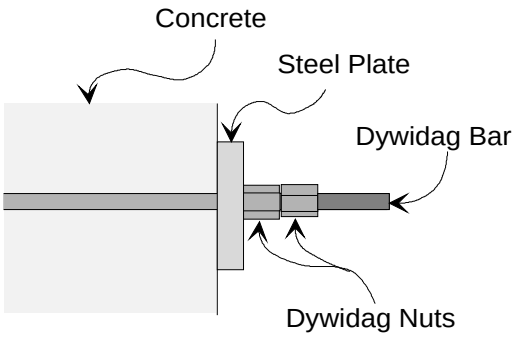

Figure 3.16 Post-Tensioning Hardware

3.3.5 Grout

The mix design for the grout used to fill the ducts containing the post-tensioning bars is shown in Table 3.3. An expansive agent, Interplast N, was added to ensure the ducts were filled completely. Several cubes 5.08 cm (2.0 in.) on a side were cast to test the grout strength. Tests on the bent specimens were not initiated until the grout reached a compressive strength of at least 17.2 MPa (2500 psi). Compressive test results are shown in Figure 3.17.

Table 3.3 Grout Mix Design

Component	Amount	
Cement	13.61 kg	(30.0 lbs)
Water	6.62 kg	(14.6 lbs)
Expansive Agent	0.14 kg	(0.3 lbs)

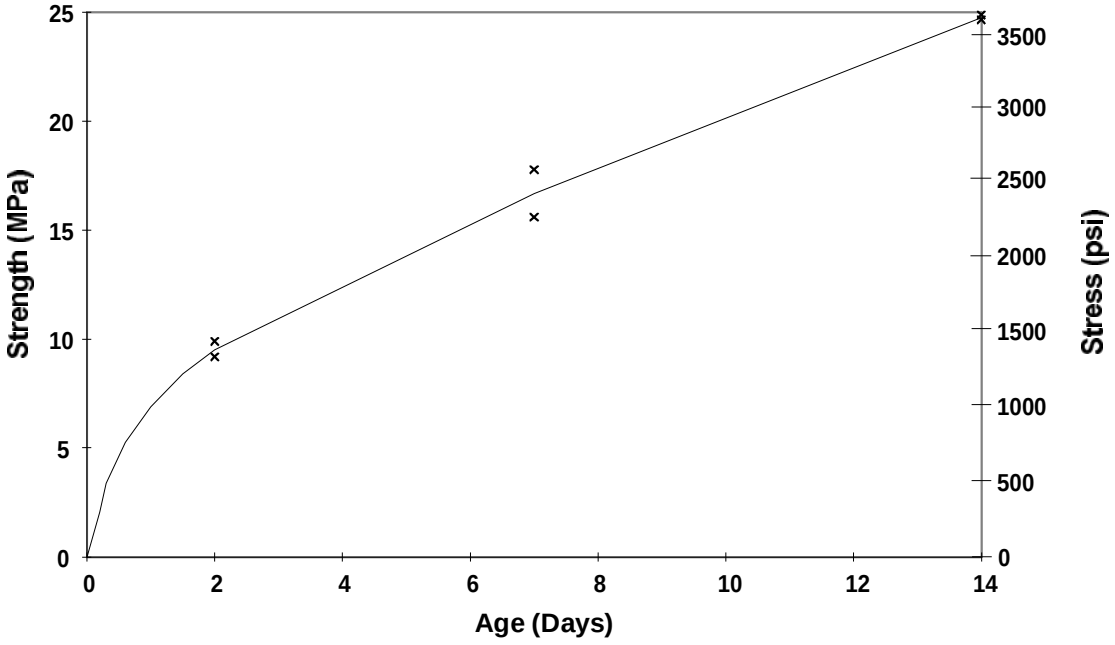

Figure 3.17 Compressive Strength Test Results for Grout

3.4 Fabrication

3.4.1 Reinforcing Cages

Specimens were cast on their sides to avoid consolidation problems that might have resulted if they were cast in their upright position. The steel cages were also constructed in a horizontal position, away from the formwork, and later transferred by crane into the casting forms. Steel reinforcement was cut and bent in the lab and tied together using both plastic and wire ties.

For the post-tensioned specimen, 12 1.73-m (68-in.) long, 3.18-cm (1.25-in.) diameter aluminum electrical ducts were inserted into the overhang for the post-tensioning bars. Eight aluminum electrical ducts were also inserted vertically into the column and joint of the reinforced concrete specimen, because a potential repair method utilizing internal post-tensioning was selected for testing, and equipment was not available for drilling the deep holes required in the specimen after it had been cast.

Reinforcing bars were ground slightly, sanded, and cleaned at locations where strain gauges were desired. The gauges were then attached with epoxy, covered with butyl rubber for protection against damage, and painted with latex for water-tightness. The lead wires were routed, parallel to expected crack patterns, to the compression zone of the column, where they were bundled together and routed down to the footing and out of the cage.

3.4.2 Formwork

Formwork was designed to be reusable and therefore was constructed in several sections from plywood and 2 x 4's as shown in Figure 3.18. These sections were sprayed

with form release compound before each reinforcing cage was placed in the formwork. After a cage was placed on chairs (bolsters) on the bottom plate of the formwork, the side pieces of the formwork were lifted into place and secured. The cage was then shifted, if necessary, to ensure consistent concrete cover on all sides. Although the sides were stiffened with 2 x 4's, additional measures were taken to ensure that the formwork did not shift or flex when filled with concrete. The top of the formwork was braced to the floor with diagonal 2 x 4's. Furniture clamps were also used to hold the formwork together in two places: across the overhang near the joint and near midheight of the column.

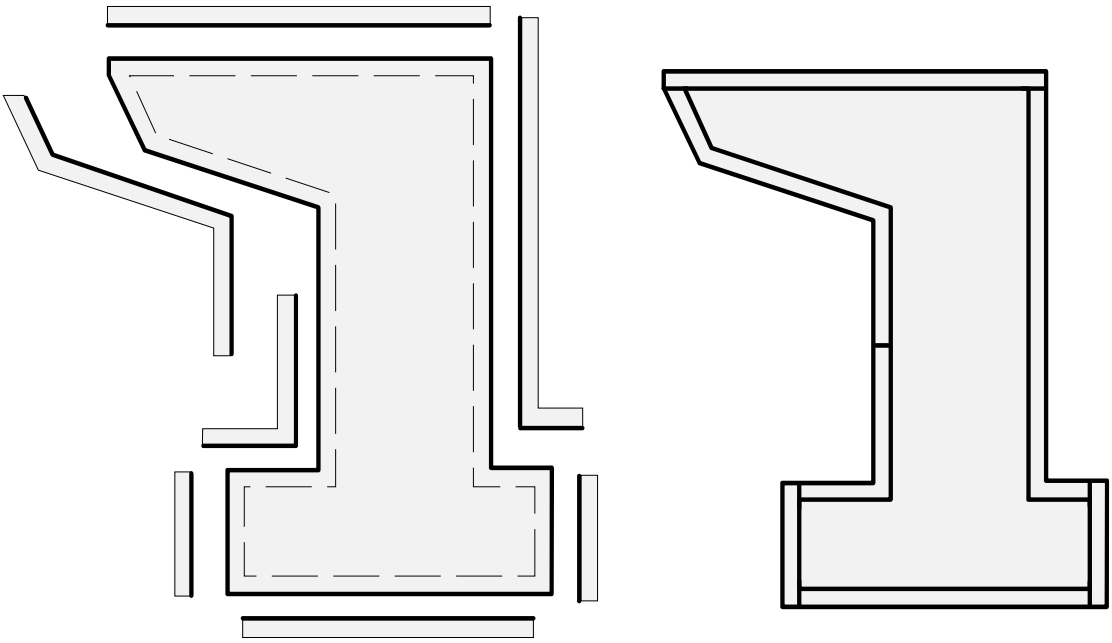

Figure 3.18 Formwork Sections and Assembled Formwork

The same formwork was used for all specimens, although the post-tensioned specimen required block-outs (for the post-tensioning hardware) to be inserted at each end of the overhang, with holes drilled for the horizontal post-tensioning ducts, while the reinforced concrete specimen required holes in the forms at the top of the specimen to accommodate the vertical ducts. Holes were also drilled in the formwork to allow the insertion of lifting hooks.

3.4.3 Placement and Consolidation of Concrete

Concrete was placed from overhead with a bucket. Mechanical vibrators were used to ensure consolidation, which was critical because of reinforcement congestion. Twenty compression test cylinders, 30.5 cm (12 in.) high and 15.2 cm (6 in.) in diameter, were cast along with each specimen. Two beams, 15.2 x 15.2 x 137.2 cm (6 x 6 x 54 in.), were also cast to measure the elastic modulus of the concrete.

3.4.4 Finishing, Curing and Form Removal

Concrete was finished by hand, using trowels, and covered with plastic sheets to prevent excessive drying. After three days, the specimens were uncovered and the sides of the formwork were removed. The specimens continued to cure until it was time for testing.

3.5 Test Set-Up

3.5.1 Loading Frame and Rams

The loading frame is shown in Figures 3.19a and 3.19b. Four columns, each consisting of a W 14 x 145 section welded to 30.5 x 30.5 x 2.5 cm (12 x 12 x 1 in.) plates, were bolted to the laboratory floor, using four 2.54 cm (1-in.) diameter, high-strength threaded rods. Two W 30 x 108 beams were bolted to the columns, at a height of approximately 3.66 m (12 ft). The flanges on one side of the web, near each end, were removed to allow the web to be bolted directly to the flanges of the columns. A W 12 x 65 section was clamped to the bottom flange of the two W 30 x 108 beams. Two 890-kN (200-kip) hydraulic rams were placed on 30.5 x 30.5 x 2.5 cm (12 x 12 x 1 in.) plates that were bolted to the bottom of the W 12 x 65 section. Each ram acted on a 61.0 x 30.5 x 3.8 cm (24 x 12 x 1.5 in.) plate resting on two 27.9 x 20.3 x 7.6 cm (11 x 8 x 3 in.) steel laminated elastomeric bearing pads, which in turn rested directly on the specimen.

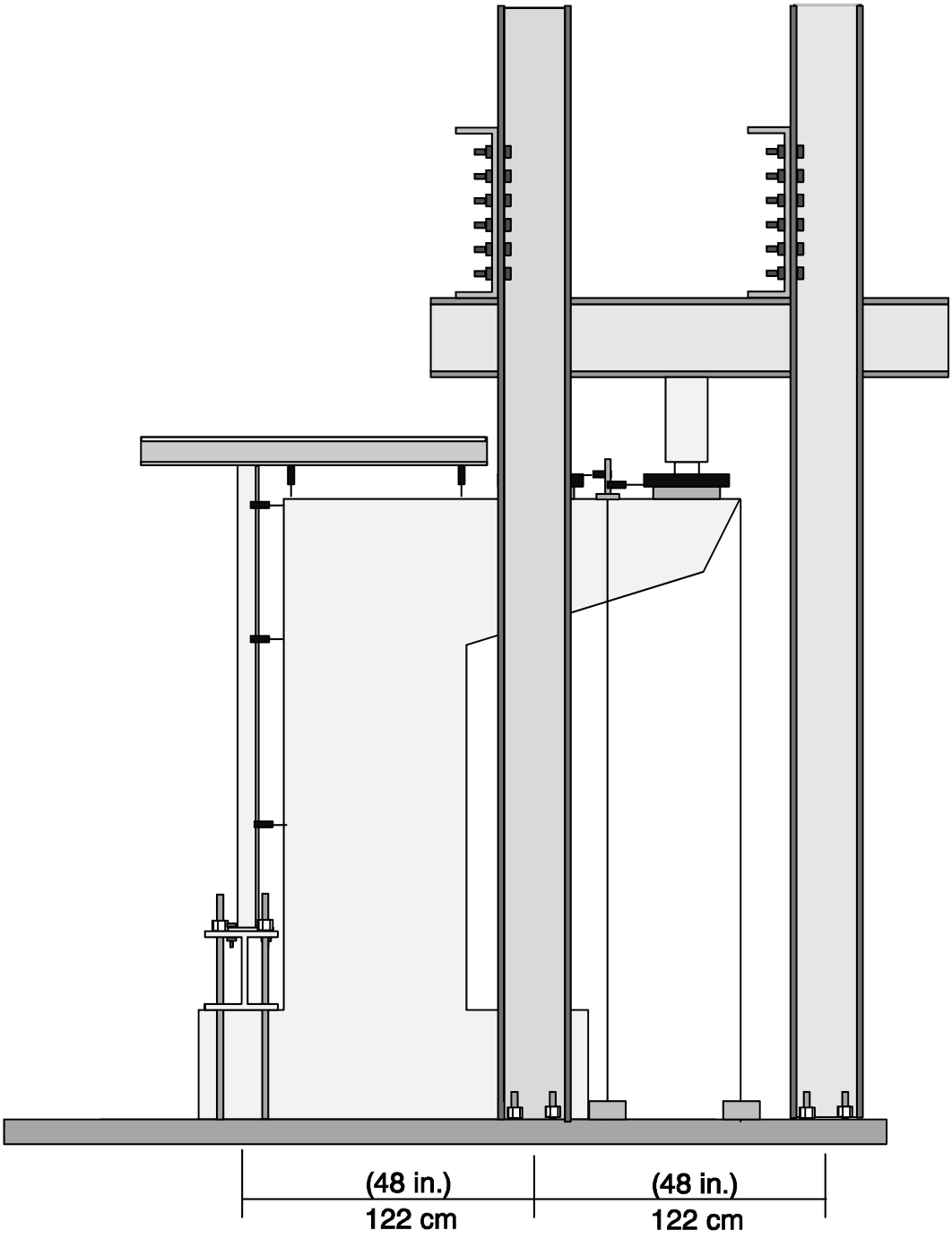

Figure 3.19a Loading Frame [Modified from Ref. 3]

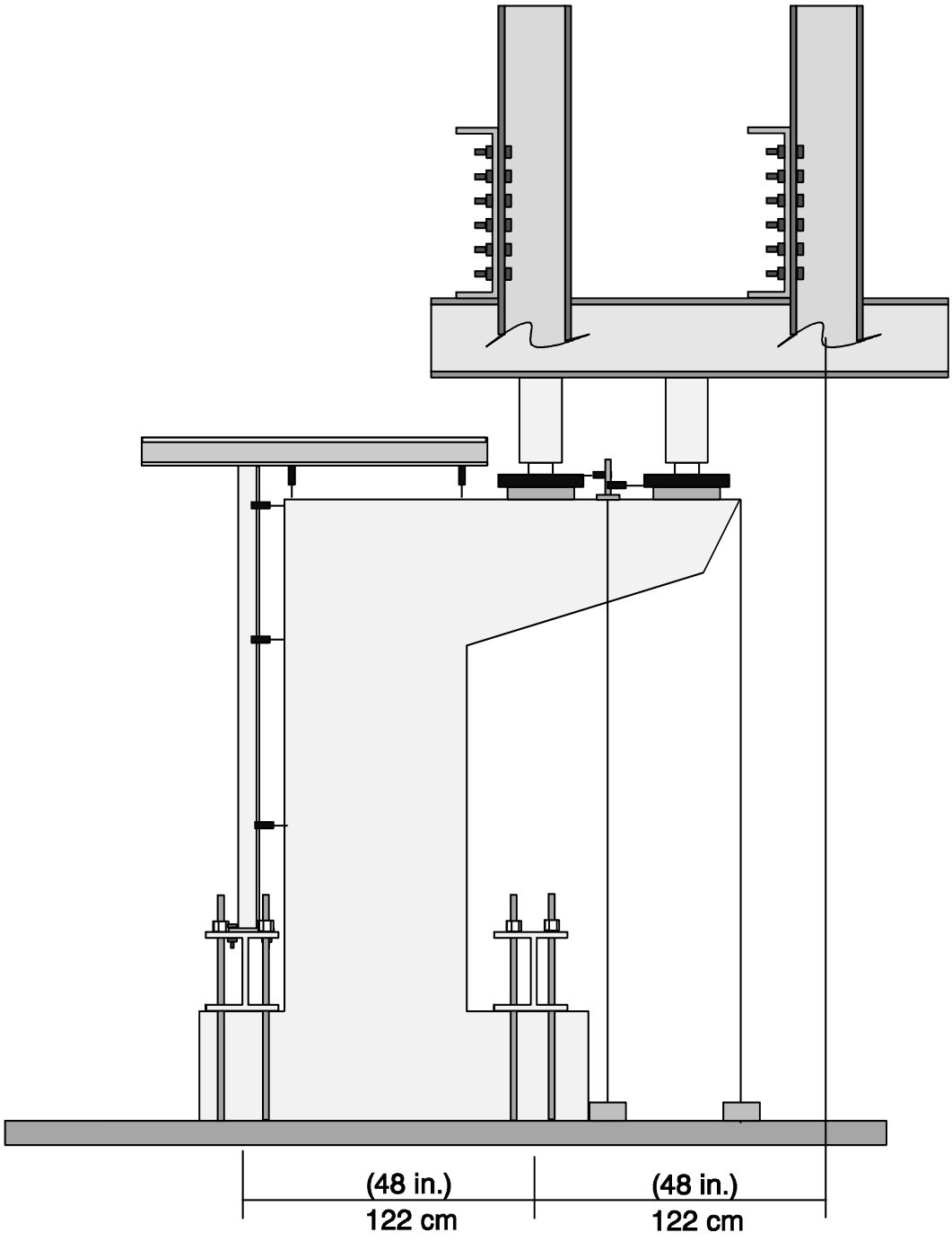

Figure 3.19b Loading Frame with Columns Cut Away to Show Rams and Floor Anchorage

3.5.2 Floor Anchorage System

The specimen was held in place by two W 12 x 65 beams that were bolted to the laboratory floor (See Figure 3.19b). The beams rested on a layer of hydrostone on the top surface of the specimen footing. Bolts on the beam located near the outer face of the specimen were post-tensioned to prevent movement of the specimen under load. Bolts restraining the beam near the inside face of the specimen were merely tightened by hand because they were not expected to resist tensile forces.

Each specimen rested on a layer of hydrostone and 30.5 x 30.5 x 7.5 cm (12 x 12 x 3 in.) steel blocks, fitted together to form a level surface with any gaps filled with hydrostone.

3.5.3 Instrumentation and Data Collection

3.5.3.1 Strain Gauges

Electronic resistance strain gauges were epoxied to the longitudinal reinforcement in the column and overhang. They were also applied to shear friction steel and post-tensioning bars. Some of the skin steel on the top face was also gauged. All gauges used on #4 and #5 bars were 5 mm (0.197 in.), while those applied to #2 bars were 2 mm (0.079 in). Both sizes of gauge were used on #3 bars. Figures 3.20 and 3.21 show the placement of all strain gauges. All gauges had 5-m (16.4-ft) lead wires to enable them to be attached to the data acquisition system without splicing. Gauges were labeled with codes showing their type and location.

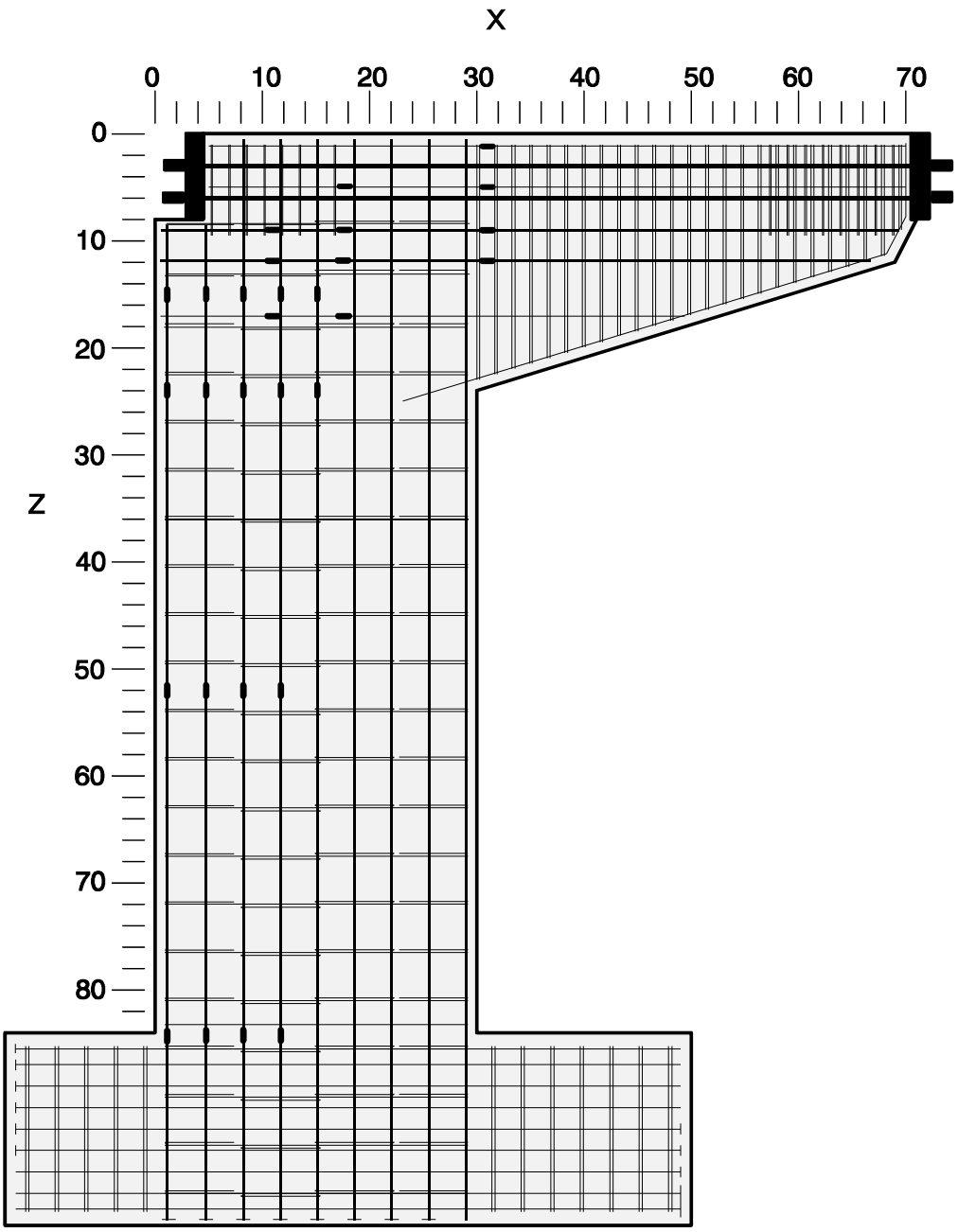

Figure 3.20 Locations of Strain Gauges in Post-Tensioned Specimen [From Ref. 3]

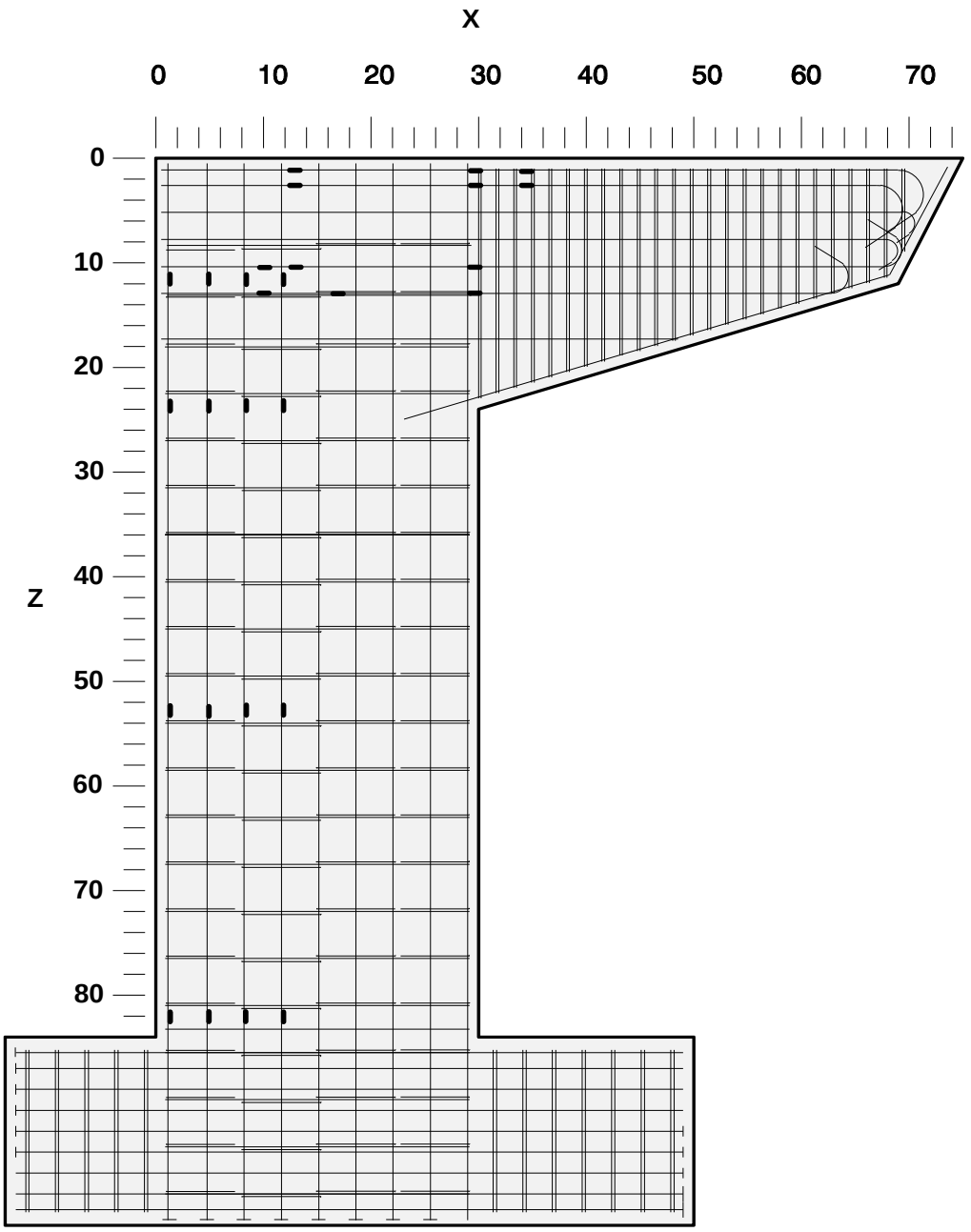

Figure 3.21 Locations of Strain Gauges in Reinforced Concrete Specimen [From Ref. 3]

The first one or two characters on the label are an alphabetic code indicating the type of reinforcement. The last character indicates the location of the gauge along the width of the

specimen. Characters in between give the location of the gauge in a Cartesian coordinate system, with the origin at the outside corner of the joint. The x-axis ran along the overhang, while the z-axis was parallel with the column. The first numbers give the location on the x-axis, while the numbers following the letter "Z" give the location on the z-axis.

3.5.3.2 Displacement Gauges

Two types of displacement gauges were used: 5.1-cm (2-in.) linear potentiometers and 12.7-cm (5-in.) displacement transducers. Linear potentiometers were used along the back of the column and the top of the joint to measure horizontal and vertical displacement of the specimen. Horizontal motion of the bearing pads was also monitored. Displacement transducers were attached to the floor and the overhang to measure vertical displacement along the overhang. On the reinforced concrete specimen, another transducer was used at the inner corner of the joint to measure relative displacement between the overhang and column. A diagram of displacement gauge locations is shown in Figure 3.22.

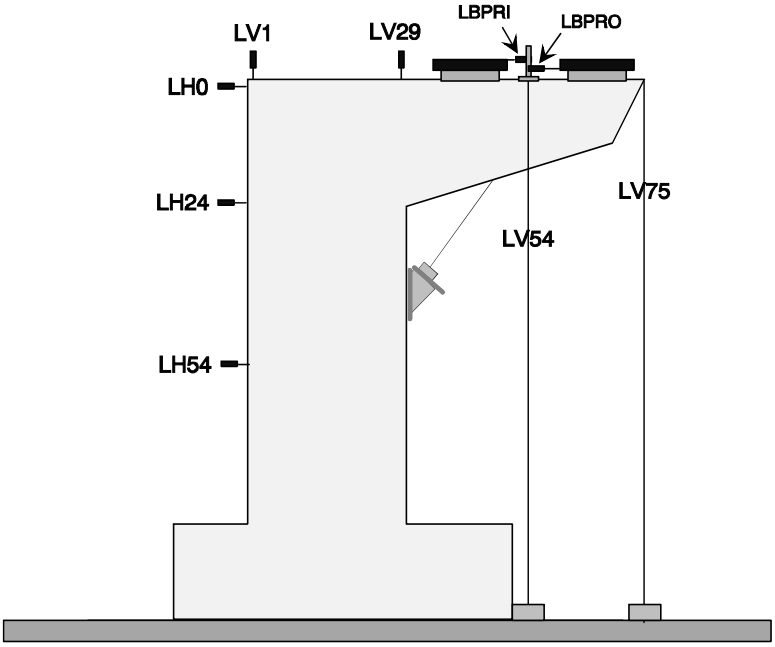

Figure 3.22 Locations of Displacement Gauges

3.5.3.3 Pressure Transducers

Pressure transducers were connected to the pumps for the hydraulic loading rams to measure the pressure applied to the rams and thereby compute the force applied to the specimen. The transducers had a range of 68.9 MPa (10,000 psi). Voltmeters were connected to the pumps to give immediate, though approximate, pressure readings during loading, to ensure that loading increments remained constant.

3.5.3.4 Data Acquisition System

The data acquisition system consisted of a 140-channel Hewlett Packard 3497A scanner and an IBM compatible Hewlett Packard XT personal computer. The system was controlled by HPDAS2, a computer program developed in Ferguson Laboratory. Strain, displacement, and pressure readings were collected by measuring voltage across each gauge

and converting the electrical measurements into the appropriate engineering values. At the beginning of each test, a zero voltage reading was taken for all strain gauges, displacement gauges, and pressure transducers. At each increment of loading, another voltage reading was taken and compared to the zero readings. The readings were stored by the computer and a printout was made showing the current readings, zero readings, and calculated differences. Calculated pressure and load values were printed for the pressure transducers, displacement values for the displacement gauges, and stress and strain values for the strain gauges.

3.6 Test Procedure

3.6.1 Installation of Specimen

3.6.1.1 Specimen Placement and Preparation

Lifting hooks were inserted in each specimen and the specimen was lifted by these hooks to a vertical position with the overhead crane. It was then transferred to a position near the test set-up. The steel blocks that provided the base for the specimen were placed and the gaps filled with hydrostone. A boundary was made around the edge of the blocks with duct tape and sealed with silicone caulk. Before the specimen was placed on the steel blocks, an approximately 0.6 cm (0.25 in.) thick layer of hydrostone was poured over the top of the steel blocks.

When the specimen was in place, it was painted with whitewash so cracks could be identified more easily. A grid was drawn on the specimen to indicate where cracks were to be measured, as shown in Figure 3.23. Horizontal lines were drawn on each side of the overhang and joint at 7.6-cm (3-in.) intervals, with an extra line at 3.8 cm (1.5 in.) from the top. On the column (beneath the joint), horizontal lines were drawn every 10.1 cm (4 in.). Vertical lines were drawn at 10.1-cm (4-in.) intervals, except for the first line, which was at 5.1 cm (2 in.) from the outer face.

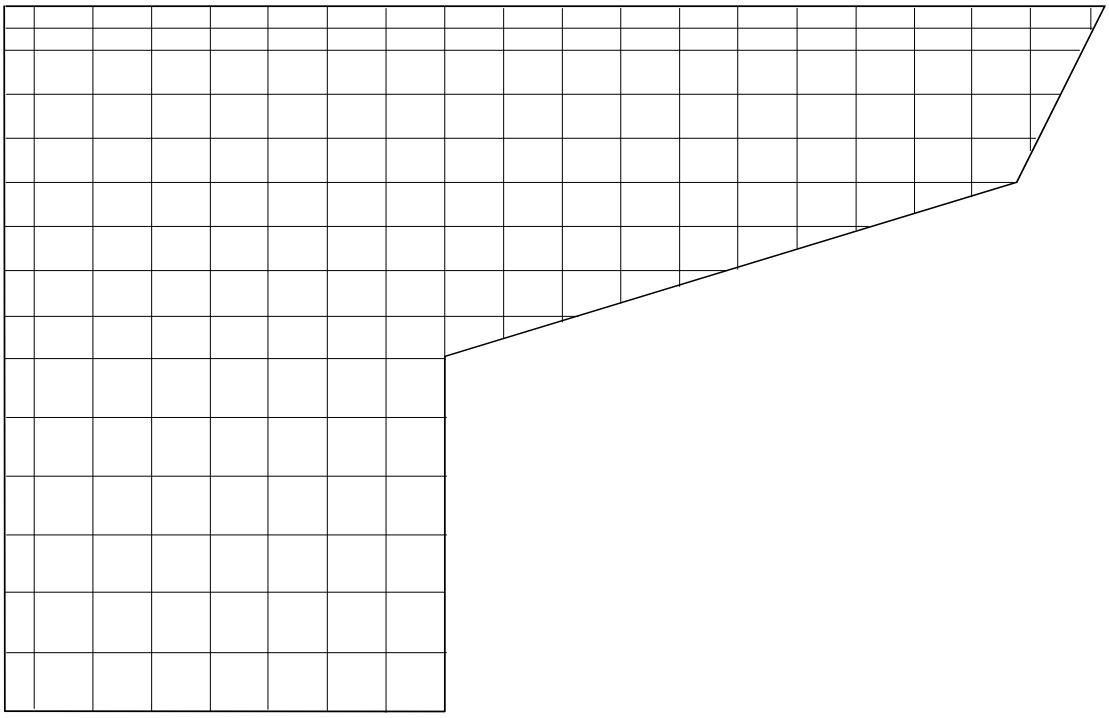

Figure 3.23 Grid Lines on Specimen

3.6.1.2 Tie-Down Attachment

After the specimen was in place, 2.54-cm (1-in.) diameter, high-strength threaded rods were screwed into the floor and W 12 x 65 beams, with appropriate holes in their flanges, were lowered over the rods until they neared the top of the specimen footing. Silicone caulk was used to form a berm at each end of the footing, to retain hydrostone that was placed before the hold-down beams were lowered the remainder of the way and leveled. After that hydrostone had cured, the twelve rods holding the beam at the back of the specimen were post-tensioned to a stress of 241 MPa (35 ksi), for a total force of 124 kN (28 kips) per bolt.

3.6.1.3 Gauge Installation

When the specimen was in place, a secondary framework was installed to support the displacement gauges, which were then attached. Strain and displacement gauges were connected to the data acquisition system and the system was checked to ensure that the gauges and channels were all functioning properly. The gauges were then zeroed and the test was started.

3.6.2 Static Load Steps

Loads were applied to the specimen in increments. Loading to dead load was divided into 20 steps. For these, each ram was loaded equally, because the dead load from the superstructure would be divided evenly between the bearings. Strain gauges, displacement gauges, and pressure transducers were read (scanned by the computer) at each step. Every two or three steps, the specimen was examined for cracks. All post-tensioning was performed at one-half dead load. After dead load was reached, the additional load required to reach service load was divided into 14 steps. After service load was reached, the load was reduced to dead load levels and again brought up to service load, at which point the tests of unrepaired specimens were concluded. For repaired specimens, loading was continued using the same increments as before, until loading equivalent to factored load divided by ϕ (FL / ϕ) was reached, or until failure or severe damage appeared imminent, whichever occurred first. When the final repair method for a specimen was tested, loading was continued until failure. Major load steps are listed in Table 3.5.

Table 3.5: Major Load Steps

Load Description	Load Factors	Ri		Ro	
		kN	(Kips)	kN	(Kips)
1/2 Dead Load	1/2 DL	146.6	32.9	146.6	32.9
Dead Load	DL	293.2	65.9	293.2	65.9
Dead Load + 1/2 Live Load	(DL + 1/2 LL)	312.3	70.2	345.9	77.8
Service Load	(DL + LL)	342.3	77.0	398.7	89.6
Dead Load + 2 Live Load	(DL + 2 LL)	391.5	88.0	504.2	113.4
Factored Load	(1.3 DL + 2.17 LL)	487.9	109.7	610.1	137.2
Factored Load / ϕ	(1.3 DL + 2.17 LL) / ϕ	542.1	121.9	677.8	152.4

3.6.3 Post-Tensioning Operation

For the post-tensioned specimen, the post-tensioning bars were tensioned after the specimen was loaded to one-half dead load. The stressing sequence was designed to prevent twisting of the overhang and excessive tensile stresses in either the top or bottom fibers. A 267-kN (60-kip) capacity hydraulic ram was used. The final tension desired in each bar was 620 MPa (90 ksi), or 123 kN (27.6 kips) per bar. Each bar was tensioned in increments of 7.0 MPa (1000 psi) on the ram, which produced about 21 kN (4.7 kips) of force in each bar, until approximately half of the desired tension was reached. After each bar had been tensioned halfway, the process was repeated, this time tensioning each to approximately 133 kN (30 kips). After all bars were tensioned, the average tension in each bar was approximately 110 kN (25 kips). However, all but three of the strain gauges were damaged during tensioning, so precise measures of final post-tensioning forces are unavailable. The tension in each bar after it had been stressed was estimated by lift-off tests. Bars tensioned earlier were stressed to higher tensions to compensate for losses incurred when later bars were tensioned. After all

bars were tensioned, grout was injected under pressure into each duct until the ducts were filled.

3.6.4 Crack Identification

Each specimen was examined for cracks every two or three load steps, depending on how much crack growth occurred during each step. For identification purposes, cracks on the north side were considered separately from those on the south side. On each side, cracks were divided into three groups: Pier (column) cracks, overhang cracks, and joint cracks. A crack was categorized depending on where it initiated, even if it crossed an interface afterwards. Cracks in each element were numbered in the same order in which they appeared.

When each crack appeared, a line was drawn alongside it with a felt-tip marker. A hatch mark was made at the point where the crack was no longer visible to the naked eye, and a number designating the current load step was written next to the mark. When a crack lengthened, the line was extended and the number of the new load step was noted.

3.6.5 Strain and Displacement Measurements

Strain and displacement measurements were collected at every load step. The voltage changes measured were stored and printed by the computer. Printouts also included calculated displacement, pressure, load, stress, and strain values as appropriate for each gauge.

3.6.6 Crack Width Measurements

The width of each crack was measured to the nearest .013 mm (0.0005 in.) wherever it crossed a grid line approximately perpendicularly. For example, if a crack started at the top of the overhang and extended approximately vertically downward, its width would be measured at every point that it crossed a horizontal line. These measurements were taken at various loads during the test: one-half dead load, dead load, dead load plus one-half live load, service load, and dead load plus twice live load. Because dead load, dead load plus one-half live load, and service load were each reached twice during the loading sequence, crack widths were measured both times.

3.6.7 Photographs

Thirty-five mm slides were taken of the specimen at one-half dead load, dead load, dead load plus one-half live load, service load, dead load plus twice live load, factored load, factored load / ϕ, and ultimate load. Photographs were taken of the overall specimen from both sides, with close-ups of the column, overhang, and joint regions and any other areas of particular interest.

3.6.8 Completion of the Tests

The initial tests on unrepaired specimens were to be continued to service loads, unless failure appeared imminent at a lower load. If the specimens were too badly damaged during the initial tests, repairing them would not be feasible. The prestressed specimen was tested to service loads, at which time the test was halted. Loading was then reduced to one-

half dead load, because complete unloading would have produced cracking in the bottom of the overhang due to the prestressing force.

The reinforced concrete specimen had not yet reached service loads when it began to deflect substantially with no increase in load. The test was stopped at this point, and the dead load/service load cycle was not attempted. The specimen was unloaded completely.

Tests on repaired specimens were continued to factored load / ϕ, except for the last test on each specimen, which was continued until failure occurred.

CHAPTER 4

REPAIR METHODS

4.1 Introduction

After the effects of the reinforcement detailing flaw in the bents had been determined, it was apparent that several bents supporting the San Antonio Y superstructure were unsafe in their existing state. New details were devised by Wood in a related study [Ref. 3], for use in future similar situations. However, replacing the existing bents with new, improved bents would be extremely difficult and expensive. Therefore, it was necessary to design methods for retrofitting the bents, to enable them to carry their full design loads, without completely disrupting traffic.

4.2 Prestressed Concrete Specimen

4.2.1 External Vertical Post Tensioning (POJ-PS-100-RP1)

4.2.1.1 Concept

Because the bents with a post-tensioned overhang experienced no distress in the overhang, it was only necessary to develop a method for effectively connecting the column to the joint. As a result, various methods of vertical post-tensioning were considered. Extreme reinforcement congestion made the prospect of drilling into the column risky, because damage to existing reinforcement could result. A system of external post-tensioning was therefore developed.

4.2.1.2 TxDOT Design

The Texas Department of Transportation (TxDOT) developed a possible retrofit design (Figure 4.1). It involved drilling horizontally through the column to accommodate bolting a steel plate assembly on each side. The steel plate assemblies included vertical stiffeners and smaller horizontal plates to form the lower anchorage for post-tensioning bars. A stiffened beam would rest on top of the joint and project out beyond the sides of the bent to provide the upper anchorage for the post-tensioning bars. Stiffened side pieces were attached to the top beam to provide additional moment capacity to the beam. Eight 3.49-cm (1-3/8-in.) post-tensioning bars would be installed on each side, with space available for four additional bars if necessary.

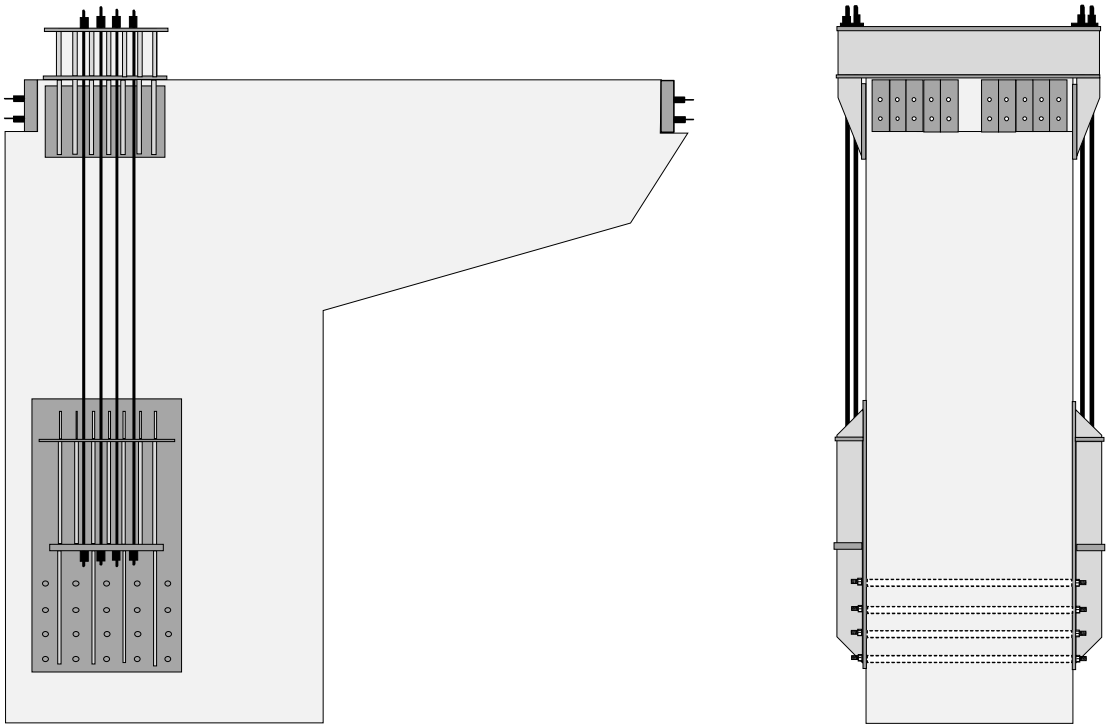

Figure 4.1 TxDOT Design for External Vertical Post-Tensioning [From Ref. 3]

4.2.1.3 Scaled and Modified Design

The TxDOT design was scaled down to the size of the test specimens. Because specimens were not exact scale models of the full-size bents, there were some difficulties encountered in attempting to duplicate the retrofit design. In particular, because the small-scale column was relatively narrow, and because the post-tensioning bar end hardware required more space than direct scaling would provide, a reduced number of post-tensioning bars had to be used to maintain the same relative location of the resultant post-tensioning force. Six 1.59-cm (5/8-in.) diameter post-tensioning bars were therefore used on each side of the column. Vertical stiffeners on the plates attached to the side faces of the column were designed to transfer forces from the post-tensioning bars into the side plates. The scaled, and slightly modified, design is shown in Figure 4.2.

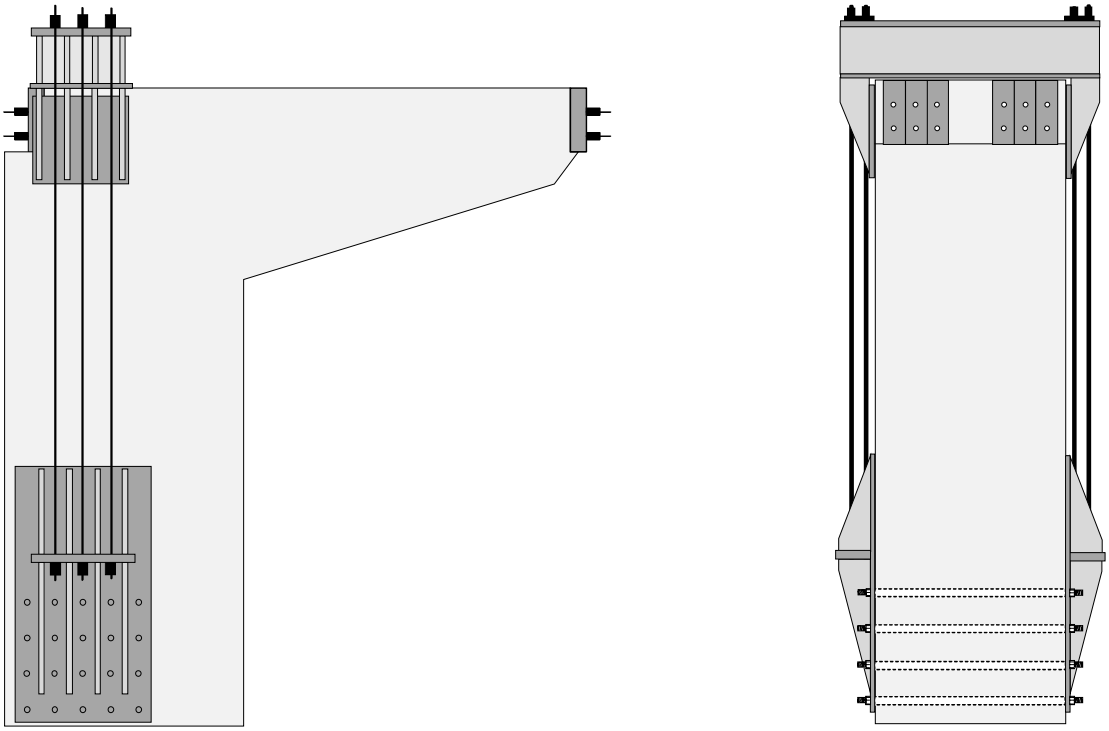

Figure 4.2 Scaled, Modified Design for Specimen [From Ref. 3]

The stiffened beam on the top of the joint was designed for moment and shear, although design was ultimately controlled by deflection. If the beam was too flexible, the ends would deflect downward under the post-tensioning force. Extreme beam deflections would concentrate compressive forces on a small area of concrete near the edges of the specimen, possibly resulting in spalling of the side-face cover. The stiffeners at the ends of the beam were designed to resist the compression forces from the post-tensioning, while bearing plates were used to transfer the forces to the stiffeners. The side pieces attached to the bottom of the beam (see Figure 4.2) were intended to help resist moment, but their effectiveness would be determined by the actual fabrication. Because the beam was designed to be very stiff, a slight gap between the side pieces and specimen would prevent the side

pieces from resisting any moment. The actual effectiveness of the side pieces could not be determined until the stiffened beam was installed on the test specimen and subjected to load.

The layout of holes in the side plates was intended to minimize the likelihood of encountering column steel when drilling through the specimen. The spacing of vertical stiffeners was designed to allow sufficient access to the nuts on the transverse bolts. Stiffeners on the side plates were evaluated for moment and compression, but their length was controlled by shear transfer through the welds. Thickness of the horizontal plate supporting the post-tensioning bars was determined by moment and shear calculations. The side plates were designed considering fracture through the net section and bearing stresses from the bolts. The transverse bolts themselves were evaluated for combined shear and tension.

4.2.1.4 Details

The top beam (Figure 4.3) consisted of four vertical plates 82.6 x 15.2 cm (32.5 x 6 in.) attached to a top and bottom plate, each 82.6 x 30.5 cm (32.5 x 12 in.). Bearing stiffeners, 15.2 x 7.0 cm (6 x 2.75 in.), were inserted between the vertical plates at the ends of the beam to provide additional bearing area to support the post-tensioning bars. Side pieces, (below the beam) each consisting of four 30.5-cm (12-in) stiffeners, connected to a 30.5-cm (12-in.) square plate, were attached to the ends of the beam to provide additional flexural rigidity. All vertical plates and stiffeners were 1.91 cm (0.75 in.) thick, as was the top plate, while the other plates were 1.3 cm (0.5 in.) thick. Dimensions of the top beam assembly are shown in Figure 4.3.

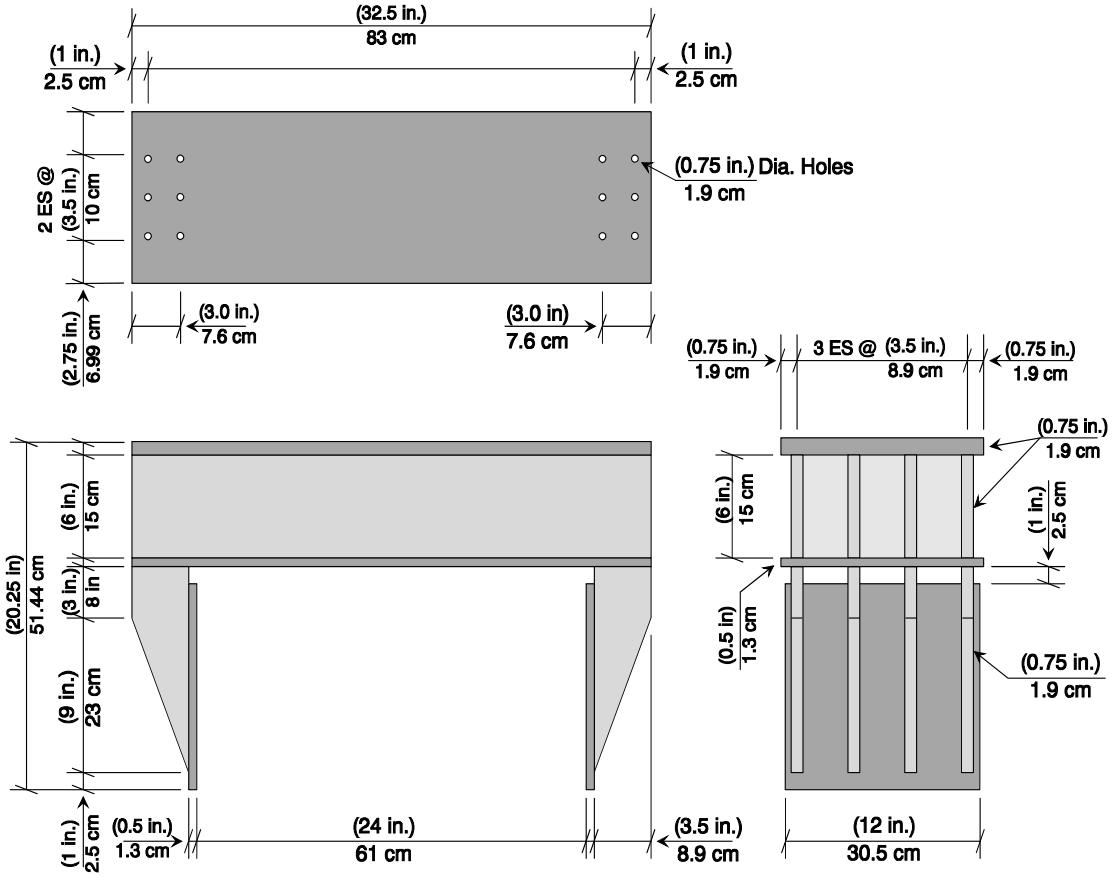

Figure 4.3 Dimensions of Top Beam Assembly [From Ref. 3]

Each side plate assembly consisted of a 43 x 81.3 x 1.3 cm (17 x 32 x 0.5 in.) plate with a horizontal 2.5-cm (1.0-in.) thick plate located approximately 31.3 cm (12.5 in.) from the top edge to support the post-tensioning bars. The horizontal plate, in turn,was supported by 10.2-cm (4-in.) deep triangular vertical stiffeners, four each above and below. The upper stiffeners were 29.2 cm (11.5 in.) long, while the lower stiffeners were 42 cm (16.5 in.) long. All stiffeners were 1.9 cm (0.75 in.) thick and were welded both to the side plate and to the horizontal plate. Side plate dimensions are shown in Figure 4.4.

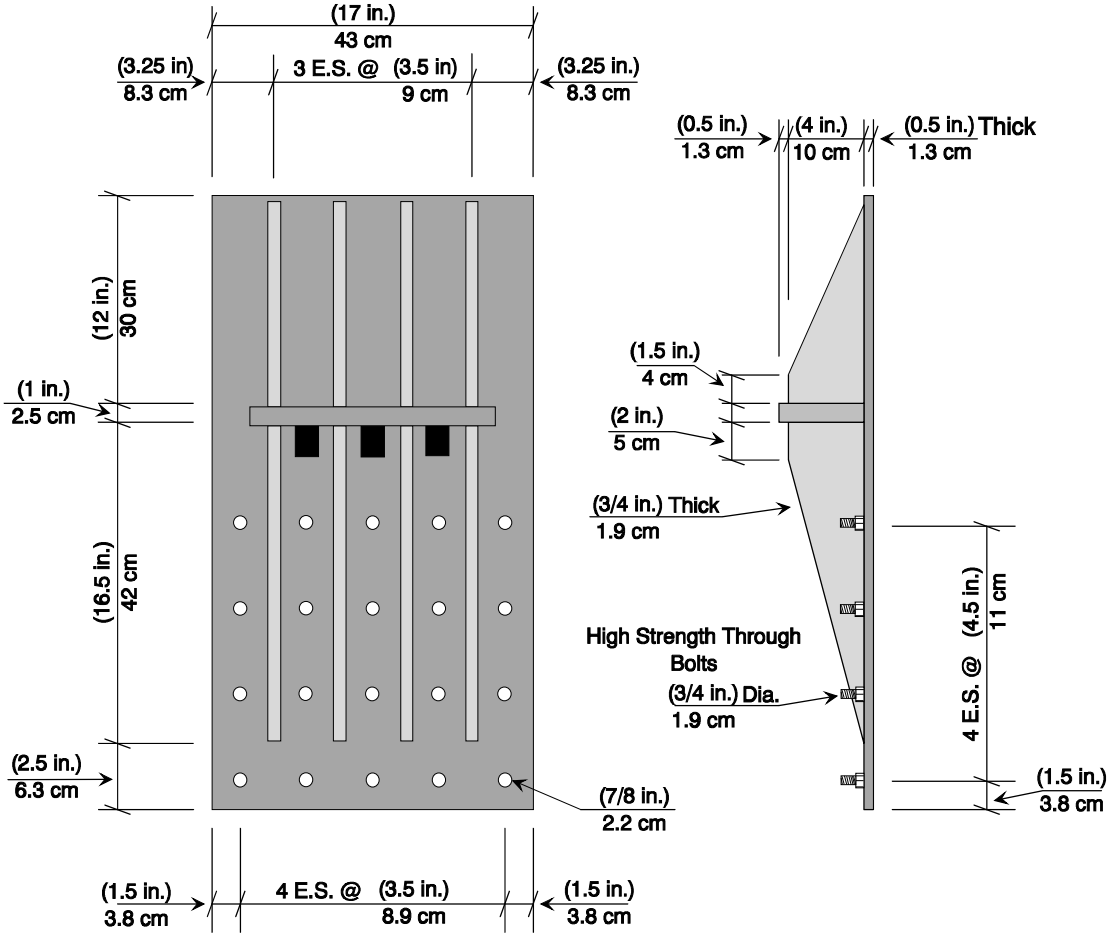

Figure 4.4 Dimensions of Side Plate Assemblies [From Ref. 3]

4.2.1.5 Materials

All plates and stiffeners were fabricated using Grade 50 steel. Post-tensioning bars were 1.59-cm (0.625-in.) diameter Dywidag bars, similar to those used to post-tension the overhang. Ultimate strength of the bars was approximately 965 MPa (140 ksi), and a tensile test of a representative bar is shown in Figure 3.15. All plates were welded with 0.64-cm (0.25-in.) welds, using an E60 electrode.

4.2.1.6 Fabrication

Holes were carefully measured, marked and drilled in the steel plates. The triangular stiffeners were cut and ground to the proper sizes. Upper stiffeners on the side plates were welded to the plates so that the bottom edges were aligned. The horizontal plates were then welded to the upper stiffeners, and the lower stiffeners were welded to the horizontal and vertical plates.

For the top beam assembly, the four vertical plates of the top beam were welded to the top plate with fillet welds on both sides. Because the sides of all vertical plates were not accessible for welding once the bottom plate was in place, fillet welds could not be used to attach the bottom plate. Instead, 1.3-cm (0.5-in.) diameter holes were drilled in the bottom plate along the center lines of the stiffeners at a spacing of 11.5 cm (4.5 in.), and the bottom plate was plug welded to the vertical plates. Stiffeners on the side pieces of the top beam were welded to their plates, then the assembled side pieces were welded to the top beam.

4.2.1.7 Installation

In order to precisely align the holes in the specimen with holes in the side plates, hole locations for both the steel and concrete were carefully measured and marked. The holes in the concrete were drilled slightly oversized from both sides of the pier with a coring drill to ensure proper alignment for both plates. The threaded bars were inserted through the specimen and the plates were lifted into place on the bars. The two washers used between each nut and side plates were split on one side so grout could be injected into the holes after the nuts were tightened. It would have been impractical to inject the grout and then bolt the plate on afterwards because the grout would leak out of the holes and possibly set before the bars could be tensioned.

After the side plates were secured in place, the holes were grouted. The grout used consisted of the same mix design as that used in the overhang (Table 3.3). It was injected under approximately 280 MPa (40 psi) pressure through the opening in the washers until it flowed from the opening in the washers on the other side of the specimen. After the grout had cured, the sides and bottom edges of the steel plates were sealed with silicone, and hydrostone was injected between the specimen and the plates to fill any gaps caused by plate warping or surface irregularities on the concrete.

The top beam assembly was lowered into place on top of the specimen with a crane. Any gaps between the end stiffeners and the sides of the specimen were filled with hydrostone as described above. All steel plates were whitewashed to indicate yielding of the steel during testing. The post-tensioning bars were slid through the holes in the top plate until the lower ends reached the holes in the side plates. Dywidag nuts were threaded onto the bottom of the bars, with 1.3-cm (0.5-in) thick steel bearing plates between the nuts and the plate. Nuts were threaded loosely onto the upper ends of the bars in preparation for post-tensioning.

Strain gauges were attached to the Dywidag bars and at various points on the top beam and side plates, as shown in Figure 4.5, to assist in evaluating their behavior. Frames were built to hold displacement gauges for measuring the movement of the plates and bolts. The locations of the displacement gauges are shown in Figure 4.6.

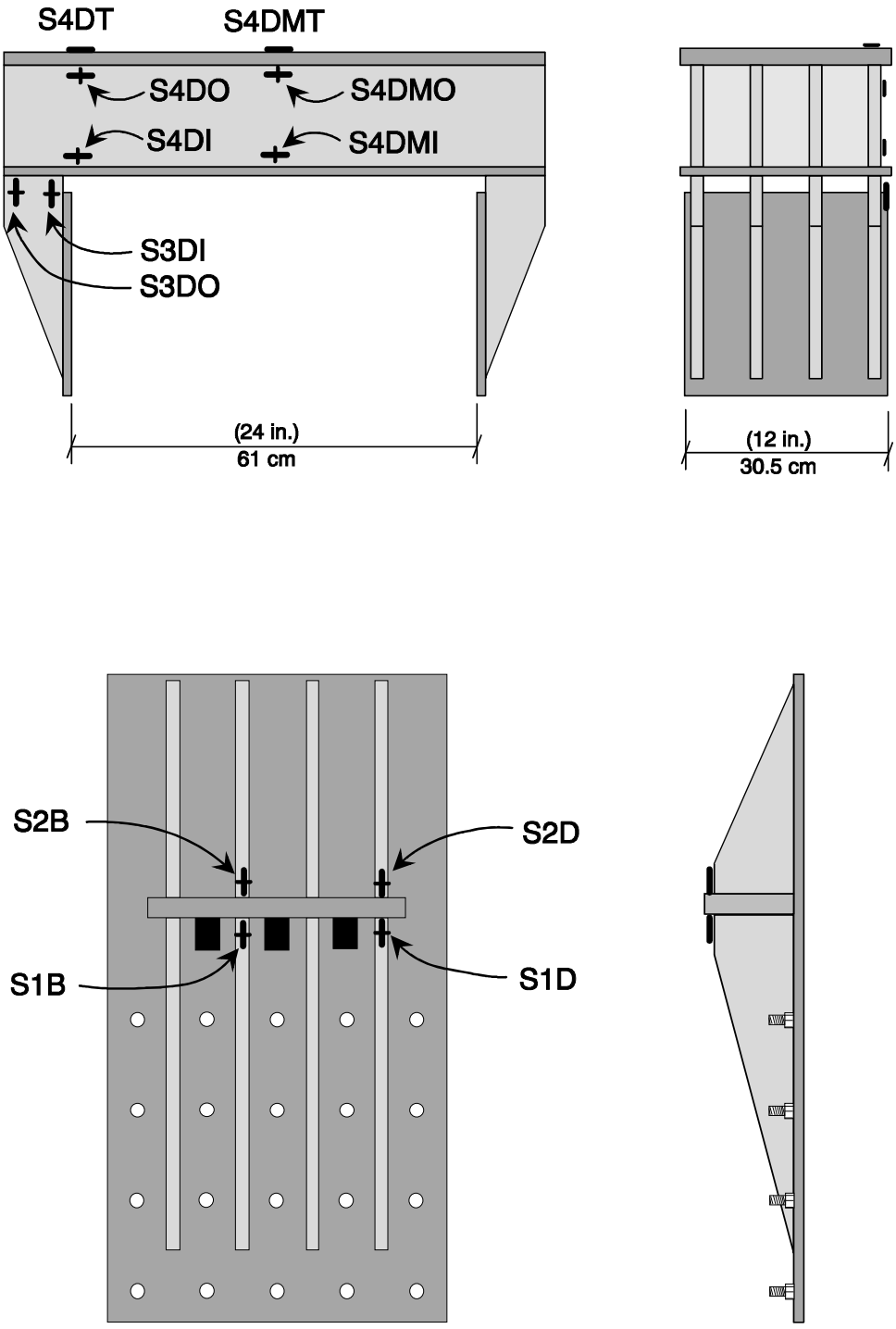

Figure 4.5 Locations of Strain Gauges on Repair Components [Modified from Ref. 3]

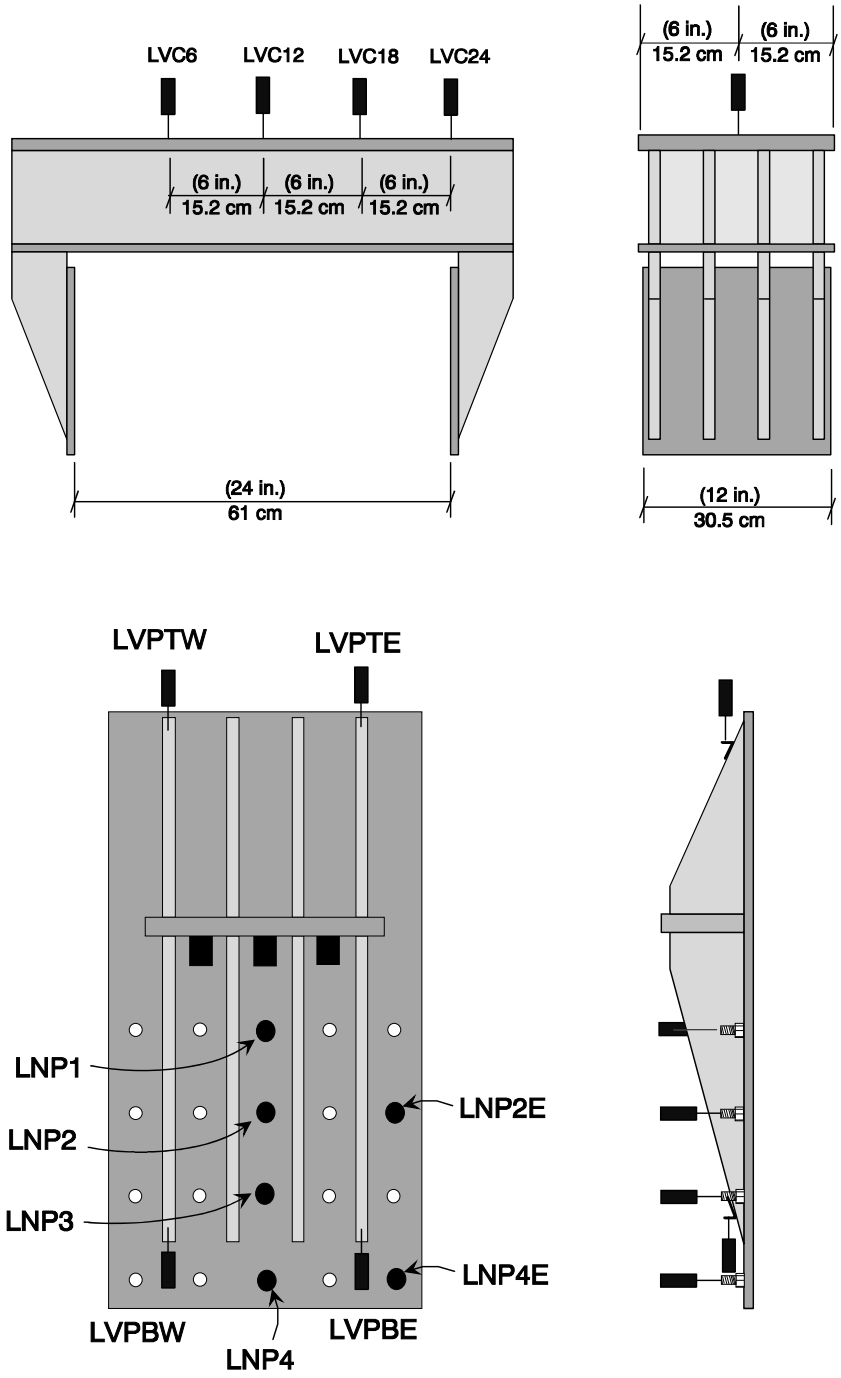

Figure 4.6 Locations of Displacement Gauges on Repair Components [Modified from Ref. 3]

4.2.1.8 Test Procedure

The repair components were attached to the specimen while one-half dead load was maintained. The post-tensioning bars were then stressed in several increments. The stessing sequence in shown in Figure 4.7. Stressing was repeated three times to ensure that the bar forces were as consistent as possible. Strain and displacement readings were taken at each stressing increment. Crack widths were measured before and after post-tensioning. The specimen was then loaded incrementally to dead load, at which point crack widths were measured again. Cracks were marked on the specimen every two or three load steps. Because cracks from the initial test were marked in red, the new cracks and extensions of old cracks were marked in green, to differentiate. The test continued in the same manner as the initial tests, but all major load steps were achieved, including the cycle from service load to dead load, to service load again, as shown in Table 4.1. Factored load divided by ϕ (FL / ϕ) was successfully achieved.

Figure 4.7 Stressing Sequence for External Vertical Post-Tensioning Bars

Table 4.1 Loading Sequence [From Ref. 3]

Stage	Condition
1	1/2 Dead Load
2	Post-Tensioning
3	Dead Load
4	Dead Load + 1/2 Live Load
5	Service Load
6	Dead Load
7	Dead Load + 1/2 Live Load
8	Service Load
9	Dead Load + 2 Live Load
10	Factored Load
11	Factored Load / ϕ

4.2.2 Modified External Vertical Post Tensioning (POJ-PS-100-RP2)

4.2.2.1 Rationale and Design

Because the specimen performed quite well, it was decided to reduce the number of post-tensioning bars to four on each side and test the specimen to failure. Because the side plates and cap beam had been designed for the ultimate force produced by six bars per side, they were more than adequate for the force which could be produced by four. Therefore, no additional calculations were necessary for the repair.

4.2.2.2 Details

The details of this repair were identical to those used in the previous method, except that the two end post-tensioning bars in the outer row on each side of the specimen were removed, leaving the inner row of three bars plus the center bar of the outer row on each side. The new bar layout is shown in Figure 4.8.

Figure 4.8 Modified Bar Layout for External Vertical Post-Tensioning

4.2.2.3 Test Procedure

The test procedure was identical to that used in the previous test, except that the loading was not stopped at FL / ϕ, but continued until the overhang deflection curve became flat (nearly zero slope). The post-tensioning bars were again stressed while one-half dead load was maintained on the specimen. The new cracks and crack extensions were marked in purple to distinguish them from cracks marked during the previous two tests. Loading was continued until approximately 1.25 times factored load was achieved, at which point the specimen was unloaded in several stages.

4.3 Reinforced Concrete Specimen (POJ-RC2)

4.3.1 External Diagonal Post Tensioning (POJ-RC2-RP1)

4.3.1.1 Concept

Unlike the bents with prestressed overhangs, reinforced concrete bents required strengthening of the joint in both the horizontal and vertical directions. This could be done by adding horizontal and vertical post-tensioning. The concept behind the strengthening method investigated here was to combine the effects of both horizontal and vertical post-tensioning by using diagonal post-tensioning. Using this approach, the external post-tensioning force would be more nearly perpendicular to the critical section, increasing its effectiveness and permitting the use of fewer post-tensioning bars (Figure 4.9).

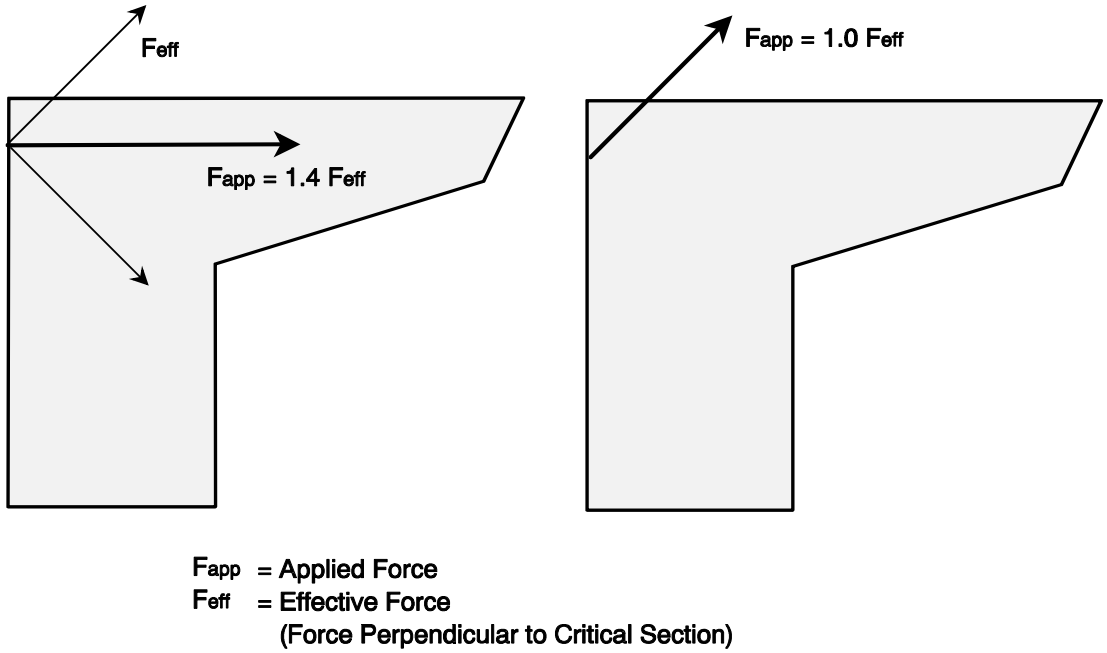

Figure 4.9 Effective Applied Force from Horizontal and Diagonal Post-Tensioning Bars

The bars would be attached to the specimen by attaching them to a cross beam welded at an angle to plates bolted to the top and back faces of the specimen (Figure 4.10). The anchor bolts resist the forces from the shear components of the post-tensioning, while the specimen resists the compressive components. In addition, the normal forces on the specimen produce a frictional force which reduces the shear component of the force, so fewer bolts can be used (Figure 4.11).

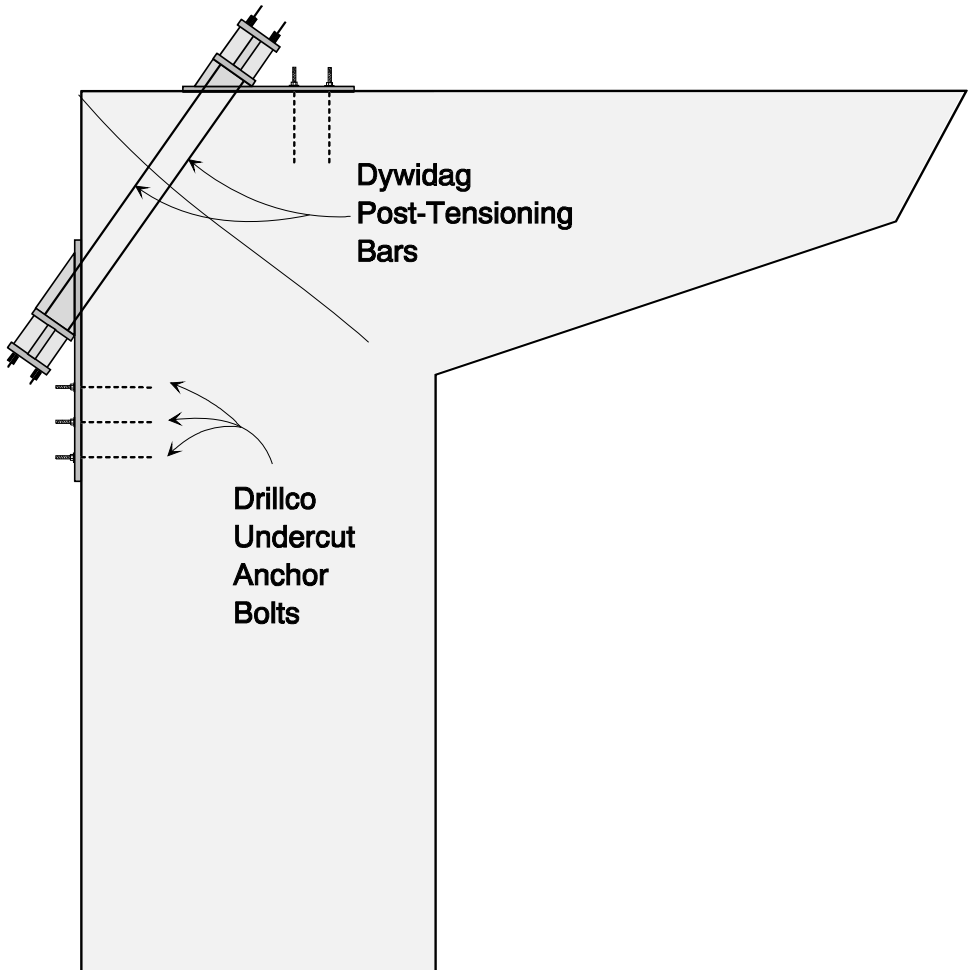

Figure 4.10 Layout of External Diagonal Post-Tensioning [From Ref. 3]

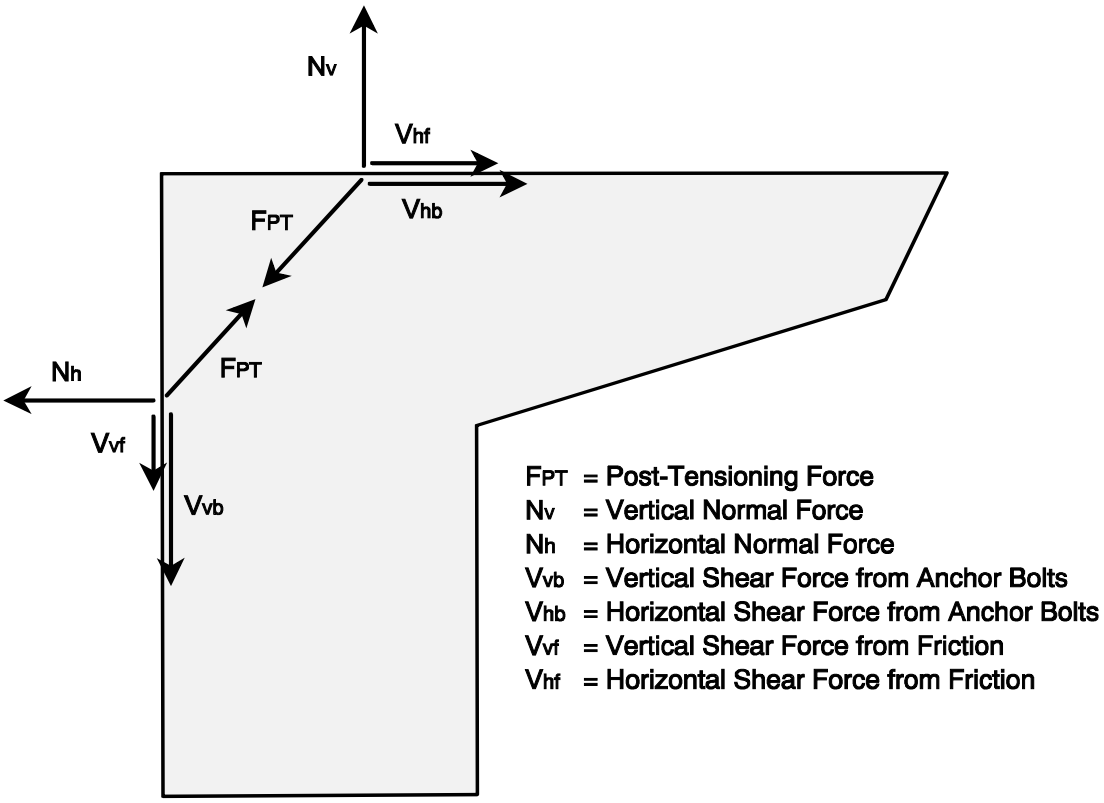

Figure 4.11 Normal and Shear Forces Produced in the Specimen by Diagonal Post-Tensioning

4.3.1.2 Design

The design of the plates depended on the force produced by the post-tensioning bars, which in turn was determined by the length of the moment arm between the bars and the concrete compression zone. While increasing the distance between the compression block and the post-tensioning bars decreased the force required, the distance was limited by the required development lengths of column and overhang reinforcement. If the plates were connected too close to the ends of the reinforcing bars, a crack could form at the edge of the plates, resulting in too little embedment beyond the crack to develop the mild steel (Figure

4.12). To prevent this, the line of bolts farthest from the outer corner of the joint had to be more than the development length of the appropriate bars away from the corner.

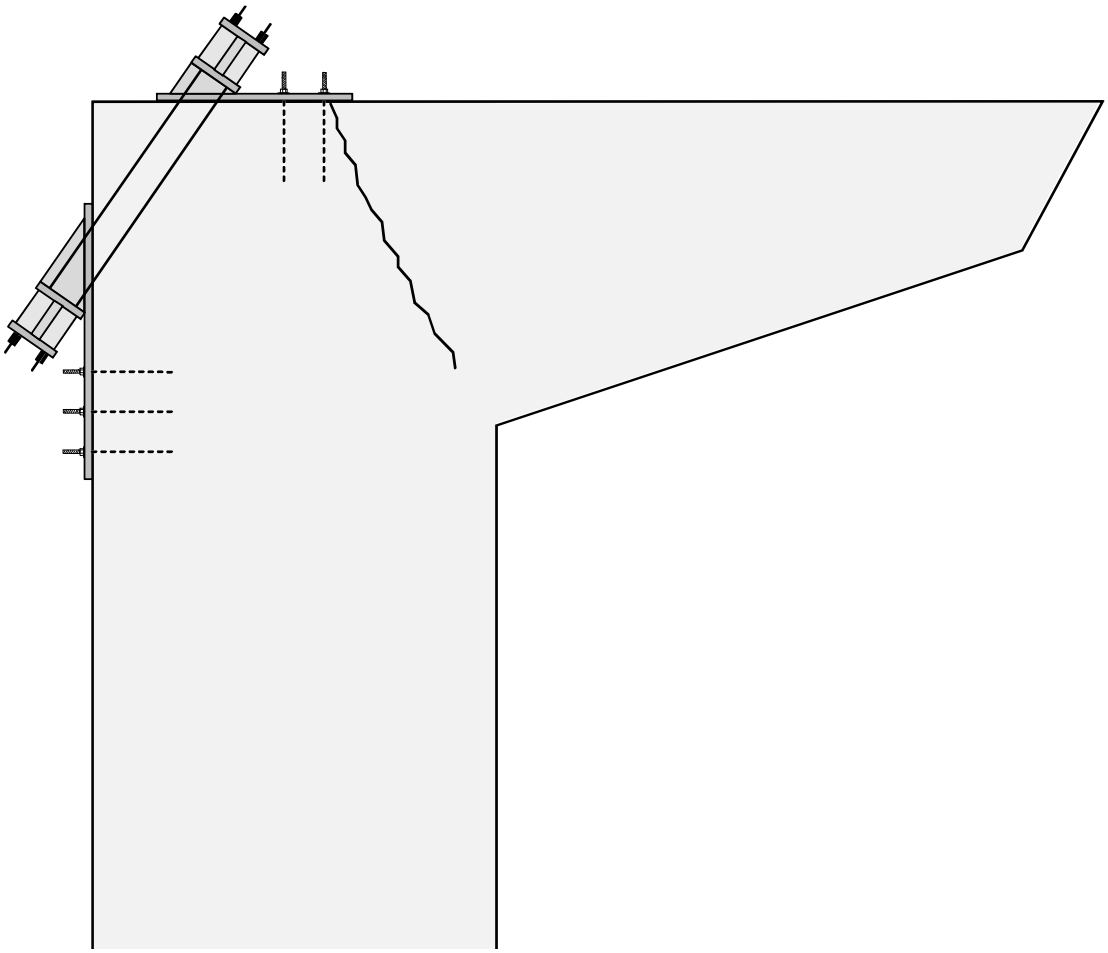

Figure 4.12 Crack at New Critical Section

In addition, the post-tensioning bars had to be as far as possible from the concrete compression zone for maximum efficiency. This could be accomplished by lengthening the plates so the bars would be much closer to the corner than the bolts (Figure 4.13). However,

lengthening the plates would require more materials and expense. Furthermore, the shorter post-tensioning bars that would result would incur higher seating losses during the post-tensioning operation. A minimum length was considered necessary to maintain a reasonable amount of prestress in the bars. The inclination of the bars would also affect their efficiency, because only the component of force perpendicular to the expected crack would add to the moment capacity of the connection.

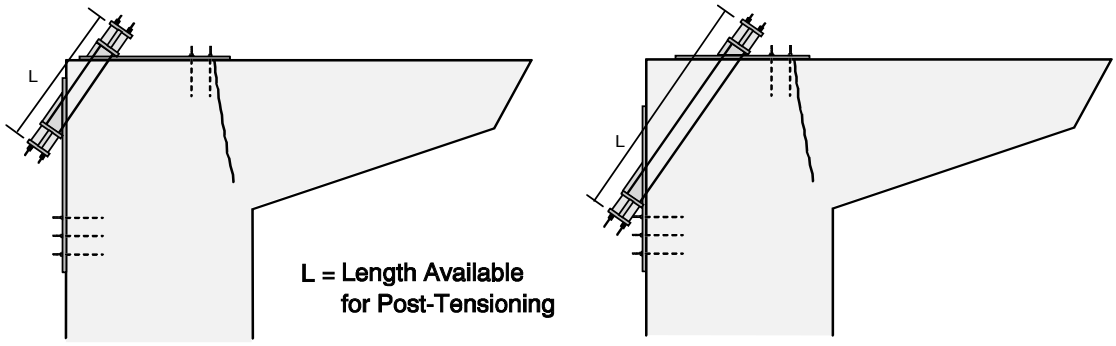

Figure 4.13 Effect of Plate Length [Modified from Ref. 3]

When all these factors were considered, it was decided to dimension and position the plates and bars as shown in Figure 4.14. At that location, the required post-tensioning force was calculated to be 683.1 kN (153.6 kips), which could be provided by 3.6 1.59-cm (0.625-in.) diameter Dywidag bars. The cross beams and plates were therefore designed to resist the ultimate strength of four bars, or 747 kN (168 kips). The number of anchor bolts necessary was determined by calculating the shear component of that ultimate force, and subtracting the frictional force, which was equal to the normal component of force multiplied by a frictional coefficient of 0.4.

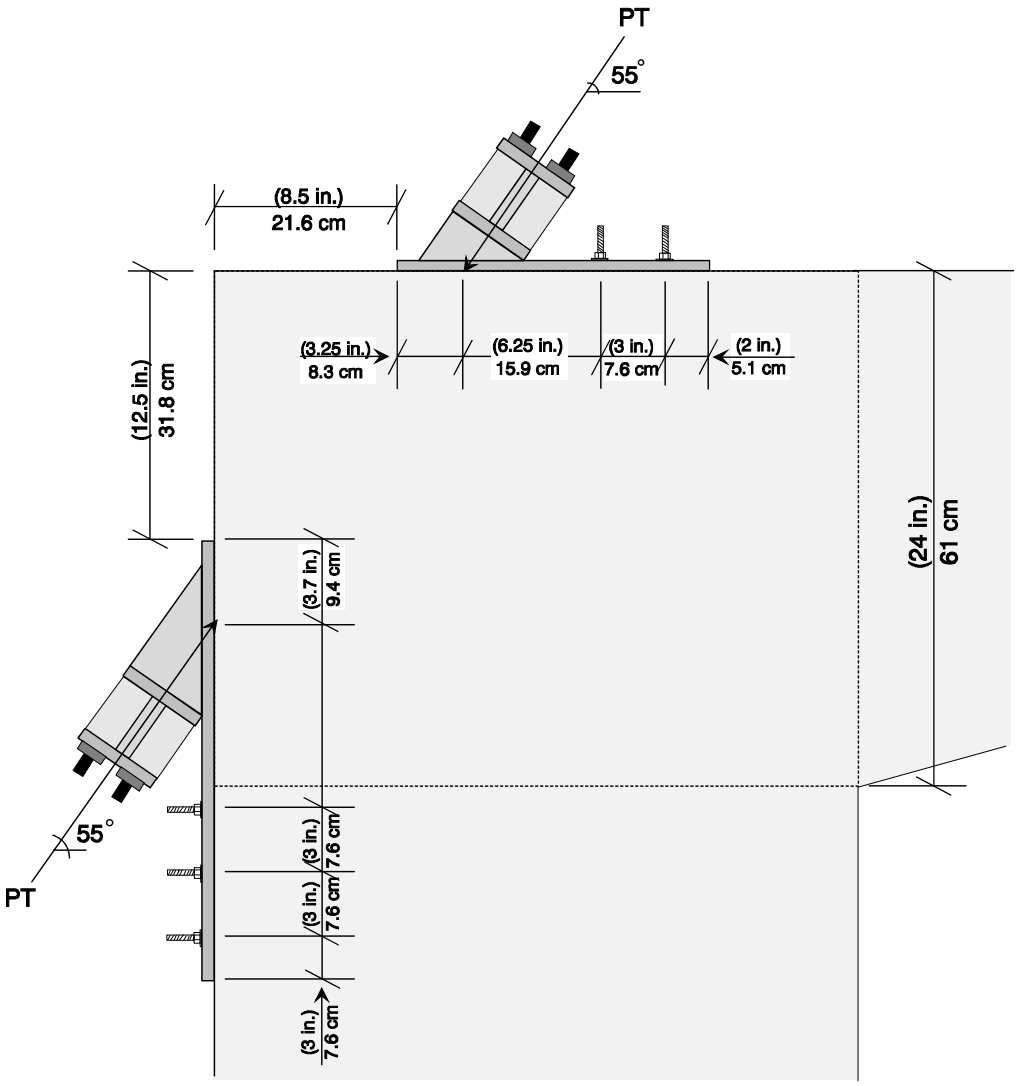

Figure 4.14 Plate Size and Position for External Post-Tensioning System [Modified from Ref. 3]

The anchor bolts were designed to resist the shear forces from the post-tensioning, minus the frictional component. The plates were designed to resist bearing stresses from the anchor bolts and fracture across a net section involving a line of bolt holes. The beams were

designed to resist moment and shear from the post-tensioning, while the stiffeners were designed for bearing forces. Welds were designed to transfer shear.

4.3.1.3 Details

The flanges of the cross beams were 77.5 x 10.2 cm (30.5 x 4 in.) steel plates. The flange plates were welded to a 77.5 x 7.6 cm (30.5 x 3 in.) web, and bearing stiffeners, at the ends where post-tensioning bars were anchored, were welded to the web and flange. The edge of one flange of each cross beam was welded to the base plate that would be attached to the specimen. The bottom of the same flange was welded to vertical triangular plates which in turn were welded to the base plates. Stiffeners were welded perpendicular to the cross beams between the vertical triangular plates. All steel was 1.3 cm (0.5 in.) thick, except for the triangular plates and the web of the beam, which were 1.9 cm (0.75 in.) thick because they were required to resist large compressive forces. The details are shown in Figs. 4.15 and 4.16.

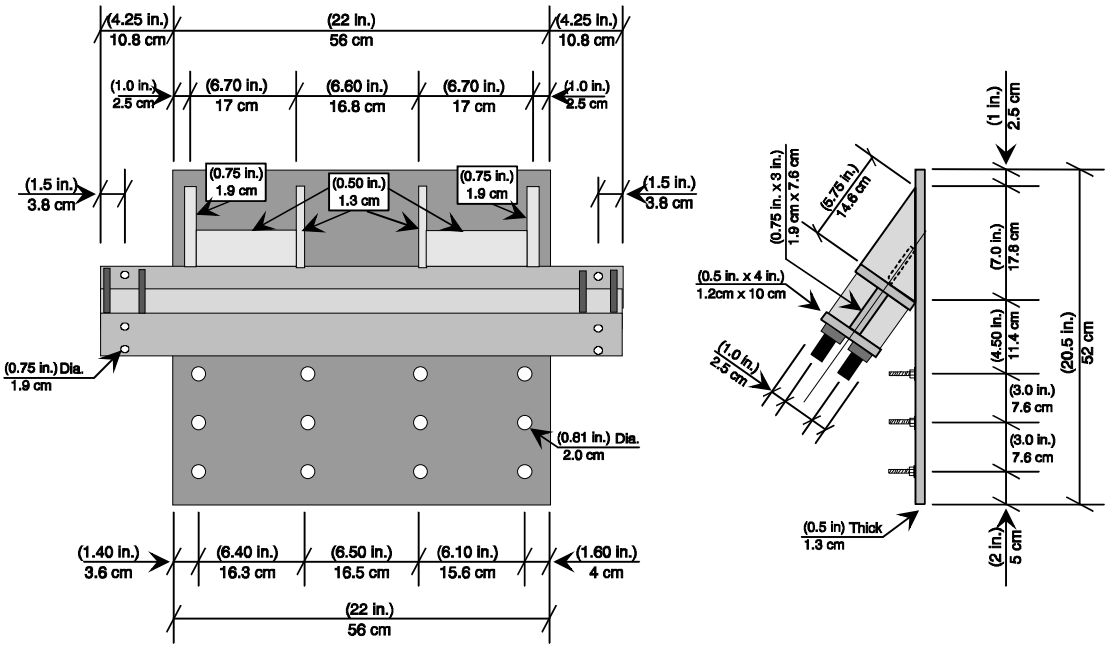

Figure 4.15 Details of Side Plate Assembly for External Diagonal Post-Tensioning [From Ref. 3]

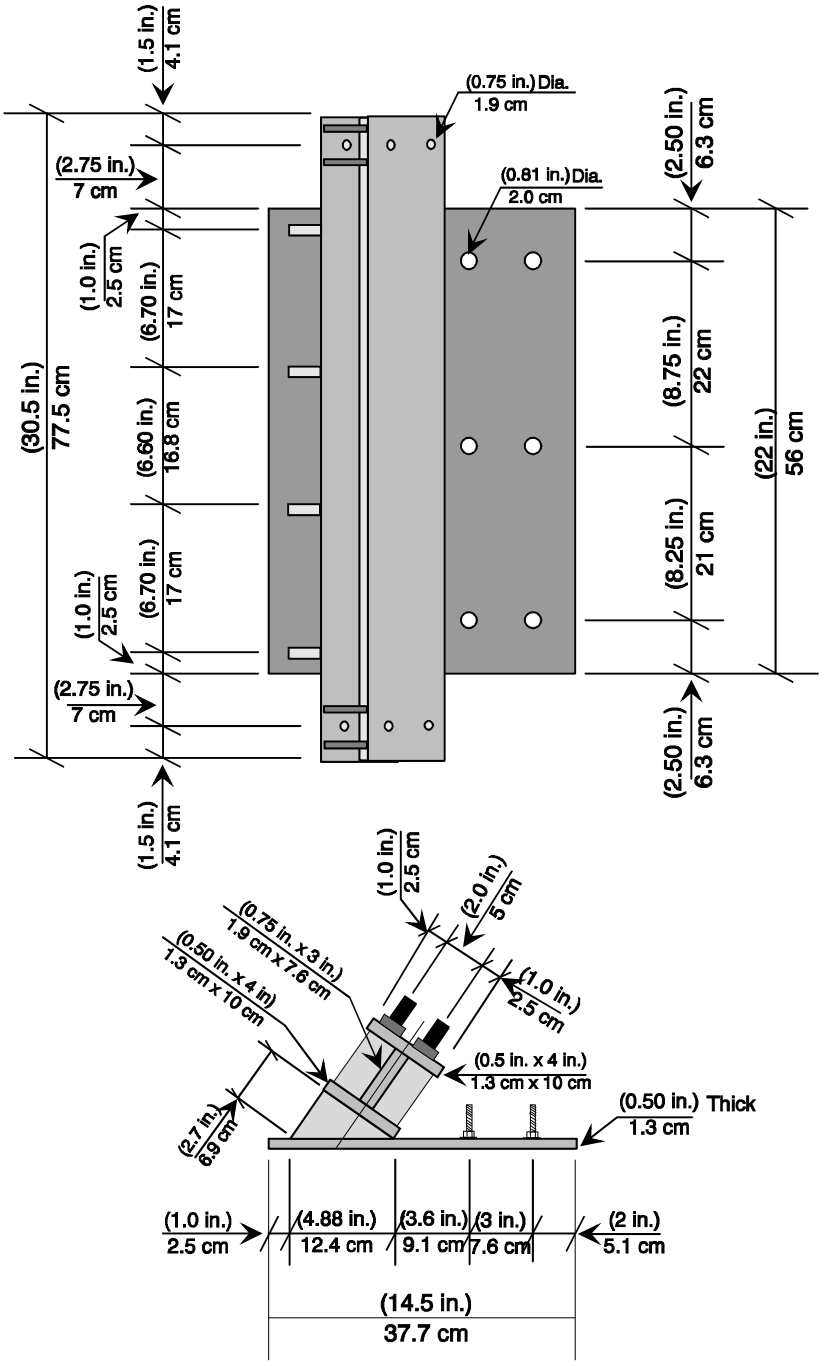

Figure 4.16 Details of Top Plate Assembly for External Diagonal Post-Tensioning [From Ref. 3]

The optimum position of the post-tensioning bars was 35 degrees from vertical. That angle produced a larger normal force on the top face of the joint and a larger shear on the back face. Because of its larger shear and lower normal force, which resulted in a lower frictional force to offset the shear, the back plate required 10 anchor bolts, while the top plate required only six. The forces due to post-tensioning and the reactions of the concrete and anchor bolts are shown in Figure 4.17.

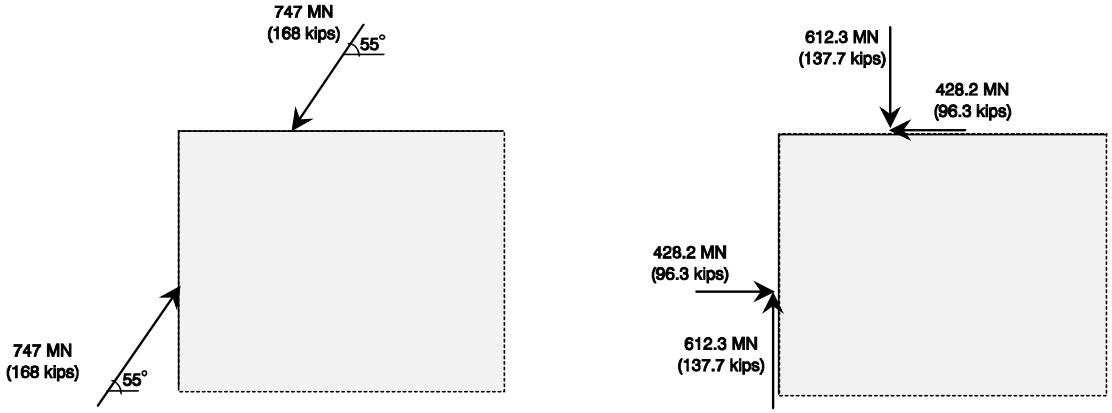

a) Post-Tensioning Forces

b) Resultants of Post-Tensioning Forces

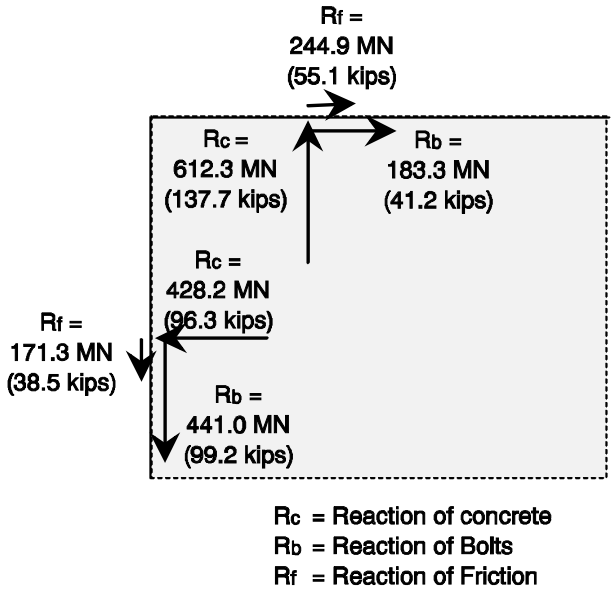

c) Reactions to Post-Tensioning Forces

Figure 4.17 Forces from Post-Tensioning Bars, Anchor Bolts, and Friction [Modified from Ref. 3]

4.3.1.4 Materials

All steel plates were Grade 50 with a nominal yield strength of 345 MPa (50 ksi) and an ultimate strength of 448 MPa (65 ksi). They were welded with 0.64-cm (0.25-in) welds, using an E60 electrode. Post-tensioning bars were the same as used in the previous repair, with a 1.59-cm (0.625-in.) diameter and an ultimate strength of approximately 965 MPa (140 ksi). Results of tensile tests are shown in Figure 3.15.

Anchor bolts were 12.7-cm (0.5-in.) diameter Drillco undercut anchor bolts with 1.90-cm (0.75-in.) diameter sleeves added to increase their area. The manufacturer's quoted ultimate tensile strength was 827 MPa (120 ksi), and a factor of 0.6 was used to estimate shear strength. Shear tests were performed on several bolts. An example of the results of one such test is shown in Figure 4.18. Based on these tests, a shear strength of 53.4 kN (12 kips) per bolt was used in design.

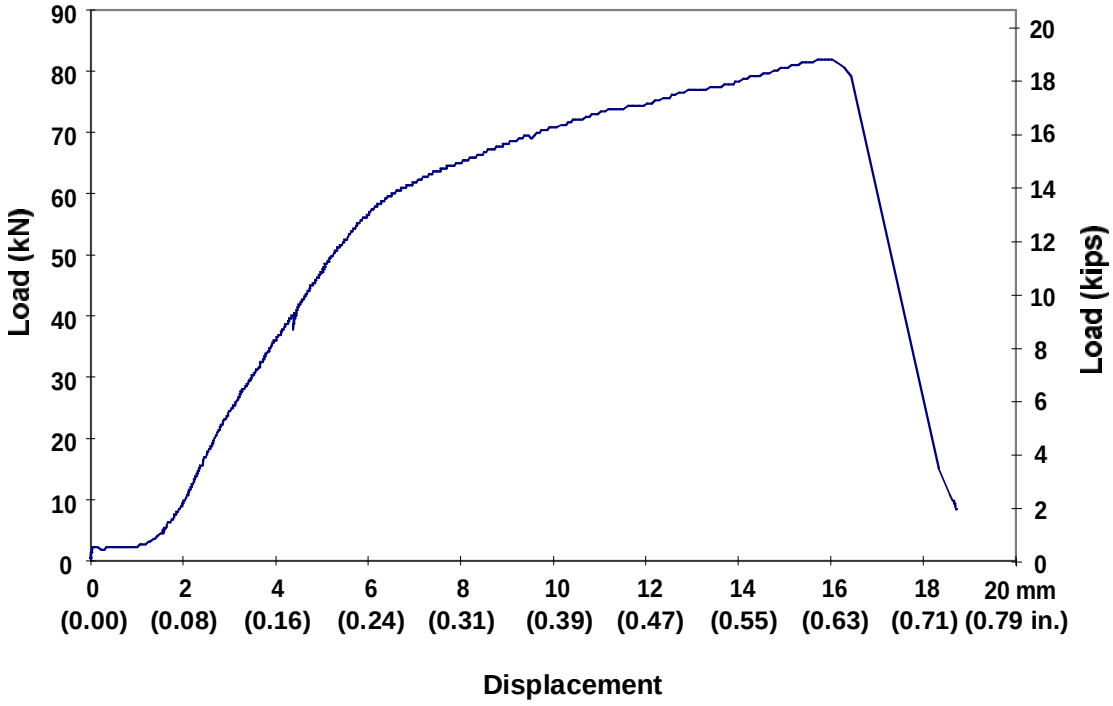

Figure 4.18 Example of Anchor Bolt Shear Test Results

4.3.1.5 Fabrication and Installation

Before installing the hardware for this repair method, the specimen was whitewashed to cover old cracks and crack markings. This way, new cracks could be marked independently of the previous tests, and measurements of existing cracks would indicate the amount of widening which occurred during the test. New grid lines were also drawn. The layout of the anchor bolts was complicated by the congestion and slight asymmetry in the main reinforcement of the column and overhang. Holes could not be drilled in a precisely symmetrical pattern without damaging the reinforcement. The exact position of the reinforcement was noted before casting the concrete because the bars were too closely spaced

to be located magnetically afterwards. Precise hole locations were determined and carefully measured and marked on the specimen.

After holes were drilled in the concrete, anchor bolts were installed and pre-tensioned. Vertical cracks appeared on one side of the column when anchor bolts on that side were tightened (Figure 4.19). Previous tests by Klingner [Ref. 7] indicated that the effectiveness of anchor bolts is reduced by approximately two-thirds in cracked concrete, so two additional bolts were installed to compensate for the reduced capacity of the three bolts affected by cracking. The final positions of the anchor bolts were measured and templates created to ensure holes in the plates would match holes drilled in the concrete.

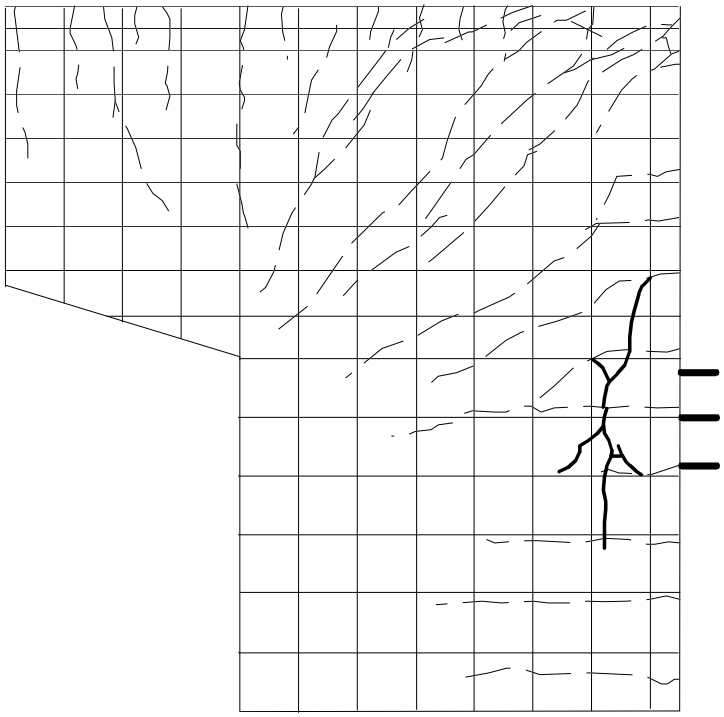

Figure 4.19 Cracks in Specimen Due to Anchor Bolt Tensioning Superimposed on Cracks from the Previous Test

Holes for the post-tensioning bars were drilled in the flanges of the cross beams, after which the flanges were welded to the webs. Bearing stiffeners were then welded to the flanges and webs. The positions of the triangular plates were carefully measured and marked on the base plates to prevent gaps between the triangular plates and the cross beams. The triangular plates were welded to the base plates, and then the cross beams were welded to the triangular plates. Additional stiffeners were ground to the proper size and shape and welded between the triangular plates, in line with the web of the cross beam.

The plate assemblies were carefully lifted by hand and placed over the anchor bolts. Washers and nuts were added, and the anchor bolts were tightened to a final torque of 81.3 N-m (60 ft-lbs). Post-tensioning bars were then forced into place. Welding had warped the base plates slightly, and the unbolted ends angled outward from the surface of the concrete, making insertion of the bars difficult. After the bars were stressed, the plates flattened against the concrete, at which point, the edges were sealed with silicone caulk and the remaining gap between each base plate and the specimen was filled with hydrostone.

After the plate assemblies were bolted in place, strain gauges were epoxied to the surfaces of the plates and stiffeners as shown in Figure 4.20. Displacement gauges were attached to steel frames which had been constructed around the plates for this purpose. The layout of displacement gauges is shown in Figure 4.21.

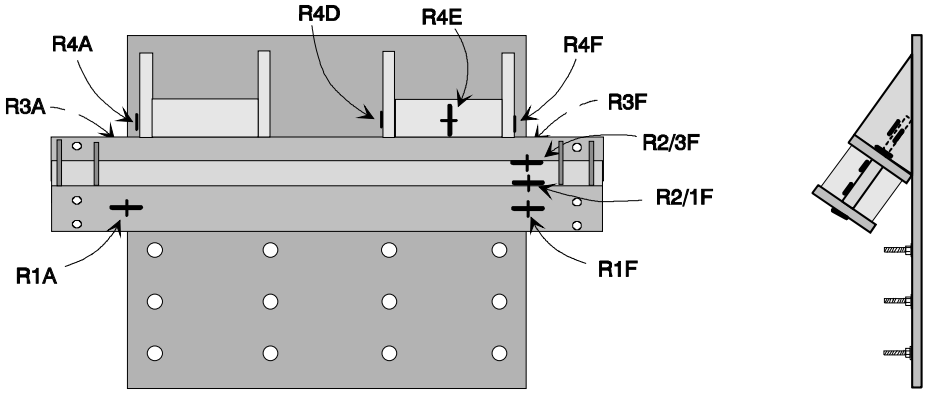

a) Side Plate

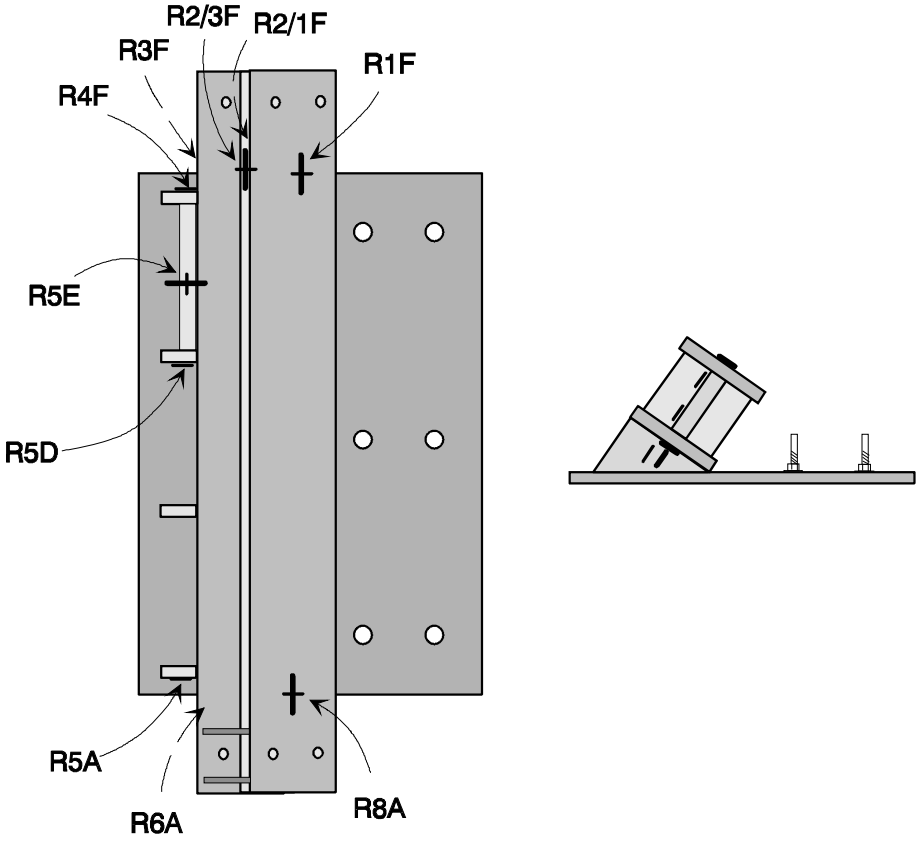

b) Top Plate

Figure 4.20 Locations of Strain Gauges on Repair Components [Modified from Ref. 3]

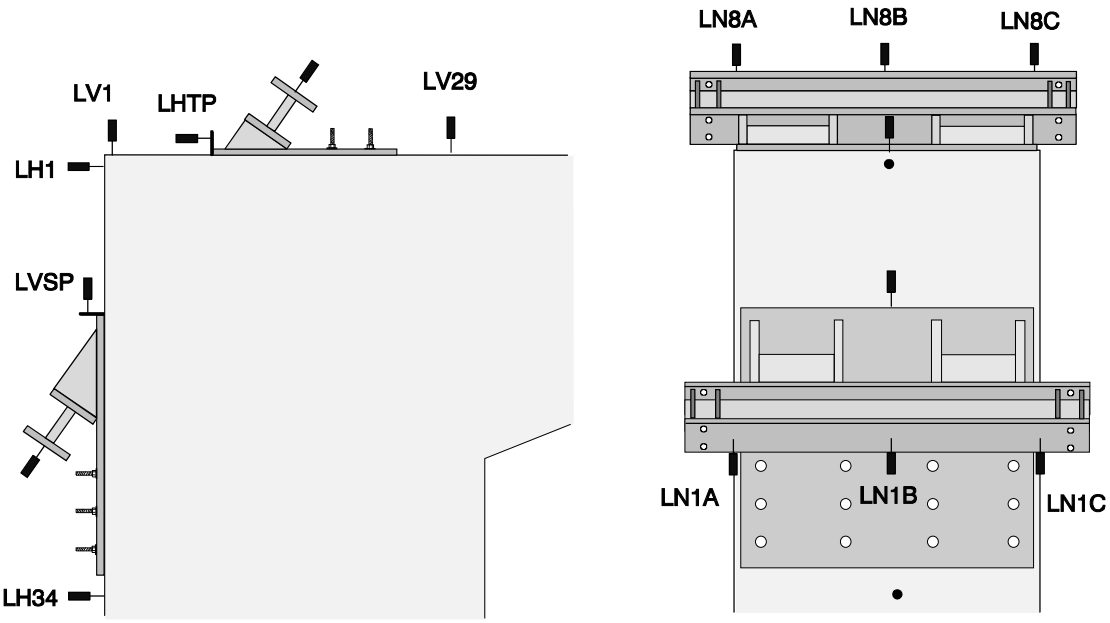

Figure 4.21 Locations of Displacement Gauges on Repaired Specimen [Modified from Ref. 3]

4.3.1.6 Test Procedure

The specimen was completely unloaded following the original test. After the plate assemblies were installed, the specimen was loaded as it was for the original tests until one-half dead load was reached, at which point the post-tensioning bars were stressed. Pairs of bars diagonally opposite each other were stressed simultaneously, alternating with the other pair, until the desired tension was reached. Strain and displacement readings were taken at each stressing increment. Loading was then resumed, and all major load steps were completed (see Table 4.1). Cracks were marked every two or three load steps. Because the specimen had been re-whitewashed, it was not necessary to differentiate crack markings from previous tests. Crack widths were measured at all major load steps. After a maximum load of FL / ϕ was reached, the specimen was unloaded.

4.3.2 Internal Vertical Post-Tensioning (POJ-RC2-RP2)

4.3.2.1 Concept

This repair option involved running post-tensioning bars vertically through the top of the joint into the column (Figure 4.22). The primary advantage of this repair method was that it would be completely hidden within the pier, except for the anchorage hardware on top. Vertical post-tensioning would directly strengthen the connection between the column and the joint. The overhang connection to the joint would also be strengthened slightly because of confinement of the overhang reinforcement afforded by the post-tensioning. However, coring through the top of the joint and inserting post-tensioning bars in the full-size pier would be complicated by the top flange of the superstructure cantilevering over the joint.

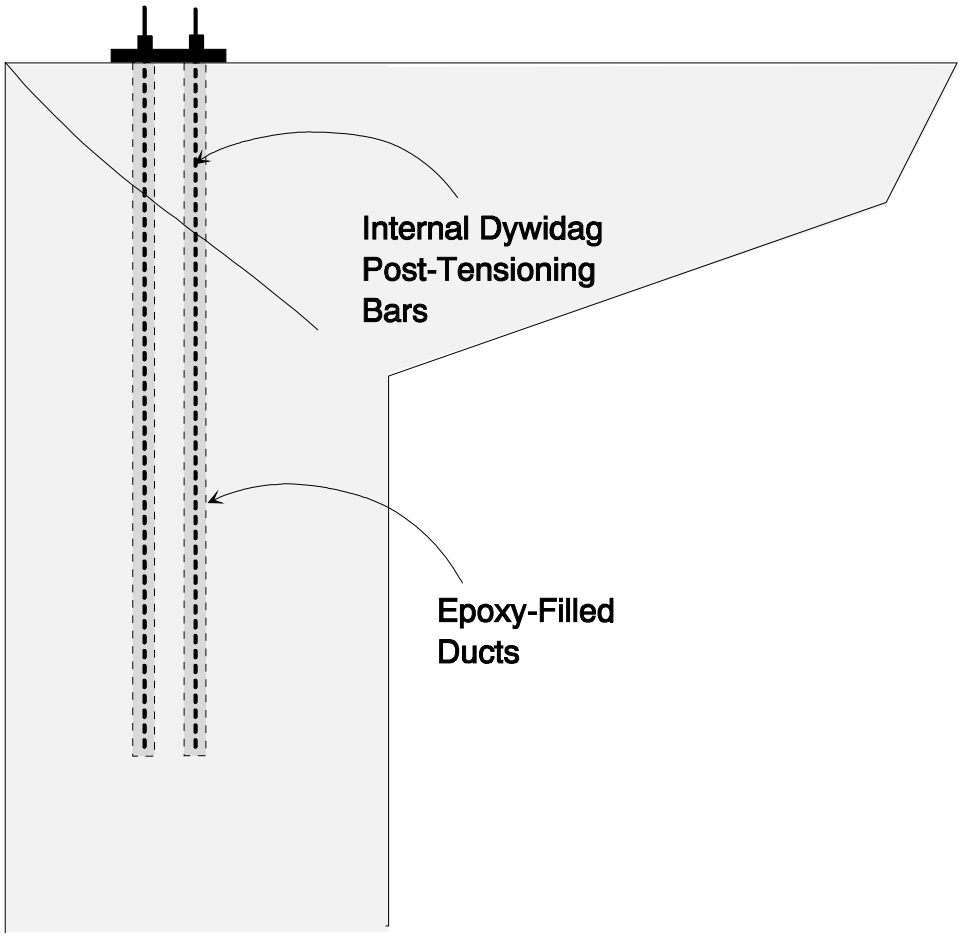

Figure 4.22 Schematic of Internal Post-Tensioning

4.3.2.2 Design

As with the previous repair, the amount of post-tensioning required depended on its perpendicular distance from the compression zone. For vertical post-tensioning, this meant the horizontal distance. The farther the post-tensioning force is applied from the compression zone, the lower the force that is needed to strengthen the joint. However, because the internal post-tensioning is provided in one direction only, it is necessary to ensure the longitudinal steel in the overhang has sufficient development length, although this would not be a

necessary consideration if the repair is applied to a bent with a prestressed overhang. The two rows of bars were positioned at 27.9 cm (11 in.) and at 38.1 cm (15 in.) from the exterior vertical face of the joint (Figure 4.23). The resultant post-tensioning force was therefore located at 33.0 cm (13 in.), allowing 31.8 cm (12.5 in.) of development length for the primary longitudinal steel in the overhang, compared to 30.5 cm (12 in.) required. This placement fixed the required post-tensioning force at 1.44 MN (324 kips), which could be provided by 7.7 1.59-cm (0.625-in.) diameter Dywidag bars. Therefore, eight bars were used. The 1.73-m (68-in.) length of the bars was controlled by the necessity to minimize post-tensioning losses.

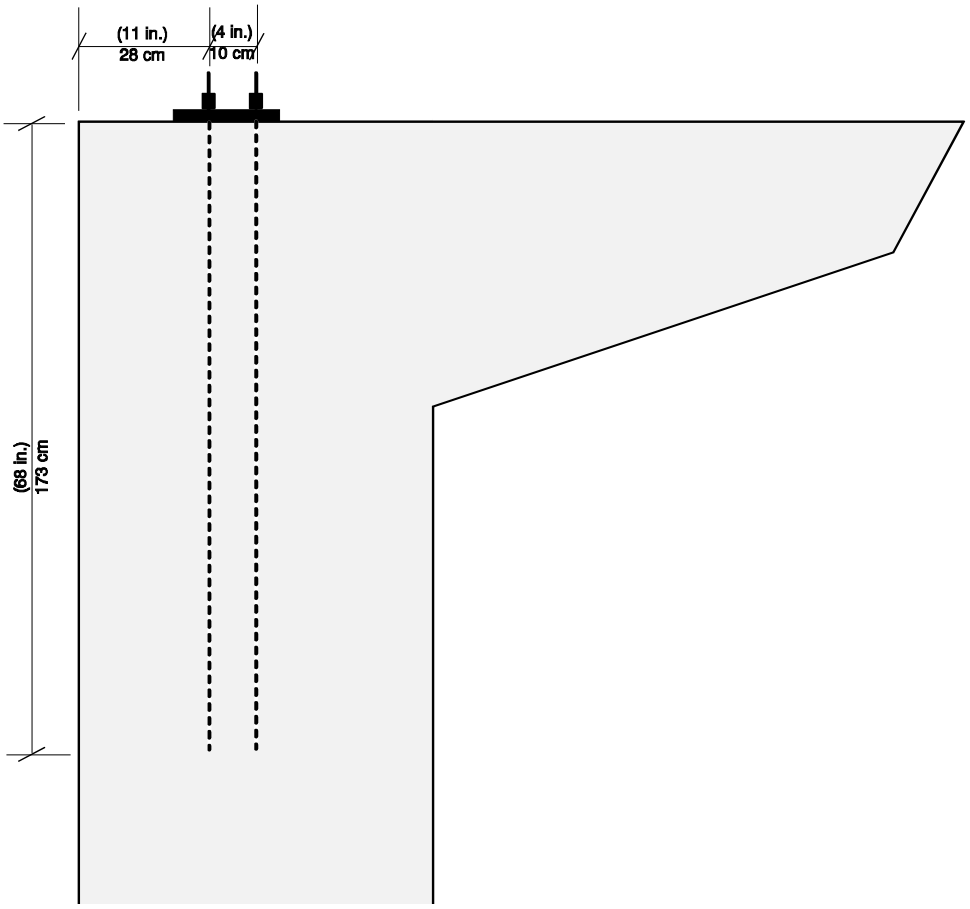

Figure 4.23 Location of Post-Tensioning Bars in Profile

4.3.2.3 Details

The locations of the eight post-tensioning bars across the joint were controlled by the location of the main reinforcement in the overhang and the desire to space the bars as evenly as possible (Figure 4.24). The lower ends of the post-tensioning bars were held in place with quick-set epoxy, while slow-set epoxy was used to fill the remainder of the holes, setting after the bars were stressed. The top of each bar was anchored with two Dywidag nuts, bearing

against a 8.9 x 22.9 x 2.5 cm (3.5 x 9 x 1 in.) steel plate, with two bars per plate, to distribute the compressive forces over a larger area of concrete.

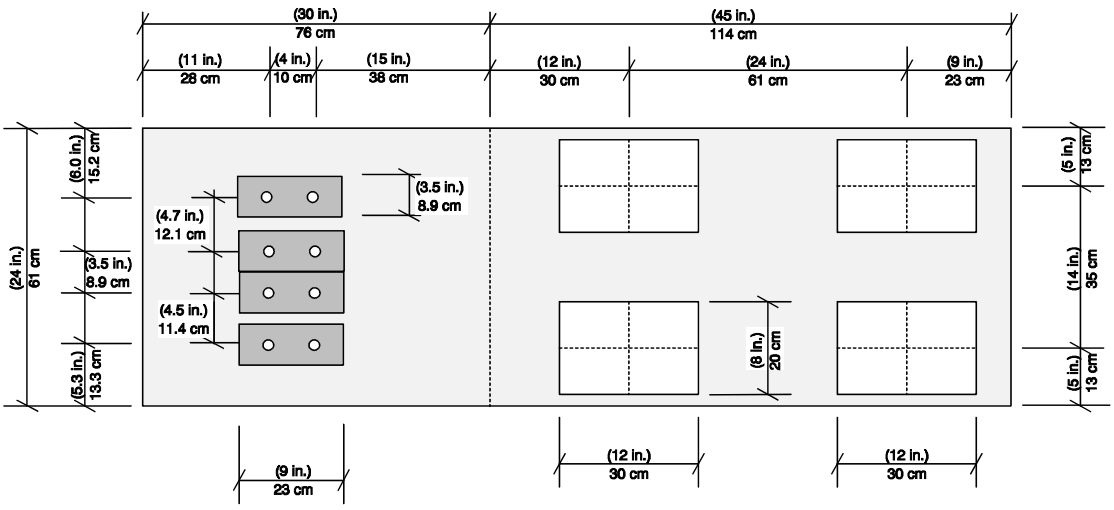

Figure 4.24 Plan View of Location of Post-Tensioning Bars

4.3.2.4 Materials

The post-tensioning bars were 1.59-cm (0.625-in.) diameter Dywidag bars, the same as used in other repairs, with an ultimate strength of approximately 965 MPa (140 ksi). Results of a representative tensile test are shown in Figure 3.15. The bearing plates were fabricated using Grade 50 steel. The quick-set epoxy used to anchor the lower ends of the bars filled the holes to a depth of 56 cm (22 in.), while the slow-set epoxy filled the remaining 112 cm (44 in.) (Figure 4.25). The quick-set epoxy had a cure time of 90 seconds, while the cure time for the slow-set epoxy was at least 23 minutes.

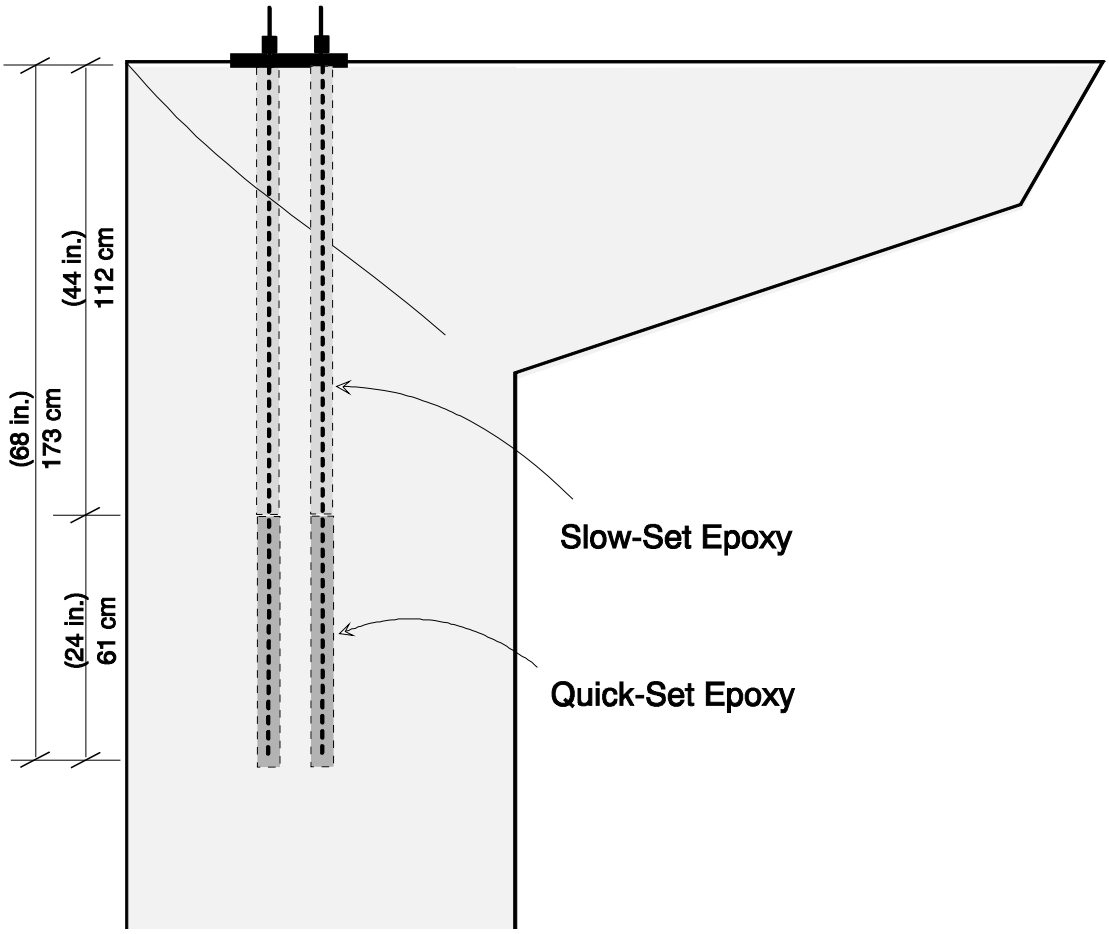

Figure 4.25 Epoxy Distribution in Holes

4.3.2.5 Fabrication and Installation

Four bearing plates were cut and two holes were drilled in each. To avoid the necessity of coring deep holes in the specimen, for which proper equipment was not available, 2.5-cm (1-in.) diameter aluminum ducts were cast in the specimen and removed after the concrete had cured. The epoxy came in sealed plastic tubes which were inserted into the holes. Two tubes of quick-set epoxy were inserted first, followed by enough tubes of slow-set epoxy to fill the holes. The Dywidag bars were attached to a drill and inserted while

spinning in order to break the plastic epoxy tubes and mix the two components. After each bar was inserted, the quick-set epoxy as allowed to set, after which the bar was tensioned. Because only a limited time was available for stressing, each bar was stressed to its full tension in one stage, relying on the pressure gauge on the hydraulic pump to provide the necessary stressing data. Two practice trials were conducted, by inserting bars in a block of concrete remaining from another test, in order to confirm the curing times of the epoxies and to practice the procedure. It was determined that strain gauges attached to the bars were too badly damaged by the insertion procedure to function afterwards, so they were not used on the bars installed in the specimen.

4.3.2.6 Test Procedure

The specimen was completely unloaded following the previous test. It was re-whitewashed to cover old cracks and crack markings, and new grid lines were drawn. It was then loaded to one-half dead load for installation of the post-tensioning bars, which were inserted as described above. The stressing sequence is shown in Figure 4.26. The specimen was then unloaded so complete load-displacement response curves could be generated. Gauge readings were rezeroed before testing began. The test procedure was the same as for the initial test of the unrepaired specimen. The specimen was ultimately loaded to factored loads divided by ϕ, with readings taken at each step. The specimen was then unloaded.

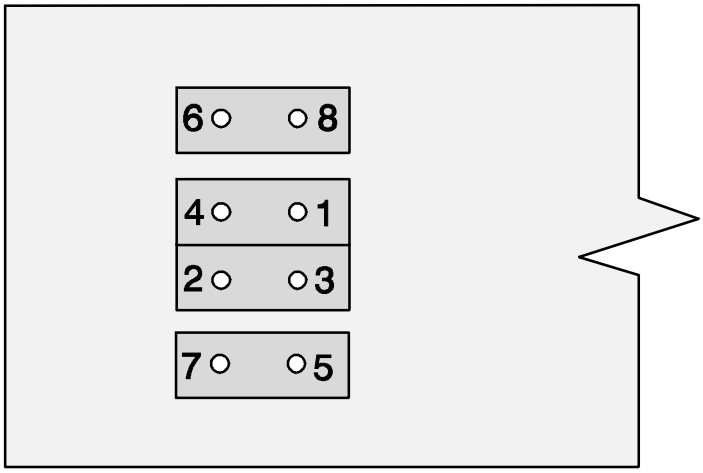

Figure 4.26 Stressing Sequence for Vertical Internal Post-Tensioning

4.3.2.7 Modification (POJ-RC2-RP2a)

The internal post-tensioning bars were inserted into ducts which were cast into the original specimen. This was done because equipment was not available to core 1.73-m (68-in.) deep holes in the specimen. However, in an actual repair, holes would need to be cored. Because of congestion in the overhang, some of the overhang steel would be damaged or cut completely during coring. The damage to the reinforcement could weaken the joint strength at the section on the overhang side of the post-tensioning bars. In order to test the possible effects of this damage, holes were cored from the top of the joint, on the overhang side of the post-tensioning bars, to a depth just beyond the shear friction steel in the middle of the overhang (Figure 4.27). A worst-case scenario was created by coring through as many bars as possible.

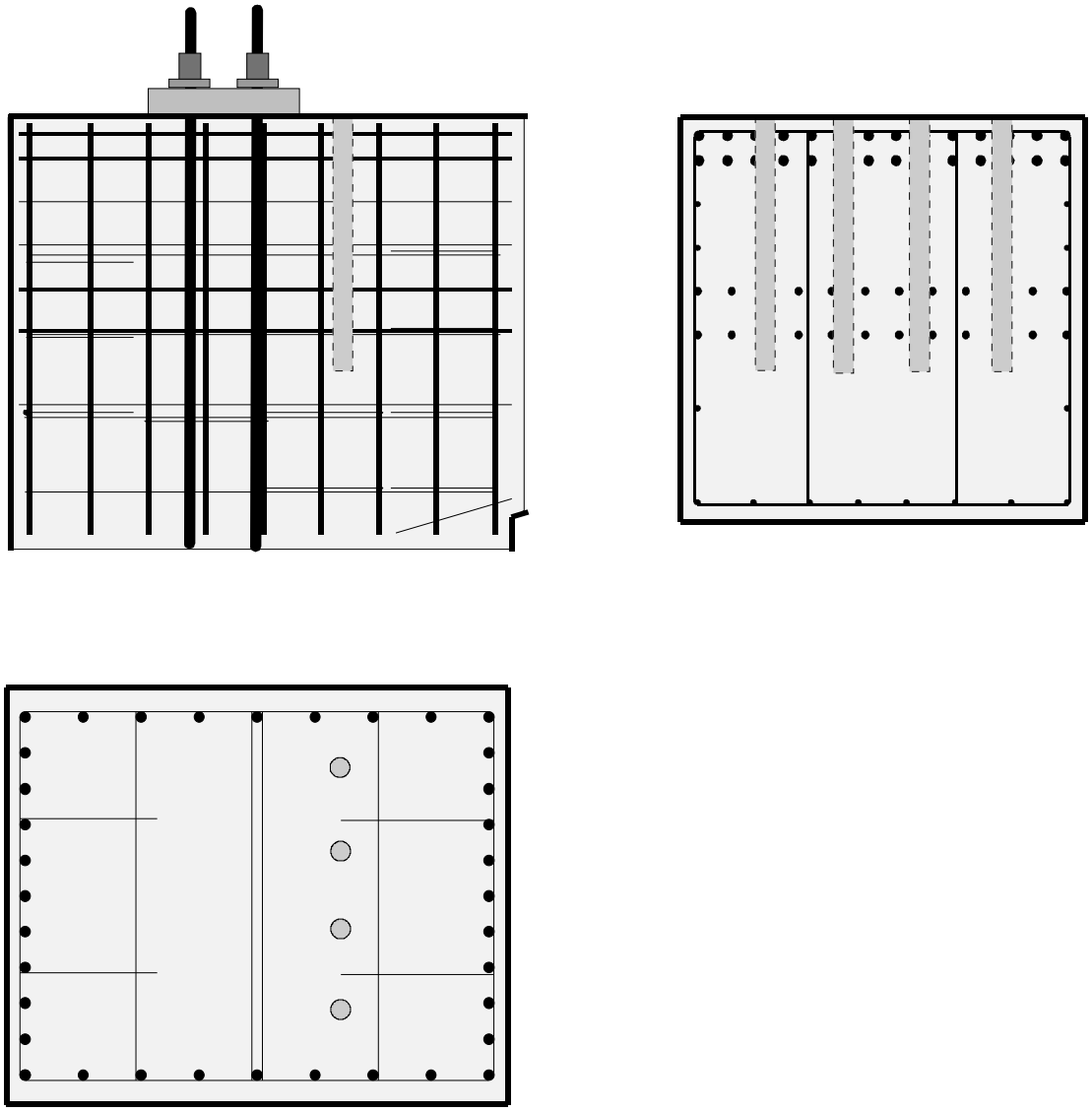

Figure 4.27 Location of Holes in Plan and Profile Views

After the holes were drilled, the specimen was re-whitewashed, new grid lines were drawn and the gauges were rezeroed. The modified test was conducted in an identical manner to the previous test.

4.3.3 Shear Test (POJ-RC2-RP2s)

4.3.3.1 Concept

During testing of the repair methods, TxDOT became concerned about a diagonal crack which was observed in Piers I-4C and I-5C. It was not especially wide, but it extended from the inner bearing pad towards the inside corner of the joint, over almost the entire depth of the overhang (Figure 4.28). No similar cracks were observed on any of the test specimens. It was hypothesized that the wide crack in Pier I-2C had caused the superstructure to shift, resulting in more of its weight being applied to the inner bearing pad than the outer pad.

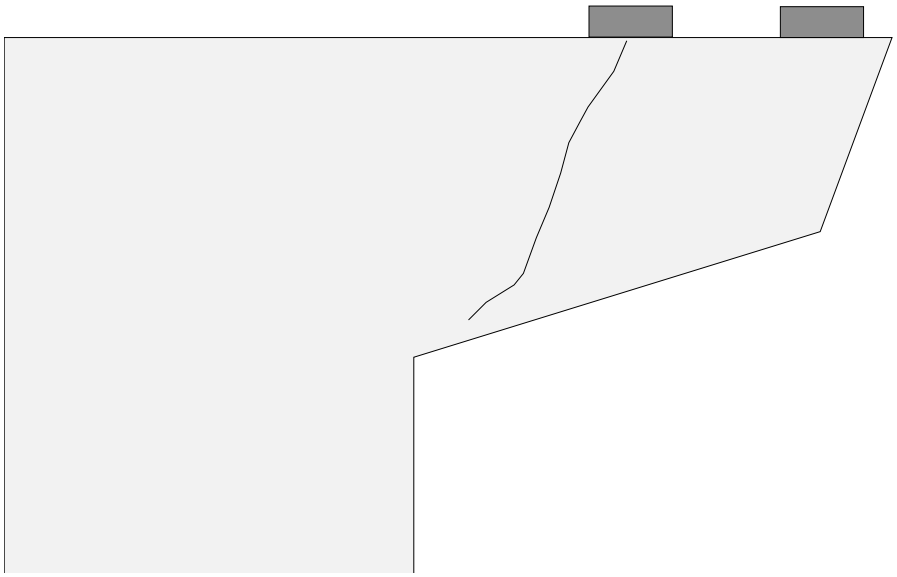

Figure 4.28 Location of Diagonal Crack in Pier I-4C

4.3.3.2 Modification of Loading Frame

To partially test this hypothesis and examine the behavior of a bent with a similar diagonal crack, a new test was designed in which all the load from the superstructure was

applied to the inner loading point. The new configuration would require a larger ram and would place nearly all the reaction force on only two of the columns in the loading frame. The loading frame was not strong enough to resist these loads. Therefore, the loading frame was reconfigured. The specimen was moved forward two feet to place the inner loading point in the middle of the loading frame. Because holes in the floor for anchorage bars were no longer in the correct place to hold down the specimen, the tie-down system was modified as shown in Figure 4.29. A new ram, with a capacity of 2.67 MN (600 kips), was obtained and attached to a new beam that was clamped between the two upper beams which were bolted to the columns. The reconfigured loading frame is shown in Figure 4.30.

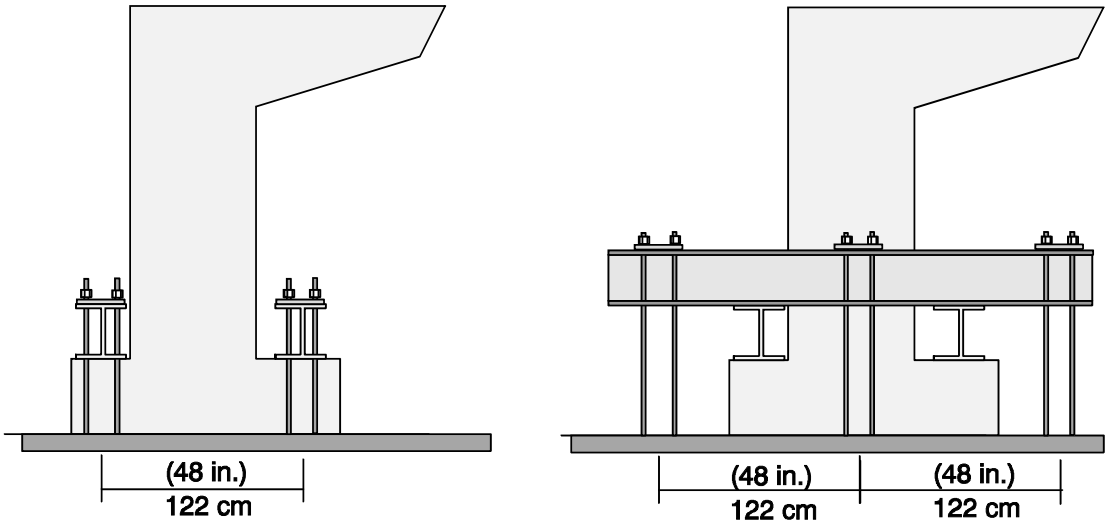

a) Original Tie-Down System b) Redesigned Tie-Down System

Figure 4.29 Specimen Tie-Down Systems

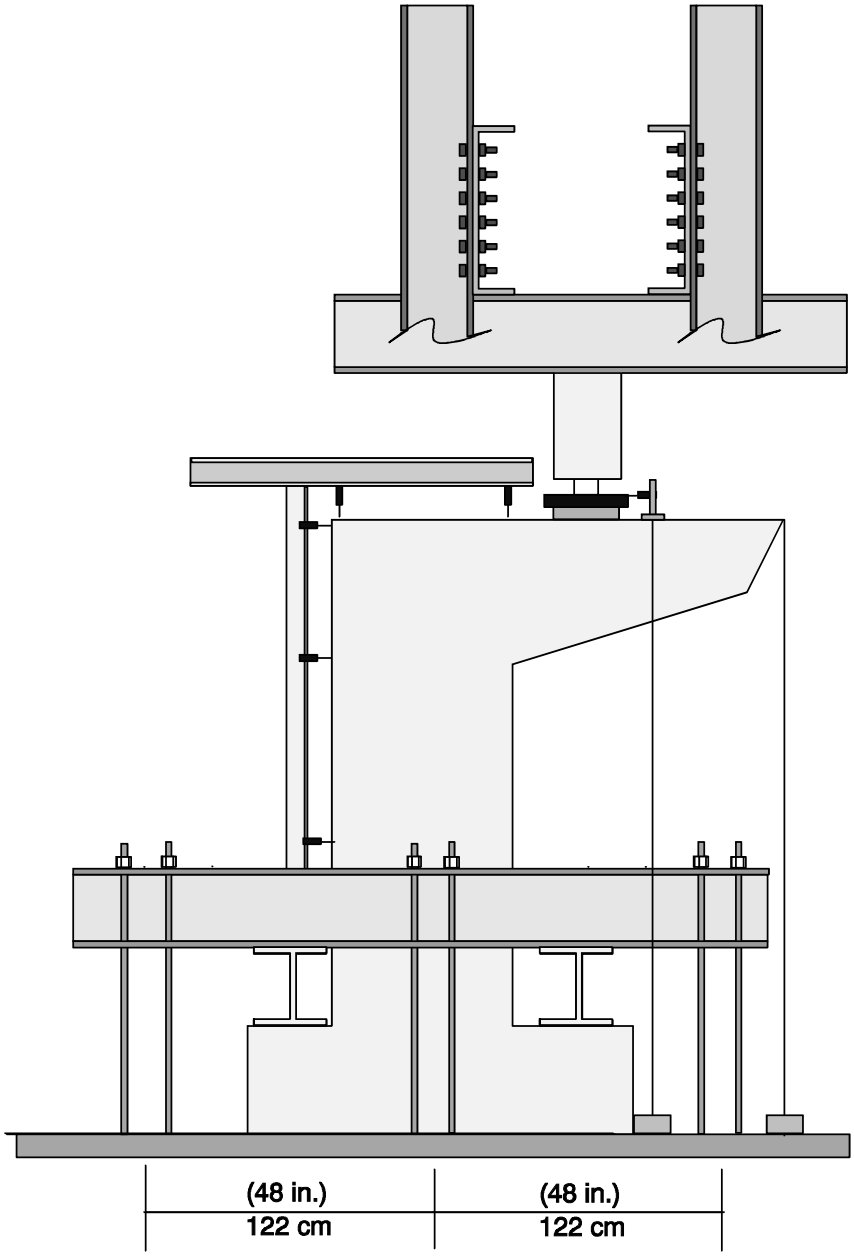

Figure 4.30 Reconfigured Loading Frame

4.3.3.3 Modification of Specimen

Because Piers I-4C and I-5C were designed without shear friction steel, the effects of this reinforcement on the specimen had to be eliminated. To this end, holes were cored horizontally through the overhang, to cut the shear friction steel at or near the expected location of the diagonal crack (Figure 4.31). The holes were then filled with expansive grout, so that the holes themselves would have as little effect as possible on crack formation and propagation. After the holes were filled, the specimen was re-whitewashed and new grid lines were drawn.

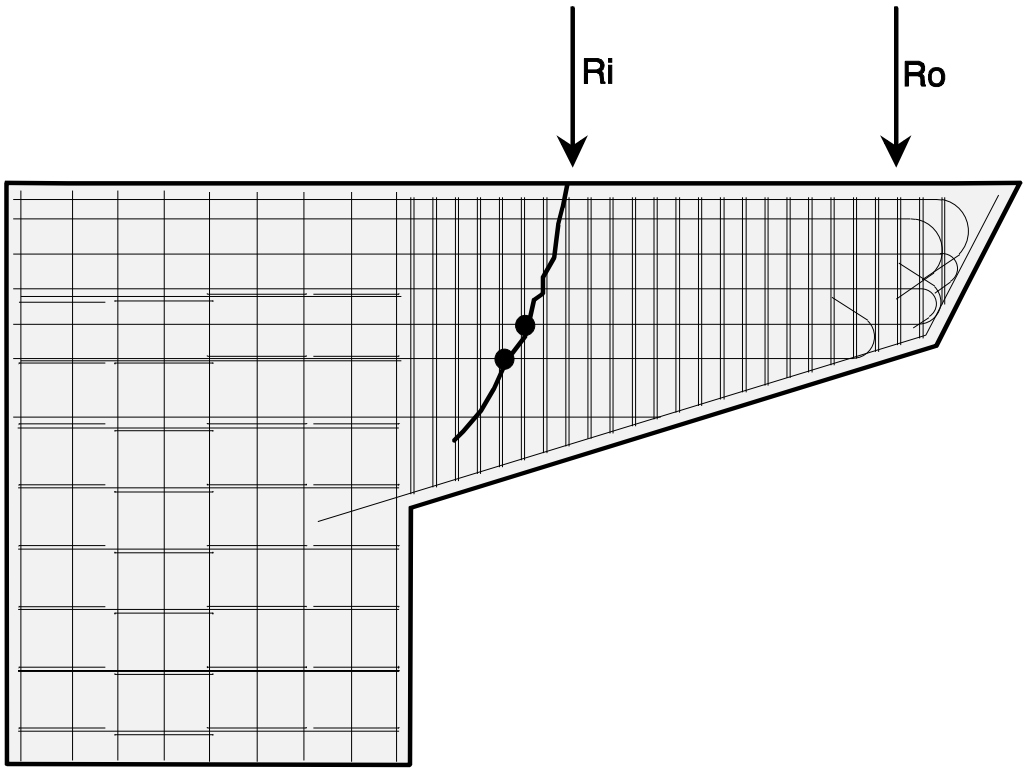

Figure 4.31 Expected Diagonal Crack and Holes Cored through Shear Friction Steel

4.3.3.4 Modification of Test Procedure

New load steps were calculated to reflect the new loading configuration intended to provide critical shear forces rather than moment. Because this was to be the final test, the load was intended to be carried up to the maximum capacity of the bolts restraining the loading frame, approximately 2.0 MN (450 kips), or until the specimen failed. Because of differences in the test, crack widths for the specimen could not be compared with those from previous tests. Therefore, only the main shear crack was measured to monitor its progress. Otherwise, the test was conducted in the same manner as previous tests. When the specimen was loaded to near the maximum load considered safe for the loading frame, one of the two top beams buckled, and the test was terminated.

4.4 Discarded Repair Options

4.4.1 External Horizontal and Vertical Post-Tensioning

This repair method would be applied only to the reinforced concrete bents, because the others already have horizontal post-tensioning. The basic design involved post-tensioning bars positioned along the top of the overhang and down the back of the column. Both sets of bars would be anchored in a block attached to the outside corner of the joint and to other blocks attached to the column or overhang (Figure 4.32). Two variations on this method were considered: concrete anchorage blocks and steel anchorage blocks.

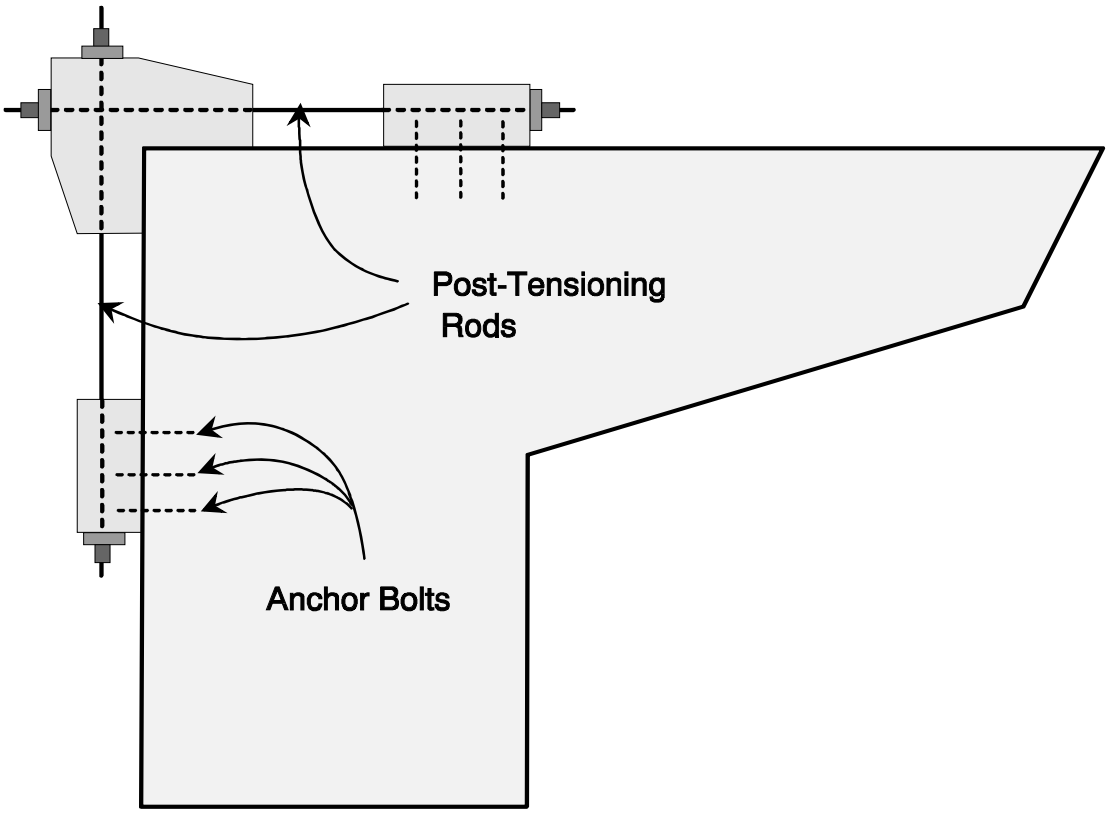

Figure 4.32 Schematic of External Horizontal and Vertical Post-Tensioning

The design was inherently inefficient, in that each set of bars would need to resist most of the moment in the joint on its own. In addition, the distance between the bars and the surface of the concrete bent would need to be sufficient to allow installation of the anchorage hardware, resulting in high overturning forces on the anchorage blocks. The design of the corner anchorage block was made impractical by the large forces it would be required to withstand. If the anchorage blocks were made large enough to resist the forces involved, they would present an extremely unaesthetic appearance. Another problem was the lack of space for the horizontal post-tensioning bars, due to the presence of the bearing pads for the superstructure. The final factor in the decision not to test this option was that the post-

tensioning forces on the joint would be applied at the corner only, putting excessive stress on a small area of concrete.

4.4.2 Internal Diagonal Post-Tensioning

The main problem with this option (Figure 4.33) was the congestion of reinforcement in the bent and the difficulty of drilling diagonally through the joint without damaging a significant amount of reinforcement. In addition, angled bearing plates would be required on the surface of the pier.

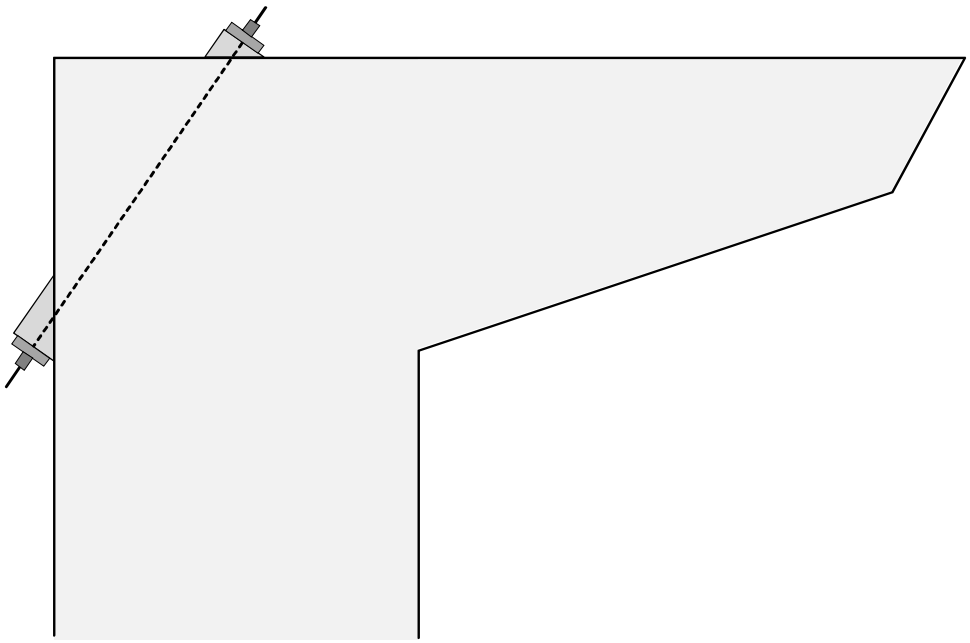

Figure 4.33 Schematic of Internal Diagonal Post-Tensioning

4.4.3 Concrete Strut

This option was originally proposed and designed by TxDOT. It involved increasing the depth of the column by approximately 38 percent by adding reinforced concrete to the face of the column under the overhang (Figure 4.34). This would decrease forces in the joint and increase the distance between the compression zone and joint reinforcement. The construction presented some difficulties in casting the new concrete under the overhang, even though some existing concrete would be removed to allow the new reinforcement to be interconnected with the old.

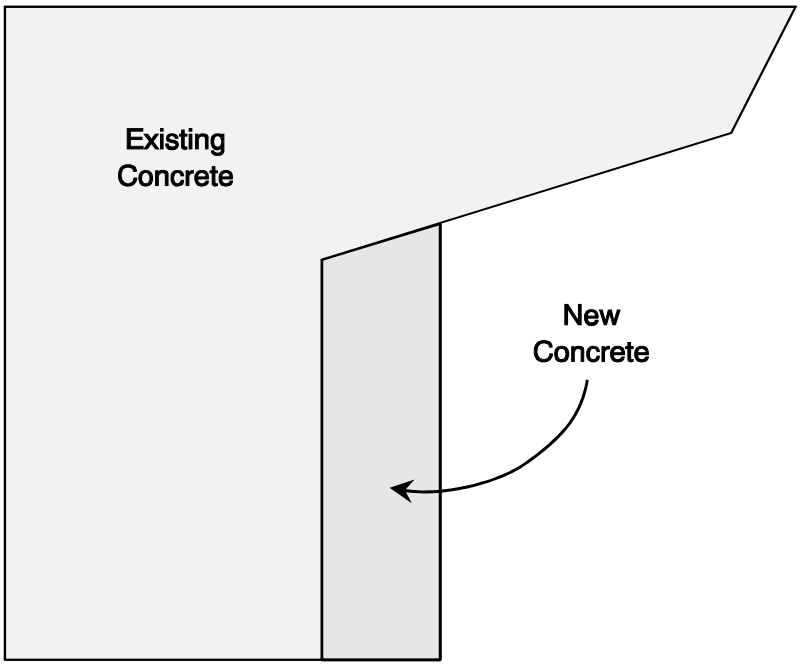

Figure 4.34 Layout of Concrete Strut

However, the main problem was based on the difference in stiffness between the new and old concrete. As concrete ages, it gains in strength and stiffness. The new concrete

would therefore be much less stiff than the old and carry less stress for the same displacement. Although the overhang was to be jacked up to remove as much load as possible, the existing concrete would still carry residual stresses, which would not be experienced by the new concrete. Furthermore, the new concrete would creep more than the existing concrete and would gradually shed its load to the existing concrete after the bent was loaded. Because of these two factors, the new concrete would provide very little assistance to the existing bent in resisting moment.

4.4.4 Steel Haunch

The principle behind this repair option was similar to that for the concrete strut. A steel haunch would be built to fit in the inside corner where the column meets the overhang (Figure 4.35). Steel plates would be bolted against the front face of the column and the underside of the overhang with stiffeners welded between them. Because steel is much stiffer than concrete and does not creep, the haunch was expected to provide additional compression area, allowing compressive forces from the superstructure to be transmitted more directly into the column. However, during the initial test of the reinforced concrete specimen, it was determined that the relative displacement between the column and the overhang in the vicinity of the corner was very small. Because the haunch was to be bolted in place, gaps between the bolts and holes in the plate, as well as movement of the anchor bolts in the concrete, would require relatively large displacements to fully engage the bolts against the plates.

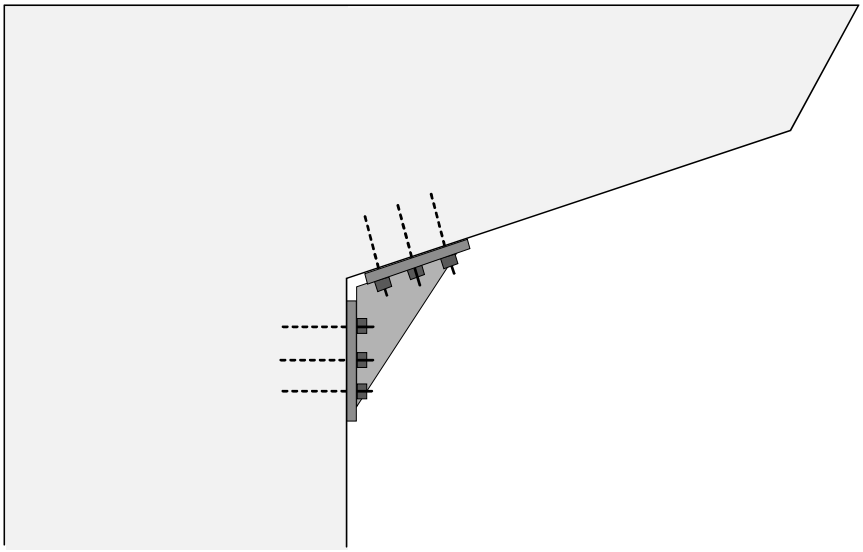

Figure 4.35 Layout of Steel Haunch

4.4.5 Internal Horizontal and Vertical Post-Tensioning

This repair method (Figure 4.36), like the method utilizing external horizontal and vertical post-tensioning, would only be applied to reinforced concrete bents. There was no basic problem with this approach, other than the difficulty associated with accurately drilling long holes and avoiding interference between the horizontal and vertical bars. Furthermore, following the test involving only vertical internal post-tensioning, horizontal post-tensioning was not determined to be necessary to provide the required capacity.

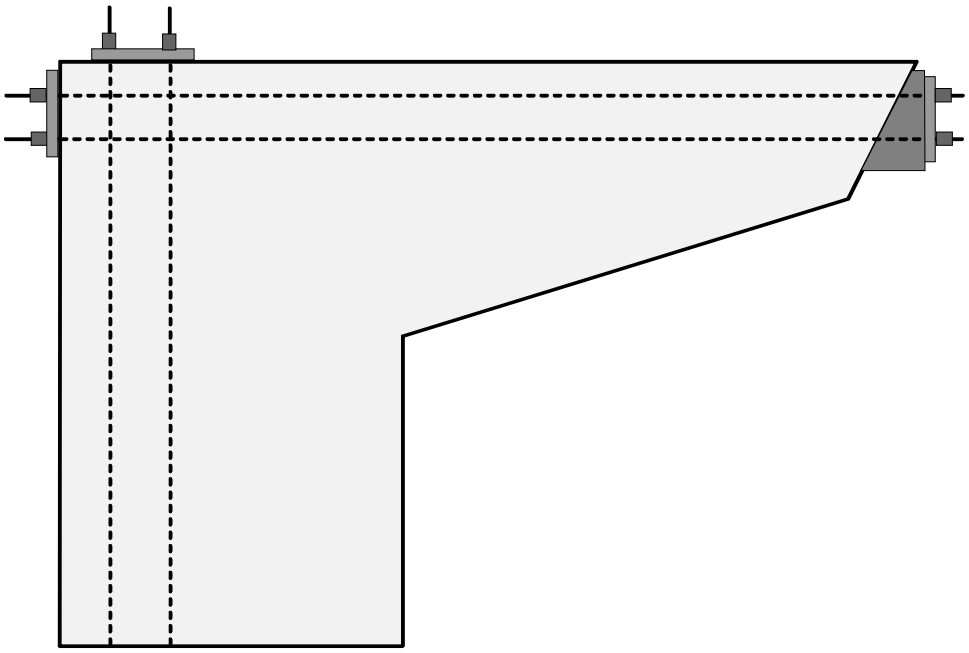

Figure 4.36 Schematic of Internal Horizontal and Vertical Post-Tensioning

CHAPTER 5

PRESENTATION OF TEST RESULTS

5.1 Introduction

This chapter presents the results of tests conducted on both repaired and unrepaired specimens. Four types of results are included: strength, deflection, cracking, and, where applicable, performance of the repair components themselves. All loads were normalized to avoid confusion associated with dual units. Factored loads were used to normalize the loads. Because cracking is a serviceability concern rather than a strength concern, all crack measurements were compared at service load, unless indicated otherwise.

5.2 Tests on Prestressed Concrete Specimens

5.2.1 POJ-PS-100

5.2.1.1 Strength

The unrepaired specimen with the post-tensioned overhang (POJ-PS-100) was intended to be loaded to service load to illustrate its performance at that level and to create a cracked specimen on which to test the repair schemes. The test was temporarily interrupted at dead load, but the decision was made to continue. At a normalized load of 0.58 (approximately dead load plus one-half live load), load began to drop off until it reached dead load. Although the specimen resistance remained steady at dead load during increasing deflection, the test was discontinued in order to avoid excessive damage to the specimen. Strains in selected pier reinforcing bars at mid-depth of the joint are shown in Figure 5.1 for

the initial loading up to dead load, followed by unloading to one half dead load. The strains resulting from the additional loading cycle are not shown because of some loss of bond strength between the bars and the concrete. The resulting strain readings fluctuate and do not provide any useful data.

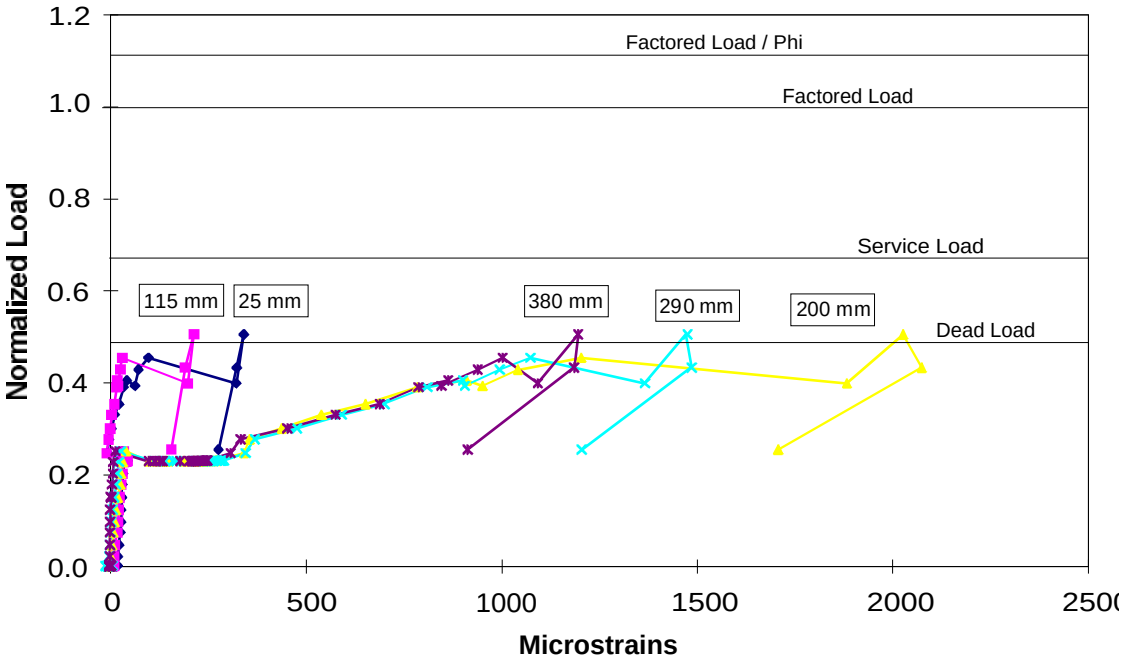

Figure 5.1 Pier Reinforcement Strains in the Joint of Specimen POJ-PS-100. (Labels indicate the distance of the bars from the exterior face of the pier.)

5.2.1.2 Deflection

A plot of tip deflection versus normalized load is shown in Figure 5.2. The maximum tip deflection achieved was approximately 63 mm (2.5 in.). Specimen response during unloading is not shown for the sake of clarity.

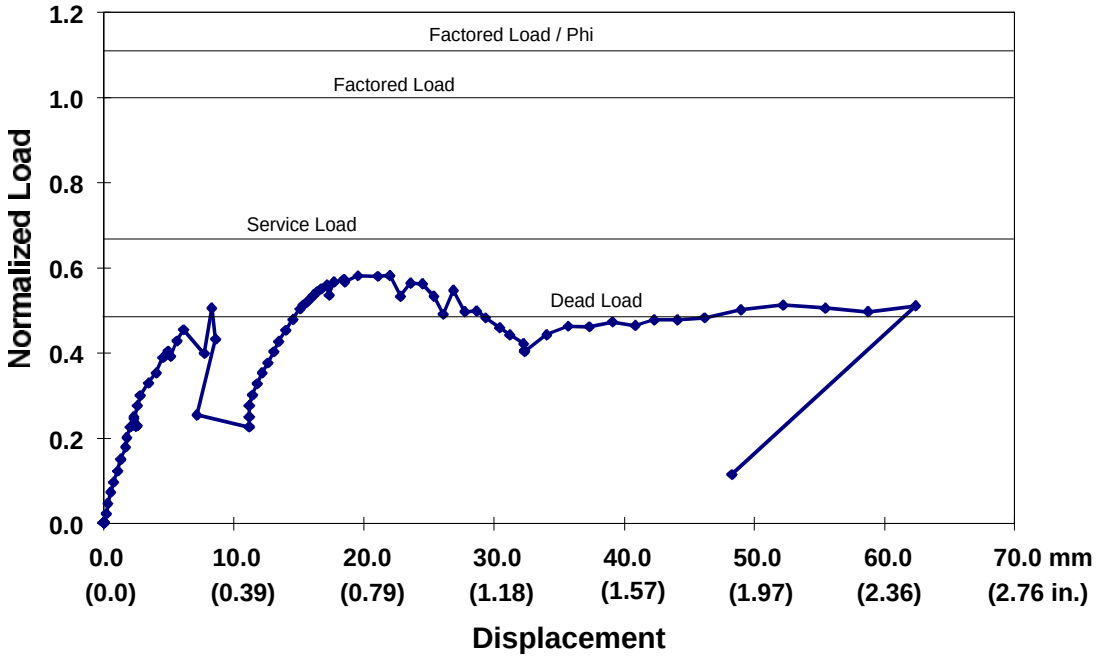

Figure 5.2 Tip Displacement vs. Normalized Load Response for Specimen POJ-PS-100

5.2.1.3 Cracking

Cracks that developed in the specimen by the time dead load was reached are shown in Figure 5.3. Note that no cracks formed in the overhang at this stage. A total of 81 crack width measurements (from both sides of the specimen) were made at dead load. The number of cracks and the maximum crack width in each region of the specimen are listed in Tables 5.1 and 5.2. The distribution of measurements in each region is shown in Figure 5.4.

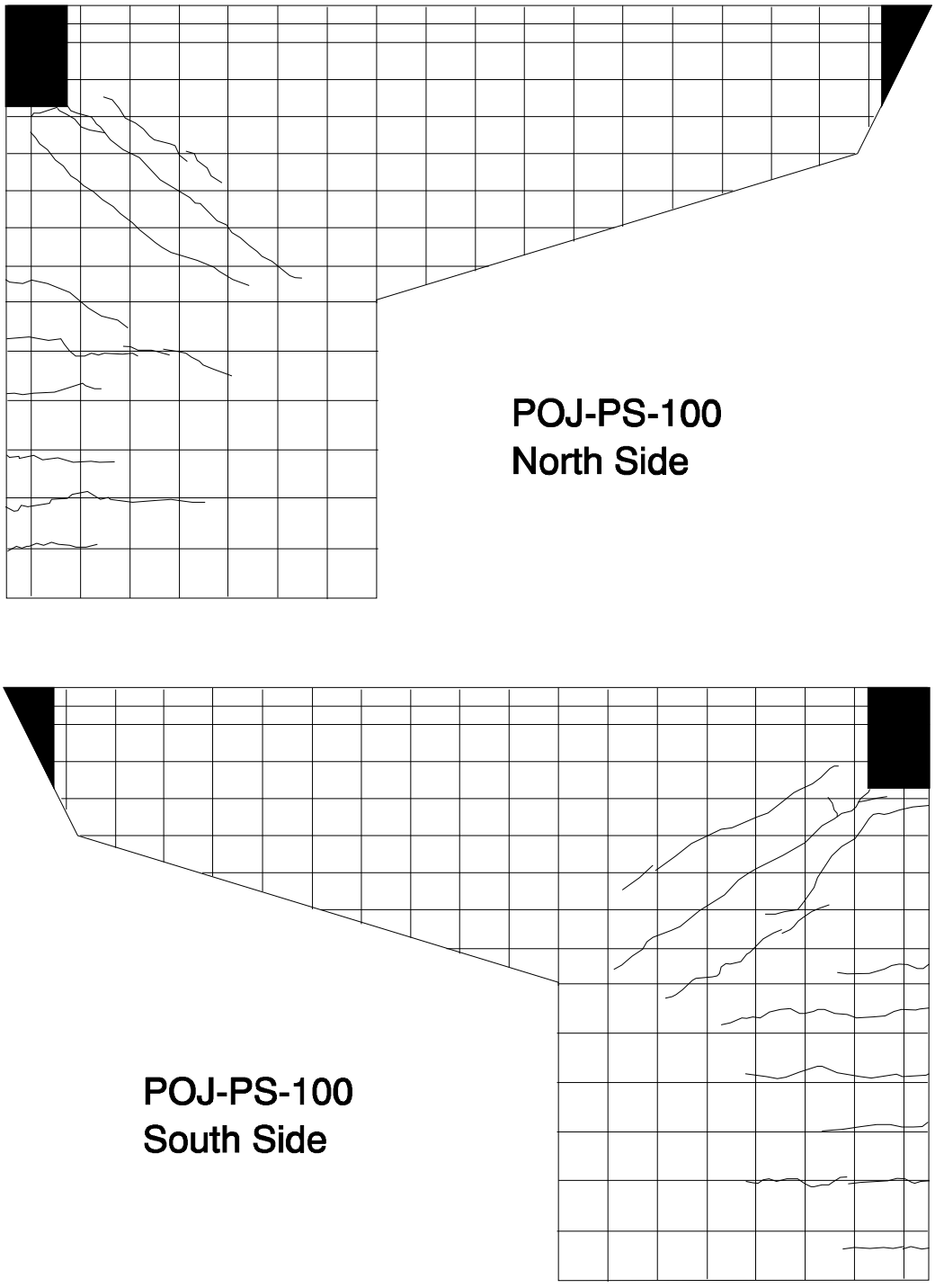

Figure 5.3 Crack Patterns on Specimen POJ-PS-100 at Dead Load

Table 5.1 Number of Cracks in Specimen POJ-PS-100 at Dead Load

	Pier	Joint	Overhang
North Side	5	5	0
South Side	5	5	0

Table 5.2 Maximum Crack Widths in Specimen POJ-PS-100 at Dead Load

	Pier		Joint		Overhang	
North Side	0.10 mm	0.0040 in.	1.02 mm	0.0400 in.	0 mm	0.0 in.
South Side	0.10 mm	0.0040 in.	0.66 mm	0.0260 in.	0 mm	0.0 in.

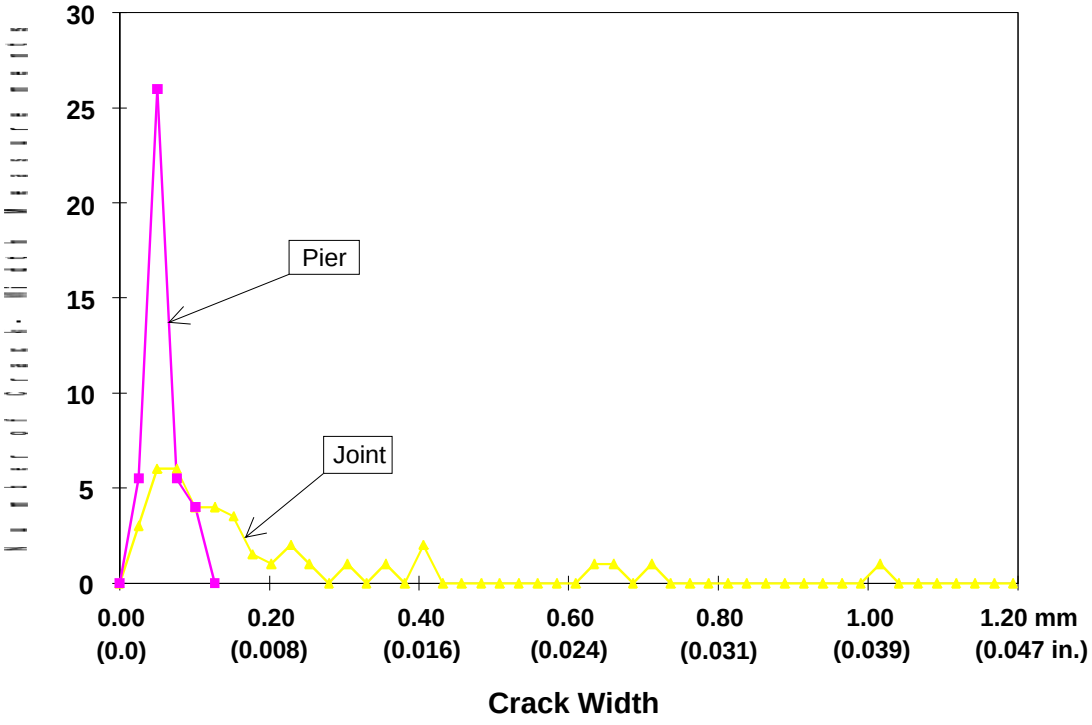

Figure 5.4 Distribution of Dead Load Crack Widths in Each Region of Specimen POJ-PS-100

5.2.2 POJ-PS-100-RP1

5.2.2.1 Strength

Specimen POJ-PS-100 was repaired with external vertical post-tensioning to become POJ-PS-100-RP1. The repaired specimen was loaded to factored load / ϕ (FL/ϕ), at which point it was unloaded to one-half dead load so that further testing could be performed. Strains in selected pier reinforcing bars at mid-depth of the joint are shown in Figure 5.5.

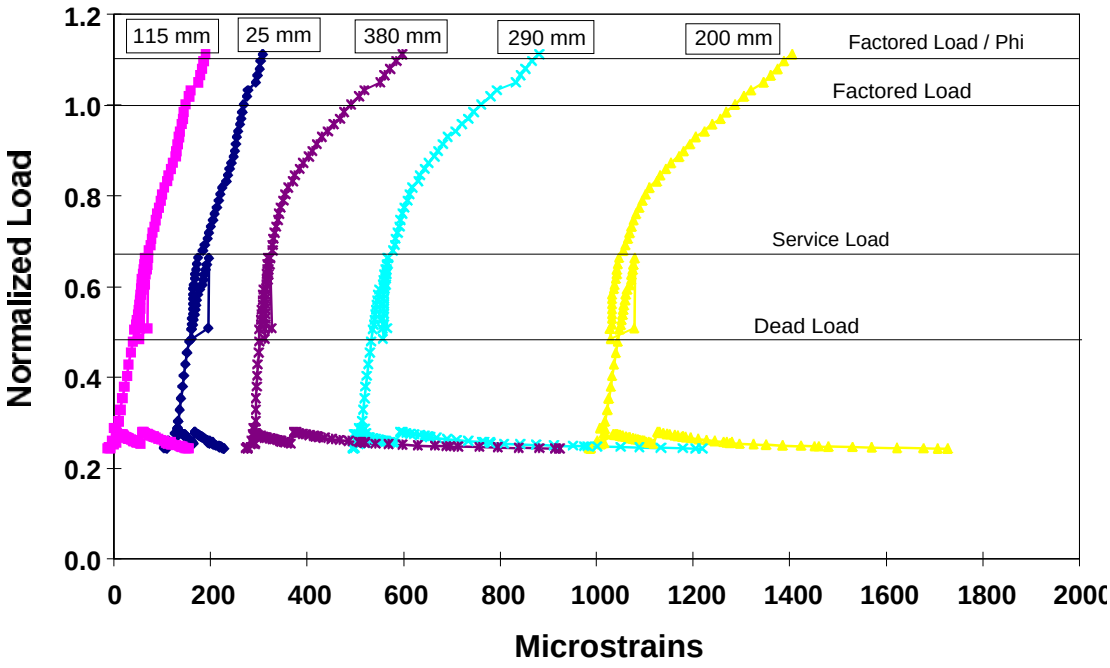

Figure 5.5 Pier Reinforcement Strains in the Joint of Specimen POJ-PS-100-RP1. (Labels indicate the distance of the bars from the exterior face of the pier.)

5.2.2.2 Deflection

A plot of tip deflection versus normalized load is shown in Figure 5.6. The maximum tip deflection, at FL/ϕ, was approximately 16 mm (0.62 in.), or approximately 10.5 mm (0.41 in.) greater than at one-half dead load. The load/displacement response is incomplete because the specimen was never fully unloaded after completion of the first test. Furthermore, the response presented in Figure 5.6 includes the residual loads and deformations from the previous test. The increase in tip deflection from dead load to FL/ϕ was approximately 9.0 mm (0.35 in.).

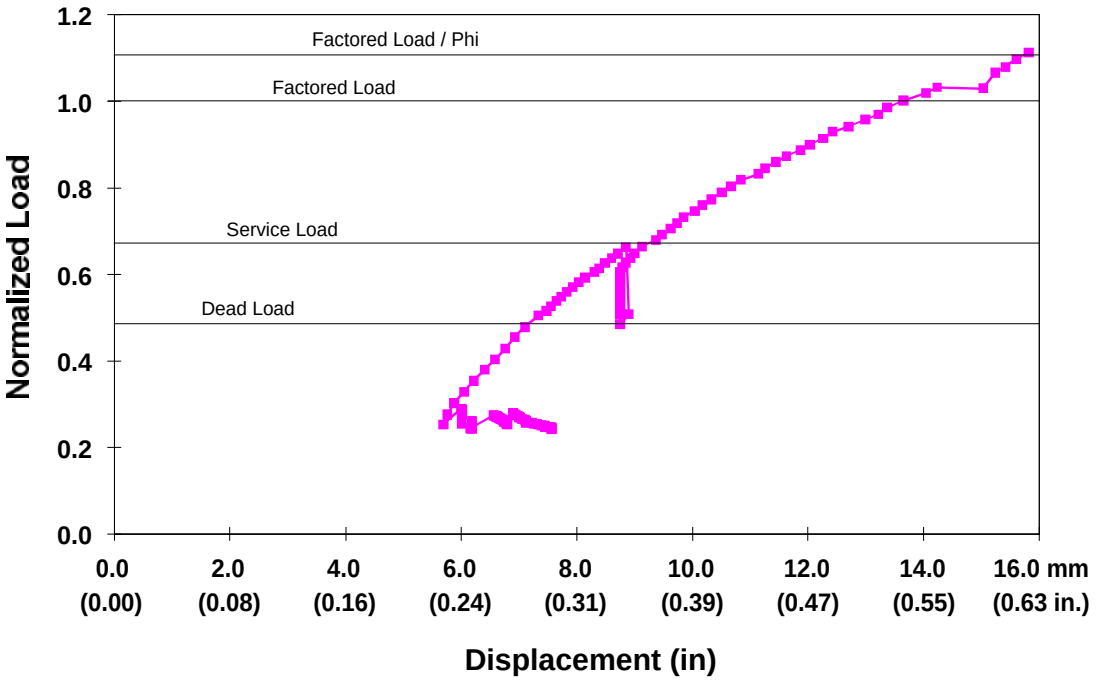

Figure 5.6 Tip Displacement vs. Normalized Load Response for Specimen POJ-PS-100-RP1

5.2.2.3 Cracking

Crack patterns on the specimen at FL/ϕ are shown in Figure 5.7. A total of 77 crack width measurements (from both sides of the specimen) were made at service load. The number of cracks and the maximum crack width in each region of the specimen are listed in Tables 5.3 and 5.4. The distribution of measurements in each region is shown in Figure 5.8. The crack width measurements are incomplete, because cracks underneath the repair could not be measured. Also, because the specimen had been tested before and cracks were not repaired, the crack widths included effects from the previous loading history. Therefore, the crack widths cannot be compared directly with those from the previous test. However, the widest cracks occurring on the repaired specimen were insignificant or nonexistent on the unrepaired specimen, so previous cracking contributed little to the maximum crack width on the repaired specimen. Even though crack widths for the two specimen configurations should not be compared directly, it is clear from examination of Tables 5.2 and 5.4 that the clamping force provided by the external post-tensioning substantially reduced maximum crack widths at comparable load levels.

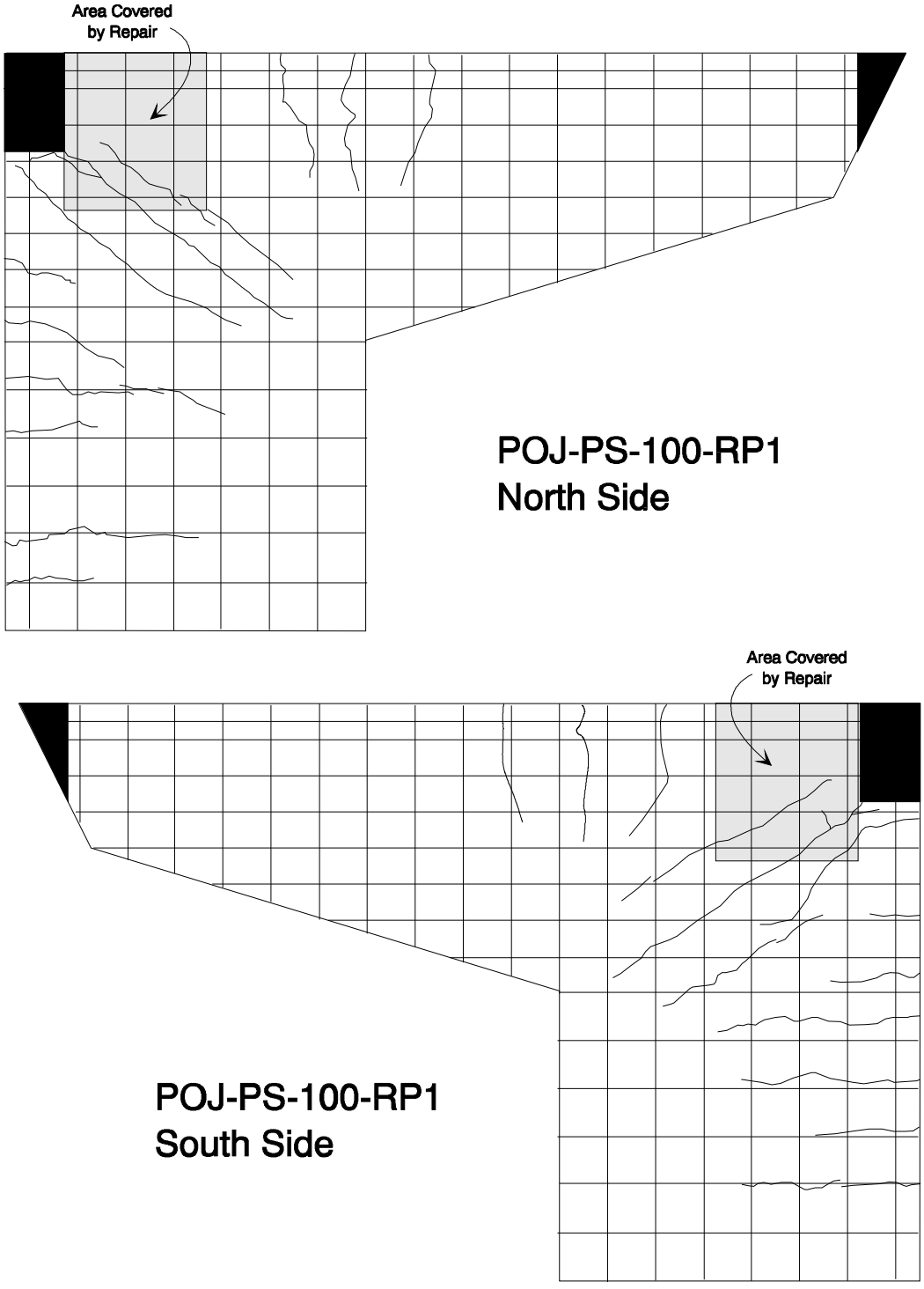

Figure 5.7 Crack Patterns on Specimen POJ-PS-100-RP1 at Factored Load / ϕ

Table 5.3 Number of Cracks in Specimen POJ-PS-100-RP1 at Service Load

	Pier	Joint	Overhang
North Side	5	6	0
South Side	5	6	0

Table 5.4 Maximum Crack Widths in Specimen POJ-PS-100-RP1 at Service Load

	Pier		Joint		Overhang	
North Side	0.03 mm	0.0010 in.	0.08 mm	0.0030 in.	0 mm	0.0 in.
South Side	0.05 mm	0.0020 in.	0.11 mm	0.0045 in.	0 mm	0.0 in.

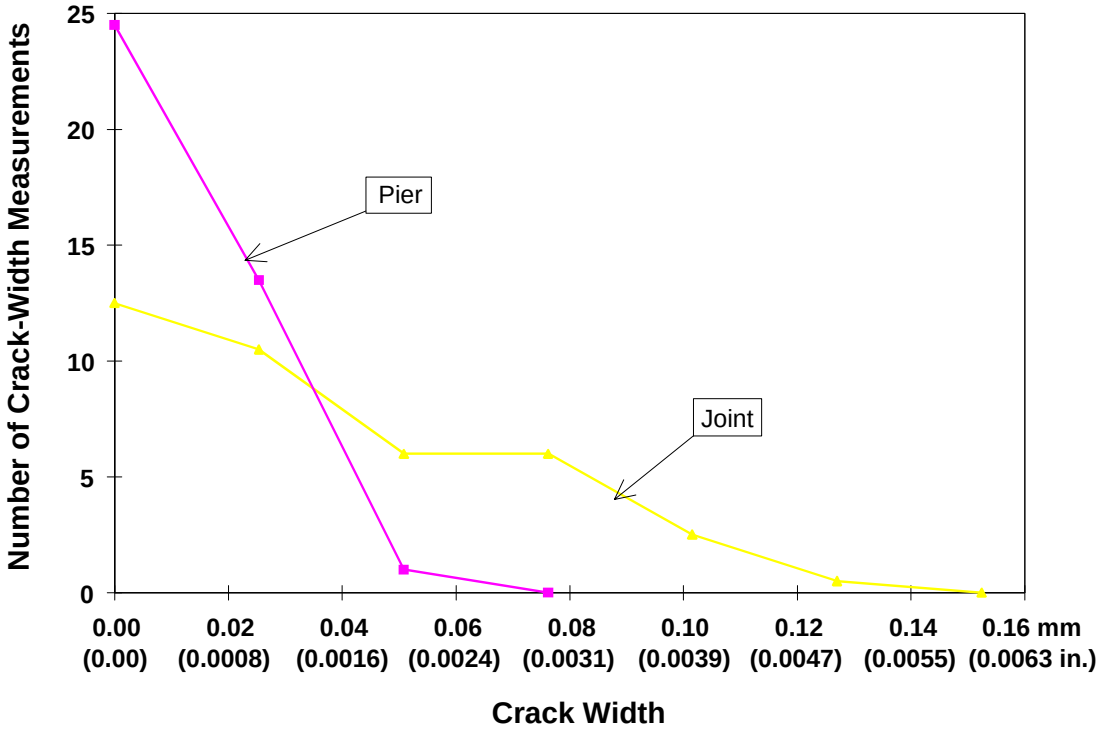

Figure 5.8 Distribution of Service Load Crack Widths in Each Region of Specimen POJ-PS-100-RP1

5.2.2.4 Performance of Repair Components

The average initial stress in the Dywidag bars after post-tensioning was approximately 593 MPa (86.0 ksi) or 61 percent of the ultimate strength. The maximum stress in the bars at FL/ϕ was approximately 615 MPa (89.2 ksi) or 64 percent of ultimate.

The maximum stress in the top beam was approximately 124 MPa (18 ksi), occurring in the middle of the top flange. The vertical displacement profiles for the stiffened top beam are shown in Figure 5.9. At FL/ϕ, the south end of the beam was approximately 0.51 mm (0.020 in.) lower than the north end. The highest difference in displacement between the ends was 0.88 mm (0.034 in.) and occurred after initial post-tensioning but before loading was resumed. The maximum curvature in the beam, indicated by a difference in vertical displacement between the center of the beam and the average displacement of the ends of 0.44 mm (0.017 in.), occurred at dead load. At FL/ϕ, the displacement was 0.36 mm (0.014 in.).

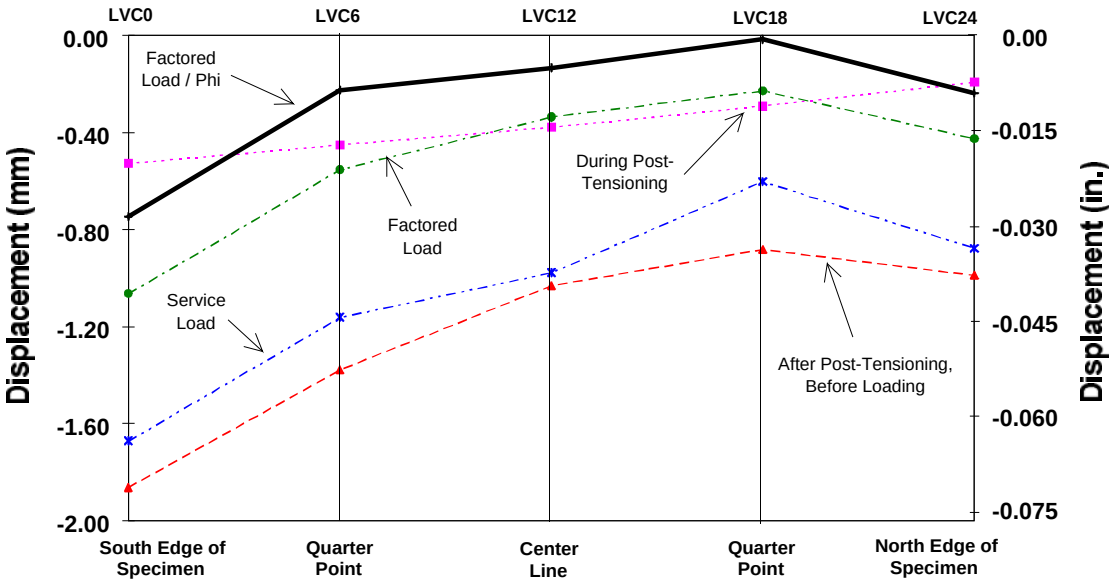

Figure 5.9 Vertical Displacement in the Top Beam for Specimen POJ-PS-100-RP1

Displacements of the side plates are shown in Figures 5.10 and 5.11. Initial movement was approximately 0.5 mm (0.020 in.) at the bottom of the plate and approximately 0.6 mm (0.025 in.) at the top. The largest displacement normal to the specimen occurred at the top row of bolts and measured approximately 0.15 mm (0.0060 in.).

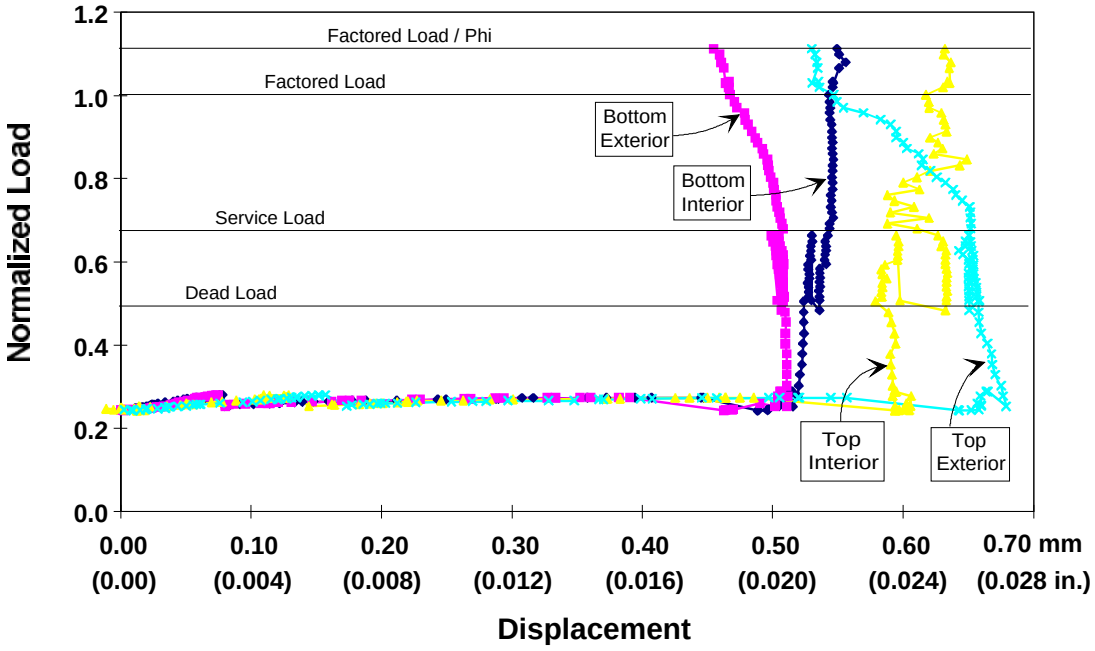

Figure 5.10 Vertical Slippage of the Side Plates on Specimen POJ-PS-100-RP1

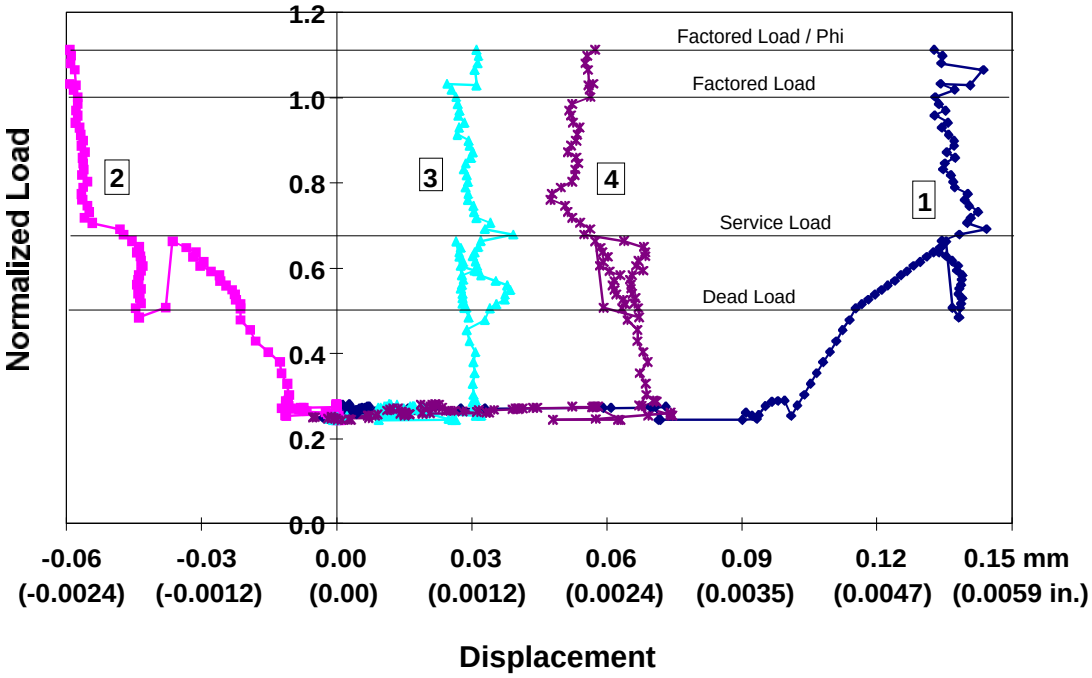

Figure 5.11 Movement of the Side Plates Normal to Specimen POJ-PS-100-RP1, Measured at Each Row of Bolts. (Gauges are numbered from top to bottom.)

5.2.3 POJ-PS-100-RP2

5.2.3.1 Strength

The repair for specimen POJ-PS-100-RP1 was modified by removing two of the six post-tensioning bars on each side. The modified specimen was designated POJ-PS-100-RP2. It was loaded to FL/ϕ; then, because this was to be the last test on specimen POJ-PS-100, loading was continued to approximately 25 percent above factored load. At this point, the deflection was great enough to pose a hazard to the testing equipment, so the specimen was unloaded. The strains in selected pier reinforcing bars at mid-depth of the joint are shown in Figure 5.12.

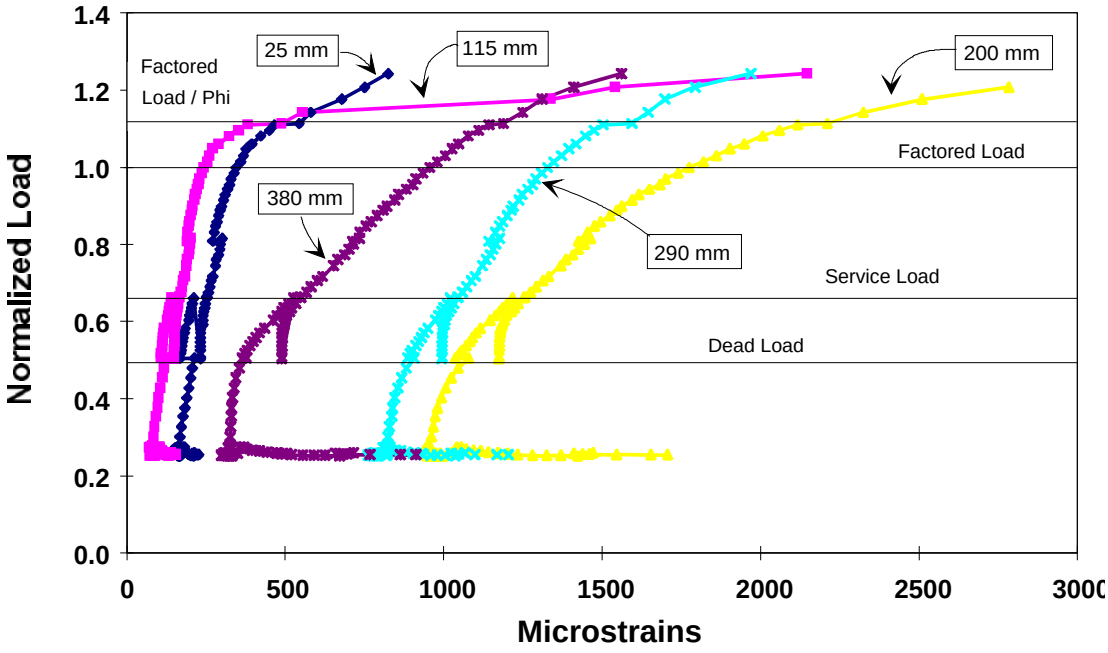

Figure 5.12 Pier Reinforcement Strains in the Joint of Specimen POJ-PS-100-RP2. (Labels indicate the distance of the bars from the exterior face of the pier.)

5.2.3.2 Deflection

A plot of tip deflection versus normalized load is shown in Figure 5.13. The maximum total tip deflection was approximately 22 mm (0.88 in.), while the deflection at FL/ϕ was approximately 17 mm (0.68 in.). The increase in deflection from one-half dead load to FL/ϕ was approximately 11 mm (0.43 in.). The slope of the curve at FL/ϕ is quite low, but load is still increasing. As was the case for the first repair, the load/displacement curve is incomplete, because the specimen was never fully unloaded after the first two tests. Figure 5.13 therefore shows the total deflection, including the residual deformations from the

two previous tests. The increase in tip deflection from dead load to FL/ϕ was approximately 9.0 mm (0.35 in.).

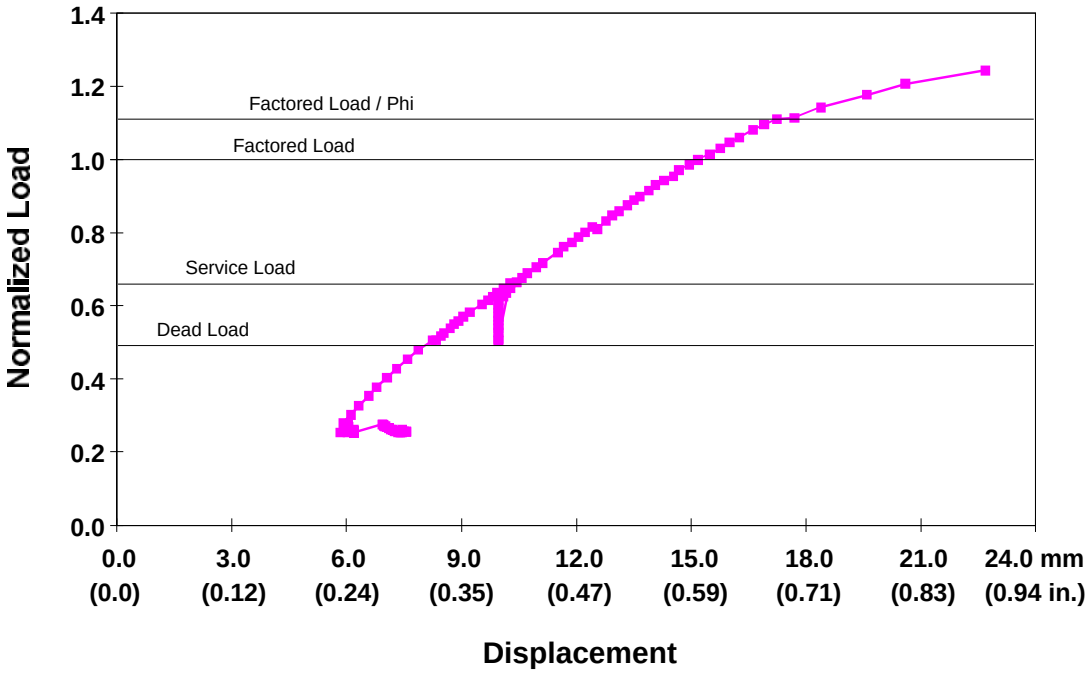

Figure 5.13 Tip Displacement vs. Normalized Load Response for Specimen POJ-PS-100-RP2

5.2.3.3 Cracking

Cracks in the specimen at ultimate load are shown in Figure 5.14. A total of 104 crack width measurements (from both sides of the specimen) were made at service load. The number of cracks and the maximum crack width in each region of the specimen are listed in Tables 5.5 and 5.6. The distribution of measurements in each region is shown in Figure 5.15. The crack width measurements are incomplete, because those cracks covered by the repair

could not be measured. Also, as discussed above, the crack widths included effects from previous loadings, so comparisons with measurements from other tests are somewhat ambiguous. Maximum measured crack widths in the pier and joint were smaller (substantially so for the joint) than crack widths measured during testing of the unrepaired specimen. Cracking in the overhang initiated during testing of specimen POJ-PS-100-RP2.

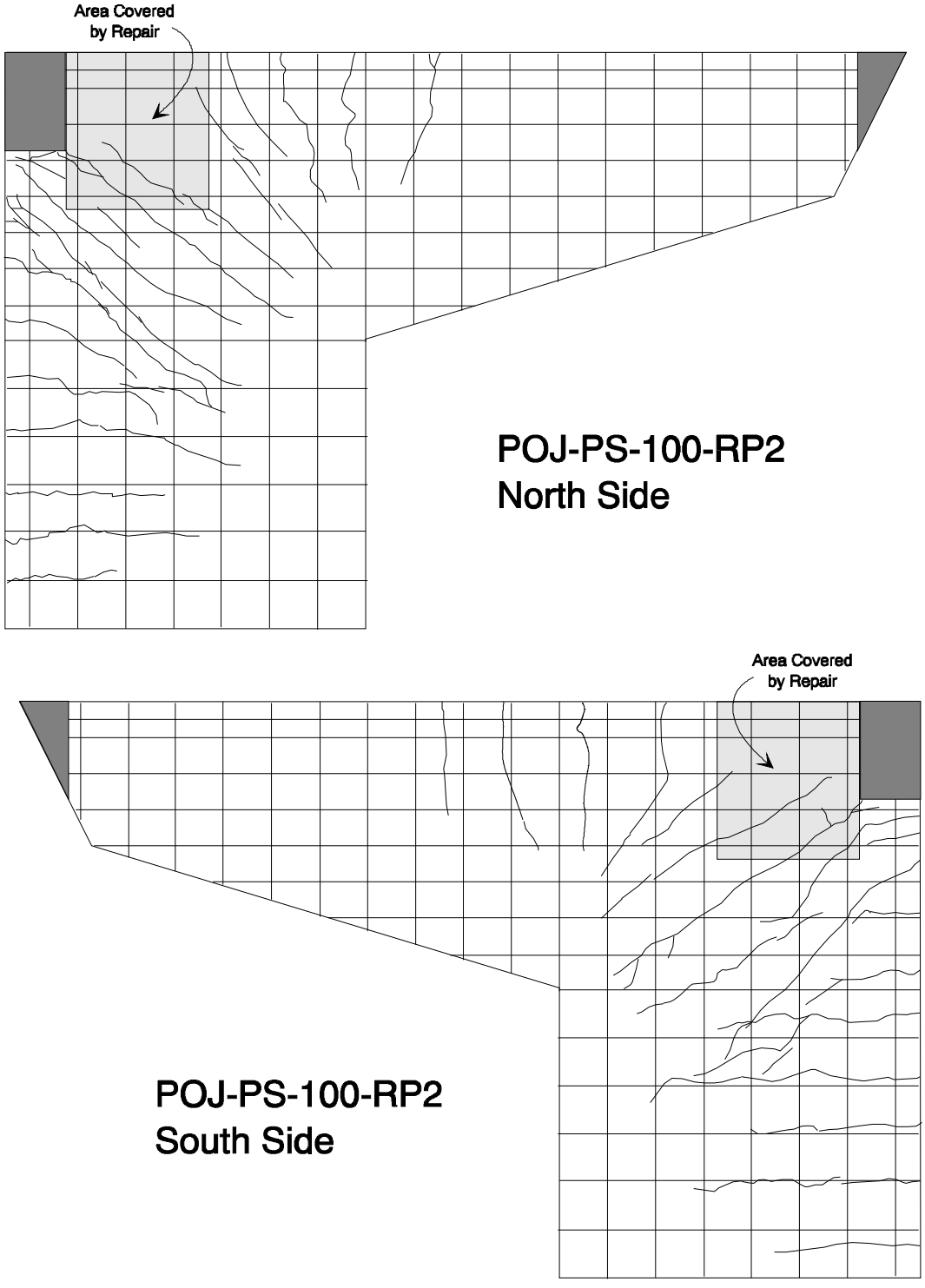

Figure 5.14 Crack Patterns on Specimen POJ-PS-100-RP2 at Ultimate Load

Table 5.5 Number of Cracks in Specimen POJ-PS-100-RP2 at Service Load

	Pier	Joint	Overhang
North Side	5	8	1
South Side	4	9	0

Table 5.6 Maximum Crack Widths in Specimen POJ-PS-100-RP2 at Service Load

	Pier		Joint		Overhang	
North Side	0.08 mm	0.0030 in.	0.14 mm	0.0055 in.	0.04 mm	0.0015 in.
South Side	0.08 mm	0.0030 in.	0.28 mm	0.0110 in.	0 mm	0.0000 in.

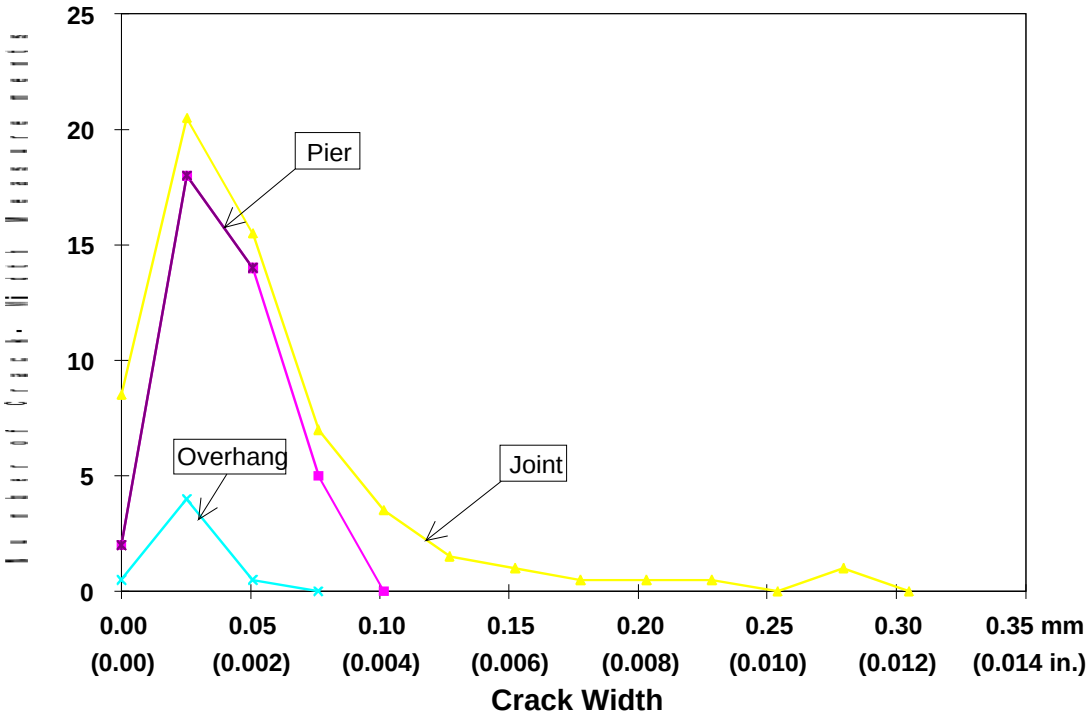

Figure 5.15 Distribution of Service Load Crack Widths in Each Region of Specimen POJ-PS-100-RP2

5.2.3.4 Performance of Repair Components

Although this test was continued to a higher load than the previous test, the decrease in number of post-tensioning bars on each side was expected to produce lower stress in the repair components. The average initial stress in the Dywidag bars after post-tensioning was 547 MPa (79.4 ksi) or 57 percent of the ultimate strength of the bars. The maximum stress in the bars was 602 MPa (87.3 ksi) or 62 percent of ultimate.

The maximum stress in the top beam was approximately 94 MPa (13.7 ksi), occurring in the middle of the top flange. The overall maximum stress was approximately 108 MPa (15.7 ksi), occurring in a triangular stiffener on the side plate assembly. The vertical displacement profiles for the top beam assembly are shown in Figure 5.16. At FL/ϕ, the north end of the beam was approximately1.23 mm (0.048 in.) lower than the south end, the maximum difference during the test. The maximum difference in vertical displacement between the center of the beam and the average of the ends was 0.31 mm (0.012 in.), occurring at service load. At FL/ϕ, the displacement was 0.13 mm (0.005 in.).

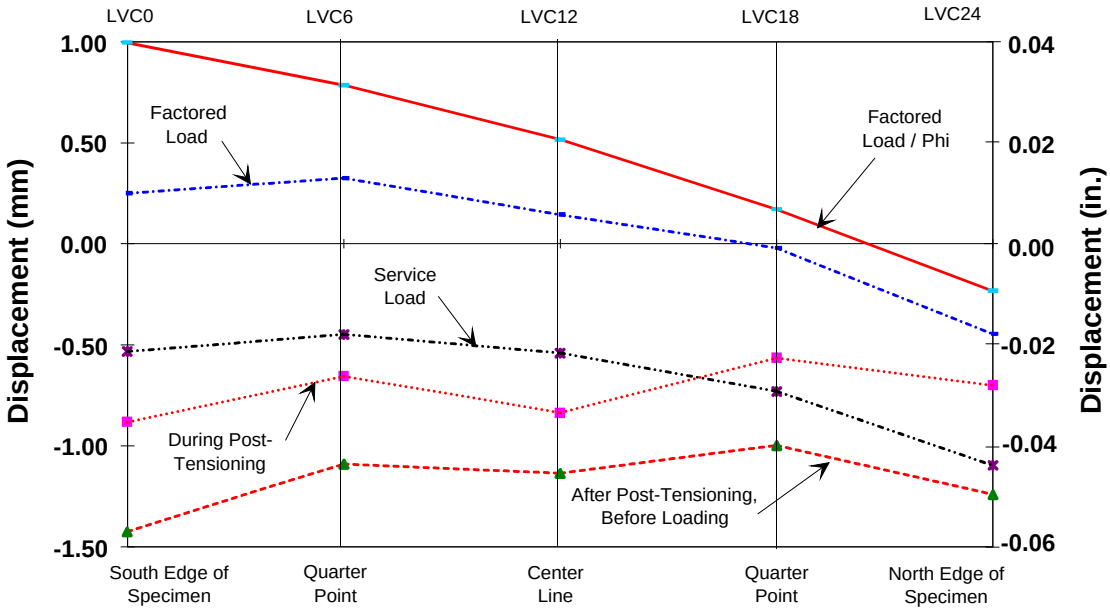

Figure 5.16 Vertical Displacement in the Top Beam for Specimen POJ-PS-100-RP2

Vertical displacements in the side plates, relative to the specimen, are shown in Figure 5.17. Maximum displacement occurred at the end of post-tensioning, after which the displacements decreased, especially at the edge of the plate closest to the exterior face of the pier. This probably indicates increased displacement of the specimen, rather than decreased displacement of the plate. Movement of the side plates normal to the specimen was less than 0.08 mm (0.003 in.) at maximum load, which was too small to plot clearly.

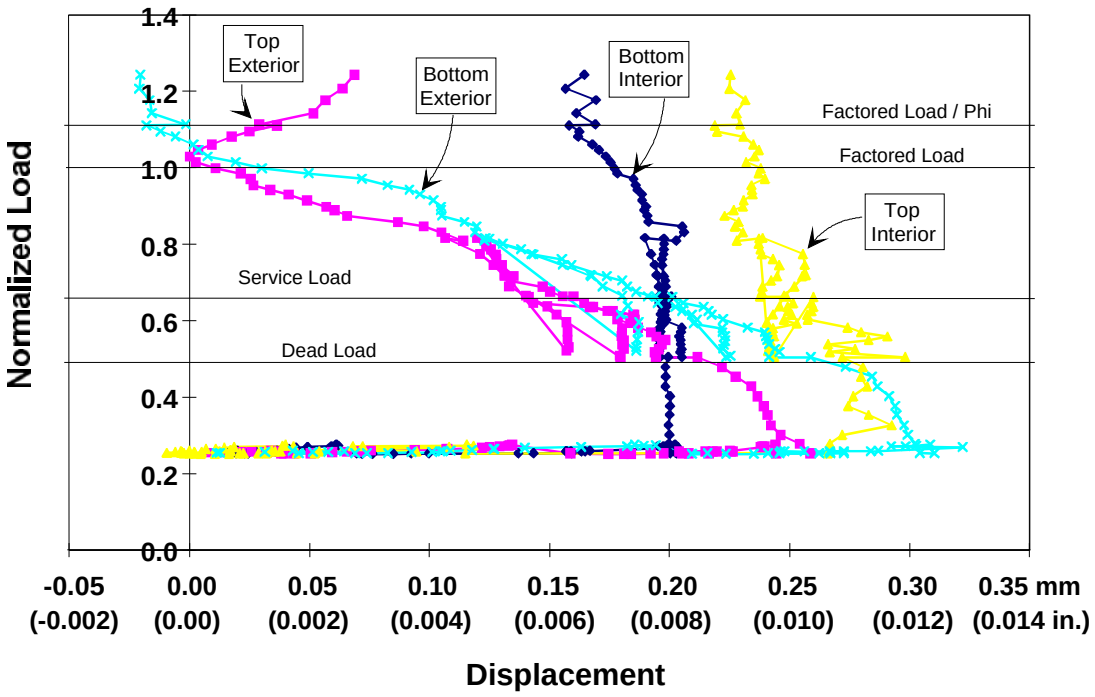

Figure 5.17 Vertical Slippage of the Side Plates on Specimen POJ-PS-100-RP2

5.3 Reinforced Concrete Specimen Tests

5.3.1 POJ-RC2

5.3.1.1 Strength

The unrepaired reinforced concrete specimen (POJ-RC2) was intended to be tested to service load. However, substantial deflection under sustained loading began to occur at a normalized load of 0.65, or about 98 percent of service load. To prevent further damage to the specimen, loading was discontinued at that point. Therefore, its actual normalized ultimate strength was approximately 0.65. Strains in the pier reinforcement at mid-depth of the joint are shown in Figure 5.18.

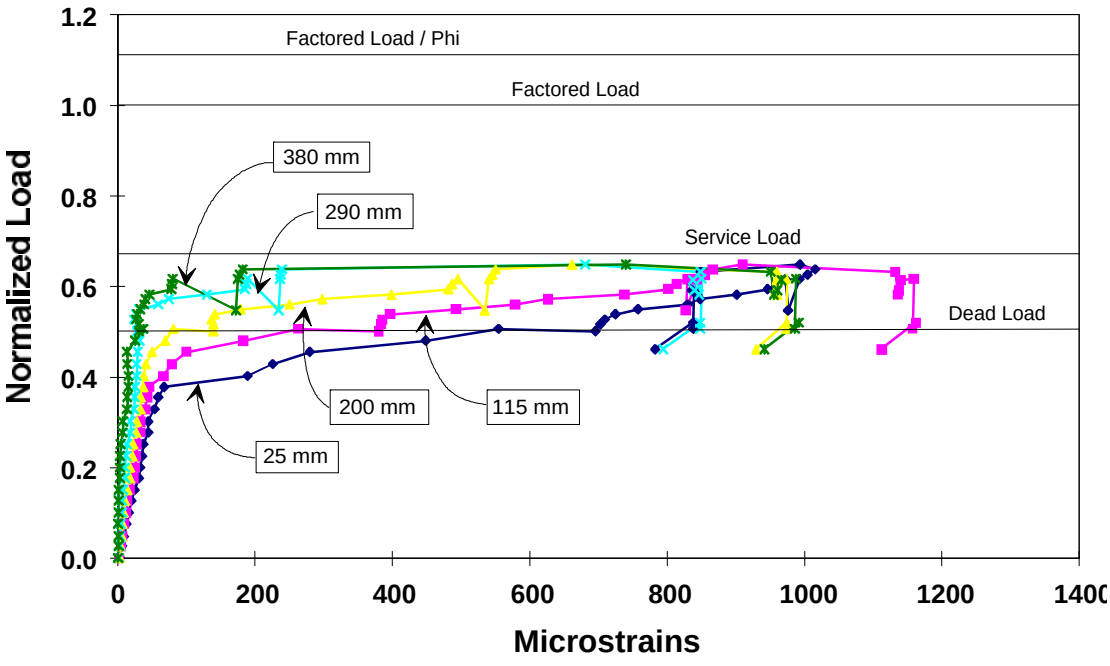

Figure 5.18 Pier Reinforcement Strains in the Joint of Specimen POJ-RC2. (Labels indicate the distance of the bars from the exterior face of the pier.)

5.3.1.2 Deflection

A plot of tip deflection versus normalized load is shown in Figure 5.19. A maximum tip deflection of approximately 15 mm (0.59 in.) was reached when the test was stopped.

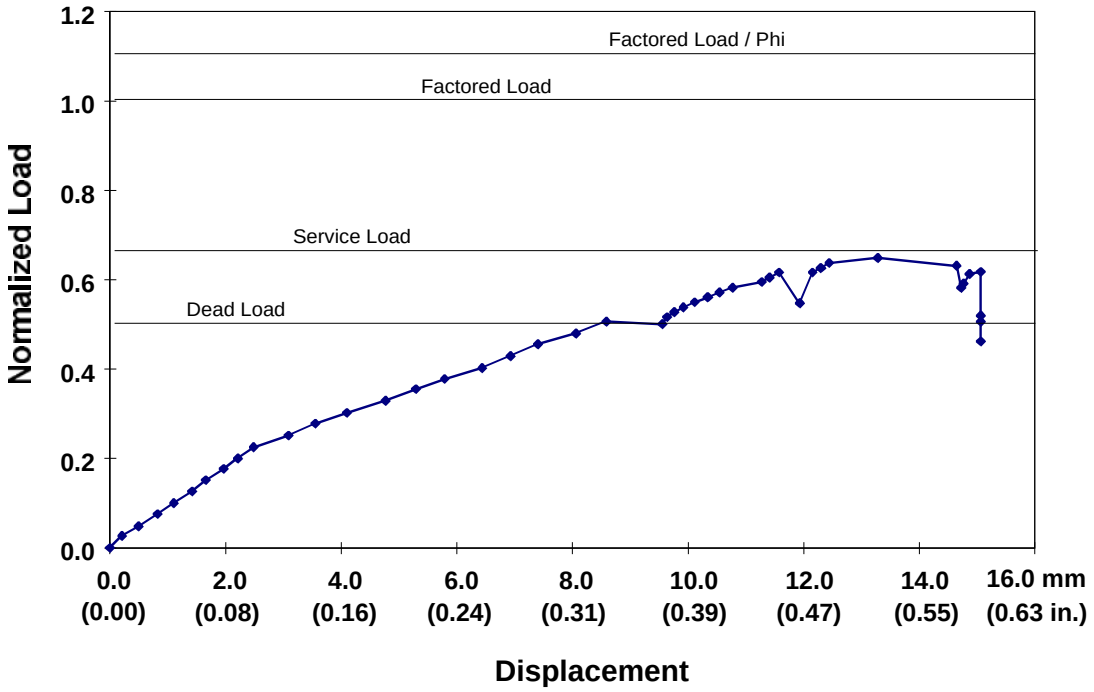

Figure 5.19 Tip Displacement vs. Normalized Load Response for Specimen POJ-RC2

5.3.1.3 Cracking

The pattern of cracking in the specimen at its ultimate load of 0.65 is shown in Figure 5.20. A total of 273 crack width measurements (from both sides of the specimen) were made at that load. The number of cracks and the maximum crack width in each region of the

specimen are listed in Tables 5.7 and 5.8. The distribution of crack widths measurements is shown in Figure 5.21.

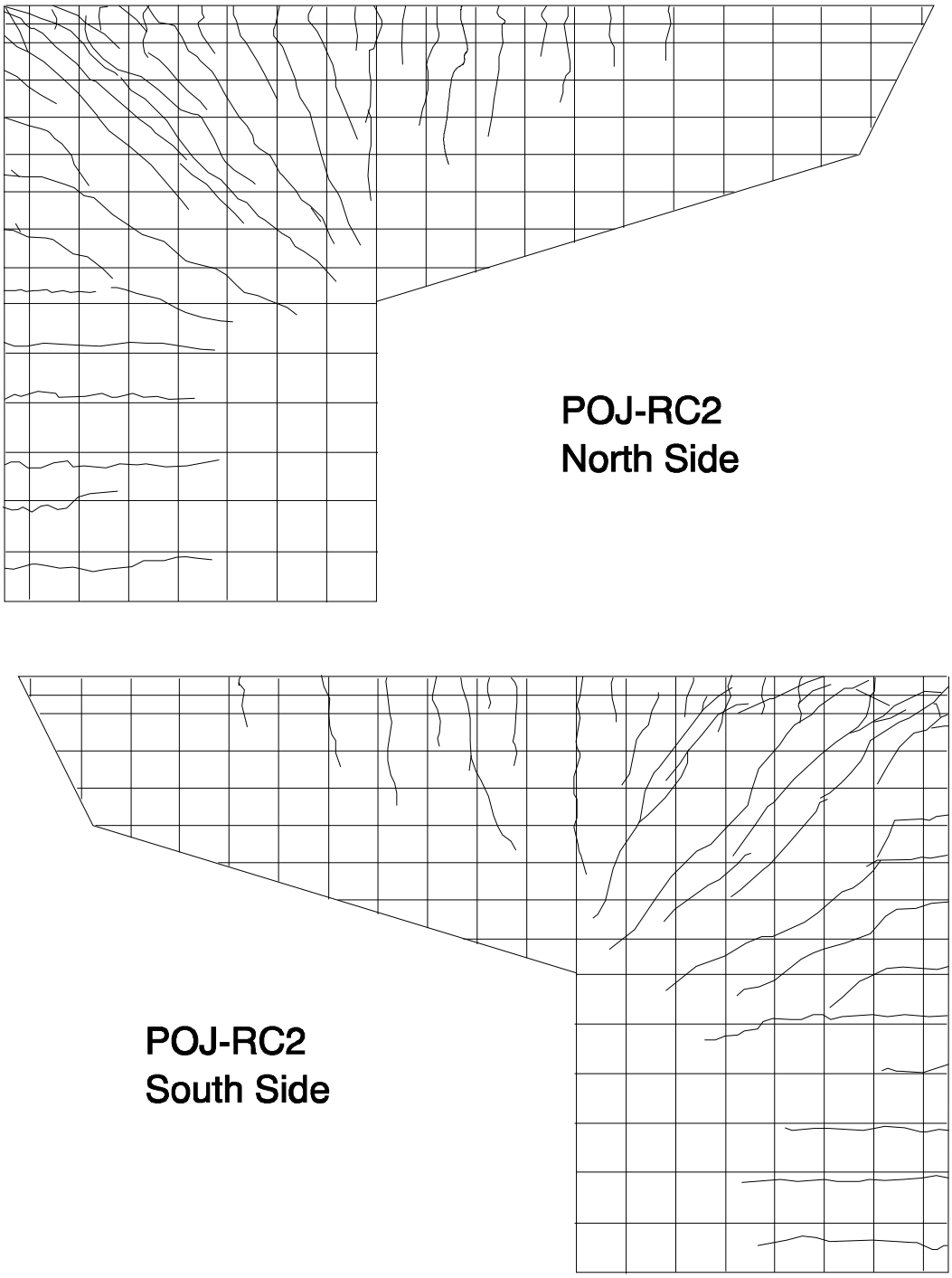

Figure 5.20 Crack Patterns on Specimen POJ-RC2 at its Ultimate Load

Table 5.7 Number of Cracks in Specimen POJ-RC2 at its Ultimate Load

	Pier	Joint	Overhang
North Side	5	18	8
South Side	5	17	7

Table 5.8 Maximum Crack Widths in Specimen POJ-RC2 at its Ultimate Load

	Pier		Joint		Overhang	
North Side	0.17 mm	0.0065 in.	0.51 mm	0.0200 in.	0.10 mm	0.0040 in.
South Side	0.15 mm	0.0060 in.	1.68 mm	0.0660 in.	0.10 mm	0.0040 in.

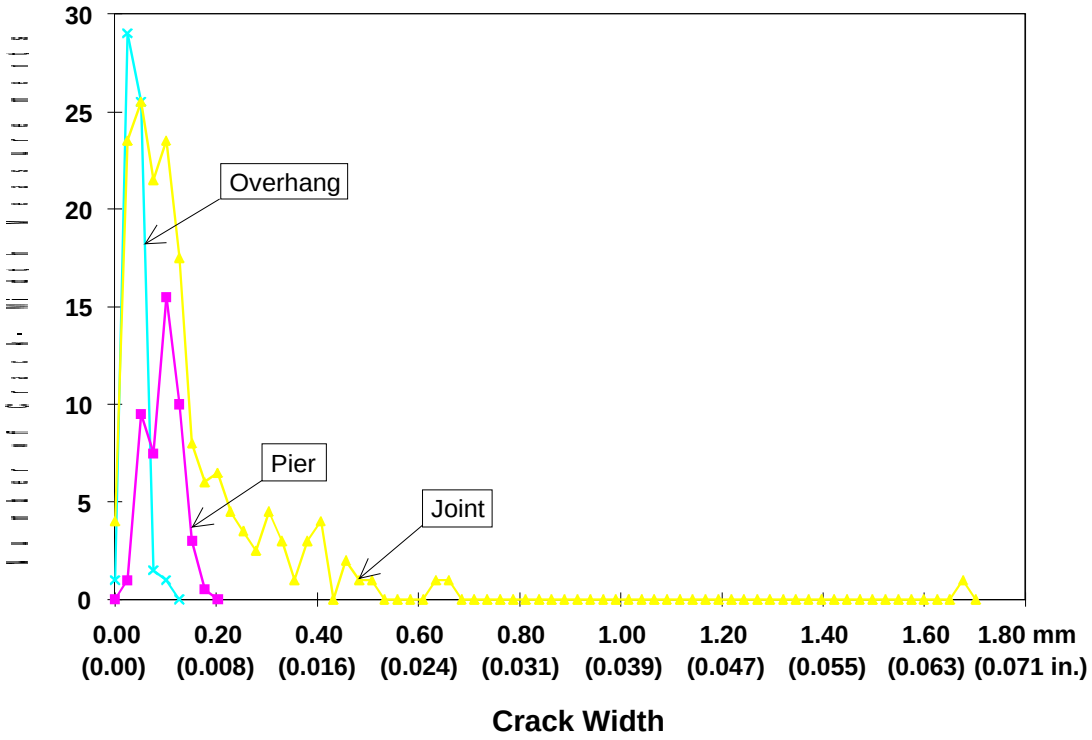

Figure 5.21 Distribution of Service Load Crack Widths in Each Region of Specimen POJ-RC2

5.3.2 POJ-RC2-RP1

5.3.2.1 Strength

Specimen POJ-RC2 was repaired with external diagonal post-tensioning to become POJ-RC2 -RP1. The repaired specimen was loaded to FL/ϕ, at which point it was unloaded to one-half dead load so that further testing could be accomplished. Its actual strength was therefore not determined, although it clearly exceeded design requirements. The strains in pier reinforcement at mid-depth of the joint are shown in Figure 5.22. The discontinuity in the plot is due to the effects of the post-tensioning operation, which occurred at one-half dead load.

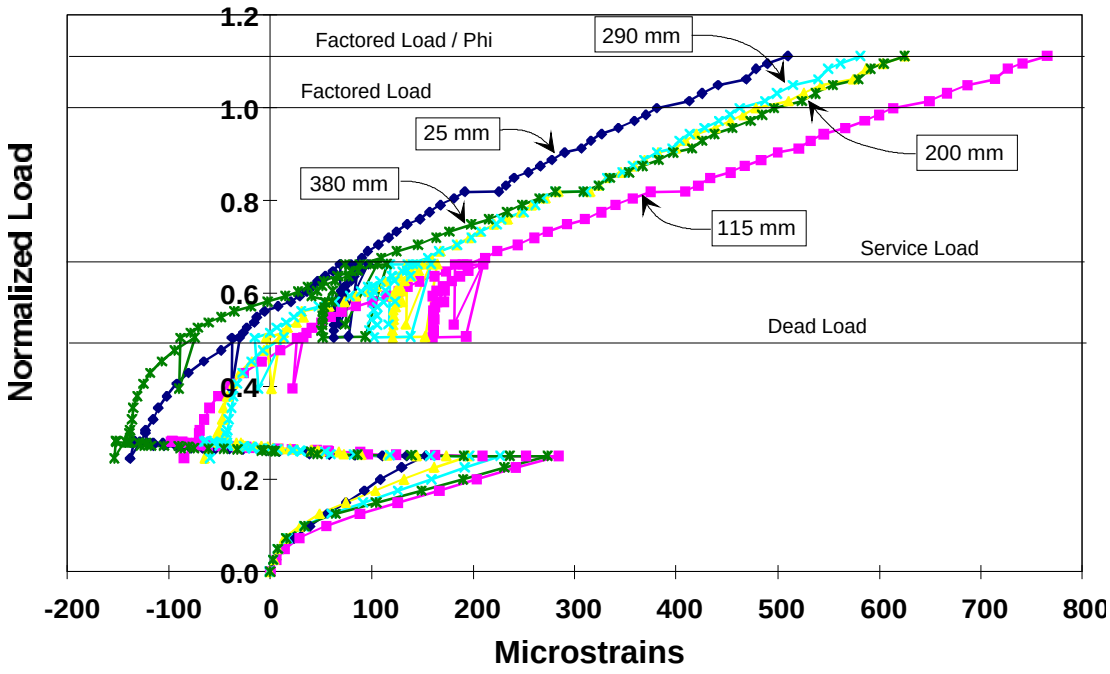

Figure 5.22 Pier Reinforcement Strains in the Joint of Specimen POJ-RC2-RP1. (Labels indicate the distance of the bars from the exterior face of the pier.)

5.3.2.2 Deflection

A plot of tip deflection versus normalized load is shown in Figure 5.23. The discontinuity at one-half dead load is due to the post-tensioning operation. The deflection at FL/ϕ was approximately 19 mm (0.74 in.). The increase in tip deflection from dead load to FL/ϕ was approximately 13 mm (0.51 in.).

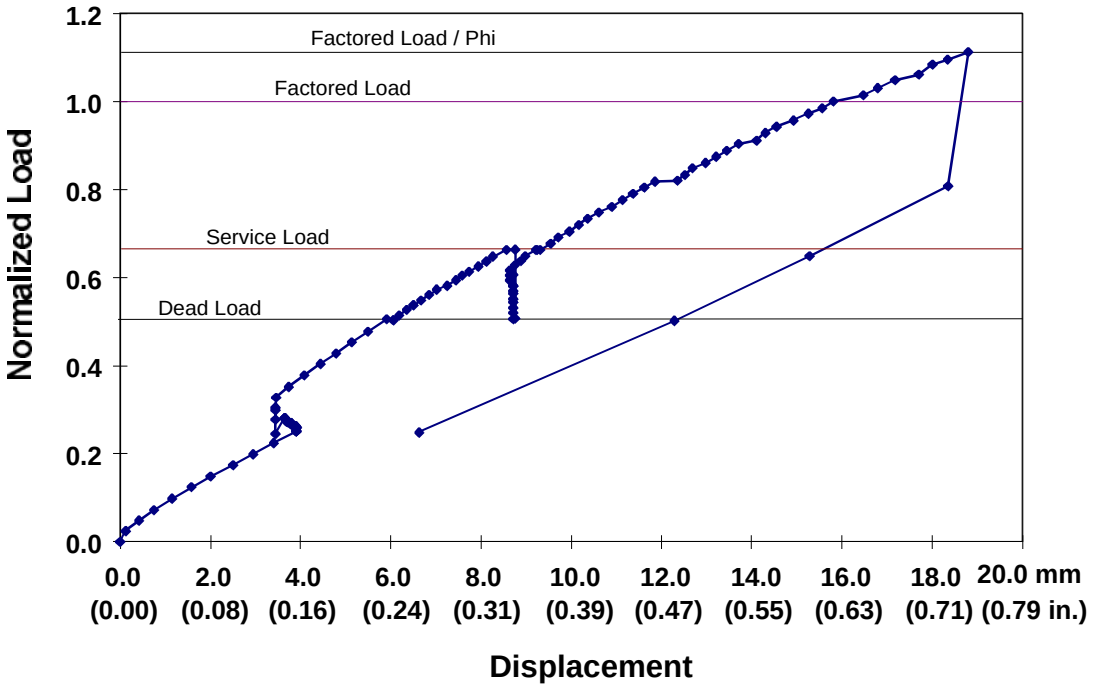

Figure 5.23 Tip Displacement vs. Normalized Load Response for Specimen POJ-RC2-RP1

5.3.2.3 Cracking

Cracks in the specimen at FL/ϕ are shown in Figure 5.24. The number of cracks and the maximum crack width in each region of the specimen at service load are listed in Tables 5.9 and 5.10. The distribution of crack widths is shown in Figure 5.25. Crack widths include residual effects from the previous loading. Therefore, direct comparisons of crack widths with those from other tests may be of dubious value. In any case, maximum measured crack widths generally exceeded those measured during testing of specimen POJ-RC2, in part because service loads applied to specimen POJ-RC2-RP1 exceeded those applied to specimen POJ-RC2. Growth of the major joint crack was monitored by measuring the horizontal displacement of the concrete on each side of the crack and calculating the difference between the readings. While this does not provide the actual change in crack width, it does give an indication of relative growth. A plot of the horizontal component of crack width growth is shown in Figure 5.26.

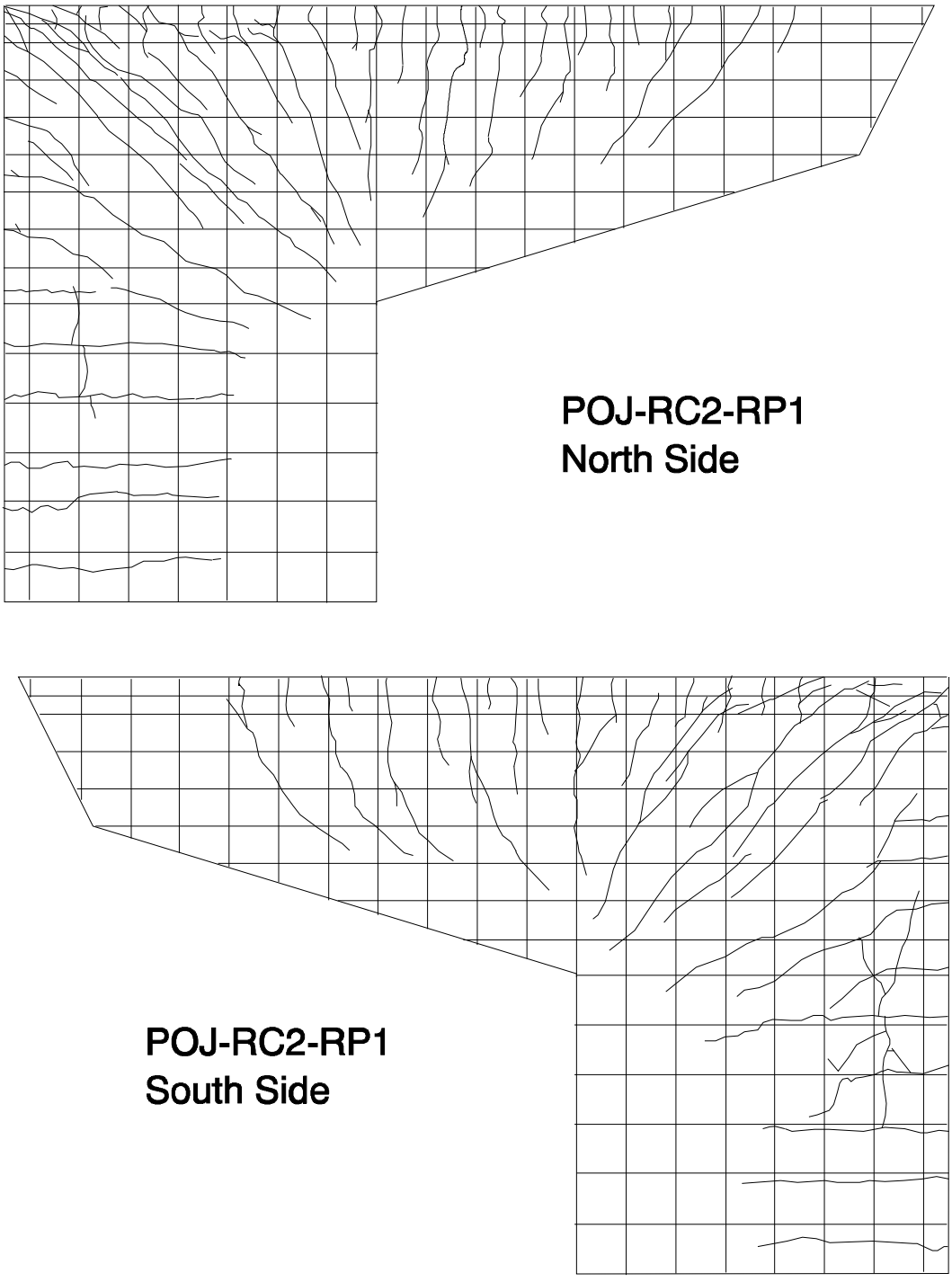

Figure 5.24 Crack Patterns on Specimen POJ-RC2-RP1 at Factored Load / ϕ

Table 5.9 Number of Cracks in Specimen POJ-RC2-RP1 at Service Load

	Pier	Joint	Overhang
North Side	5	18	8
South Side	5	17	9

Table 5.10 Maximum Crack Widths in Specimen POJ-RC2-RP1 at Service Load

	Pier		Joint		Overhang	
North Side	0.31 mm	0.0120 in.	0.79 mm	0.0310 in.	0.10 mm	0.0040 in.
South Side	0.46 mm	0.0180 in.	0.94 mm	0.0370 in.	0.13 mm	0.0050 in.

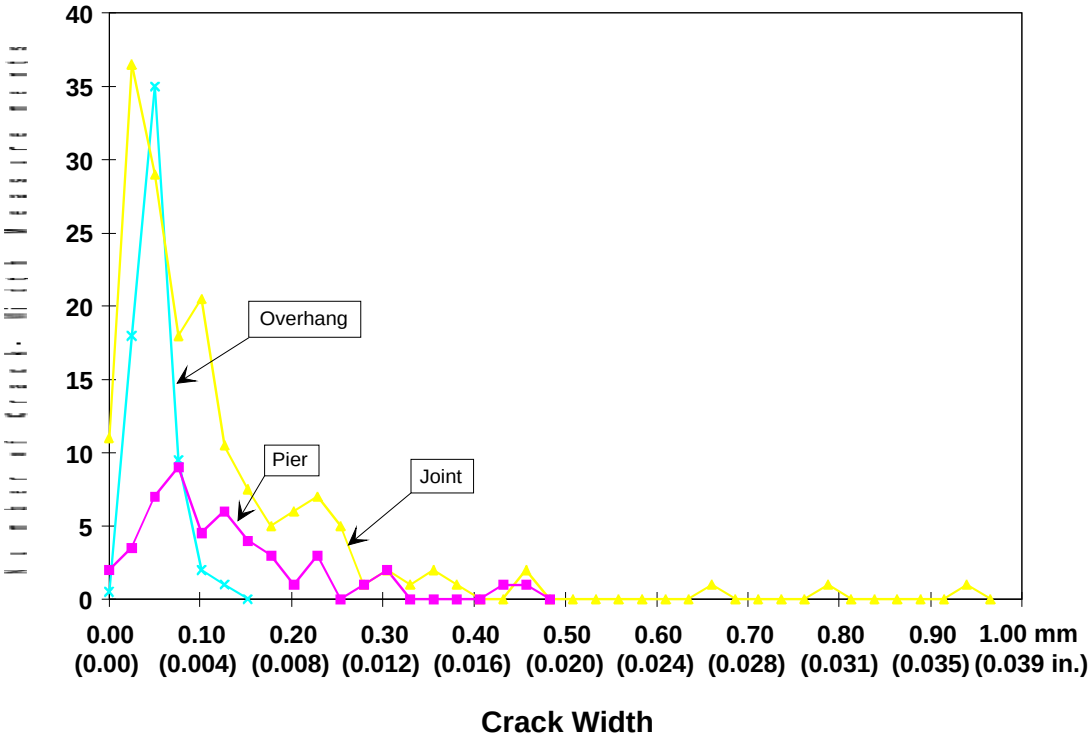

Figure 5.25 Distribution of Service Load Crack Widths in Each Region of Specimen POJ-RC2-RP1

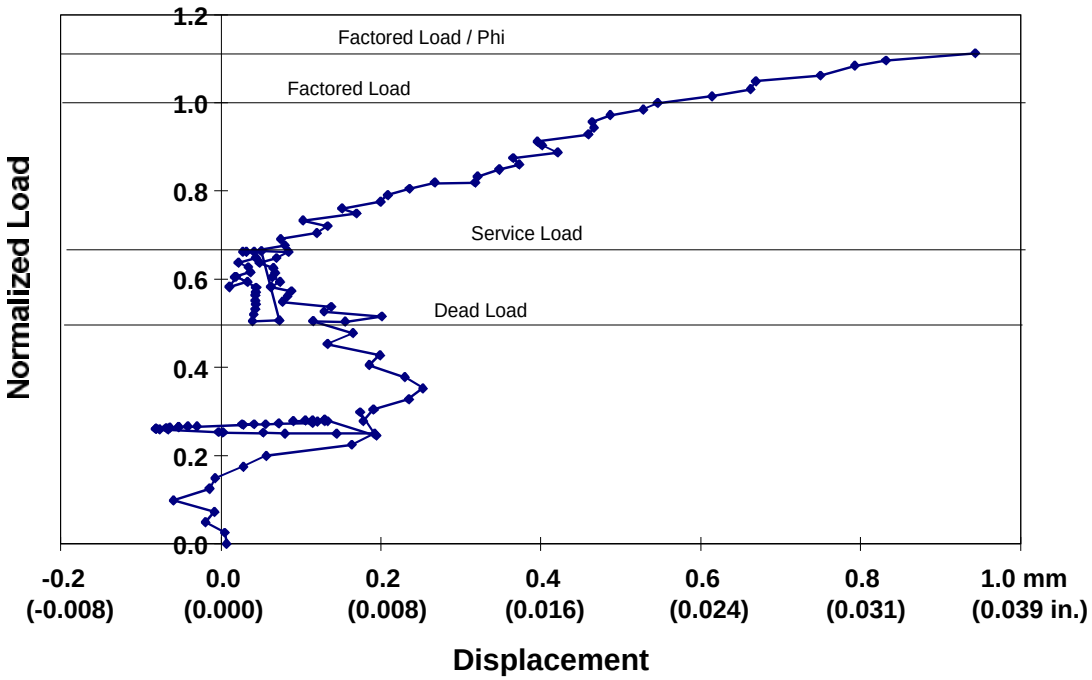

Figure 5.26 Horizontal Component of Growth of Main Joint Crack on Specimen POJ-RC2-RP1

5.2.2.4 Performance of Repair Components

The readings from strain gauges attached to plates in the repair hardware indicated that the maximum stress was slightly under half of yield stress. Displacements of the plates are shown in Figure 5.27. Initial slippage consisted of approximately 6.4 mm (0.25 in.) for the side plate and approximately 7.6 mm (0.30 in.) for the top plate. During loading, the top plate moved an additional 0.7 mm (0.03 in.), while the extra displacement on the side plate was too small to be measured.

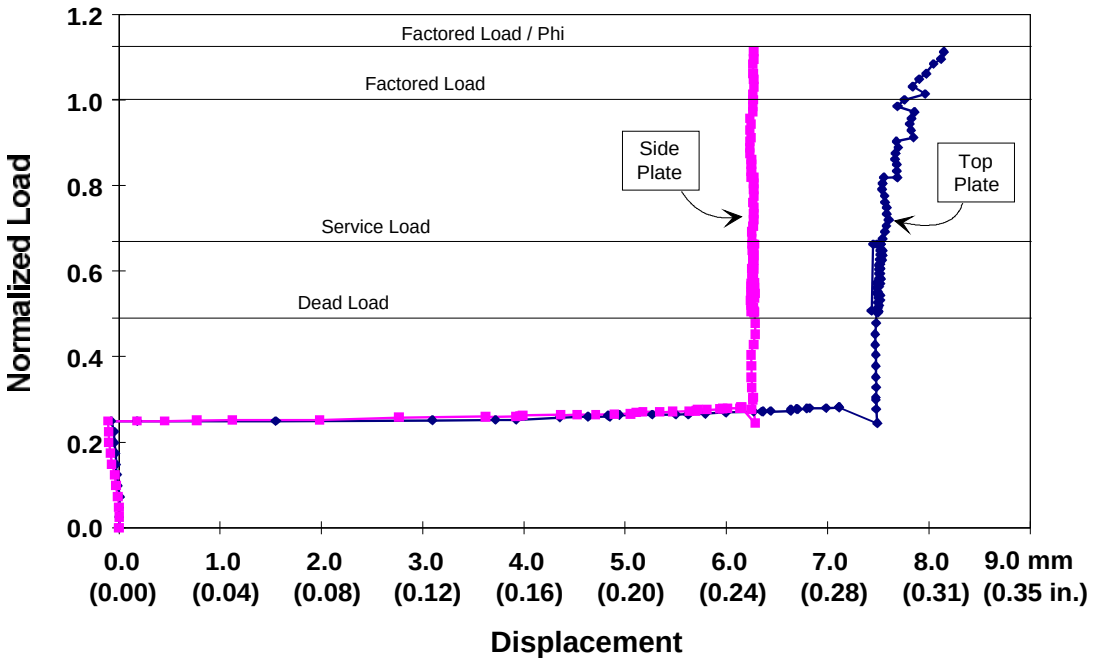

Figure 5.27 Normalized Load vs. Plate Slippage Curves for Specimen POJ-RC2-RP1

5.3.3 POJ-RC2-RP2

5.3.3.1 Strength

The external diagonal post-tensioning was removed from specimen POJ-RC2 and internal vertical post-tensioning was installed to create POJ-RC2 -RP2. The repaired specimen was loaded to FL/ϕ, at which point it was unloaded so that further testing could be accomplished. Its actual strength was therefore not determined, although, obviously, it exceeded design requirements. Strains at mid-depth of the joint in the pier reinforcing bars are shown in Figure 5.28.

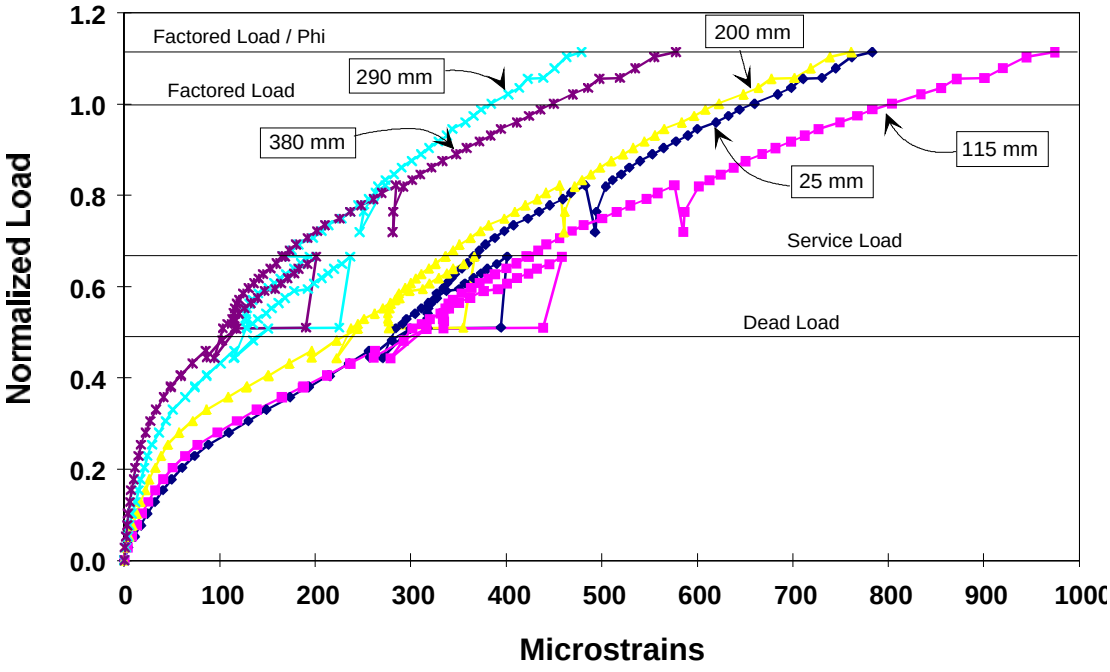

Figure 5.28 Pier Reinforcement Strains in the Joint of Specimen POJ-RC2-RP2. (Labels indicate the distance of the bars from the exterior face of the pier.)

5.3.3.2 Deflection

A plot of tip deflection versus normalized load is shown in Figure 5.29. No discontinuities appear due to the post-tensioning, because the specimen was completely unloaded after post-tensioning and the gauges were re-zeroed at that time. The tip deflection at FL/ϕ was approximately 20 mm (0.78 in.), while the increase in tip deflection from dead load to FL/ϕ was approximately 12.5 mm (0.49 in.).

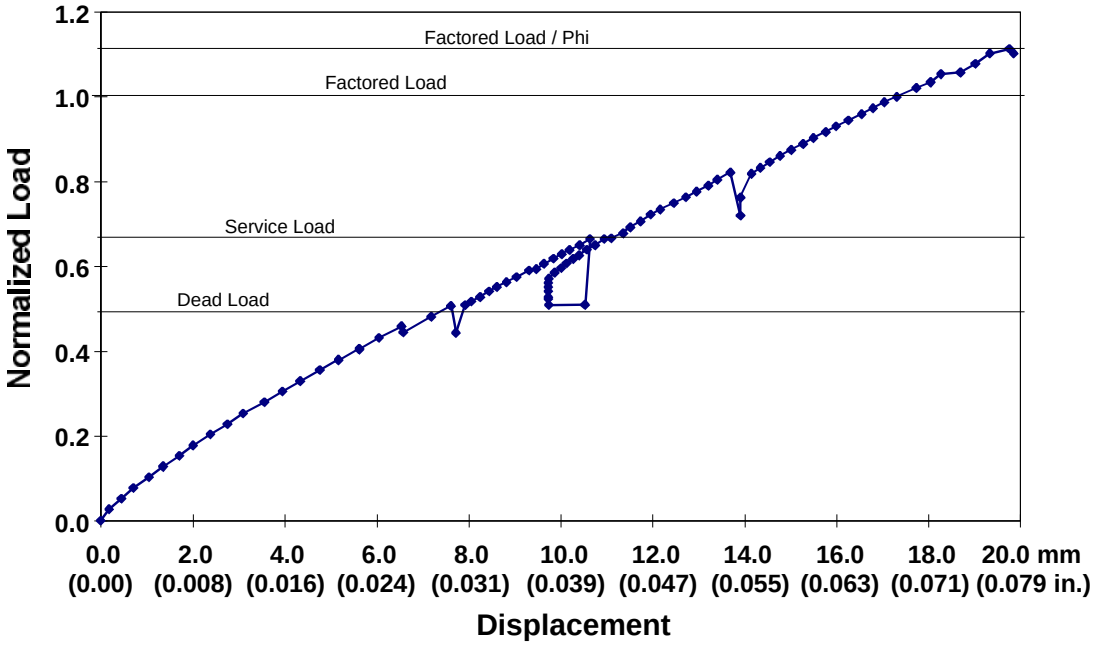

Figure 5.29 Tip Displacement vs. Normalized Load Response for Specimen POJ-RC2-RP2

5.3.3.3 Cracking

Cracks in the specimen at FL/ϕ are shown in Figure 5.30. The number of cracks and the maximum crack width in each region of the specimen at service load are listed in Tables 5.11 and 5.12. Maximum crack-width measurements indicate the internal post-tensioning retrofit reduced maximum crack widths at service load in all regions of the reinforced concrete cantilever bent. The distribution of crack widths is shown in Figure 5.31. Monitoring of the major joint crack, begun in the prior test, was continued. The horizontal displacement of the specimen on either side of the crack is shown in Figure 5.32, while the difference in displacement, representing the change in the horizontal component of the crack width, is shown in Figure 5.33.

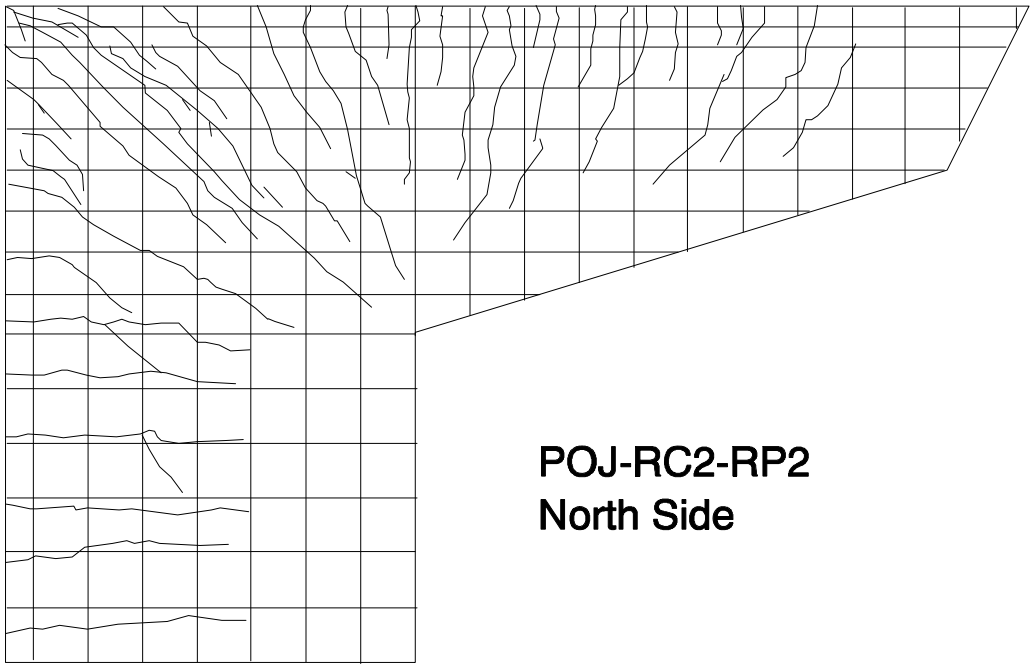

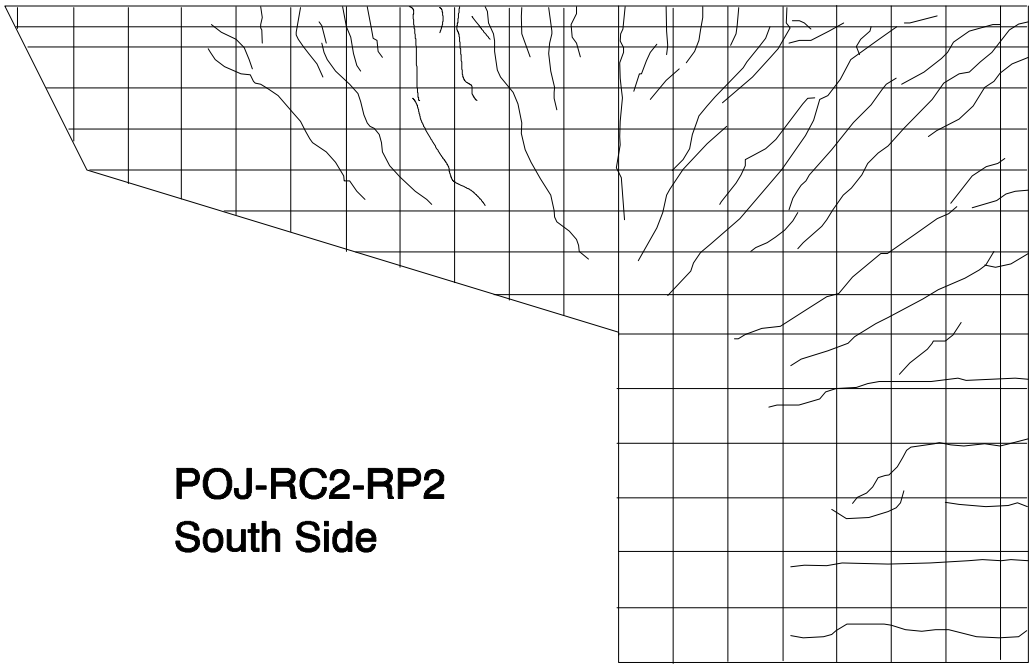

Figure 5.30 Crack Patterns on Specimen POJ-RC2-RP2 at Factored Load / ϕ

Table 5.11 Number of Cracks in Specimen POJ-RC2-RP2 at Service Load

	Pier	Joint	Overhang
North Side	5	17	9
South Side	4	14	13

Table 5.12 Maximum Crack Widths in Specimen POJ-RC2-RP2 at Service Load

	Pier		Joint		Overhang	
North Side	0.11 mm	0.0045 in.	0.23 mm	0.0090 in.	0.05 mm	0.0020 in.
South Side	0.15 mm	0.0060 in.	0.22 mm	0.0085 in.	0.09 mm	0.0035 in.

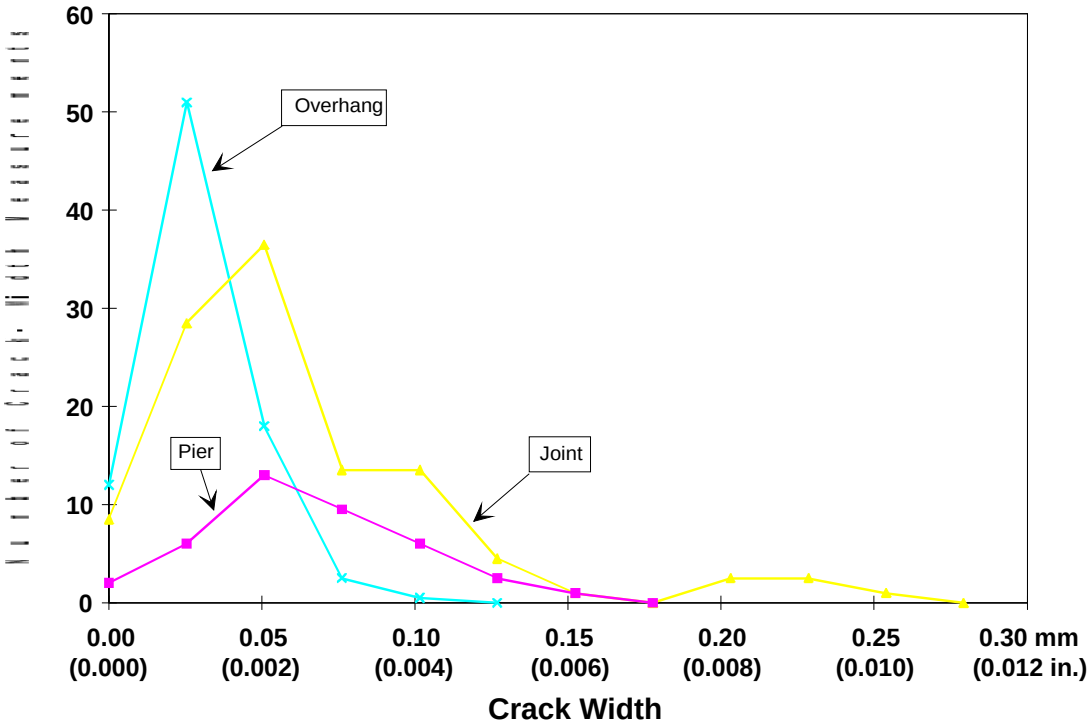

Figure 5.31 Distribution of Service Load Crack Widths in Each Region of Specimen POJ-RC2-RP2

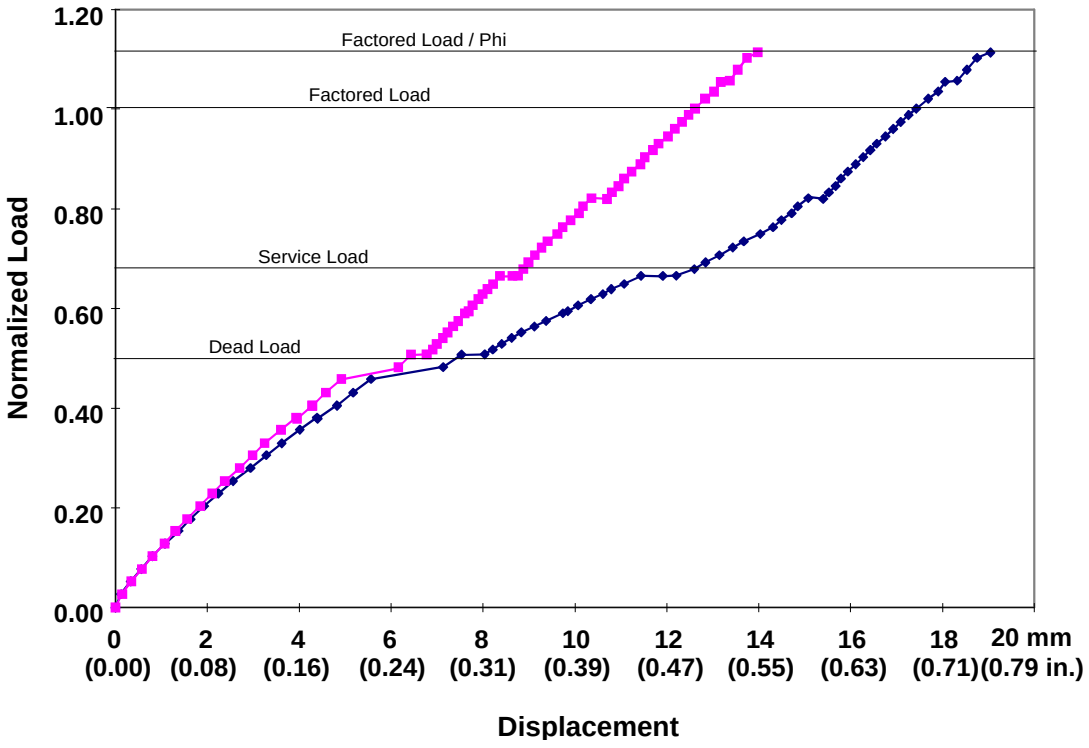

Figure 5.32 Displacement on Either Side of Main Joint Crack on Specimen POJ-RC2-RP2

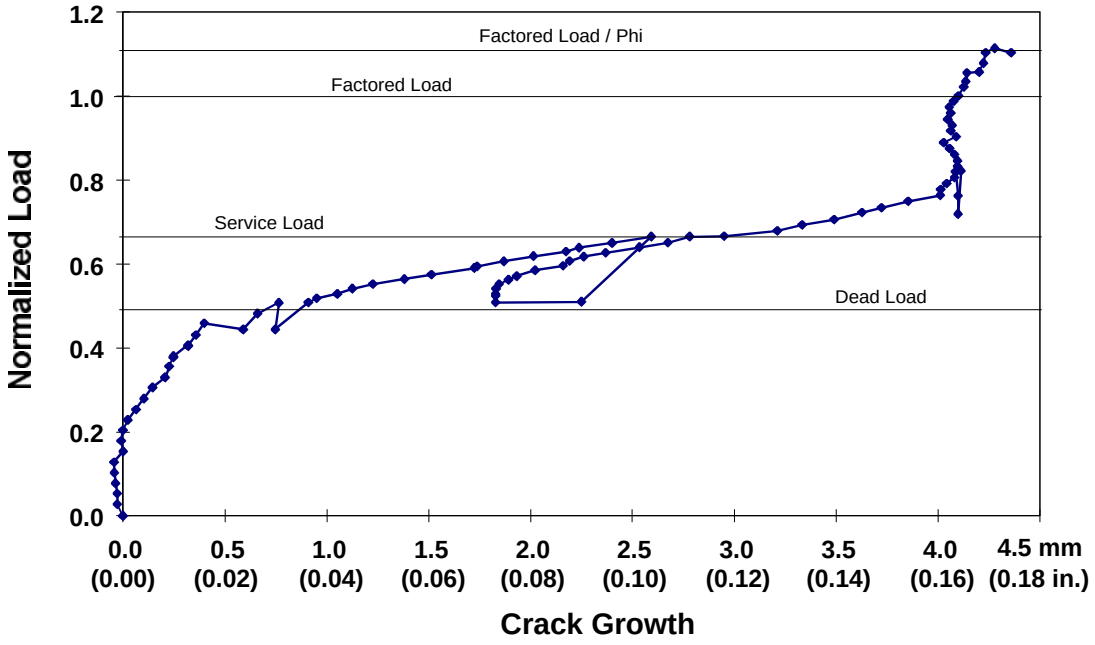

Figure 5.33 Horizontal Component of Crack Width for Growth of Main Joint Crack on Specimen POJ-RC2-RP2

5.3.4 POJ-RC2-RP2a

5.3.4.1 Strength

Specimen POJ-RP2 was modified by coring holes through the top of the joint to damage the main overhang steel and simulate the damage which might be caused by coring holes for field installation of internal vertical post-tensioning. The modified specimen, POJ-RC2-RP2a, was loaded to FL/ϕ, at which point it was unloaded so that further testing could be accomplished. Its actual ultimate strength was therefore not determined, although it was well above the design requirements. Strains at mid-depth of the joint in the pier reinforcing bars are shown in Figure 5.34.

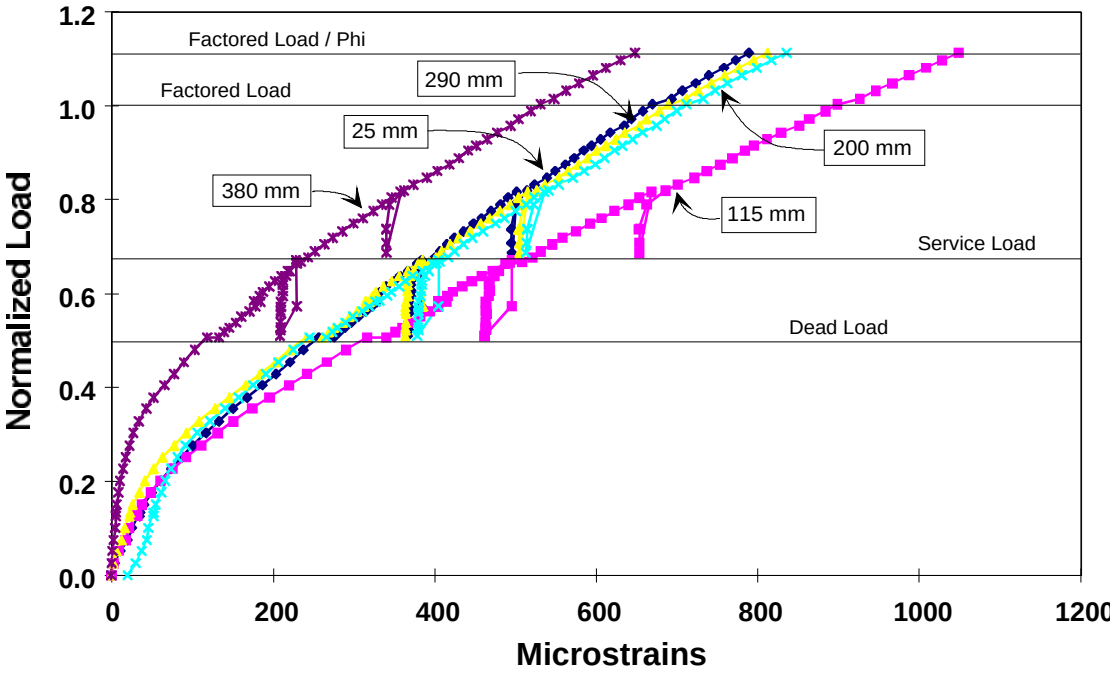

Figure 5.34 Pier Reinforcement Strains in the Joint of Specimen POJ-RC2-RP2a. (Labels indicate the distance of the bars from the exterior face of the pier.)

5.3.4.2 Deflection

A plot of tip deflection versus normalized load is shown in Figure 5.34. No discontinuities appear in the plot becuase no additional post-tensioning was performed for this test. The tip deflection at FL/ϕ was approximately 20 mm (0.78 in.), increasing approximately 12.5 mm (0.49 in.) from dead load to FL/ϕ.

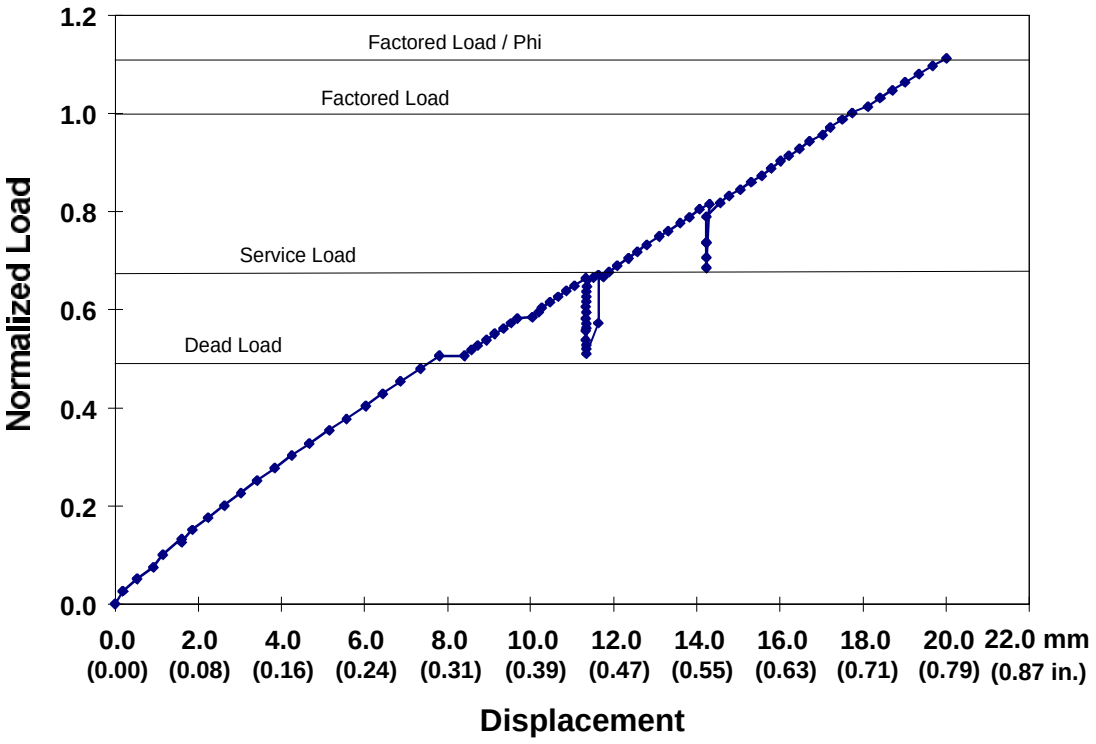

Figure 5.35 Tip Displacement vs. Normalized Load Response for Specimen POJ-RC2-RP2a

5.3.4.3 Cracking

Cracks in the specimen at FL/ϕ are shown in Figure 5.36. The number of cracks and the maximum crack width in each region of the specimen at service load are listed in Tables 5.13 and 5.14. Maximum crack widths for this case generally exceeded those measured for specimen POJ-RC2-RP2. The distribution of crack widths is shown in Figure 5.37. Monitoring of the major joint crack width was continued. The horizontal displacement of the specimen on either side of the crack is shown in Figure 5.38, while the difference in displacement, representing the change in the horizontal component of the crack width, is shown in Figure 5.39.

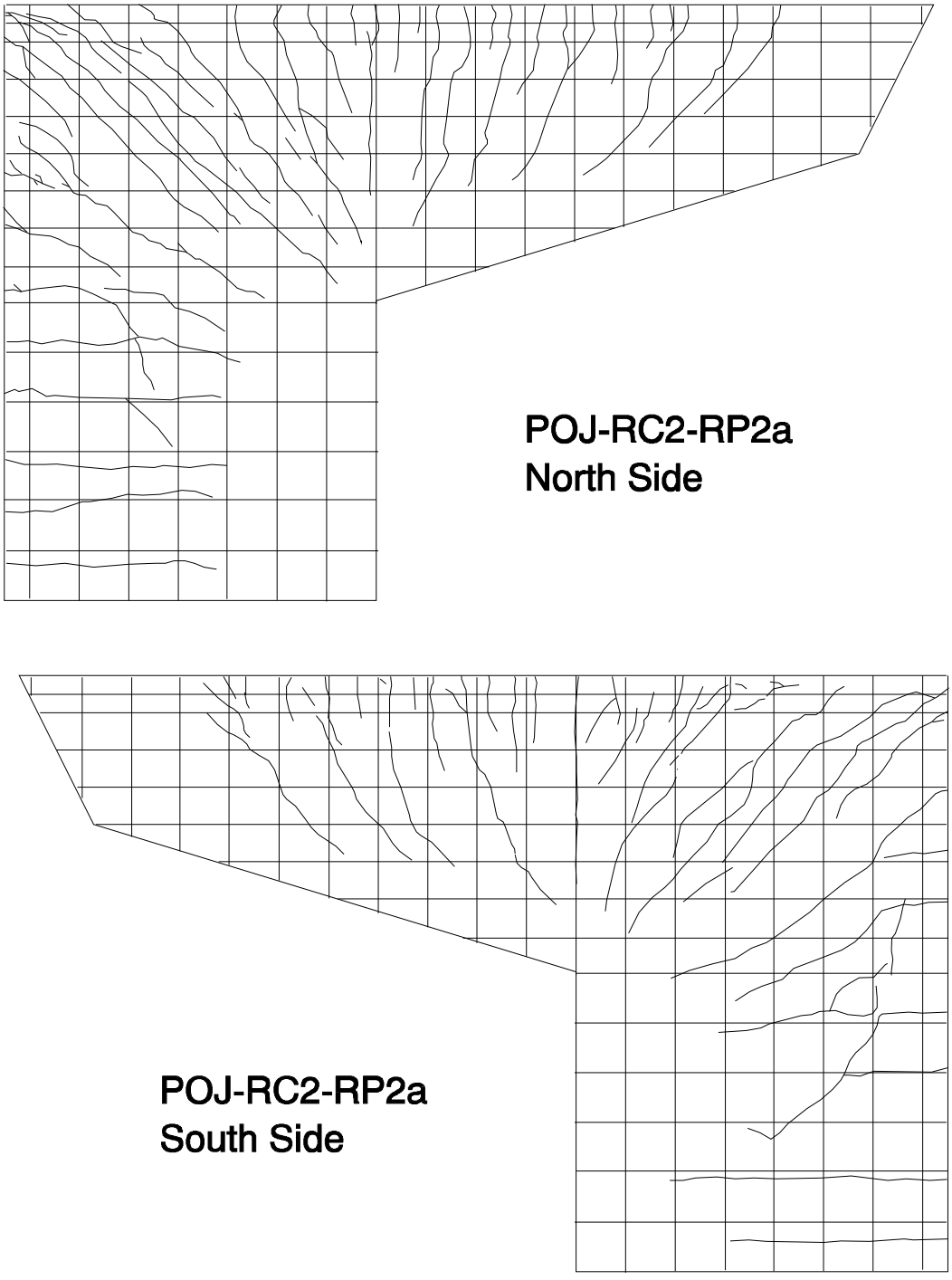

Figure 5.36 Crack Patterns on Specimen POJ-RC2-RP2a at Factored Load / ϕ

Table 5.13 Number of Cracks in Specimen POJ-RC2-RP2a at Service Load

	Pier	Joint	Overhang
North Side	5	20	11
South Side	4	17	13

Table 5.14 Maximum Crack Widths in Specimen POJ-RC2-RP2a at Service Load

	Pier		Joint		Overhang	
North Side	0.15 mm	0.0060 in.	0.28 mm	0.0110 in.	0.08 mm	0.0030 in.
South Side	0.17 mm	0.0065 in.	0.48 mm	0.0190 in.	0.09 mm	0.0035 in.

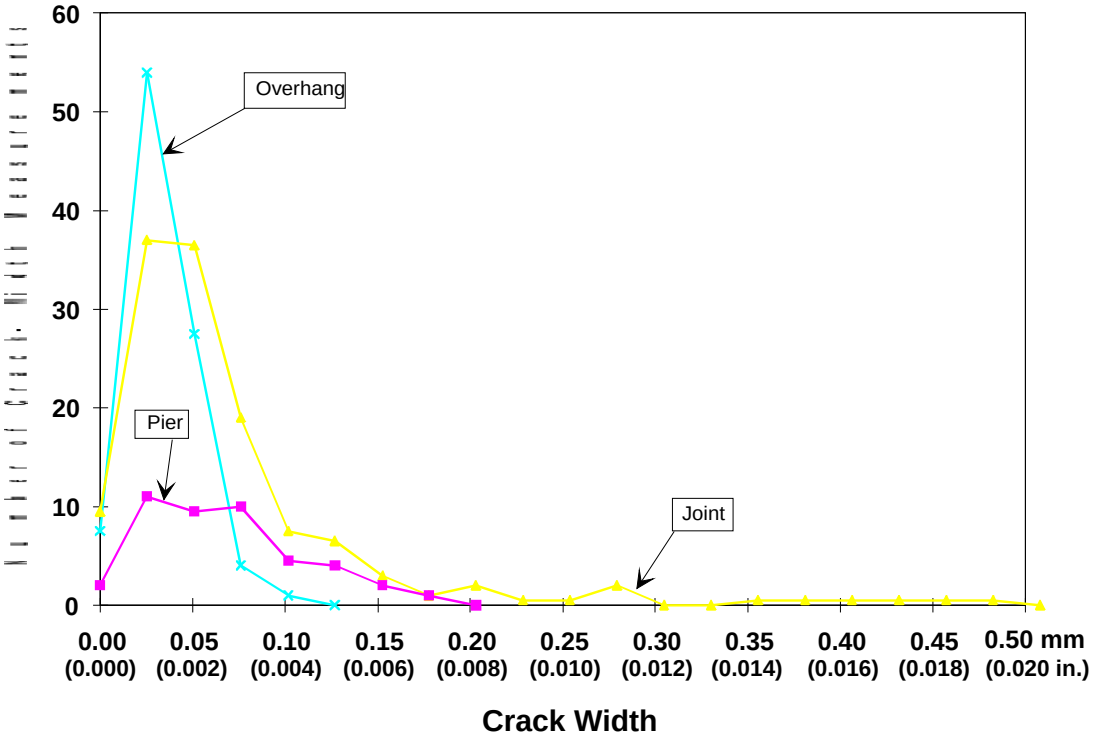

Figure 5.37 Distribution of Service Load Crack Widths in Each Region of Specimen POJ-RC2-RP2a

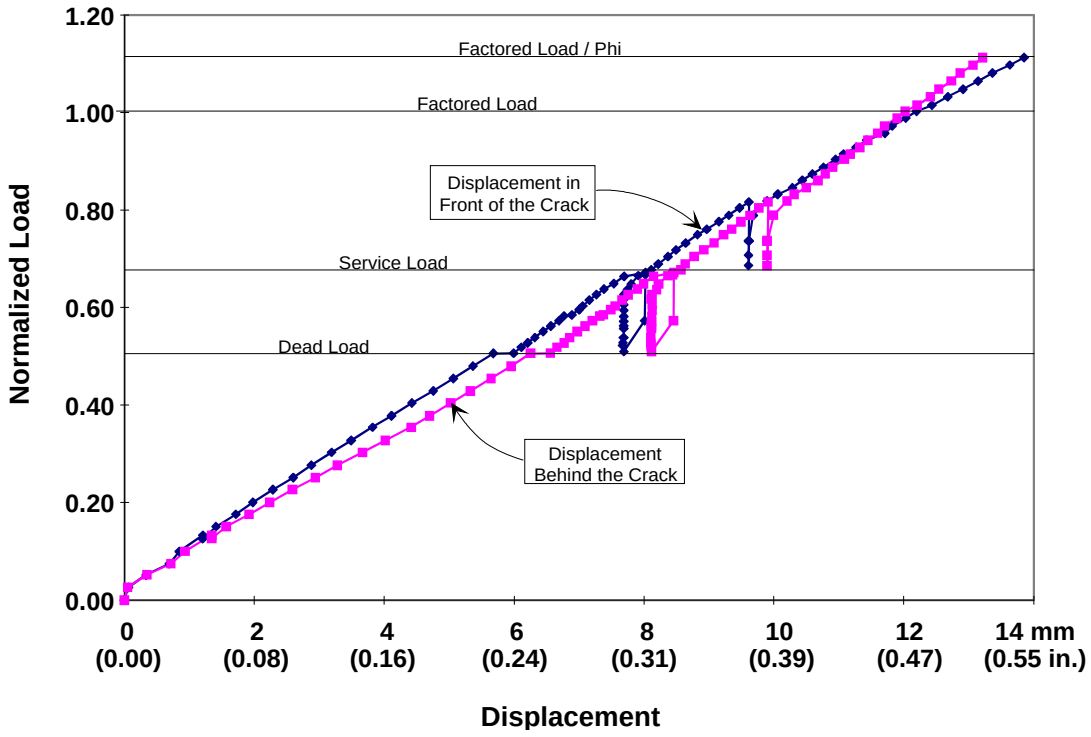

Figure 5.38 Displacement on Either Side of Main Joint Crack on Specimen POJ-RC2-RP2a

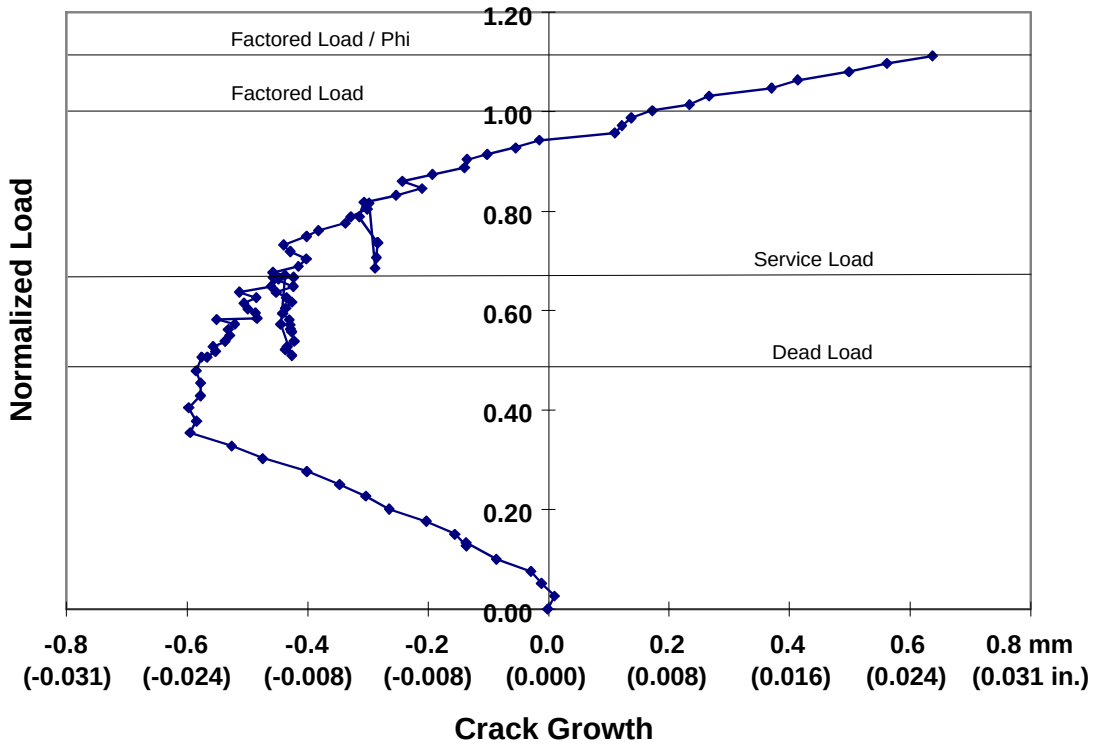

Figure 5.39 Horizontal Component of Crack Width for Growth of Main Joint Crack on Specimen POJ-RC2-RP2a

5.4 Shear Test (POJ-RC2-RP2s)

5.4.1 Strength

Specimen POJ-RP2-RP2a was modified in an attempt to simulate the conditions leading to a long shear crack in Piers I-4C and I-5C. This was accomplished by coring holes horizontally through the overhang to cut the shear friction steel, which was not included in the design of Piers I-4C and I-5C. The loading was also modified to shift all of the applied load to the inner bearing pad. The modified specimen, POJ-RC2-RP2s, was loaded to a normalized load of 1.86, at which point failure appeared imminent. An unexpected failure in the loading frame prevented further loading to capture the post-ultimate behavior of the specimen. However, the load reached its intended maximum. Because the specimen was heavily cracked and concrete spalling had started at the inside corner of the joint, its ultimate strength could not have been significantly higher than the 2.03 MN (457 kips) achieved in the test.

The estimated capacity of Specimen POJ-RC2-RP2s could not be calculated using the joint capacity spreadsheet program described in Chapter 3, because the program was not designed to calculate shear strength. A strut-and-tie model was therefore developed to estimate the specimen's capacity (Figure 5.40). Because the main longitudinal reinforcement in the overhang (T1) was damaged during installation of the internal post-tensioning repair, the capacity of the specimen could not be accurately estimated. Based on the strut-and-tie model and the assumption that an area of reinforcement equivalent to four bars was removed during coring, the capacity of Specimen POJ-RC2-RP2s was estimated at 169 MN (381 kips) or a normalized load of 1.54.

Because the location of the resultant of the applied loads differed from that of the previous tests, the loads were normalized with respect to the factored shear forces, rather than moment at the joint. The normalized loads shown are therefore different from those used for the previous tests and cannot be directly compared.

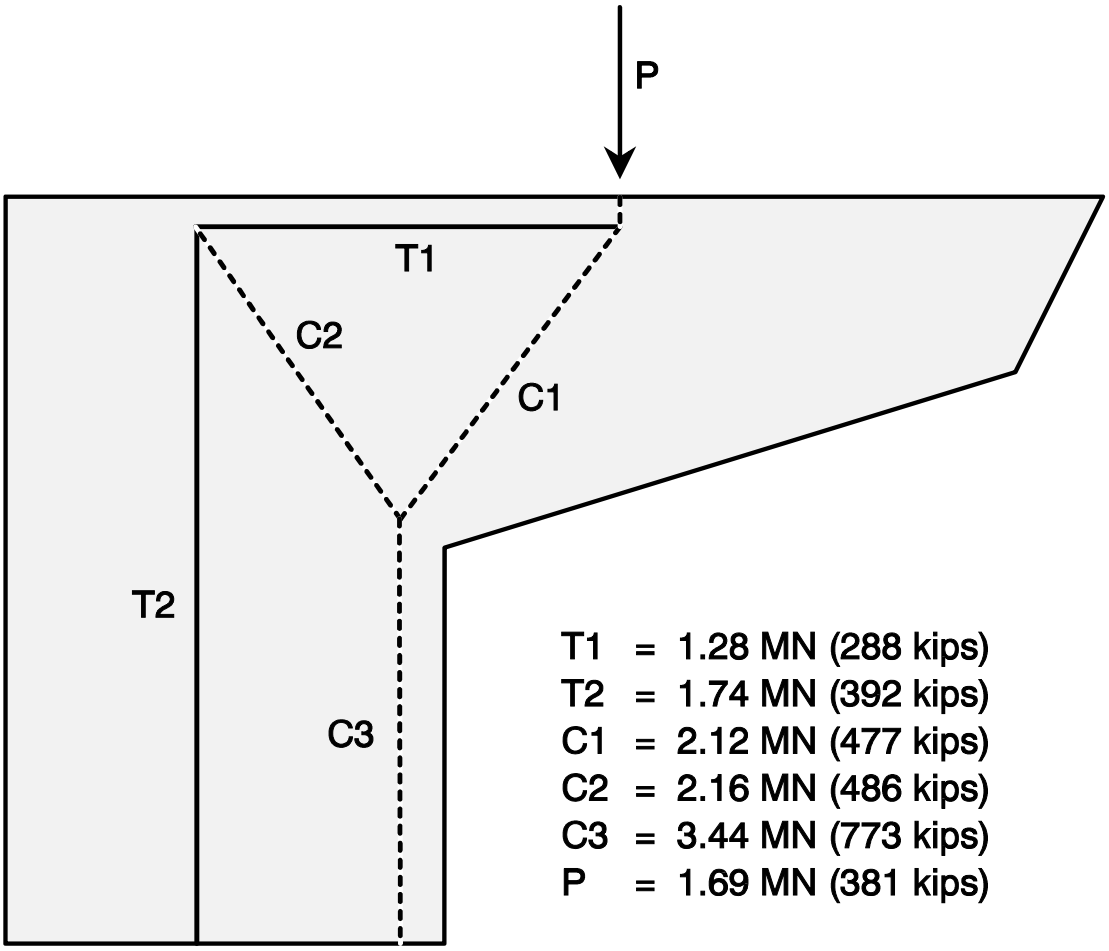

Figure 5.40 Strut-and Tie Model of Specimen POJ-RC2-RP2s

5.4.2 Deflection

A plot of tip deflection versus normalized load is shown in Figure 5.41. The maximum deflection reached was approximately 20 mm (0.80 in.). While the test was not continued to failure, it is clear from the flatness of the load-deflection curve that little if any additional load could have been applied. This is supported by the fact that small pieces of concrete had spalled from the high compression zone in the vicinity of the inner corner of the joint.

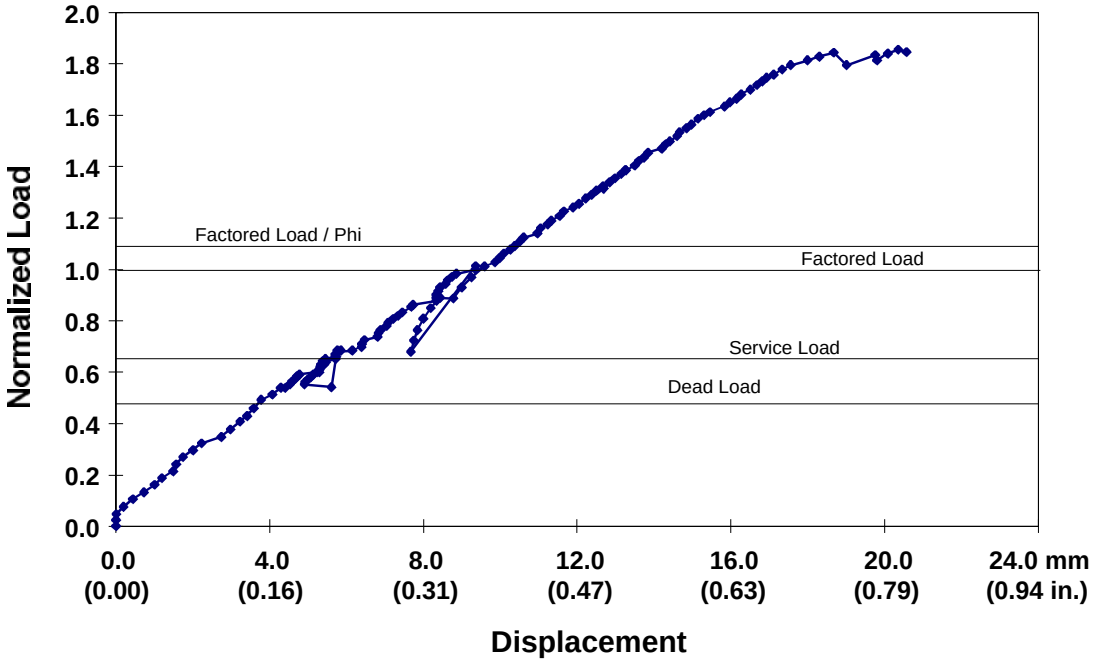

Figure 5.41 Tip Displacement vs. Normalized Load Response for Specimen POJ-RC2-RP2s

5.4.3 Cracking

Cracks in the specimen at ultimate load are shown in Figure 5.42. The shear crack, the examination of which was the purpose of the test, appeared at a normalized load of 0.55 (approximately 10 percent over dead load). It grew to a maximum width of 0.84 mm (0.033 in.) on the south side and 0.58 mm (0.023 in.) on the north side at a normalized shear of 1.68. The growth of the main shear crack is shown in Figure 5.43.

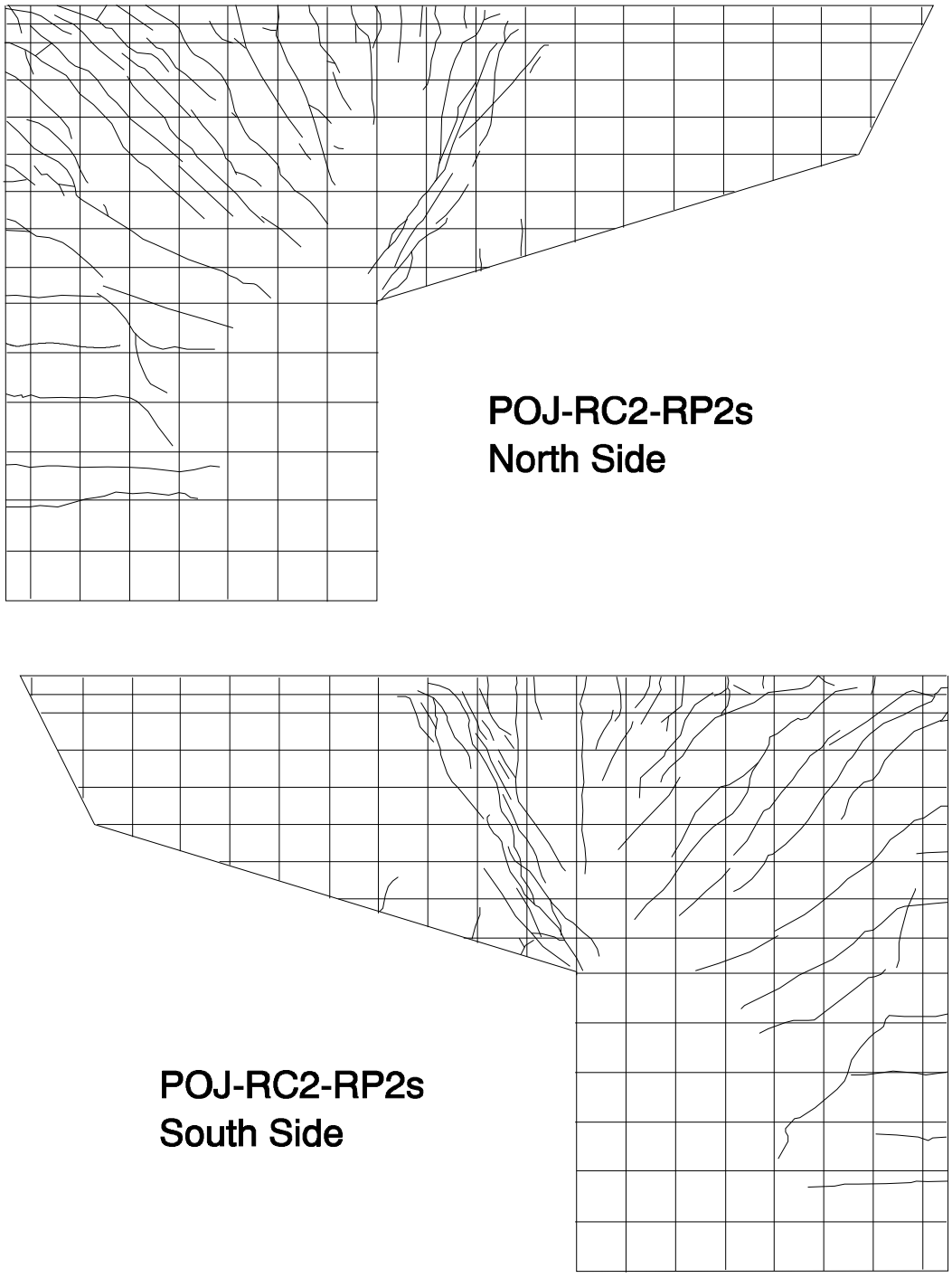

Figure 5.42 Crack Patterns on Specimen POJ-RC2-RP2s at Ultimate Load

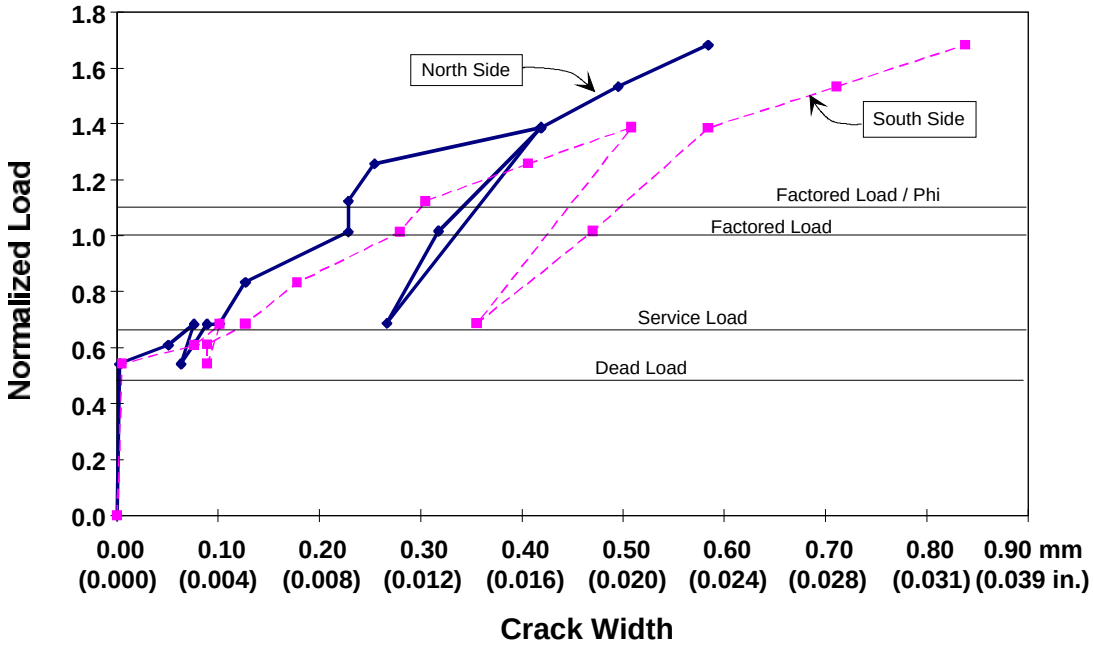

Figure 5.43 Horizontal Component of Growth of Main Shear Crack on Specimen POJ-RC2-RP2s During Loading

CHAPTER 6

DISCUSSION OF TEST RESULTS

6.1 Introduction

This chapter discusses the test results which were presented in Chapter 5. Included are comparisons of actual and expected performance and examination of any anomalies or unexpected developments. As mentioned previously, all crack width measurements apply to service load conditions, while strength, deflection, and crack pattern figures refer to conditions at either ultimate load or factored load / ϕ (FL/ϕ), as appropriate for each case.

6.2 Prestressed Concrete Specimen Tests

6.2.1 POJ-PS-100

The estimated normalized ultimate strength of the unrepaired post-tensioned specimen, based on the joint capacity model (spreadsheet program) described in Chapter 3, was 0.518. The maximum load achieved by the specimen was 0.58, after which the load dropped off to 0.50 (approximately dead load) and substantial deflections occurred (Figure 5.2). The specimen also displayed a surprising amount of ductility, deflecting over 30 mm (1.2 in.) with little increase in applied load, for a total tip deflection of approximately 63 mm (2.5 in.). Because the specimen was not tested to failure, the post-ultimate loading curve is not available. However, it would appear that more deflection could be expected before failure, but no additional load.

Strains in the pier longitudinal reinforcement in the joint showed a marked difference between the two sets of cut-off bars (on the outer face) and the three sets of full-length bars closest to them (Figure 5.1). During overhang post-tensioning at one-half dead load, the cut-off bars appeared to lose anchorage. When loading was resumed, the full-length bars showed substantial increases in strain, while the strain in the cut-off bars remained low. The sudden increase in strain in the full-length bars with little or no increase in load indicates the onset of cracking of the concrete in that region.

No cracks appeared in the overhang at service load and only one extended down from the top face of the joint, indicating, as expected, that the overhang design is not deficient for the post-tensioned specimens (Figure 5.3). Several cracks appeared in the pier and joint region. The pier cracks were mainly small in width, parallel, and horizontal, while the larger

joint cracks extended from the back face of the joint to within a few inches of the inner corner. The crack widths in the pier at dead load were all at or below 0.10 mm (0.004 in.) (Table 5.2). In the joint, several crack widths were as high as 0.41 mm (0.0160 in.), with three large cracks in the 0.64–0.71 mm (0.0250–0.0280 in.) range and one very large crack, in the corner of the joint, that was 1.02 mm (0.040 in.) wide (Figure 5.4).

6.2.2 POJ-PS-100-RP1

6.2.2.1 Specimen Performance

The estimated normalized ultimate strength of the repaired specimen, based on the joint capacity model, was 1.39. Because of the irregularities in the load-displacement curve (Figure 5.6), it is difficult to estimate the ultimate load that could have been reached had the loading continued. The repaired specimen was much stiffer than the unrepaired version, with only 11.5 mm (0.45 in.) of tip deflection between one-half dead load and FL/ϕ and 9.0 mm (0.35 in.) between dead load and FL/ϕ . The maximum tip deflection reached was approximately 16 mm (0.63 in.). The stiffness inferred from the load/displacement plot at factored load was approximately 50 percent of the stiffness at dead load. Because the specimen was never completely unloaded after the first test and the gauges were not rezeroed, the final deflection is not the same as that which would have occurred had the repair been applied to the specimen before it was loaded to failure. Had the specimen not been tested previously, the final tip deflection would have been somewhat lower, perhaps approximately 11 mm (0.43 in.) (Figure 5.6). The specimen was not tested to failure, so the post-ultimate response is not available and the maximum deflection cannot be estimated. The ductility is therefore also unknown.

Strains in the pier reinforcing bars did not show as much difference in behavior between the cut-off bars and the full-length bars (Figure 5.5). The general shape of the load-strain curves was the same for all of the bars: strains increased throughout loading with a decrease in slope of the load-strain response at higher loads. This indicates that all bars remained at least partially bonded with the concrete in the joint. However, the two cut-off bars showed the lowest strains, indicating some loss of anchorage, while the strains in the full-length bars followed an approximately linear strain profile (plane sections remaining plane). Because much of the tensile stress in the pier was carried by the external post-tensioning bars, overall strains in the mild reinforcing bars were much lower than those in the unrepaired specimen. There was no indication of yielding in any of the pier reinforcing bars.

Only one new crack appeared along the back face of the specimen by the end of the test, but two new cracks extended down from the top face of the specimen, near the joint/overhang interface, where the largest moments were expected (Figure 5.7). The original crack in the top of the joint lengthened significantly. The pre-existing cracks in the joint and pier region closed somewhat when the external post-tensioning was applied at one-half dead load. As loading increased, existing cracks began to open again, but were never longer than they were on the unrepaired specimen. The maximum crack widths in the pier at service load were quite small, from approximately 0.03–0.05 mm (0.0012–0.0020 in.), because the cracks were held closed by the external post-tensioning (Table 5.4). Joint cracks were also held closed, although to a lesser extent, with a maximum crack width of approximately 0.11 mm (0.0045 in.). Because the widest cracks observed in this test did not exist in the original, unrepaired specimen, the previous load history had little effect on the maximum crack widths.

The smaller cracks, those in the 0.08–0.10 mm (0.003–0.004 in.) range, were significantly affected.

6.2.2.2 Performance of Repair Components

The average initial stress in the Dywidag bars after post-tensioning was approximately 593 MPa (86.0 ksi) or 61 percent of the ultimate strength. The maximum stress in the bars was approximately 615 MPa (89.2 ksi) or 64 percent of ultimate. The slight increase in bar stress indicates the bars were not fully utilized, either because deflections at the top of the joint were small or because the top retrofit beam was not stiff enough to effectively transmit the forces to the Dywidag bars. However, the small displacements of the center of the retrofit beam relative to the ends argues against the latter possibility. The average stress in the bars on the north side tended to be slightly lower than the average stress in the bars on the right side. Precise values are not available because strain gauges were attached to only two bars on the north side, while all six of the south side bars were gauged.

Because the design of the stiffened top beam of the repair was controlled by stiffness rather than strength, no yielding was expected to occur in that component. The maximum stress of approximately 35 percent of yield stress measured in that component was therefore not surprising. Displacements measurements for the top beam indicated it displaced slightly further on the south side than on the north side, possibly due to a lack of symmetry in the post-tensioning or uneven initial seating of the cap (Figure 5.9). Use of bearing pads rather than hydrostone might have mitigated this.

Movement of the side plates indicates that the top of the plate displaced further than the bottom by approximately 0.15 mm (0.006 in.) during initial post-tensioning, indicating

significant average tensile stresses in the plate (Figure 5.10), although the stresses would have varied along the length of the plate. During loading, displacements measured by the gauges toward the exterior face of the pier decreased slightly, while those of the interior gauges (toward the inner face) remained fairly constant. This could indicate greater opening of cracks in the middle of the joint than towards the back This could also have resulted from differential movement of the frame supporting the gauges. Displacements of the plate normal to the specimen (Figure 5.11) indicated the largest displacement occurred at the top row of bolts and that it was away from the specimen. The second largest displacement was measured in the opposite direction at the second row of bolts . The two gauges on the edge of the plate indicated smaller displacements than the corresponding gauges in the center. Because the plate was more flexible on the edges, the bolts there would experience lower stresses than those in the middle.

6.2.3 POJ-PS-100-RP2

6.2.3.1 Specimen Performance

The maximum normalized load reached by the specimen with its modified repair was 1.24, approximately 5.6 percent higher than the estimate of 1.17 from the joint capacity model. Judging by the slope of the load-displacement curve (Figure 5.13) at the point loading was discontinued, only a slight amount of additional load could have been applied. Its ultimate strength was nevertheless well above the required design strength of 1.11. The overall stiffness of the specimen was similar to that of the first repair, with only 11 mm (0.43 in.) of tip deflection between one-half dead load and FL/ϕ and 9.0 mm (0.35 in.) between dead load and FL/ϕ . The stiffness at factored load was approximately 70 percent of the

stiffness at dead load. The final tip deflection was approximately 22.5 mm (0.89 in.). Because the specimen was only unloaded to one-half dead load after the second test and the gauges were not rezeroed, the final deflection was not the same as that which would have occurred had the repair been applied to the specimen before either the test on the original deficient specimen or the test of the initial retrofit. If the specimen had not been previously loaded into the nonlinear range, the final tip deflection would probably have been in the range of 16–18 mm (0.63–0.71 in.). The specimen was not tested completely to failure, so the post-ultimate loading curve is not available and the maximum deflection cannot be estimated. The ductility is therefore also unknown.

Strain measurements for the pier reinforcing bars in the joint (Figure 5.12) were similar in shape to those for specimen POJ-PS-100-RP1 (Figure 5.5). The strains increased with increasing load for all of the bars, although the full-length bars showed much higher increases in strain for similar load increases than did the cut-off bars. As for the previous specimen, the cut-off bars experienced the lowest strains, while strains in the full-length bars indicated an approximately linear strain profile, with strains increasing with distance from the compression zone. Because the lower number of external post-tensioning bars carried less of the pier tensile stress, measured strains in the mild reinforcement were much higher than those in bars for the previous repair, approaching yield in one case.

Many new cracks appeared in the pier and joint, and one in the overhang (Figure 5.14). Pier and joint cracks began to angle downward more sharply, crossing the earlier horizontal cracks. The maximum crack widths in the pier at service load were approximately 0.08 mm (0.003 in.) (Table 5.6). The joint cracks had a maximum width of approximately 0.14 mm (0.0055 in.) on the north side of the specimen and approximately 0.28 mm (0.011

in.) on the south side. The largest overhang crack was 0.04 mm (0.0015 in.) wide. Crack widths included residual effects from the previous tests. Because the widest cracks were in roughly the same locations as those in the previous test, this probably affected the maximum crack widths. The widest pier crack grew in width approximately 0.04 mm (0.0015 in.) during the test, while the maximum joint crack width grew approximately 0.10 mm (0.004 in.). The overhang crack, which did not exist during the previous tests, was unaffected. The smaller and medium-sized crack widths, in the 0.02–0.10 mm (0.001–0.004 in.) range, were greatly affected by the previous loading

6.2.3.2 Performance of Repair Components

The average initial stress in the Dywidag bars after post-tensioning was 558 MPa (79.9 ksi) or 57 percent of ultimate strength. At FL/ϕ, the average stress was 657 MPa (94.1 ksi), or 67 percent of ultimate. The highest stress in the bars during the test was 697 MPa (101.1 ksi) or 72 percent of ultimate. Because of the decrease in the number of bars, the stress increase was much higher than for the previous test.

The maximum stress in the top beam used in the retrofit was lower than that for the previous test: approximately 27 percent of yield strength. The overall maximum stress was 31 percent of yield. All stresses were well below yield levels. The displacements of the top beam indicated that it remained closer to level during the second test than during the first (Figure 5.16).

The vertical movement of the side plates was much smaller for the second test, approximately half as great as for the earlier test, because initial slippage had already occurred (Figure 5.17). Some slippage still occurred, and the maximum movement was again

greater for the top of the plate than for the bottom. All displacements decreased during loading, but those at the side of the plate toward the back face of the pier decreased substantially more than those on the other side. Movement of the side plates normal to the specimen was less than 0.08 mm (0.003 in.) at maximum load, but fluctuations in the readings prevented any meaningful analysis.

6.3 Reinforced Concrete Specimen Tests

6.3.1 POJ-RC2

The unrepaired reinforced concrete specimen was loaded to a normalized load of 0.66 when load began to drop off. The negative slope of the load-displacement curve (Figure 5.19) at this point indicated that the ultimate strength had been reached. The estimated normalized ultimate strength of the specimen, based on the joint capacity model described in Chapter 3, was 0.71. This was approximately 7.0 percent above its actual normalized ultimate load of 0.66. The specimen displayed a slight amount of ductility, deflecting under gradually decreasing load. Because the specimen was required for further testing, only a small portion of the post-ultimate loading curve could be examined.

The gauged pier reinforcement demonstrated an approximately linear strain response up to approximately 80 percent of dead load (Figure 5.18), because the outer bars were not cut off as was the case in specimens with post-tensioned overhangs. The outer bars displayed a gradual increase in strain above a normalized load of approximately 0.4. At failure, the strains suddenly decreased, indicating a partial loss of anchorage. On the other hand, the bars closer to the compression zone showed no significant increase until higher loads were reached, after which the strains increased suddenly to approximately the same levels as for the outer bars. As for the unrepaired post-tensioned specimen, the high strain increases with little or no increase in load indicated the initial cracking of the concrete in that region.

There was extensive cracking throughout the pier, joint, and overhang regions of the specimen at its ultimate load of slightly less than service load (Figure 5.20). The main joint crack reached a width of 1.68 mm (0.0660 in.) on the south side, although its maximum width

was only 0.51 mm (0.020 in.) on the north side (Table 5.8). In comparison, no cracks on the pier were more than 0.17 mm (0.0065 in.) wide, and the largest crack on the overhang was only 0.10 mm (0.0040 in.) wide. However, all crack widths were measured on the surface. The main joint crack was actually wider between the side faces. Displacement gauges were therefore attached at the centerline of the specimen to monitor the increase in crack width during future tests by measuring the horizontal displacement of the specimen above and below the crack.

6.3.2 POJ-RC2-RP1

6.3.2.1 Specimen Performance

The estimated normalized ultimate strength of the reinforced concrete specimen with diagonal post-tensioning, based on the joint capacity model, was 1.15, but the specimen was only tested to a normalized load of 1.11 or FL/ϕ. The total tip deflection was approximately 19.0 mm (0.74 in.), with 13.0 mm (0.51 in.) deflection occurring between dead load and FL/ϕ. The stiffness at factored load was approximately 60 percent of the stiffness at dead load. Therefore, judging by the nearly constant slope of the load/displacement curve (Figure 5.23) up to the point where loading was discontinued, the estimated ultimate capacity could easily have been reached and exceeded had the loading been continued. The estimated strength was therefore probably low.

Strain responses in the pier reinforcing bars were all quite low and nearly linear above dead load (Figure 5.22), although strains in the outermost bars were the lowest due to loss of anchorage which occurred in the previous test. However, because the load-strain

curve for those bars was essentially the same shape as for the inner bars, no noticeable additional anchorage loss occurred during this test. The overall strains remained well below yield levels throughout the test, and the steep slope at maximum load confirmed the above conclusion of substantial reserve capacity.

Crack patterns were essentially the same as for the previous test (Figure 5.24). More cracks appeared in the overhang, while existing cracks lengthened. Little or no change occurred for cracks in the pier or joint region. Near the top of the joint, however, some small horizontal cracks appeared, indicating debonding of longitudinal overhang reinforcement. The maximum service load crack widths in the pier were 0.31 mm (0.012 in.) on the north side and 0.46 mm (0.018 in.) on the south side (Table 5.11). The widest pier crack occurred just below the bottom anchor bolt and was probably influenced by stresses from the bolts, because cracks at higher and lower locations were narrower. The joint cracks reached a maximum service load width of 0.79 mm (0.031 in.) on the north side and 0.94 mm (0.037 in.) on the south. The maximum width of overhang cracks was 0.13 mm (0.005 in.).

These crack measurements refer to widths measured on the surface, while the widest point on the main joint crack was inside the joint, between the side faces of the specimen. The displacement gauges assembled to measure the horizontal increase in crack width at this point indicated that the crack increased in width by nearly 1.0 mm (0.038 in.) (Figure 5.26), between service load and FL/ϕ. The large width at that point was partly due to the horizontal confinement of the concrete. The concrete on the outer surfaces was able to expand outward, increasing the debonding of the longitudinal reinforcement in that region. The decreased bond transmitted lower forces to the concrete in the immediate vicinity of the main crack, resulting in higher growth of nearby cracks, but lower growth of the main crack. In contrast,

the reinforcement in the middle of the joint continued to apply force to the crack region. In addition, the maximum post-tensioning force was applied at the sides of the specimen, with less closing force on the cracks inside the joint.

6.3.2.2 Repair Performance

The average initial stress in the Dywidag bars after post-tensioning was 641 MPa (93.0 ksi) or 66 percent of the ultimate strength of the bars. At FL/ϕ, the average stress was 750 MPa (108.8 ksi), or 78 percent of ultimate. Because design of the repair components was controlled by stiffness rather than strength, no yielding was expected in the steel, and the maximum measured strain of slightly less than half the yield strain required no explanation. Slippage of the plates along the specimen was of greater interest (Figure 5.27). Nearly all slippage occurred during post-tensioning. During loading, the top plate moved an additional 0.7 mm (0.03 in.), while the extra displacement on the side plate was too small to be measured. Because the post-tensioning imposed larger normal and smaller shear forces on the top surface than on the side, friction accounted for a large part of the assumed shear resistance of the top plate. This assumption may account for the extra movement of the top plate. The readings from the gauges intended to measure relative displacement between the middle and the ends of the top beam were unreliable, so no estimate can be made of the amount of beam bending.

6.3.3 POJ-RC2-RP2

The estimated normalized ultimate strength of the reinforced concrete specimen with internal post-tensioning, based on the joint capacity model, was 1.12. The total tip deflection

was approximately 20.0 mm (0.74 in.), with 12.5 mm (0.51 in.) between dead load and FL/ϕ . The stiffness at factored load was approximately equal to the stiffness at dead load. Judging by the slope of the load-displacement curve (Figure 5.29) at the point loading was discontinued, the estimated ultimate load would have been reached and exceeded had the loading continued. The estimated strength was therefore almost certainly low. Because the specimen was not loaded to failure and apparently had a great deal of reserve capacity, no information on the post-ultimate loading curve or specimen ductility is available.

Strains in the pier reinforcing bars were quite low and approximately linear above dead load (Figure 5.28). Strains in the outermost bars were lower than those measured in the next set of bars, but higher than in the others, reflecting the partial loss of anchorage from the first test. However, because the load-strain response for those bars was essentially the same shape as for the other bars, no noticeable additional anchorage loss occurred during the test. The overall strains remained well below yield levels throughout the test, and the slope of the measured response at maximum load, though flatter than that in the previous test, confirmed the above conclusion of substantial reserve capacity.

There was extensive cracking throughout the pier, joint, and overhang regions of the specimen at FL/ϕ (Figure 5.30). The main joint crack only reached a width of 0.23 mm (0.0090 in.) on the side faces of the specimen (Table 5.12). The displacement gauges mounted on each side of the crack, on the other hand, registered an increase in the horizontal component of crack width of nearly 3.0 mm (0.12 in.) at service load (Figure 5.33). The crack growth slowed substantially at a normalized load of about 0.8, possibly indicating the increased growth of other cracks, and began to increase again above factored load. Maximum service load crack widths for the pier and overhang were 0.15 mm (0.0060 in.) and

0.09 mm (0.0035 in.) on the pier and overhang, respectively. These widths appear to be much smaller than those for the previous test; however, as the specimen was whitewashed between tests, the crack widths cannot be directly compared. The cracks in the joint tended to become more horizontal near the top exterior corner, indicating some splitting in the plane of the longitudinal reinforcement.

No information is available on the stress in the post-tensioning bars at any point other than initial stressing for each individual bar. Because of the installation method, it was impractical to attach strain gauges to the bars.

6.3.4 POJ-RC2-RP2a

The estimated normalized ultimate strength of the reinforced concrete specimen with internal post-tensioning and damaged overhang reinforcement, based on the joint capacity model, was 1.05. The estimated normalized ultimate load was exceeded in the test, and the nearly constant slope of the load/displacement curve (Figure 5.35) indicates that a much higher load could have been achieved had testing continued. The load-deflection behavior was very similar to that shown in the previous test, with a total tip deflection of approximately 20.0 mm (0.74 in.), and an increase of 12.5 mm (0.51 in.) between dead load and FL/ϕ. The stiffness at factored load was approximately equal to the stiffness at dead load.

Strains in the pier reinforcing bars were similar to those in the previous test (Figure 5.34), although strains in the outermost bars were lower than the next three sets of bars, reflecting the partial loss of anchorage from the previous test. However, because the load-

strain curve for those bars had essentially the same shape as those for the inner bars, no noticeable additional anchorage loss was detected during the test. The overall strains remained well below yield levels throughout the test, and the steep slope at maximum load confirms the above conclusion of reserve capacity.

There was extensive cracking throughout the pier, joint, and overhang regions of the specimen at FL/ϕ (Figure 5.36). The main joint crack reached a width of 0.48 mm (0.0190 in.) on the side faces of the specimen (Table 5.14), which was more than twice the size of the crack width measured for specimen POJ-RC2-RP2. The previous loading history may have been responsible for a large portion of this increase. The displacement gauges, on the other hand, registered a slight initial decrease in width up to just below dead load, after which the crack began to reopen, with a net increase of approximately 0.7 mm (0.03 in.) at FL/ϕ (Figure 5.39). Possibly other cracks had begun to open, decreasing the early stress at the main crack. In particular, the damage to the longitudinal overhang reinforcement would tend to increase cracking in the top of the joint, just in front of the post-tensioning bars.

Cracks on the pier and overhang were similar to those for the previous test, with maximum widths of 0.17 mm (0.0065 in.) on the pier and 0.09 mm (0.0035 in.) on the overhang. The cracks in the joint showed an increased tendency to flatten near the top, indicating more splitting in the plane of the longitudinal reinforcement.

As discussed before, no information is available on the stress in the post-tensioning bars at any point other than initial stressing for each individual bar.

6.4 Shear Test (POJ-RC2-RP2s)

The estimated capacity of specimen POJ-RC2-RP2s could not be calculated using the joint capacity model described in Chapter 3, because the program was not designed to calculate shear strength. Also, because the location of the resultant of the applied loads differed from that of the previous tests, the loads were normalized with respect to the factored shear forces, rather than moment at the joint. The normalized loads shown were therefore different from those used for the previous tests and cannot be directly compared. A strut-and-tie model (Figure 5.40) was used to estimate the shear capacity of the specimen and produced normalized capacity of 1.54. This estimate was based on the assumption that the damage to the longitudinal reinforcement resulted in a net loss of four bars. The maximum normalized shear achieved was approximately 1.85 (Figure 5.42), about 20 percent higher than estimated.

Cracking in the specimen reflected the change in loading conditions (Figure 5.41). The region from the applied load to the inner corner of the joint was covered with approximately parallel shear cracks, some extending almost to the inside corner of the bent. There were no overhang cracks beyond the point of load application, and flexure cracks at the joint/overhang interface were relatively shallow. Two or three compression cracks appeared on the bottom of the overhang, approximately beneath the point of load application. The joint and pier cracks, on the other hand, were not significantly different from those in the previous test. The primary shear crack, the examination of which was the purpose of this test, appeared at approximately 1.1 dead load. Its maximum width was approximately 0.11 mm (0.0045 in.) at service load, growing to 0.84 mm (0.033 in.) on the south side and 0.58 mm (0.023 in.) on the north side at a normalized shear of 1.68, as shown in Figure 5.42. Crack width measurements were not taken above that load. Despite the early appearance of the

crack, the high load resisted by the specimen indicated that the crack was not a symptom of shear strength deficiency in the overhang. Therefore, no corrective measures are needed.

CHAPTER 7

PERFORMANCE AND COST COMPARISONS

7.1 Introduction

This chapter compares the test results which were presented in Chapter 5 and discussed in Chapter 6. Because of concerns about the capacity of existing cantilever bents in the San Antonio "Y" structure, the first and most important parameter to be considered is the ultimate capacity of each repair. The effectiveness and performance of each repair at service load, including deflections and crack control, are compared next, both as measures of serviceability and as indicators of general repair behavior. The effectiveness and performance of each repair at factored load divided by ϕ (FL/ϕ) are also discussed, although these loads should be reached rarely if ever during the life of the bents. An analysis of approximate cost and constructibility data is then conducted. Finally, miscellaneous subjective factors, such as aesthetics, are discussed. The behavior of specimen POJ-RC2-RP2s is not compared directly with the results of the other tests, because the test did not constitute a separate repair scheme, but was intended to examine a specific problem, namely the questionable shear strength of the reinforced concrete overhang with no shear friction steel.

7.2 Projected Ultimate Strength

Because none of the repaired specimens were tested to complete failure, the actual ultimate strength for each repair scheme could not be determined with certainty. In all cases, however, the ultimate strength of the repaired specimens was above FL/ϕ; for one case, it was well above. The load versus displacement response for each repaired specimen is shown in Figure 7.1.

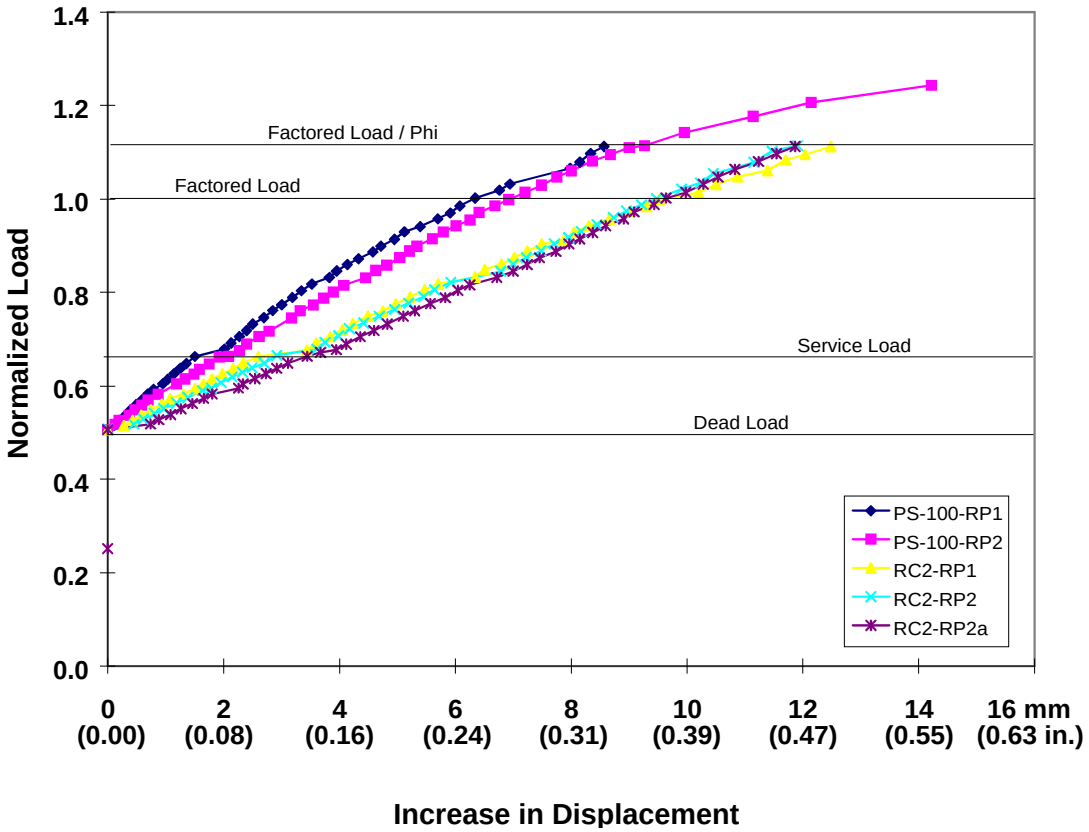

Figure 7.1 Load vs. Tip Displacement Curves up to Maximum Tested Load

The maximum normalized strengths calculated using the joint capacity model described in Chapter 3 are shown in Table 7.1 along with the maximum normalized load

actually attained by each specimen. Two normalized capacities are shown for the specimens with post-tensioned reinforcement, either in the unrepaired specimen or in the repair itself. The first column shows the load at which the post-tensioning bars would reach their nominal yield strength. Because high-strength post-tensioning bars do not have a well defined yield plateau, as do mild reinforcing bars, initial yielding of the bars would not necessarily produce substantial deflections in the specimen. Therefore, a second column lists the capacity of each specimen assuming the post-tensioning bars achieve their ultimate strength. When the two values are identical, as in the case of the unrepaired specimens, post-tensioning does not affect the specimen capacity.

Table 7.1 Original Calculated Normalized Strengths and Maximum Normalized Test Loads

	Original Calculated Strength		Maximum Load
Specimen	PT Yield	PT Ultimate	Achieved
POJ-PS-100	0.55	0.55	0.51
POJ-PS-100-RP1	1.18	1.67	1.11
POJ-PS-100-RP2	1.18	1.36	1.25
POJ-RC2	0.65	0.65	0.65
POJ-RC2-RP1	1.13	1.29	1.11
POJ-RC2-RP2	1.16	1.30	1.11
POJ-RC2-RP2a	1.07	1.21	1.11

7.3 Effectiveness/Performance at Service Load

7.3.1 Deflections

The tip deflection response up to service load for the specimens with post-tensioned overhangs are shown in Figure 7.2. Both repaired specimens performed substantially better than the unrepaired specimen. The first repair, POJ-PS-100-RP1, with six post-tensioned Dywidag bars on each side of the repair, was, as might be expected, stiffer than the second repair, POJ-PS-100-RP2, with four bars per side. The tip deflection of POJ-PS-100-RP1 at service load was about 3.7 mm (0.147 in.), which was approximately 37 percent lower than the 5.9 mm (0.232 in.) deflection of POJ-PS-100-RP2. Both tip deflection response curves followed the same general shape.

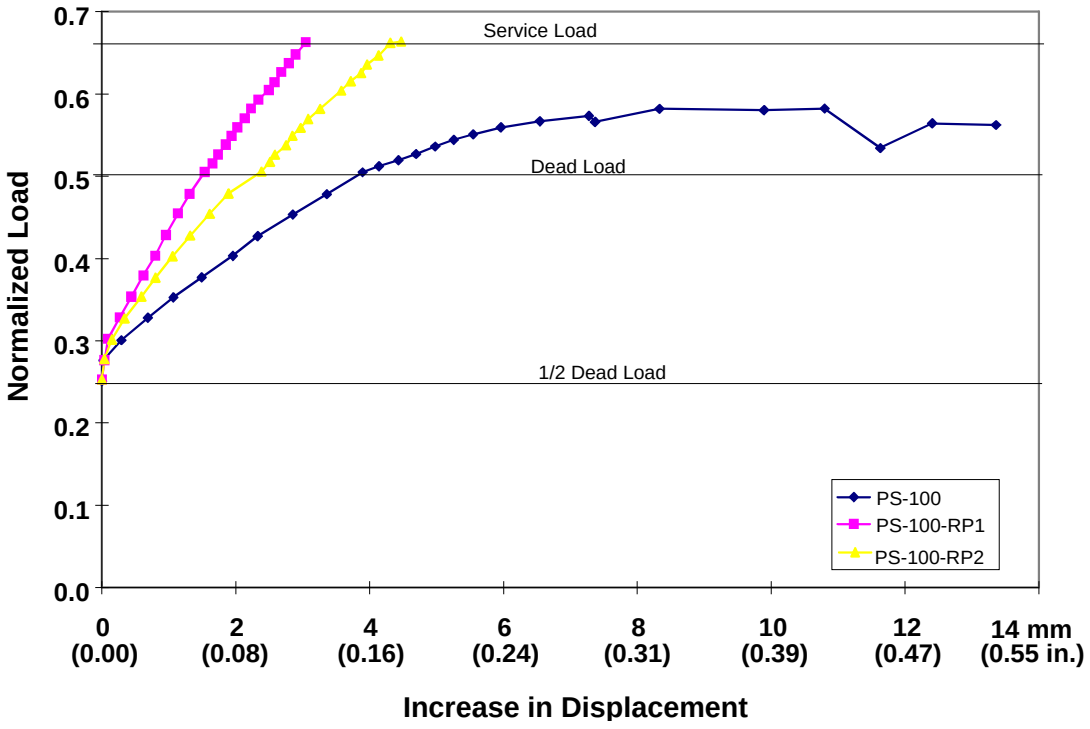

Figure 7.2 Comparison of Service Level Tip Deflection Response for Specimens with Post-Tensioned Overhangs

The tip deflection responses up to service load for the reinforced concrete specimens are shown in Figure 7.3. All three repaired specimens performed substantially better than the unrepaired specimen. The first repair, POJ-RC2-RP1, with diagonal external post-tensioning was slightly stiffer than the two repairs using internal post-tensioning. The tip deflection of POJ-RC2-RP1 at service load was about 8.5 mm (0.334 in.), which was approximately 19 percent lower than the 10.5 mm (0.413 in.) deflection of POJ-RC2-RP2 and 26 percent lower than the 11.4 mm (0.449 in.) deflection of POJ-RC2-RP2a. However, the responses for the latter two do not include the immediate effects of the post-tensioning operation, because no displacement readings were taken before post-tensioning was performed. It is not completely

clear how the responses would have compared if post-tensioning in specimen POJ-RC2-RP1 had been performed with no load on the specimen.

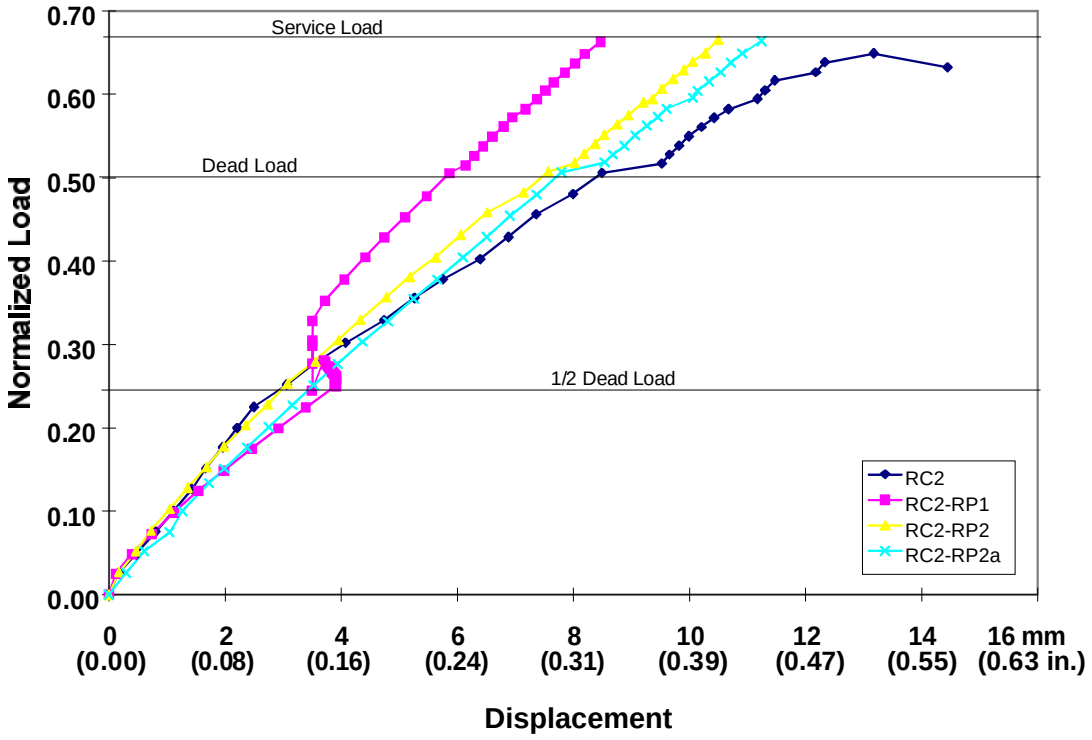

Figure 7.3 Comparison of Service Level Tip Deflection Response for Reinforced Concrete Specimens

Load-displacement responses for all of the repaired specimens are shown in Figure 7.4. The two repairs involving external vertical post-tensioning were significantly stiffer than the other two repair schemes. However, both of the repairs with external vertical post-tensioning were applied to specimens with post-tensioned overhangs, so part of the apparent stiffness is due to the higher stiffness of the overhang. The other two repairs, external diagonal post-tensioning and internal vertical post-tensioning, were applied to specimens

with fully reinforced overhangs, which had a lower stiffness due to cracking, especially at service load. This is evident by comparing the initial slopes of the load-displacement curves up to one-half dead load, which correspond approximately with the relative initial stiffnesses of the unrepaired specimens.

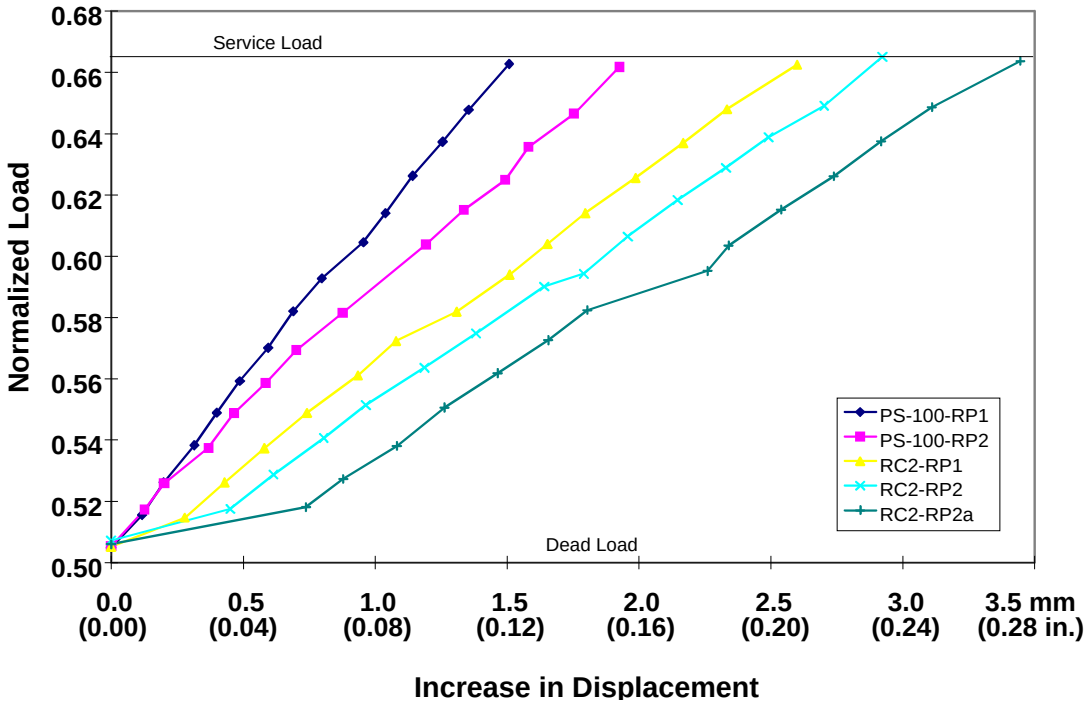

Figure 7.4 Comparison of Service Level Tip Deflection Response for All Repaired Specimens

A more accurate indication of the relative stiffnesses of the repaired specimens (excluding overhang deformations) was obtained by comparing rotations of the joint region (Figure 7.5), which still indicate the first two repairs to be stiffer, but by a lesser margin. Figure 7.6 attempts to eliminate the direct effects of the post-tensioning process that was

performed at one-half dead load by plotting the joint rotation response between one-half dead load (after post-tensioning was complete) and service load. This figure clearly shows the two vertical external post-tensioning repairs were the stiffest, while the stiffnesses of the other repairs were approximately the same (external diagonal post-tensioning was slightly stiffer than internal vertical post-tensioning) and about half the stiffness of the two repairs that utilized vertical external post-tensioning.

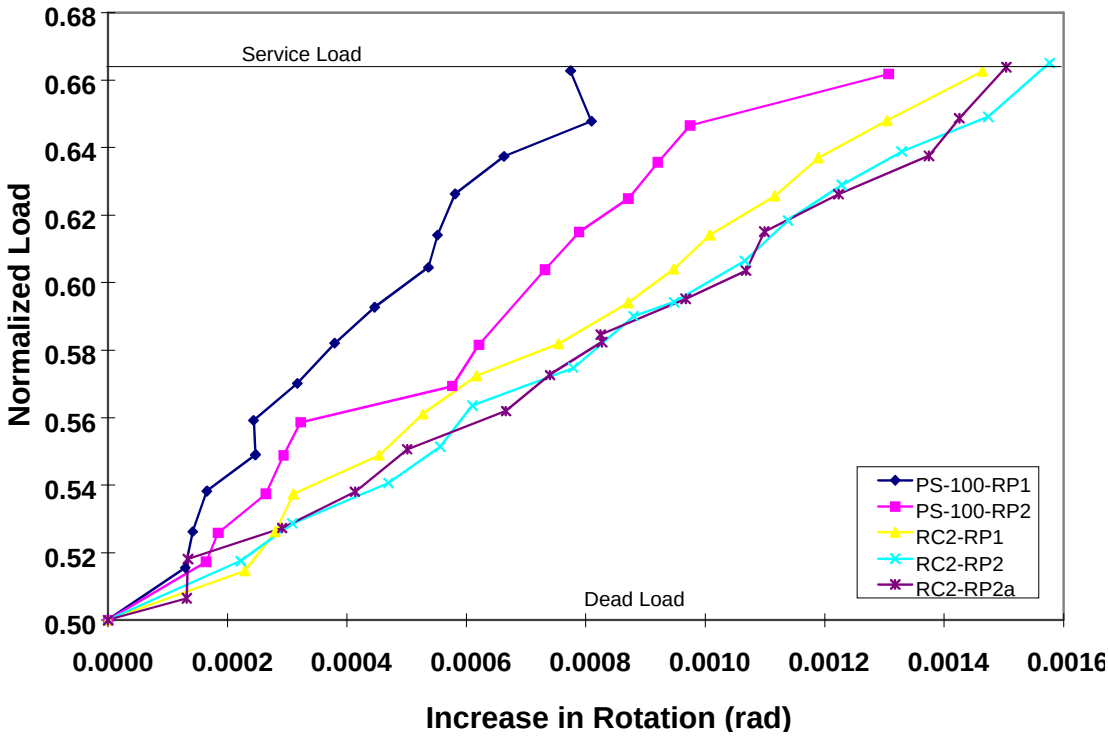

Figure 7.5 Comparison of Service Level Joint Rotations for All Repaired Specimens

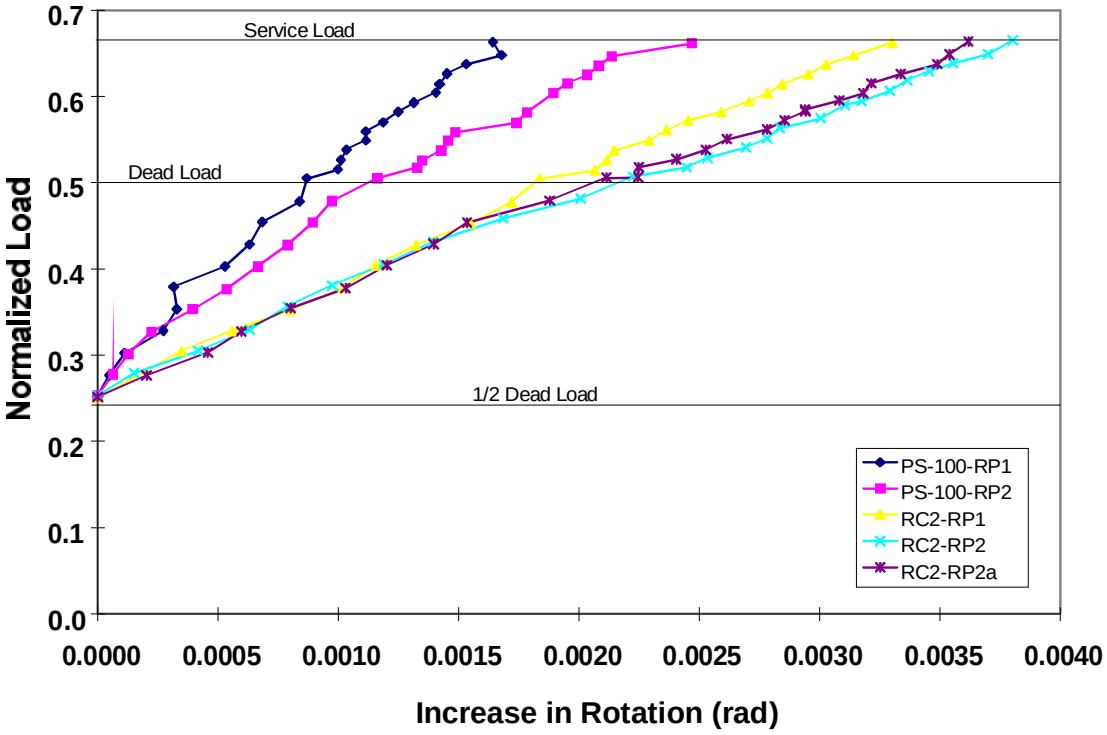

Figure 7.6 Comparison of Increase in Joint Rotations from One-Half Dead Load to Service Load for All Repaired Specimens

7.3.2 Crack Control

Figure 7.7 compares the number of cracks in each region of the repaired specimens, averaged between the north and south sides. As expected, the two specimens with post-tensioned overhangs, POJ-PS-100-RP1 and POJ-PS-100-RP2, developed fewer or no cracks in the overhang region. Also, because the overhang post-tensioning continued into the joint region, the two specimens developed fewer cracks in the joint than did the reinforced concrete specimens. The number of cracks in the pier were approximately equal for each specimen. The second repair on the post-tensioned specimen, POJ-PS-100-RP2, generally

developed more cracks than did the first repair, because it utilized less external post-tensioning force. The two tests with vertical internal post-tensioning, POJ-RC2-RP2 and POJ-RC2-RP2a, developed approximately the same number of joint cracks as the diagonally post-tensioned specimen, POJ-RC2-RP1, and developed slightly more overhang cracks.

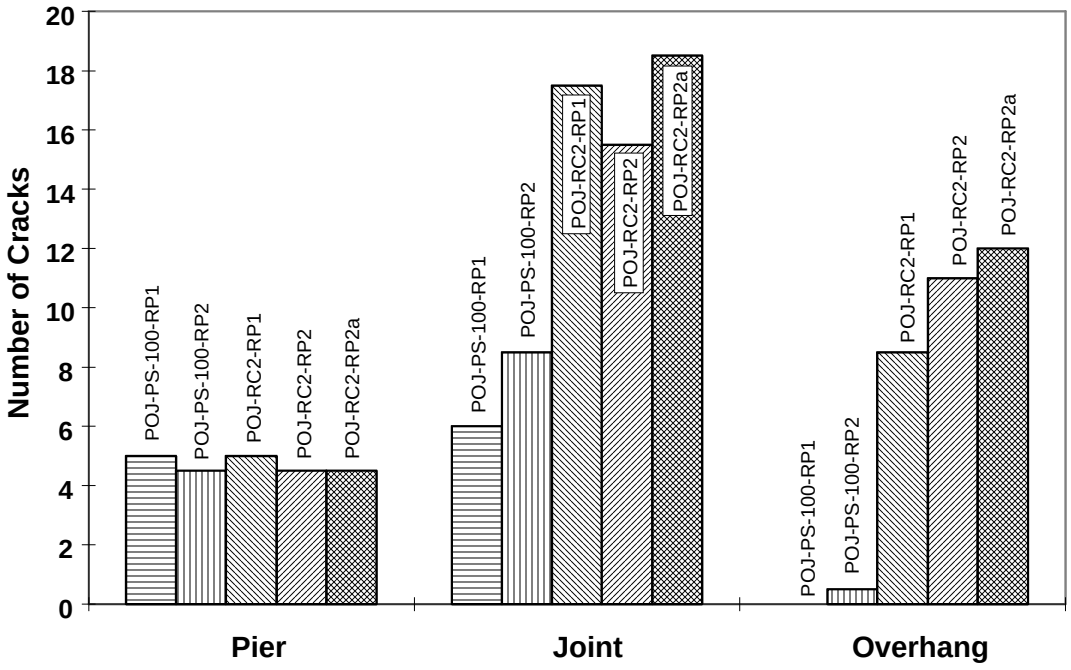

Figure 7.7 Average Number of Cracks in Each Region of the Repaired Specimens at Service Load

If only cracks emanating from the back face of the joint and pier are considered, in order to more fairly compare the reinforced concrete specimens with the post-tensioned specimens, the number of cracks is closer to equal, as shown in Figure 7.8.

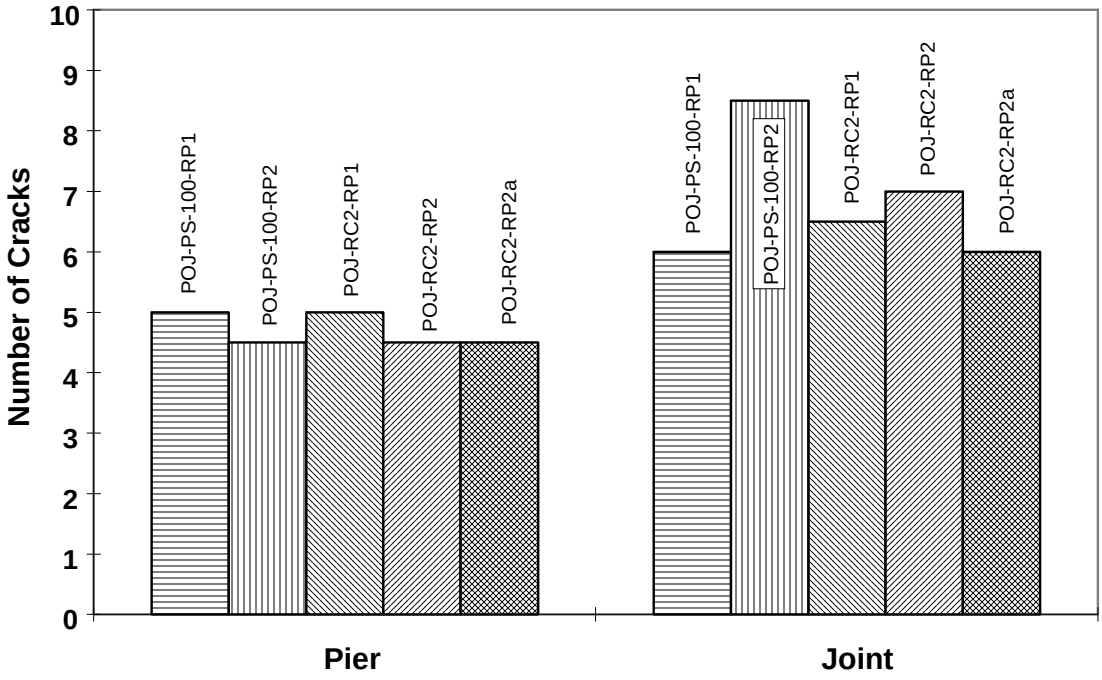

Figure 7.8 Average Number of Cracks Emanating from the Back Face of Each Repaired Specimen at Service Load

The maximum crack width for each region of each repaired specimen is shown in Figure 7.9. The large pier crack width for POJ-RC2-RP1 is due to the additional cracking in the vicinity of the anchor bolts, which could be reduced by increasing the distance between the bolts and the edge of the concrete. The small pier crack widths for the post-tensioned specimens reflect the fact that all the measured cracks were within the post-tensioned zone, while some of the measured cracks in the reinforced concrete specimens were unaffected by post-tensioning. POJ-PS-100-RP1 showed smaller maximum crack widths in all regions than did the more lightly post-tensioned POJ-PS-100-RP2. The extreme crack width in POJ-RC2-RP2a reflects spalling of concrete from the edges of a single crack due to accumulated

damage from previous tests. Each successive repair test conducted on a given original specimen tended to produce higher maximum crack widths than did the previous test.

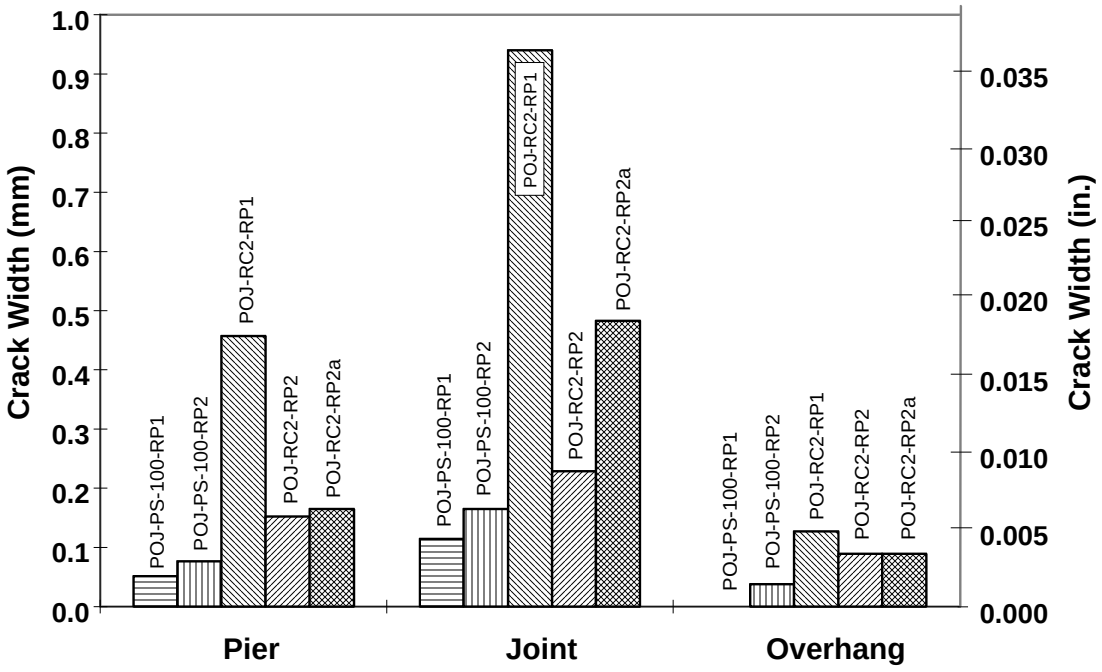

Figure 7.9 Comparison of Maximum Crack Widths at Service Load

Figure 7.10 shows the crack width distributions for the joint region of all repaired specimens. POJ-RC2-RP1 developed the largest number of wide cracks, followed by POJ-RC2-RP2a, POJ-RC2-RP2, POJ-PS-100-RP2, and POJ-PS-100-RP1. However, the reader is reminded that these figures include residual effects from previous tests. If these effects were not present, the crack width distributions might have resembled those shown in Figure 7.11. Adjusted crack widths were calculated by subtracting the difference in crack widths at dead load for the repaired specimen and the corresponding unrepaired specimen from crack widths

measured at service load. This would remove some of the increase in crack width sustained during the previous loadings.

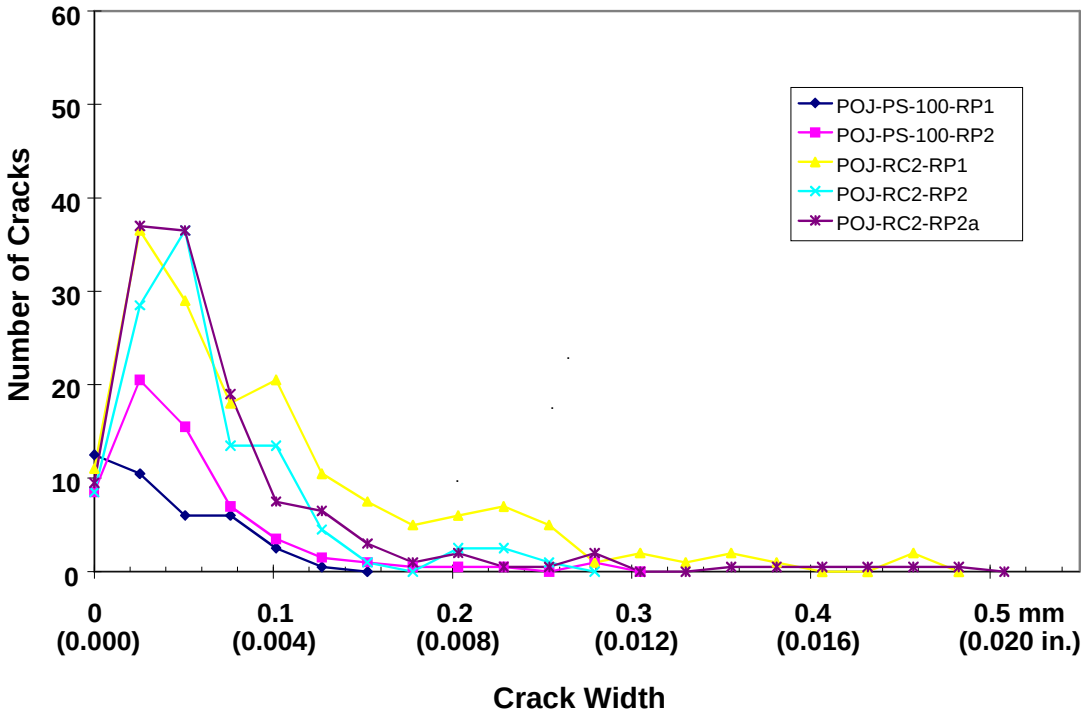

Figure 7.10 Comparison of Crack Width Distribution at Service Load

Figure 7.11 indicates that POJ-RC2-RP1 developed the highest number of very small cracks (less than 0.05 mm (0.002 in.)), but fewer large cracks than either of the other two reinforced concrete specimens. As mentioned above, the low number of cracks in the joints of the post-tensioned specimens is partly due to the lack of cracks in the top portion of the joint, where the overhang post-tensioning prevents significant cracking.

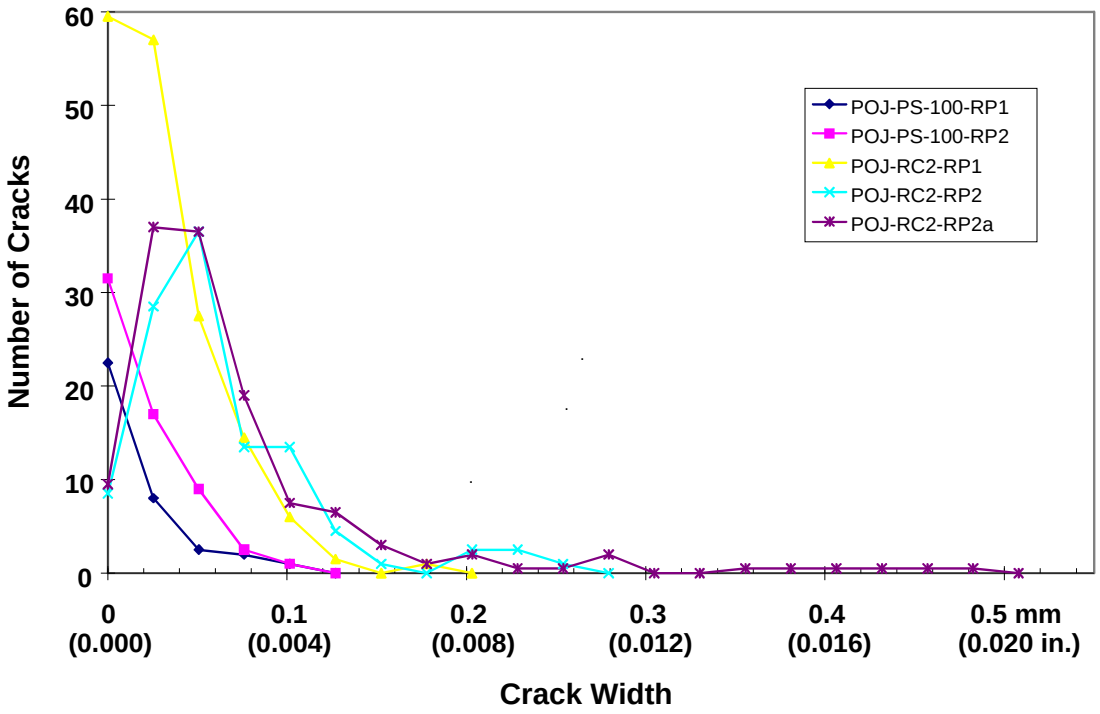

Figure 7.11 Comparison of Adjusted Crack Width Distribution at Service Load

All of the adjusted crack widths are hypothetical values which might have occurred had the repair been applied to a relatively undamaged specimen at one-half dead load. Because the actual piers would have been subjected to at least full dead load before being repaired, the adjusted crack widths are intended for the purposes of comparing relative specimen performances, rather than as a measure of crack widths to be expected in the field. In addition, the cracks in the actual piers in San Antonio would have been injected with epoxy before the repair was post-tensioned. This procedure was too costly and time-consuming to be implemented in the smaller model. Finite element analyses of the repairs by Wood [Ref. 3] indicated that had the cracks been epoxy injected, the maximum tensile

stresses in the repaired specimens would not have been sufficient to reopen the filled cracks or to introduce new cracks in the joint concrete.

7.4 Effectiveness/Performance at Factored Load / ϕ

7.4.1 Deflections

The tip deflection response up to factored load for the specimens with post-tensioned overhangs are shown in Figure 7.12. Again, both repaired specimens performed substantially better than the unrepaired specimen. The first repair, POJ-PS-100-RP1, was stiffer than the second repair, POJ-PS-100-RP2, up until approximately service load, after which the stiffnesses were very similar. The tip deflection of POJ-PS-100-RP1 at FL/ϕ was about 10.8 mm (0.425 in.), or approximately 13 percent lower than the 12.4 mm (0.490 in.) maximum deflection of POJ-PS-100-RP2. Both tip deflection response curves followed the same general shape, with one or two slight irregularities.

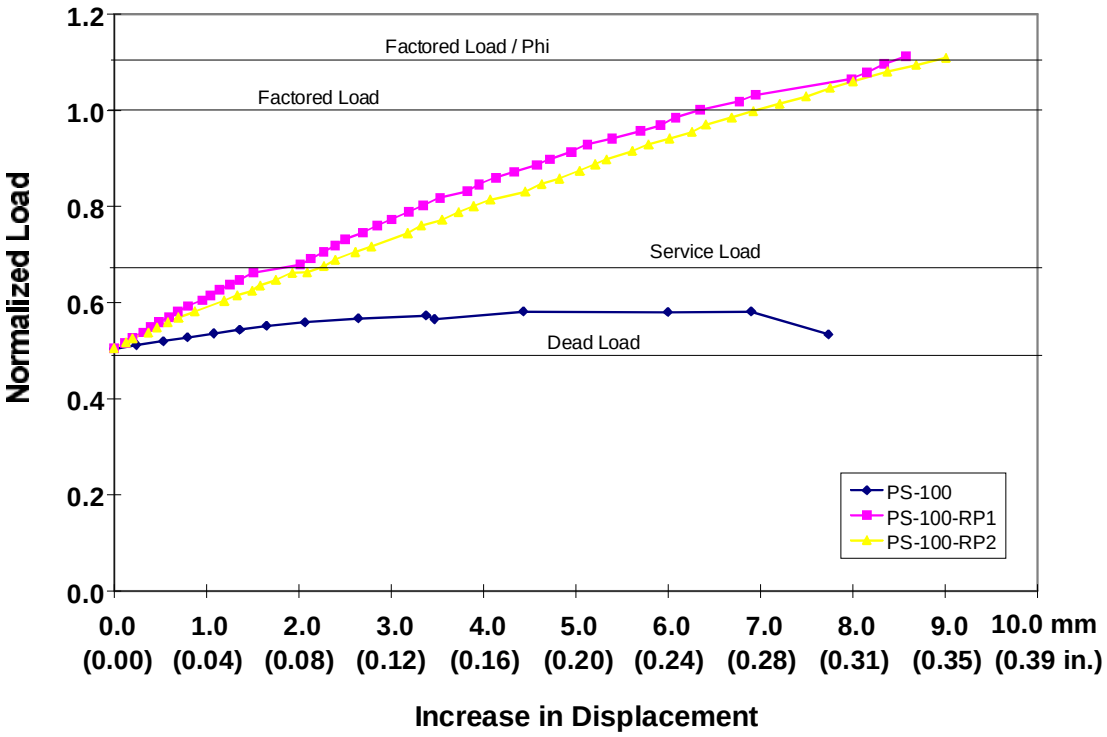

Figure 7.12 Comparison of Tip Deflection Response at Factored Load / ϕ for Specimens with Post-Tensioned Overhangs

The tip deflection responses up to FL/ϕ for the reinforced concrete specimens are shown in Figure 7.13. All three repaired specimens performed substantially better than the unrepaired specimen. The first repair, POJ-RC2-RP1, with diagonal external post-tensioning was stiffer than the two repairs using internal post-tensioning, up until service load. Above service load, the stiffness of POJ-RC2-RP1 decreased. The load-deflection curves for POJ-RC2-RP2 and RP2a are sufficiently similar that they need not be discussed separately. The tip deflection of POJ-RC2-RP1 was approximately 18.4 mm (0.723 in.) at FL/ϕ, which was approximately 6 percent lower than the 19.5 mm (0.767 in.) deflection of POJ-RC2-RP2 or the 19.7 mm (0.775 in.) deflection of POJ-RC2-RP2a. However, as discussed earlier, the

measured tip deflections for the latter two specimens were probably higher than they would have been had the original specimen not been loaded to FL/ϕ during previous tests.

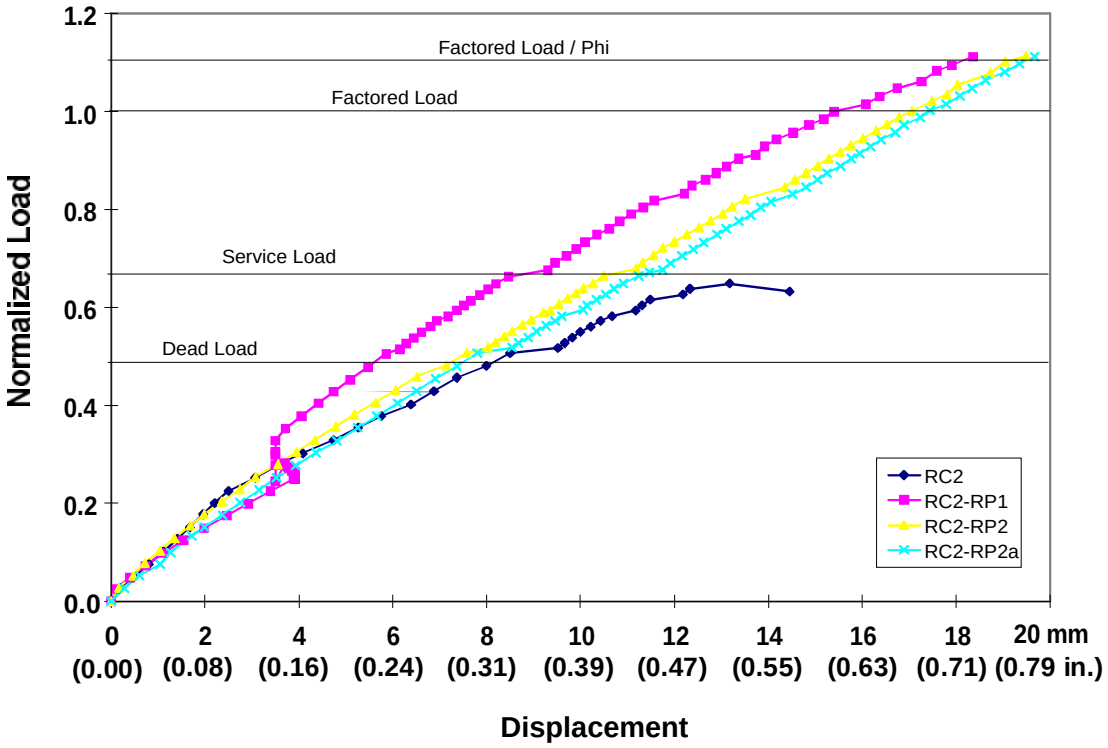

Figure 7.13 Comparison of Tip Deflections at Factored Load / ϕ for Reinforced Concrete Specimens

Load-displacement curves for all of the repaired specimens are shown in Figure 7.14. The two repairs on specimens with post-tensioned overhangs were significantly stiffer than the other two repairs, both above and below service load. Above service load, the stiffness of the displacement response curves for the specimens with post-tensioned overhangs decreased to approximately the same stiffness as the reinforced concrete specimens, while the stiffness

for the reinforced concrete specimens was approximately constant. The stiffness at FL/ϕ was significantly lower than the corresponding service load stiffness for all repairs. The stiffness of the two repairs with vertical external post-tensioning decreased the most between service load and FL/ϕ, by approximately 50-55 percent for POJ-PS-100-RP1 and approximately 40–45 percent for POJ-PS-100-RP2. The stiffness of POJ-RC2-RP1 decreased approximately 35–40 percent, while that of the two internally post-tensioned repairs, POJ-RC2-RP2 and RP2a, decreased the least, approximately 25–30 percent.

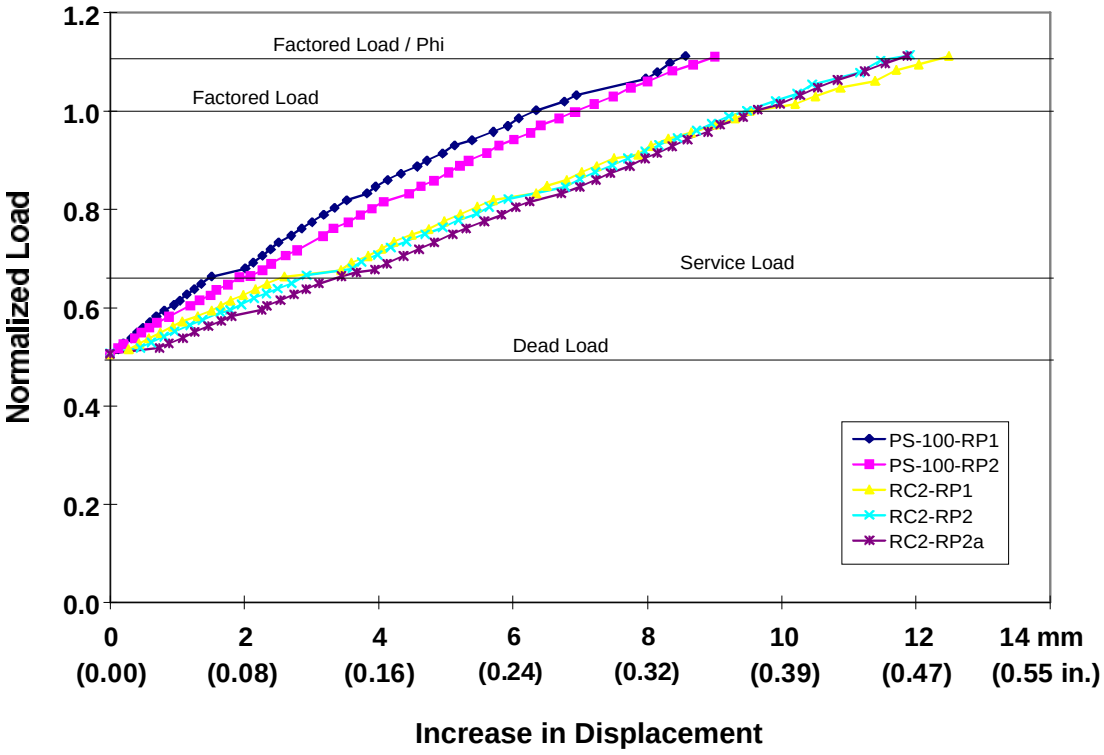

Figure 7.14 Comparison of Tip Deflections at Factored Load / ϕ for All Repaired Specimens

The rotation of the joint region gives a more accurate indication of the relative stiffnesses of the repairs by excluding the deformations of the overhang (Figure 7.15). Figure 7.16 shows the increase in joint rotation between one-half dead load (after post-tensioning was complete) and factored load / ϕ. This figure clearly shows the two vertical external post-tensioning repairs to be the stiffest, while the stiffnesses of the other repairs are approximately the same, with the repairs of the reinforced concrete specimens displaying half the stiffness of the post-tensioned concrete repairs. Note that the specimen with the external diagonal post-tensioning softened slightly above service load, relative to the reinforced concrete repairs.

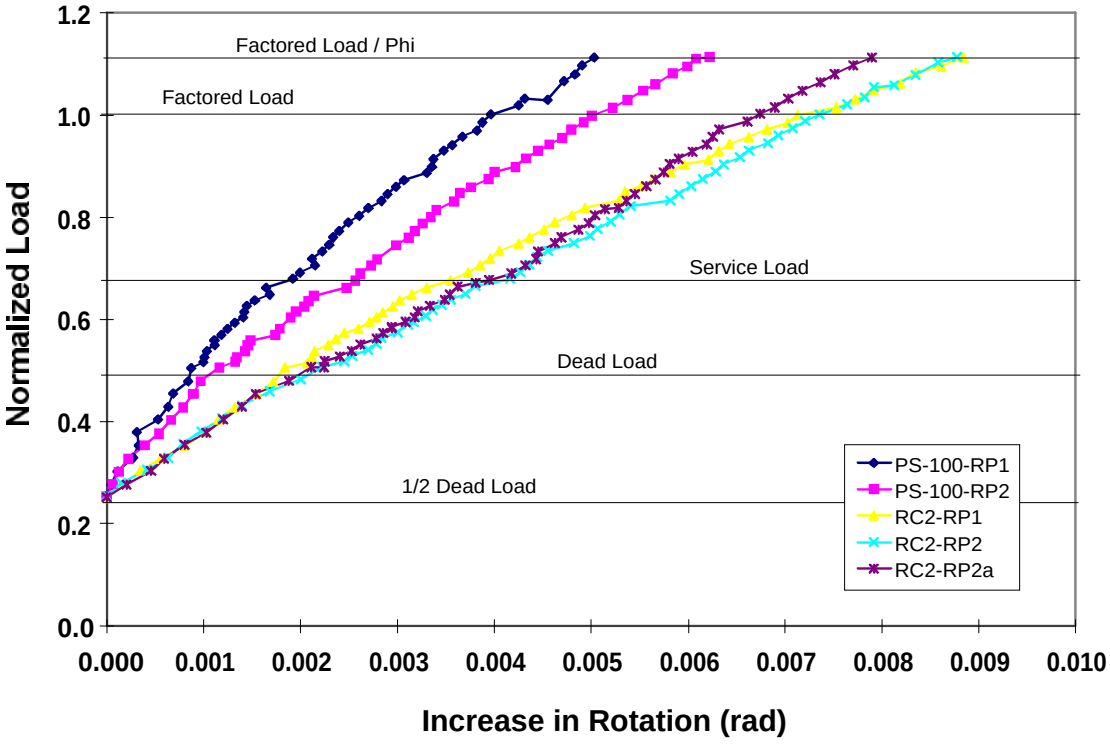

Figure 7.15 Comparison of Increase in Joint Rotations from One-Half Dead Load to Factored Load / ϕ for All Repaired Specimens

The two specimens with internal vertical post-tensioning (POJ-RC2-RP2 and RP2a) showed slight differences in joint rotation above service load (Figure 7.16), although the tip displacements were nearly identical (Figure 7.17). This would seem to indicate that the coring had little effect on the behavior of the repair. The small increase in joint rotation at higher loads may have been caused as much by additional damage from the previous test as by the coring itself.

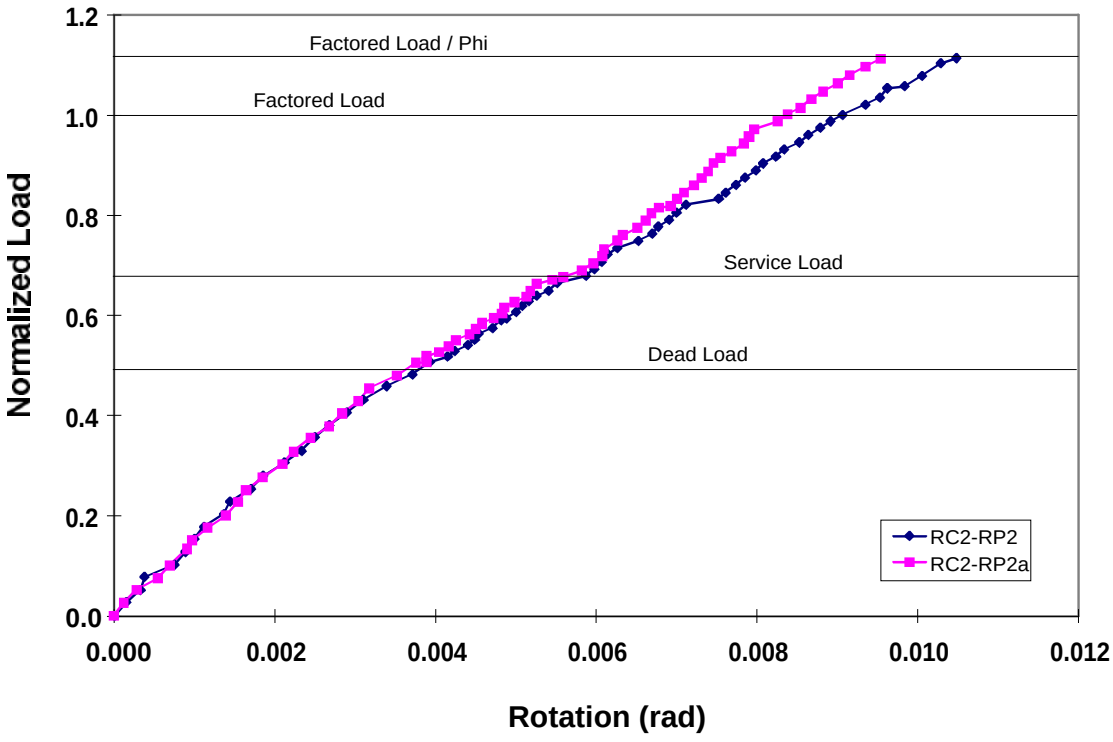

Figure 7.16 Comparison of Joint Rotations for Specimens with Internal Post-Tensioning

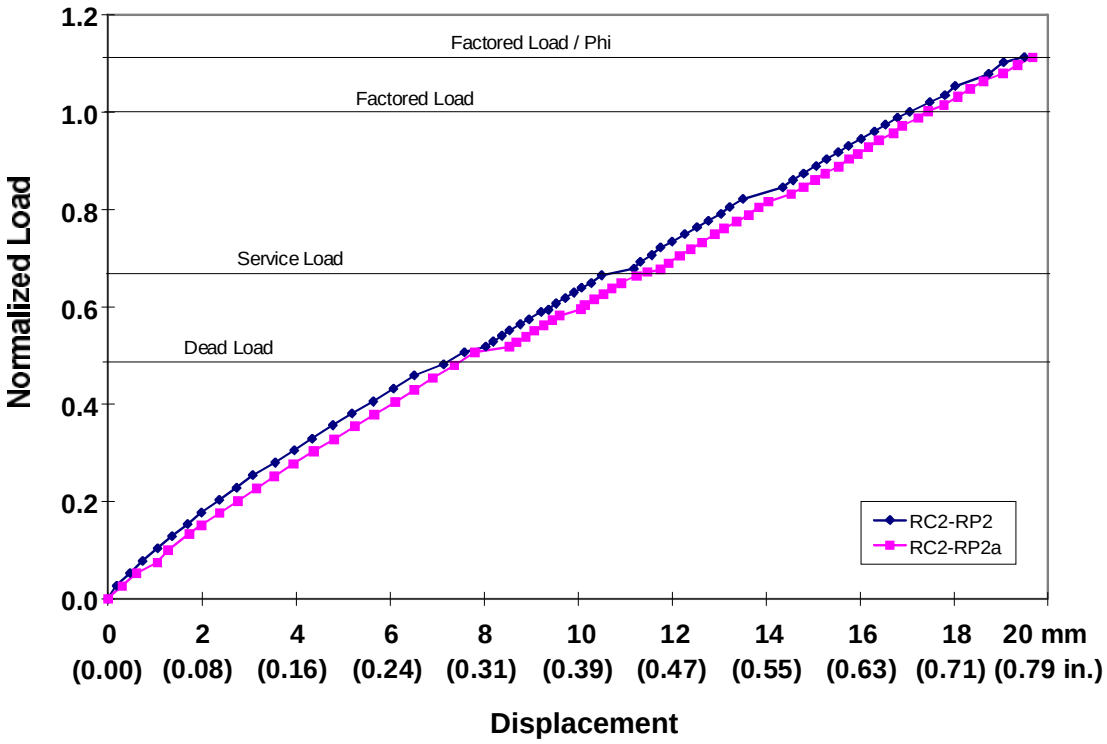

Figure 7.17 Comparison of Load-Deflections Curves for Specimens with Internal Post-Tensioning

7.4.2 Cracking and Overall Distress

Figure 7.18 compares the number of cracks in each region of the repaired specimens, averaged between the north and south sides. As expected, the two specimens with post-tensioned overhangs, POJ-PS-100-RP1 and POJ-PS-100-RP2, developed little or no cracking in the overhang region. Also, since the overhang post-tensioning continued into the joint region, the two specimens developed less cracking in the joint than did the reinforced concrete specimens. The number of cracks in the column were approximately equal for each specimen. The second repair on the post-tensioned specimen, POJ-PS-100-RP2, generally developed more cracks than did the first repair, because it utilized less external post-

tensioning force. The two tests with vertical internal post-tensioning, POJ-RC2-RP2 and POJ-RC2-RP2a, developed approximately the same number of joint cracks as did the diagonally post-tensioned specimen, POJ-RC2-RP1, and slightly more overhang cracks.

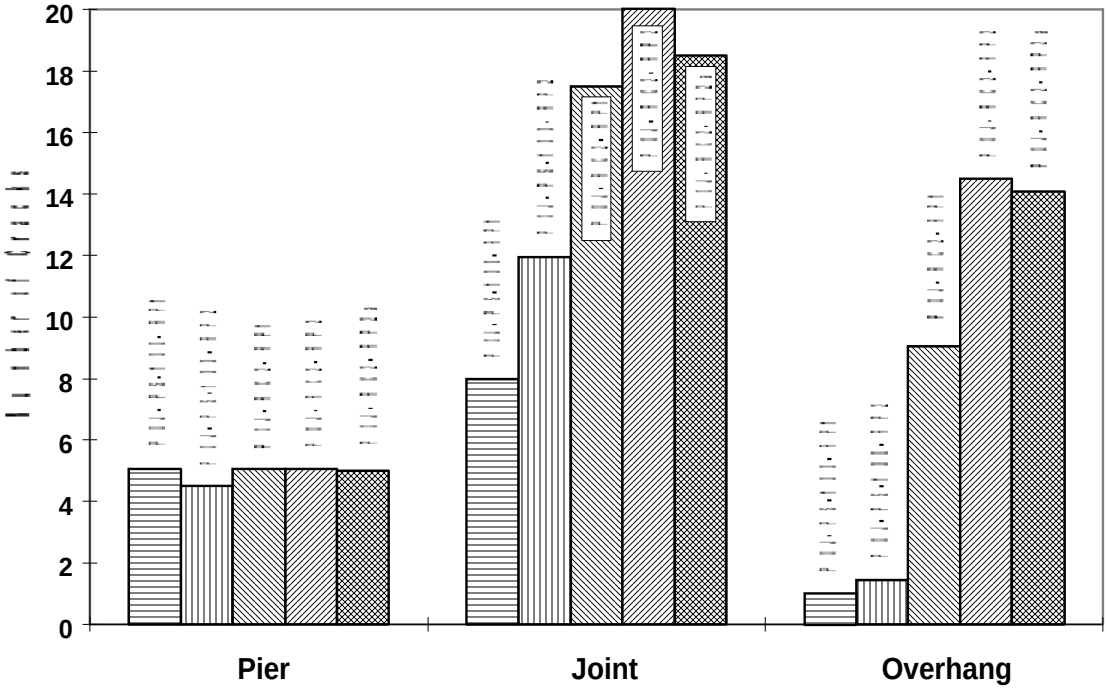

Figure 7.18 Average Number of Cracks in Each Region of the Repaired Specimens at Factored Load / ϕ

In order to more equitably compare the reinforced concrete specimens with the post-tensioned specimens, if only cracks emanating from the back face of the joint and pier are considered, the number of cracks in those regions is much more similar, as shown in Figure 7.19. Because no crack widths were measured at FL/ϕ, no crack width comparisons were made among the specimens.

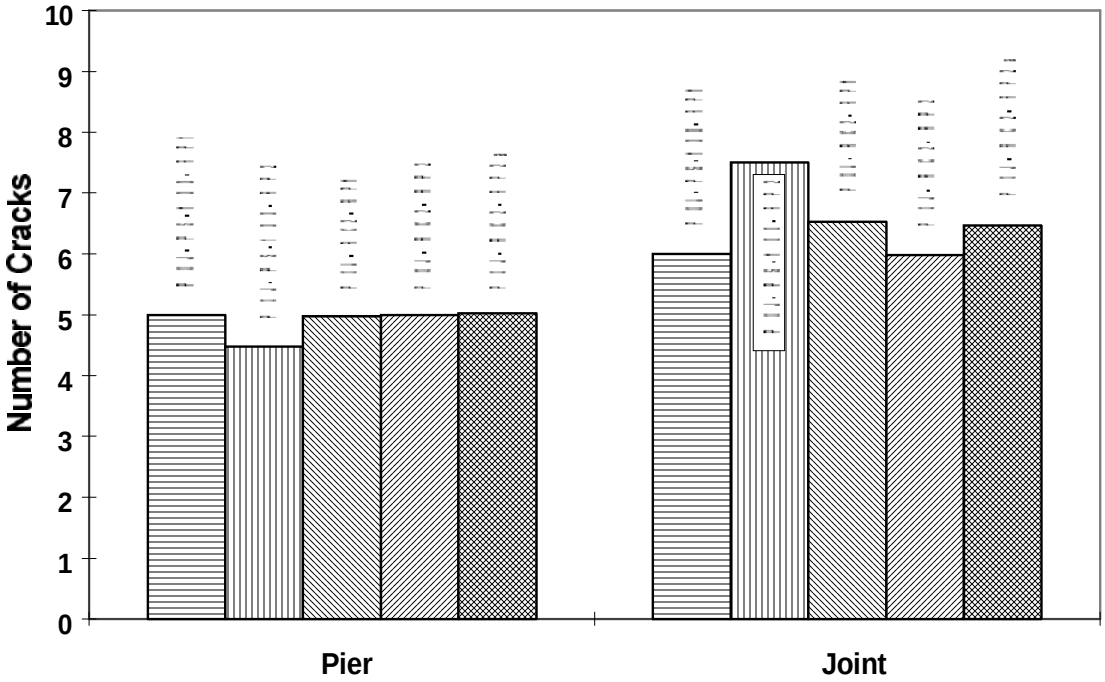

Figure 7.19 Average Number of Cracks Emanating from the Back Face of Each Repaired Specimen at Factored Load / ϕ

7.5 Cost/Constructibility

7.5.1 General

Cost and constructibility comparisons are based on estimates for full-scale repairs. Repair components were scaled up from model details using a scale factor of 2.75. All estimates of material, labor costs, and installation time are based on figures gathered by Wood [Ref. 3] from material suppliers and TxDOT personnel. Wood provides a more complete breakdown of these estimates.

7.5.2 Costs of Materials and Labor

Cost was based upon the amount of materials and labor required for each repair, including fabrication costs, multiplied by a unit cost estimate. A summary of unit costs is listed in Table 7.2. The external vertical post-tensioning repair was the most expensive, as illustrated in Figure 7.20, costing an estimated $54,000. The other two repairs were much cheaper; the cost of the internal vertical post-tensioning repair was estimated at $23,000, and the external diagonal post-tensioning repair was $15,000.

Table 7.2: Unit Costs of Repair Components

Component	Unit Cost	Unit	Unit Cost	Unit
Steel Fabrication	$4.41	Kilogram	$2.00	Pound
Anchor Bolts	$228.77	Each	$228.77	Each
Dywidag Bars	$0.63	Centimeter	$1.59	Inch
Dywidag Nuts	$10.40	Each	$10.40	Each
Dywidag Plates	$15.60	Each	$15.60	Each
Threaded Bar	$0.55	Centimeter	$1.40	Inch
Coring (7.6 cm (3") Diam)	$4.23	Centimeter	$10.75	Inch
Coring (8.9 cm (3.5") Diam)	$4.94	Centimeter	$12.55	Inch
Epoxy	$31.20	Cartridge	$31.20	Cartridge

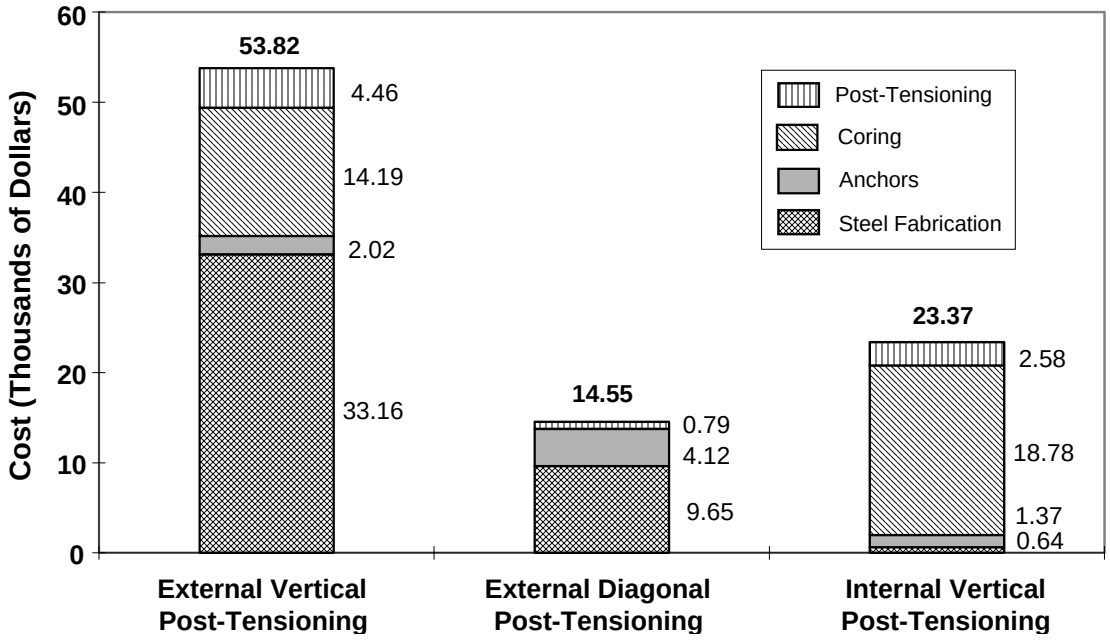

Figure 7.20 Costs of Repair Options

The high cost for the external vertical post-tensioning repair was mainly due to the massive and complicated side and cap pieces and the extensive, high-precision coring necessary for the repair. The fabricated steel sections were estimated to cost $33,000, which was more than the total cost of either of the other two repairs. The coring costs were estimated at $14,000 for 20 holes, 1.67 m (66 in.) long and 7.62 cm (3.0 in.) in diameter. The remainder of the costs consisted of anchor bolts and post-tensioning rods and hardware.

The cost of the external diagonal post-tensioning repair was also dominated by the cost of the fabricated steel sections. Since they were much lighter than those for the vertical post-tensioning repair (about 21.5 N (4.82 kips) compared to 73.7 N (16.6 kips)), they were

only estimated to cost $9650. The anchor bolts were the next major expense, at $4050, with the post-tensioning rods and hardware accounting for the remaining costs.

In contrast to the two external repairs, coring costs were the major cost item in the internal vertical post-tensioning repair. Despite the need for only eight 8.9-cm (3.5-in.) diameter holes, the 4.75-m (187-in.) length of the holes increased their cost to an estimated $18,780, which was higher than the cost of the 20 holes for the external vertical post-tensioning repair. The epoxy cost an additional $1370, and the remaining costs were associated with the post-tensioning rods and hardware.

7.5.3 Installation Time

This factor was based on the total time required to install each repair. The external diagonal repair was estimated to require about four weeks, the least amount of time for installation. The vertical post-tensioning repairs, both internal and external, were estimated to require 30 weeks or more.

The long installation time for the external vertical post-tensioning repairs was partly due to the fabrication of the complicated top and side pieces. Part of the steel elements could be prefabricated to reduce installation time in the field. However, the holes in the side pieces had to precisely match the holes in the pier, and the cap piece had to fit closely over the joint. Another factor was the difficulty of coring 20 holes through the pier using sufficient precision to install the anchors.

The internal vertical post-tensioning repair had very little steel fabrication required, but the coring of the 4.75-m (187-in.) holes would be very time-consuming. The presence of

the superstructure, which generally extended over the joint region of the piers in question, prevented the holes from being cored without the use of drill extenders, and also required the post-tensioning rods to be coupled together in several sections and threaded into the holes. Because the rods would be anchored with epoxy, the installation time for the rods is critical.

The external diagonal post-tensioning repair had less fabricated steel than the external vertical repairs, while its only drilling requirements consisted of shallow holes for anchor bolts.

7.6 Other Factors

7.6.1 Durability/Service Life

The internal vertical post-tensioning was estimated to have the greatest durability and service life [Ref. 3], because the post-tensioning would be inaccessible, and no maintenance would be necessary or possible, other than monitoring for cracks. The external post-tensioning repairs, being exposed to the atmosphere, would have lower service lives and require periodic inspection and perhaps painting. One alternative would be to encase the entire repair in concrete, which would increase its initial cost. The durability and service life of the external diagonal post-tensioning repair was estimated to be similar to that of the external vertical post-tensioning repair [Ref. 3].

7.6.2 Aesthetics

Being the least obtrusive, the internal vertical post-tensioning was deemed the most aesthetic. It would not be visible to passing motorists or vulnerable to vandalism. The external post-tensioning repairs would both be much more visible. The diagonal post-tensioning would be smaller and located higher on the bent, with lower visibility and accessibility than the vertical post-tensioning. The side plates on the external vertical post-tensioning would need to be located low on the pier to increase the length of the post-tensioning rods and minimize seating losses. This would increase the visibility of the repair and render it more susceptible to damage. The external repairs could be painted to reduce their obtrusiveness, but this would require increased maintenance.

CHAPTER 8

CONCLUSIONS AND RECOMMENDATIONS

8.1 Introduction

This chapter briefly describes the background and purpose of the study. A summary of the results of the testing program is presented, and recommendations are made to the Texas Department of Transportation based on those results.

8.2 Summary

8.2.1 Background

A design flaw was discovered in the joint region of several cantilever bridge piers supporting a major highway interchange in San Antonio. These piers or bents consisted of two basic types. One type was composed solely of concrete with mild reinforcement, while the other utilized post-tensioning in the cantilever element. Due to inadequate development length for the longitudinal reinforcement in the column of the post-tensioned bents and in both the column and overhang of the reinforced concrete bents, the flow of tensile forces through the joint between the column and the overhang was impeded. This resulted in a substantially-reduced load carrying capacity for the bents. The study described in the preceding chapters was developed to examine methods for remediating this problem.

8.2.2 Scope

The purpose of this study was to develop retrofit designs which could be applied to existing bents to restore their capacity. To this end, various repair methods were devised. The most promising schemes were fabricated and tested on scale models of typical cantilever bents. All repair methods tested were successful in restoring strength, so the repair methods were then evaluated based on serviceability, cost, constructibility, durability/service life, and aesthetics.

8.2.3 Limitations

Due to limited time and funding, only two model bents could be constructed. Each was tested several times, with a different repair scheme installed for each test. This resulted in several difficulties. The repair methods could not be tested to failure, because the specimen had to be re-used. Cumulative damage from previous tests resulted in increasingly larger crack widths and decreasing stiffness in each specimen with each test. As a result, comparisons of these quantities from test to test were meaningless or dubious at best.

8.3 Conclusions

8.3.1 Specimen Performance at Factored Load / ϕ

8.3.1.1 Strength

Because the repaired specimens were not tested to failure, the ultimate strength of each repair remains unknown. However, all specimens reached factored load / ϕ (FL/ϕ), which was the only requirement for strength. Therefore, all of the repairs tested are

acceptable by this criterion. The final test indicated that, despite the ominous cracking observed in the field, shear strength of the cantilever bents was not deficient.

8.3.1.2 Stiffness

For the specimen with the post-tensioned overhang, the repair with vertical external post-tensioning bars was the stiffest. The repairs for the reinforced concrete specimen were similar in stiffness, with the external diagonal post-tensioning repair being slightly stiffer at FL/ϕ than the internal vertical post-tensioning repair.

8.3.2 Specimen Performance at Service Load

8.3.2.1 Cracking

Due to the multiple tests performed on each specimen, measured crack widths for the different repair methods could not be compared directly. However, each repair resulted in a substantial reduction in crack widths at comparable load levels from those in the corresponding unrepaired specimen. In addition, finite element analyses by Wood [Ref. 3] indicated that if the cracks were epoxy injected in the field, tensile stresses in the concrete would not be sufficient to re-open filled cracks or to produce new cracks. Therefore, cracking is not expected to be a problem in the San Antonio bents for any of the repair methods.

8.3.2.2 Stiffness

Stiffness comparisons at service load are comparable to those at FL/ϕ. The vertical external post-tensioned repair was determined to be the stiffest for the specimen with the

post-tensioned overhang. Insignificant differences in stiffness were found for the repairs applied to the reinforced concrete specimen.

8.3.3 Other Factors

8.3.3.1 Installation Cost

The external diagonal post-tensioning repair was estimated to be the least expensive, at approximately $15,000, followed by the vertical internal post-tensioning repair at $23,000 and the vertical external post-tensioning repair at $54,000. The external diagonal post-tensioning repair was also estimated to require the shortest installation time, approximately four weeks, as compared to possibly over 30 weeks for the other two.

8.3.3.2 Durability/Service Life

The repair with the highest durability and longest service life was estimated to be the internal post-tensioning repair. Because the post-tensioning bars would be completely encased in concrete, they would be protected from deterioration and require no maintenance. The post-tensioning bars of the two external repairs would be exposed to the atmosphere and require periodic maintenance.

8.3.3.3 Aesthetics

The internal post-tensioning repair would be the most unobtrusive, and therefore, the most aesthetically pleasing. The external repairs would be highly visible, and the vertical external post-tensioning repair, in particular, would require large steel components to be exposed to view by the public.

8.4 Recommendations

8.4.1 Repair Method

8.4.1.1 Post-Tensioned Bents

While the vertical external post-tensioning repair provided the most stiffness for specimens with post-tensioned overhangs, its high cost and visibility render it impractical for use in the field. Although it was not specifically tested on post-tensioned specimens, the vertical internal post-tensioning repair could be modified for that purpose. The modification would increase the stiffness of the repair, which would have significant advantages in installation time, cost, service life, and aesthetics over the vertical external post-tensioning repair. Therefore, it is recommended that vertical internal post-tensioning be utilized to repair deficient bents with post-tensioned overhangs.

8.4.1.2 Reinforced Concrete Bents

Both of the repairs installed on the reinforced concrete specimen produced similar results for strength and stiffness. The external diagonal post-tensioning repair was estimated to be less expensive and require a shorter installation time. The vertical internal post-tensioning repair, on the other hand, was determined to be more durable and less obtrusive. Both repair methods are therefore recommended for use on deficient reinforced concrete bents in the field. Based on the results of the final test, no additional modifications are needed to enhance shear strength in these bents.

8.4.2 Continued Monitoring

While the immediate performance of the repair methods was estimated by the tests on scale models of the cantilever piers, these tests did not reveal anything about the long-term

behavior of the repairs. It is therefore prudent to monitor the repairs that were actually installed in order to detect any long-term problems. If any problems are observed, further corrective action may then be undertaken. In this manner, additional data may be acquired which may prove useful in similar situations in the future.

8.4.3 Further Research

Due to the limited scope of this study, several tests were performed on each specimen. As a result, specimens could not be tested to failure and ultimate strengths were not determined. In addition, serviceability data, including crack widths and tip deflections, were affected by previous loading of each specimen. In order to obtain more meaningful data related to ultimate strength and service, more tests could be conducted.